USING PHYSICAL PRINCIPLES TO ENHANCE THE MEASUREMENT, INTERPRETATION AND UNDERSTANDING OF SOIL RESPIRATION

by

Nicholas R. Nickerson

Submitted in partial fulfillment of the
requirements for the degree of
Doctor of Philosophy

at

Dalhousie University
Halifax, Nova Scotia
July 2014

Table of Contents

List of Tables

List of Figures

Abstract

Atmospheric concentrations of greenhouse gases (GHGs) play an extremely important role in regulating Earth's climate system. Researchers need to understand how GHGs are produced at a process-level in order to predict what might happen under future climate scenarios. A great deal of work has gone into understanding the fundamental processes that control GHG production and consumption, but many questions remain. To date, much of this research has focused on the biology of the soil system but there are also many physical processes that control the transport of decomposable substrate, nutrient supply, the local-environment (e.g. temperature and moisture) as well as the eventual emission of GHGs to the atmosphere (i.e. diffusion and advection). Some recent soil respiration studies suggest that the physical aspects of the soil have an equal or greater influence on the measurement and interpretation of soil respiration data.

Here a combination of numerical and analytical models, laboratory experiments and field studies are used to help understand the effect that soil physics has on the measurement and interpretation of soil respiration data. These analyses focus mainly on high-resolution and istopologue techniques for understanding soil respiration, and how considerations including gas diffusion and thermal conduction affect results obtained using these methods. The interpretation of soil respiration data is also carefully considered, again with a focus on how physical drivers can explain patterns in field measurements, and how physical and biological processes might be disentangled in GHG investigations. The results presented here show clearly how gaseous diffusion, thermal conduction and poor methodological assumptions can bias the measurement and interpretation of GHG emissions data. These biases and misinterpretations can often be resolved through application of physical principles and mathematical modelling. The physical and mathematical approaches presented here form a basis for making robust measurements of GHG emissions and also for forming process-based models that can be more universally applicable across space and time.

Acknowledgements

I must thank (profusely) my supervisory committee who have provided much needed guidance, motivation and leeway in all aspects of my PhD work. Firstly, my supervisor Dave Risk, who has provided guidance and support (including the freedom for me to pursue whatever research my heart so desired) for many years now. Secondly to Claire Phillips, who has not only been a great friend, but also a great mentor who never loses sight of the larger picture (which I tend to forget quite frequently). Finally to Lawrence Plug who, despite me disappearing for months out a time without communication or any sign of life, is always happy to show up to last minute committee meetings and provide feedback and advice at a moments notice.

Many thanks to my codependent partner in science, Jocelyn Egan, who has motivated me and distracted me in equal amounts during my PhD, but who has always been there to help when I needed it, pondered the meaning of soil respiration and life with me and of course is always happy to provide just the right amount of sass to keep me in line. Many of my friends should have also been my coauthors on the manuscripts in this thesis, because without their advice much of the work would have never made it out of my head and on to paper. For this I would like to thank Chance Creelman, Bruce Stevens, Emily Burns, Gordon McArthur, Robert Garbary, Carl Adams, Jamie Powell, Jen Owens, Melodie Adamson (Need), Sigrid Dengel and of course, the many undergraduate and graduate students in the StFX Flux Lab. Of course an equal amount of people distracted me from finishing my papers with promises or beer and good times (note that these two lists are not mutually exclusive) including Erin Quigley, Marc & Tiffany Thibodeau (and Oliver as of recently), Jillian Smith, Marcia Kehoe, Cheryl MacPherson, Allison Stevens, Meaghan Cormier, Fiona McCool, Lir Fry, Liz Faour, Amanda MacDonald, Etor Lucio, Pablo Ortega, and I am almost certain a fistful of others who will likely cause me grief for forgetting them.

Finally thank you to my family, who have encouraged me through all my years of school, and motivated me to finish by asking if I am "done school yet" at every family gathering over the past 10+ years.

Chapter 1

Introduction

1.1 General Introduction & Objectives

Atmospheric concentrations of greenhouse gases (GHGs) play an extremely important role in regulating Earths climate system. Decades of research have shown that, until recently, atmospheric greenhouse gas concentrations have remained relatively stable or varied slowly over geologic time scales (IPCC, 2001). Post-industrial era anthropogenic activities have caused rapid and sustained increases in the concentrations of many GHGs, most notably carbon dioxide (CO_2), methane (CH_4), nitrous oxide (N_2O) and water vapour (H_2O). There is significant potential for these anthropogenically-induced changes in GHG concentrations to affect local and global climate, thereby upsetting natural balances between uptake and release of GHGs and creating climate feedback loops (Holland et al., 2000; Davidson et al., 2006a; Bond-Lamberty and Thomson, 2010a). Ultimately researchers need to understand how GHGs are produced in natural systems at a process-level in order to then predict what might happen to these balances under various future climate scenarios. A great deal of research has gone into understanding the fundamental processes that control GHG production and consumption and how changes in Earths climate could potentially affect these processes, but many questions remain (Davidson et al., 2006b).

As an example, carbon dioxide (CO_2), which is produced primarily by aerobic respiration and consumed by photosynthetic activity, is arguably the most well studied GHG to date. While the processes underlying photosynthetic uptake of CO_2 by autotrophs are well understood, much of the literature regarding respiration (particularly in soil systems) suggests that a process-based understanding is lacking (e.g. Davidson et al. (2006b)). Researchers have made progress in this direction by improving the understanding of the fundamental soil biology and ecology (Schimel and Weintraub, 2003; Tang et al., 2005a; Risk et al., 2008a; Davidson et al., 2012), developing robust methodologies for measuring GHG exchanges (Davidson et al.,

2002; Subke et al., 2004; Livingston et al., 2005; Senevirathna et al., 2007; Risk et al., 2008b), and adopting more complex mathematical techniques for analysis and predictive modelling (Pumpanen et al., 2003; Reichstein et al., 2005; Ryan and Law, 2005; Livingston et al., 2005; Graf et al., 2008), to name a few.

However, to date soil respiration research has focused largely on the biology of the soil system, as the soil organisms are ultimately the producers of CO_2. But, there are many physical processes that control the transport of decomposable substrate (Davidson et al., 2012), nutrient supply (Schimel and Weintraub, 2003), the local-environment (e.g. temperature and moisture) (Xu et al., 2004; Wei et al., 2010; Falloon et al., 2011; Moyano et al., 2012; Suseela et al., 2012) as well as the eventual emission of the produced gas to the atmosphere (i.e. diffusion and advection) (McCarthy et al., 1995; Moldrup et al., 2000; Kayler et al., 2010; Bowling and Massman, 2011). While researchers acknowledge these physical complexities they have not, until recently, received as much attention as the biological aspects. Some recent soil respiration studies suggest that the physical aspects of the soil have an equal or greater influence on the measurement and interpretation of soil respiration data (Moyes et al., 2010b; Phillips et al., 2011; Martin et al., 2012). These physical aspects will affect every part of the study of GHG emission, from measurement to data interpretation. The overall goal of this work is to evaluate the impact that soil physics - with a particular focus on thermal and gaseous diffusion dynamics - has on the study of CO_2 emissions (including carbon (C) isotopologues ($^{12}CO_2$, $^{13}CO_2$, $^{14}CO_2$)).

This overarching goal was accomplished in two parts. First methodologies for measurement and monitoring of GHG emissions were examined using a combination of theoretical, experimental and field data sets. The specific methods presented in this thesis were chosen either because they are likely to become prominent in the near-future due to recent advances in analytical equipment, or because the methods offer potential solution to already identified methodological biases (most of which are caused by soil physical considerations). Secondly, the influence of soil physics (i.e. gas and heat transport) on the interpretation of soil respiration measurements was characterized. This work sought to qualitatively match in-situ data collected by researchers and show that patterns they interpret as being biological could equally

be physical in nature. This was demonstrated mainly through numerical modelling approaches and subsequent comparison to field data gathered during this thesis research or by other researchers. After qualitatively demonstrating the importance of these physical considerations, the focus shifted towards showing that these physical patterns can be corrected for, or removed from the data, to get at the underlying biological and biogeochemical processes. This was accomplished through careful theoretical consideration of how physical processes (in this case temperature) and biological processes are linked.

1.2 Thesis Outline

This thesis consists of 7 manuscripts that together explore the influence of soil physics on the measurement and interpretation of soil respiration data. These manuscripts are presented in two distinct sections, the first topic being measurement methodologies for CO_2 and its carbon isotopologues with 4 manuscripts: 1) Forced Diffusion Soil Flux: A New Technique for Continuous Monitoring of Soil Gas Efflux; 2) Iso-FD: A novel method for measuring the isotopic signature of soil flux; 3) Subsurface Approaches for Measuring Soil CO_2 Isotopologue Flux: Theory and Application, and; 4) A numerical examination of $^{14}CO_2$ chamber methodologies for measuring fluxes at the soil surface. The second section looks at how this data can be interpreted robustly so as to answer questions about biological and soil processes that lead to soil respiration and includes 2 manuscripts: 1) Interpreting Diel Hysteresis Between Soil Respiration and Temperature, and; 2) Using production weighted heat to disentangle the environmental sensitivities of soil respiration. Finally a preliminary manuscript that outlines a conceptual framework for interpretation of soil respiration data is presented (Chapter 8). Each chapter begins with a preamble, describing my contribution to the work in question as well as its status as a publication. Many of the manuscripts have been accepted for publication, with several under review currently and one in preparation for submission.

Chapter 2

Forced Diffusion Soil Flux: A New Technique for Continuous Monitoring of Soil Gas Efflux

2.1 Preamble

This chapter presents a new method used to monitor the flux of soil gas to the atmosphere. Authorship on this manuscript is as follows: Dave Risk, Nick Nickerson, Chance Creelman, Gordon McArthur and Jen Owens. Dave Risk was responsible for much of the manuscript text, design of the instrument, and field and lab testing along with Gordon McArthur and Jen Owens. I was involved in the initial proof of concept experiments and in the theoretical derivation of the method and computational simulation efforts (along with Chance Creelman) presented in the manuscript, as well as a portion of the lab data collection and interpretation. A version of this manuscript was published in Agricultural and Forest Meteorology in December 2011 (Volume 151, Issue 12). Copyright permission for this publication can be found in Appendix E.

2.2 Abstract

Measurements of soil carbon dioxide efflux provide critical information on soil carbon balance. In light of increasing interest in monitoring carbon balance of northern soils, it is important that new methodologies are developed that are better suited to long-term, remote, and off-grid deployments. In this study, a Forced Diffusion (FD) dynamic chamber is described, in which a gas permeable membrane passively regulates mixing of atmosphere and soil air in the chamber, in place of the active pumping system inside a regular dynamic efflux chamber system. A combination of methodologies are used to explore the FD chamber technique, including numerical modelling, laboratory benchmarking, mesocosm testing, and year-round field studies in northern temperate ecosystems. Not surprisingly, FD chambers are functionally

similar to regular dynamic chambers, but the passive regulation of gas flow means that internal concentration sensors can be switched off between measurements, thereby achieving very low power consumption and high reliability. In numerical modelling experiments and controlled lab tests, FD chambers deliver data that are comparable to commercially available instruments. As with other efflux techniques, calibration, design geometry, and deployment methodology are critical issues for generating good accuracy and precision with FD chambers.

2.3 Introduction

Soil efflux is a commonly measured ecological parameter that is critical to the current and future understanding of ecosystem carbon dynamics and overall carbon balance. "Open" or "dynamic" soil chambers have been shown as among the best systems for accurate measurements of soil flux (Pumpanen et al., 2004). These systems have good potential for making long-term measurements because they generally have fewer moving parts than automated static chambers, which require arms or pistons to open and close the chamber during measurement cycles. However, dynamic systems are expensive to build and operate (Subke et al., 2004) and improvements or simplifications can be of high value to researchers, especially as instrumental limitations still compromise the ability to collect continuous long-term soil respiration records (Elberling and Brandt, 2003).

Dynamic chambers are active devices, and require a pump, flow controller and sustained power supply to maintain equilibrium between atmospheric air and soil-source gases. These components consume power, and have limited lifetimes. For example, few small pumps have rated lifetimes that exceed one year of continuous use. There is, however, reason to think that dynamic chambers could be built as passive devices. For a decade, passive diffusion-based sensors have been widely used by ecological researchers, and there are many applications where permeable membranes are used as an alternative to pumps. In a dynamic chamber, water-resistant gas permeable diffusion membranes could potentially replace pump and controller, to maintain equilibration by diffusive means.

The aim of this experiment is to build and test a dynamic diffusion soil CO_2 efflux instrument, using diffusion-based (open) CO_2 sensors and commonly available

gas-permeable membranes. While most similar manuscripts tend to describe new hardware by using either laboratory evidence (Martin et al., 2004; Pumpanen et al., 2004), comparative field/mesoscosm data (Bjorkman et al., 2010), or results from numerical modelling (Senevirathna et al., 2007; Nickerson and Risk, 2009c), this study is intended to have a multifaceted approach which relies on all of the above. The objectives are threefold: to test the theory in a modelling environment for identification of important operational parameters and uncertainty; to build and verify embodiments using flux generator (Martin et al., 2004) benchmarking devices; and to test the technique in the field.

2.4 Methods

2.4.1 Theory

Though designs vary somewhat, dynamic chamber systems are comprised of a closed cylinder through which atmospheric air is pumped at a controlled rate in order to establish equilibrium mixing between the atmosphere and soil gases moving upward into the chamber (Rayment and Jarvis, 1999). The path of soil gas flow is from the soil to the chamber exhaust, and is continually diluted by incoming atmospheric air. The concentration inside a dynamic chamber is always intermediate between that of the atmosphere and the soil. Both inlet (atmospheric) and exhaust (mean chamber) concentrations must be measured to calculate flux by mass balance, as the difference between incoming and outgoing concentrations:

$$F_s = \frac{\Gamma(C_{chamb} - C_{atm})}{A_s} \tag{2.1}$$

where Γ is the pump speed ($m^3\ s^{-1}$) at which air is being drawn through the chamber, C_{chamb} (μmol m^{-3}) is the concentration of the chamber as measured in the exhaust, C_{atm} (μmol m^{-3}) is the concentration entering the chamber and A_s is the area of the chamber in contact with the soil (m^2).

It is possible to consider the same system with two straightforward design modifications: 1) traditional closed-path analyzers are substituted for open path sensors and 2) in lieu of a pump and flow controller a proportion of the closed cylinder surface is covered by gas-permeable membrane. Like the traditional technique,

a continuous dynamic equilibrium will be established between soil gases and the atmosphere, and CO_2 concentration can still be measured at the same points.

This new system differs from the traditional dynamic system in two important ways. Firstly, the chamber is no longer mixed by a pump, with free air diffusion and thermal convection now acting as the agents of mixing. Chambers that have a small volume can be well mixed by convection and diffusion because the free-air transport rate of CO_2 is fast relative to the rate at which gases are passing across the soil or atmospheric membrane interfaces. The second and more important difference is that Eq 1. no longer applies. Consider the mass balance for this new system:

$$V\frac{\partial C_{cham}}{\partial t} = A_s F(t) - A_a\left(D\frac{C_{cham} - C_{atm}}{L}\right) \tag{2.2}$$

where V is the chamber volume (m^3), $\partial C/\partial t$ is the time rate of change in the concentration in the chamber (μmol m^{-3} s^{-1}), F(t) is the time dependent soil flux rate (μmol m^{-2} s^{-1}), A_a is the area of the membrane in contact with the atmosphere (m^2), D is the diffusivity (m^2 s^{-1}) through the chamber volume and across the membrane to the atmosphere and L is the characteristic path length (m) for diffusion. Assuming the soil system is in steady state, $\partial C/\partial t$=0 (similarly F(t)=F_s) and rearranging Eq. 2.2 to solve for F_s:

$$F_s = \frac{A_a}{A_s}\left(D\frac{C_{cham} - C_{atm}}{L}\right) \tag{2.3}$$

For simplicity constants (D, L, A_a and A_s) can be combined into a single term, G, which has units of m s^{-1}:

$$F_s = G(C_{chamb} - C_{atm}) \tag{2.4}$$

In relation to the original dynamic chamber mass balance, pump speed (Γ) has been replaced with a diffusive term that describes the overall diffusive transport properties of the membrane-chamber system (G) but the units of the equation remain unaffected (Γ/A_s has units of m s^{-1} as does G).

Membrane material, chamber geometry, and membrane surface areas A_s and A_a can be adjusted to manipulate the proportional relationship of $C_{chamber}$-C_{atm} as a function of F_s. This technique is called "Forced-Diffusion" (FD) flux because the membranes control chamber equilibration and gas flow by imposing a strict, constant, and known (via calibration) diffusive regime at the soil surface.

Like pump flow rate in the traditional dynamic chamber, G must be empirically quantifiable. While it is possible to measure membrane D, it will differ somewhat between batches of a given membrane material. It is also possible to estimate a diffusive path length (L), but owing to obstructions in the flowpath (Vaisala sensor) and complex geometries (membranes on bottom and sides), this is difficult. It is easiest to empirically measure the characteristic G of each soil chamber by rearrangement of Eq 2 to solve for G on a laboratory apparatus where F_s is known. Any known flux environment would allow the proportionality (G) between flux and internal concentration to be quantified. Benchmarking devices such as flux generators (Martin et al., 2004) should serve this purpose adequately.

It should be noted that FD is *not* a gradient technique, either in time or in space. It is a single point measurement technique based on a traditional flow-through dynamic chamber.

2.4.2 Modelling

Numerical modelling is used as validation of theory and to inform design and construction of FD embodiments. Modelling of soil respiration chambers (Senevirathna et al., 2007; Nickerson and Risk, 2009c) is a powerful tool for exploring chamber performance under a wide range of scenarios, across which exhaustive empirical tests are impractical or impossible. Chambers interact with and perturb their natural environment in several ways. In particular, when high chamber CO_2 values (relative to ambient) decrease the surface concentration gradient under the chamber, soil-source CO_2 begins to move laterally, resulting in under-reporting of fluxes in the chamber. Pumpanen et al. (2004) documents this downward bias experimentally for several chamber types.

Overall, this modelling approach is similar to Nickerson and Risk (2009c) except with a more flexible cubic grid geometry rather than the previous radial form. The coupled soil and atmosphere model simulates 3-D diffusive transport of CO_2 through soil subsurface and atmosphere layers into an infinite atmosphere. Each cell has its own layer specific total, air-filled and water-filled porosity; six diffusivity values (corresponding to the boundaries of the six nearest neighbours); and an internal CO_2

production rate. Exchange of CO_2 between cells is controlled by Fick's law:

$$F_{1,2} = D_{1,2}\frac{\Delta C_{1,2}}{\Delta(ijk)_{1,2}} \tag{2.5}$$

where $D_{1,2}$ is the diffusion coefficient (m^2s^{-1}) between cells, $\Delta\ C_{1,2}$ is the difference in CO_2 concentration (μmol m^{-3}) and $\Delta\ (ijk)_{1,2}$ is the coordinate difference in the positions (m) of the cells. Each soil column has uniformly distributed production of CO_2, summing to 1.0 μmol m^{-2} s^{-1}. Within the model, the chamber always sits on the soil surface, occupying cells in the middle of the lowest layers of the atmosphere. The bottom of this chamber exchanges CO_2 with the soil whereas the top of the chamber interacts with the atmosphere, in both cases using Fick's Law and the diffusivity coefficients of soil and free air respectively. The model was validated using both steady- and non-steady-state analytical solutions to the diffusion equation and the coupled chamber models were validated using the non-steady-state analytical solution described by Livingston et al. (2005).

Using Atlantic Computational Excellence Network (ACEnet) computing resources, model runs were used to evaluate the range of parameters summarized in Table 1. Tested parameters included soil diffusivity, chamber diffusivity (function of membranes and surface areas), collar length, and atmospheric diffusivity. These tests were repeated for a range of FD chamber geometries, membrane diffusivities and surface areas, but for simplicity results are presented only for the embodiment (described below) that was used in empirical validation testing. To force 1-D behaviour, the soil collar was extended to the bottom of the model soil.

2.4.3 Embodiment

For this study, small FD dynamic chambers were built (PVC, 5 cm internal diameter, 8 cm tall) into which a Vaisala GMP343 CO_2 sensor is mounted in a downwards fashion without its factory diffusion shield. Two opposing UV-resistant Tyvek^{TM} (part number 1460CL) membranes are installed on the sides of the chamber to communicate to the atmosphere, where they sit in a vertical orientation to help shed dust and water, though they are already highly hydrophobic and naturally resist water films. A third membrane is installed on the bottom of the chamber. The relative areas of the top and side membranes are key determinants in the overall gas

transport through the chamber, and in the described embodiment they are roughly equal, at 18.92 cm^2 and 20.10 cm^2 for bottom and outlet, respectively. With a rated water-resistance of 3 m, the membranes simultaneously regulate dynamic chamber equilibration and protect the optics of the open path chamber from standing water, dust, etc. A soil collar of 2.5 cm is attached to the chamber to create a gas seal with the soil surface, and legs to provide firm support in continuous deployments. An external reference sensor (C_{atm}) is placed adjacent to the soil chamber inside a separate chamber that is identical except for the fact that a thick piece of rubber substitutes for the bottom (soil) membrane and blocks communication with the soil. Since the soil and reference chambers are almost identical, they should respond at the same rate to changes in atmospheric concentration. While the C_{chamb} and C_{atm} measurements could readily be integrated, it is convenient to separate them so that a common reference measurement could be used for several nearby soil chambers, as the Vaisala 343 sensors are rather expensive. Figure 2.1 provides a schematic of this typical form. Many other embodiments and geometries are possible, including those with clear or opaque chambers, or with sensors for other gases of interest such as methane. A second set of embodiments were built for mesocosm tests with the same proportional geometries of bottom and side membrane surface areas, but the overall package was somewhat narrower (3.175 cm diameter) and housed the smaller Vaisala GMM222 0-2000 ppm sensors.

The probes above were initially based around the size and shape of the Vaisala 343 sensor, with membrane sizes optimized afterwards. However, many possible embodiment shapes, sizes, and configurations are possible so long as they allow for a reasonable G value (sufficient membrane area), and that internal mixing would proceed at an adequate rate without pumps (shorter is typically better). There is however no theoretical limit to scale, and inevitably embodiments can be built for various field environments. Small chambers can be placed between plants or clumps of vegetation, but do not integrate fluxes across a large area. Larger chambers do not allow for continued plant growth and might create a non-representative soil surface in systems where photosynthesis occurs near the ground, as in grasslands. In forests with relatively bare understory, however, larger FD chambers could be quite suitable. The preferred shape and size of FD chambers will no doubt vary as the technique

comes into wider use, but these geometries were suitable for development.

Overall, one target of development was to minimize the long-term concentration footprint of the FD chamber (and lateral diffusion impacts) by selecting fast-diffusing membranes and high surface areas, while allowing for a reasonable concentration increase in the housing per unit increase in flux. The latter is required to generate reasonable precision. Although modelling helped inform these choices, comparative data was drawn from the literature to shape the frame of reference. Using published information on geometries and flowrates and by applying Eq 1 or 2 (as appropriate) for a variety of well-cited studies where dynamic chambers were used, C_{chamb}-C_{atm} values were estimated. These values are presented in Table 2 and include the Subke (2002) and Kutsch et al. (2001) chambers that performed very well in the Pumpanen et al. (2004) tests. There is a surprising range in the values deemed to be acceptable, and relative to the other dynamic chambers the lateral diffusion footprint of the FD embodiments is likely to be rather low. Lateral diffusion error does, however, remain an important consideration that will be addressed in this study using 3D modelling, and specifically for the FD chamber embodiments used here.

Pressure venting is an important aspect of chamber design. It has been established that pressure gradients in efflux chambers cause measurement errors (Davidson et al., 2002) and as a result, chamber systems of all types rely on venting to equilibrate pressures with the free atmosphere. In the FD chamber, the membrane itself is used to accommodate pressure changes. Somewhere between 1% and 10% of the membrane surface is made up of pores of micron scale, which allows free passage of all gases. Liquid water is excluded simply due to its strong surface tension on the hydrophobic surface. In the embodiment described above, the total membrane porosity would equate to a vent tube of 1 cm diameter, which is very large for the small chamber volume under consideration. In addition to cross-membrane pressure equilibration, the membranes are somewhat flexible. Although supplementary venting does not appear to be necessary, this topic merits further research. Ideally, this would take the form of a comparative laboratory study comparing several efflux techniques where artificial wind is generated.

2.4.4 Flux Generator Experiments

A reference apparatus provides a good platform for empirical tests of FD dynamic chambers. Performance was benchmarked in both a 1-D environment (no lateral diffusion), and a 3-D environment, using several soil gas diffusivities.

A flux generator similar to that of Martin et al. (2004) was built using a Li-Cor LI-820 infrared gas analyzer (IRGA) with 0-20,000 ppm range to continuously measure CO_2 concentration inside a reservoir. A small diaphragm pump (Gast 3D1060-1-1-1073) was used for loop circulation. A 234.23 L reservoir was used, in which air was mixed by a fixed-speed fan which circulated air from top to bottom and mixed the entire volume in ∼15 s. On top of the reservoir sat a 0.324 m^2 tray holding a glass bead soil, or in some cases a homogenized soil free of organics (as processed by loss on ignition) to a depth of ∼14 cm. A four-port exhaust manifold coupled to a Nederman exhaust arm was used to keep the soil surface concentration near ambient levels. The flux generator was automated using a National Instruments Data Acquisition device and a custom-designed Labview interface. Pure CO_2 was introduced into the reservoir downstream of the Li-Cor IRGA by automated valving (Clippard). Two Vaisala GMM222 0-2000 ppm sensors were used to monitor ambient (C_{atm}) and soil surface concentrations as required. Otherwise, all operational parameters and mass balance equations for calculating flux were as presented in Martin et al. (2004). Flux rates up to 12 μmol m^{-2} s^{-1} were produced on the generator, with a decay time of at least 12 hours before reaching flux rates less than 0.5 μmol m^{-2} s^{-1}. In the 3-D tests, the FD soil and reference chambers were deployed together on the surface. In this large soil area, lateral diffusion was allowed to proceed as it would in the field.

For 1-D tests, the smaller apparatus shown in Figure 2.2 was used, with a reservoir of 0.412 litres in which a Vaisala 0-5000 ppm GMP343 sensor is mounted integrally. The FD chamber was coupled directly to the generator, excluding the synthetic soil used by Martin et al. (2004), creating a 1-D flow system and preventing development of lateral diffusion gradients around the chamber. A flow of CO_2-free air (N_2, high purity) was circulated through a larger cylinder that covered the side (exhaust) membranes. The C_{atm} value does not have to be measured in this case because the N_2 flow maintains a zero CO_2 concentration. G is measured by first spiking the concentration of the reservoir by injection of pure CO_2, waiting for the system

to equilibrate (∼20 minutes), and then logging the decay rates of reservoir and FD chamber concentration. The process takes roughly one hour. While 3-D testing is obviously a more realistic analogue to field deployment environments, 1-D testing provides an opportunity to validate the technique without the complicating noise of lateral diffusive effects.

1-D and 3-D flux generator runs were used to evaluate: linearity between C_{chamb} and F; the value of G for each FD chamber; the consistency of G between 1-D and 3-D environments; the effect of controlled and uncontrolled C_{atm}; and lastly to compare against modelling simulation of similar systems.

2.4.5 Comparative Mesocosm Tests with Li-Cor LI-8100

Instrument intercomparison is important for method validation, and in recognition of this comparative tests were undertaken in a real packed soil to determine relative response between Li-Cor LI-8100 and FD dynamic chambers. For these tests, an experimental mesocosm was used where CO_2 was produced in a soil by an active microbial community responding to forced changes in temperature. This experiment provided a more realistic environment than the flux generator, but also allowed us to minimize the complicating factors of spatial variability that might be encountered in side-by-side field tests.

The synthetic soil was made using a mix of silica, sand and commercial topsoil, homogenized and packed into a round 0.25 m^2 column approximately 25 cm deep. Electric soil heating cables (Nexans CSA LL23462 F AWU90 XLPE) were installed in the bottom and on the sides of the column before soil packing, controlled thermostatically by a datalogger that simulated a realistic diurnal pattern of soil temperature. Thermostatic control was carried out using a Campbell Scientific CR23x datalogger and relays, and three Campbell Scientific 107b thermistors which were installed in the soil at 5 cm depth and positioned equidistant from one another, all 10 cm from the centre of the plot. The datalogger took an average of these temperature readings and turned heating cables on or off as necessary, forcing a smooth sinusoidal temperature variation with a mean of 23°C and amplitude of 5°C. The room temperature was kept constant at 18°C. A Campbell Scientific (CS616) volumetric water content reflectometer recorded soil moisture variations during the

experiments.

Three smaller Vaisala GMM222-based FD chambers were used for this test, with 5 cm collars, and metal spikes fixed to the outside of the housings to hold the chambers stationary in the soil. The FD chambers were installed at a radial distance of 15 cm from the centre of the plot, as was the Li-Cor LI-8100. Since the soil was actively respiring at an unknown flux rate, the Li-Cor was used to measure the flux magnitudes across one diurnal cycle so that the FD G value could be established. For the balance of the experiment, the FD chambers and Li-Cor ran independently of one another. Atmospheric concentrations were not controlled, though the experimental apparatus was placed in a lesser used part of the the lab and saw somewhat smaller deviations than the core working area. Approximately one thousand Li-Cor and comparative 15-minute timescale FD flux measurements were taken over the course of a 10-day period, and no corrections were applied to the data except for routine ideal gas law corrections required by the Vaisala 222 sensors.

2.4.6 Field Tests

Data are presented here from two long-term field deployments initiated in July 2010 using Vaisala 343-based FD chambers: one at a boreal system on North Mountain, Nova Scotia (46°55'15"N, 60°25'17"W) and the other at the margin of a fallow agricultural field in Woods Harbour Nova Scotia (43°39'26"N 65°29'38"W). Two FD chambers and one FD reference chamber were deployed at each site within a footprint of roughly 1 m^2. A Campbell Scientific CR1000 datalogger was used to toggle the sensors on for 15 minutes every half hour, at the end of which data was sampled, calculations were done, and data was stored in the logger memory and/or transmitted via cellular telemetry to St. Francis Xavier University. A Sharp 80 watt solar panel, and Discovery D12550 deep cycle battery was used to power the small station. Peripheral sensors measured temperature (Campbell 107b at 2 m in air, and 0, 10, and 30 cm depth), volumetric soil water content (Campbell CS616-L at 10cm and 30 cm), shallow soil oxygen (S-200 Apogee Instruments Inc), and relative humidity (Pace Scientific). Li-Cor LI-8100 spatial flux surveys were conducted several times during the summer and fall of 2010, along the same 1 m increments in N,S,E, and W directions from the FD sensors. Flux surveys were used as a qualitative

comparator of Li-Cor and FD values, though the spatial and temporal heterogeneity of these natural environments is too high to provide reasonable controlled comparator data. The primary motivation for establishing the field sites was to assess real-world power consumption of the FD technique, test overwinter applications, establish long-term drift due to membrane degradation, and overall to consider the utility of FD chamber data.

2.5 Results and Discussion

2.5.1 Modelling Simulations

Figure 2.3 (A-C) shows the behaviour of the FD instrument in the absence of lateral diffusion (1-D diffusion only). Here the behaviour of the FD method was examined under three conditions. In panel A, 5% gaussian noise was added to the FD signal to examine the effect of potential electrical noise in the concentration measurement signal. Not surprisingly, the mean signal with noise added was the same as the noise free case and noise propagated linearly such that 5% noise in concentration manifested itself as 5% noise in the flux signal. In panel B, the effect of a step change in soil diffusivity and pore space on the probe measurement was examined. Theoretically, the probe should measure soil surface flux and be unaffected by the soil's diffusive regime once reequilibrated (at least in 1-D). As expected, the measured and actual values for flux followed each other closely before and after the step change has occurred. Finally C shows the effect of changing atmospheric concentration and the importance of an atmospheric reference. Panel C shows a FD chamber with and without atmospheric compensation, in an atmosphere where soil fluxes and atmospheric concentration are varying with the same (double diurnal) period, but with a small offset in peaks. In both cases, the atmosphere was experiencing sinusoidal variation of ± 75 ppm. Without an atmospheric reference (dotted lines), the timeseries recorded the right mean owing to the equal variation of atmospheric concentration through time, but the amplitude and temporal variation are obviously not captured properly. In the simplest terms, this last panel illustrates the consequences of assuming that C_{atm} is stable in time, and that C_{chamb} alone could be descriptive of flux. It is therefore not possible to leave terms out of Equation 2.4 and arrive at reasonable approximations of flux

rate, unless C_{atm} were truly stable, which is unlikely. The results of these simulations show clearly that atmospheric CO_2 concentration measurement is as important as the measurement within the FD chamber itself.

The 3-D model runs shown in Figure 2.4 help inform us about real-world lateral diffusion impacts and associated errors. Consistent with the relationship between lateral diffusion and C_{chamb}-C_{atm}, this error was directly related to the difference between the diffusivity of the FD chamber and the diffusivity of the atmosphere. Low chamber diffusivity values resulted in high retention of CO_2 within the chamber. As a consequence, soil CO_2 moved around the chamber in favour of quicker moving soil-atmosphere flow paths. As the difference in the atmospheric and chamber diffusivities approached zero, so did the associated 3-D error. Due to the resolution of the Vaisala sensor, however, the chamber needs to maintain a super-ambient concentration and imposes a practical limit to how much of this error can be removed. As shown in Panel C of Figure 2.4, lateral diffusion error was almost a constant offset under a wide range of real-world conditions, with <1% variation in error at common soil gas diffusivities equal to or lower than 10^{-7} m^2s^{-1}. Soil gas diffusivities and collar length were proportionately less important. Owing to compaction and the presence of moisture, soils have diffusivity values that are 10^{-7} m^2s^{-1} or lower, especially at temperate sites (Risk et al., 2008b) so that in most field settings, diffusivity should be a small determinant of error. In the case of very highly diffusive free atmospheres (high winds, thin boundary layers), the technique is still valid but more error is incurred with increasingly diffusive atmospheres, as shown in Panel D of Figure 2.4. Panel D can also be extrapolated to consider subnivean environment or environments of lower free-atmospheric diffusivity, where the FD chamber will read values that are slightly *higher* than the true flux. The explanatory mechanism is the channeling of gases through the chamber, whose diffusivity is now higher than the surrounding environment. This is inverse to the normal pattern of lateral diffusion, where CO_2 flows outwards around the chamber. The subnivean error will be enhanced as snow diffusivities are reduced below faster equivalent to CO_2 free air diffusivity ($1.6x10^{-5}$ m^2s^{-1}) but is still small overall. Typical snow diffusivities are in the 10^{-6} m^2s^{-1} range (Winston et al., 1995), where a FD chamber will read several percent above true flux. As the snowpack evolves and grains sinter, the snow diffusivity and

the lateral diffusion footprint will change. Luckily these effects are still relatively small, and a reasonable tradeoff for generating data in this difficult environment. It should be noted that in sub-snow environments, FD sensors must tolerate higher CO_2 concentrations that will be present under snow.

2.5.2 Flux Generator Trials

Figure 2.5 shows typical 1-D and 3-D flux generator runs across different flux ranges. Linearity of the technique was excellent across the tested range, and a singular G value adequately describes the proportionality between C_{soil}-C_{atm} and generator flux. The 3-D flux generator runs also fell along the same 1:1 line, indicating that no appreciable 3-D diffusion had taken place. In almost all cases the error correspondence between flux generator and the FD chamber fell within the 2% error of the Vaisala concentration sensors. Confirming the results of numerical modelling, soil gas diffusivities did not significantly affect the correspondence between flux generator and FD chamber values (not shown).

2.5.3 Comparative Mesocosm Experiment

As shown in Figure 2.6, the Li-Cor LI-8100 and the FD chamber showed excellent correspondence over the measurement period, and linear regression yielded an R^2 of 0.901. Both FD and the Li-Cor were subject to random electrical or measurement noise, which accounted for much of the variation between the two sets of measurements. To confirm that the empirically (Li-Cor) derived G did not significantly influence the results of the experiment, the G was re-calculated using five different subsets of data from the experiment: 6 and 24 hour subsets, from both the start and end of the 10 day experiment; and by one-time correspondence between the readings at a single point randomly selected near the middle of the experiment. In all cases the G value varied slightly, but the variation was not enough to be noticeable on plots and was well within the error of the instruments and methodologies involved (Vaisala 222s at $\sim$3%; Li-Cor concentration and regression error at $\sim$2%). In all cases the regressions were linear, and with similar R^2. This confirms that the measurement of variability of FD chambers does not differ from the Li-Cor, and suggests that, within

measurement error of both instruments the FD chambers and the Li-8100 were linearly related, captured the same signal, and measured fluxes equally well under these conditions.

2.5.4 Field Deployments

Figure 2.7 shows portions of characteristic data from Woods Harbour, Nova Scotia for summer, soil frost, and old snow periods. In each case, fluxes and concentrations are shown for two FD chambers spaced 30 cm apart. Wide swings in lower boundary layer CO_2 concentrations obviously drove temporal variability in fluxes (particularly in summer), reinforcing the need for an atmospheric reference sensor to give accurate readings. While fresh snow seemed uniformly diffusive and presented little problem, aging, compact, and wet snowpacks (Panel C) appeared to have characteristically high micro-spatial variability which caused adjacent FD chambers to diverge in flux, and FD chamber concentrations fell on either side of the (subnivean) atmospheric reference concentration. This high spatial variability has been observed in other studies, for example by Winston et al. (1995). While a remote atmospheric reference is normally sufficient in the well-mixed free atmosphere, a FD chamber-mounted reference would be more suitable in theses poorly-mixed subnivean environments.

The magnitude of boundary variability in C_{atm} concentrations shown in figure 2.7 is striking. These temporal variations do not undermine the FD technique because the associated atmospheric reference probe measures C_{atm} continually. However, uneven vertical positioning of these reference chambers (such as placing the chamber in/on a hollow/hump) can lead to small deviations in the measured values. Sitting on a hump, a reference chamber would measure a lower C_{atm} value, corresponding to the boundary layer concentration decay in the upward direction. A lower C_{atm} value would increase the C_{chamb}-C_{atm} difference, and consequently the flux. The opposite would be true of a reference sensor placed in a small hollow relative to its C_{chamb} pair.

To explore this spatial boundary-layer related error, data from the North Mountain field site were used, where in conjunction to FD long-term testing, atmospheric boundary layer CO_2 concentrations were measured at 50 cm increments between 0 cm (soil surface) and 200 cm with Vaisala 222 sensors. Taking a daytime and nighttime boundary layer concentration profile from early in September 2010, concentrations

were regressed against height. The best fit relationship followed a power law, which is consistent with typical wind profiles and atmospheric mixing processes cited in other studies (Hsu et al., 1994). These relations were used to infer C_{atm} as a function of height, and re-calculated the flux values based on the new C_{chamb}-C_{atm} difference. Table 4 shows results from this analysis. In this table, F_{actual} represents the observed data for a FD chamber and immediately adjacent FD atmospheric reference chamber. If the reference C_{atm} probe were moved upwards by +2.5 cm, the measured C_{atm} would see lower concentrations and higher apparent fluxes owing to larger C_{chamb}-C_{atm} difference. The potential consequences of a misplaced reference FD chamber are clearly large, particularly in hump and hollow topography that is characteristic of temperate forests. Both the mean and amplitude of data will be affected. A simple offset or multiplier cannot be used to correct the data, because the boundary layer decay exponent varies in time. This source of error can be averted by proper sensor placement on the landscape. To avoid this issue altogether, new FD prototypes may integrate both C_{chamb} and C_{atm} sensors into a single instrument, which will no doubt become more affordable as new sensors come to market. Overall, rapid concentration change with height in the surface boundary layer is a potential issue for both FD and normal dynamic chambers. It is also a non-trivial issue for static chambers, where concentration at t=0 must be representative of the soil surface boundary layer, as opposed to knee height, which might be more typical of a survey instrument being carried between collars.

Figure 2.8 shows results of a typical spatial survey with Li-Cor LI-8100 and existing FD chambers at the Highland site where hump and hollow topography is characteristic. During the time it took to conduct the Li-Cor survey, the FD chambers onsite read between 2.0 and 2.5 μmol/m^2/s, and the Li-Cor value in close proximity (30 cm) to the FD chambers matched up well in magnitude (2.38 μmol/m^2/s). Data of this nature is, however, relatively qualitative because it is impossible to make accurate comparisons between instruments where both temporal and spatial variability are so characteristically high.

Due to membrane degradation via UV radiation, particle abrasion, or biofouling, it is likely that G will drift through time as a function of environmental conditions. However, the hydrophobic UV stabilized 1460CL Tyvek was surprisingly durable, and

during the course of these lab studies no measurable drift was found in retesting even after 4 months. Initial local field experience suggests that G is very stable over time periods of at least several months. Once a full one-year period has elapsed, the existing housings will be brought into the laboratory to re-determine their G value. A better procedure for assessing drift or re-calibration interval would be to conduct a suite of laboratory experiments, where membranes could be artificially aged by sandblasting, microbial culturing, etc. Once drift rates are known, it will be possible to define recalibration intervals, which would involve replacement of the diffusive membrane portion of the dynamic chamber with new (and recently calibrated) parts. Given the low membrane material cost, regular replacement is a feasible and prudent option, with readily available calibration equipment. The optimal membrane replacement intervals are estimated to range from several months to one year, depending on environment. Additionally, louvres or other physical protection could be designed to extend membrane lifetimes in very harsh environments.

Power consumption at the field sites was manageably low, at roughly 1 watt per hour total for one FD chamber and one atmospheric reference chamber measuring at half-hourly intervals. This compares very favourably to a continuously operating Li-Cor, which consumes about 15 watts per hour and is comparatively difficult to sustain off-grid. The data loss rate during the 8 month deployment was only $\sim$1%, usually due to temporary power loss after five or more successive days of fog. Opportunities are evident to further reduce power consumption using logic sequences to toggle the Vaisala optics heaters, or by reducing the duty cycle with a move towards CO_2 sensors with faster warmup times. It is likely that more power-thrifty and/or faster warmup sensors will reach the market in the coming years, potentially in a miniaturized form which would allow for fast warmup and for each FD chamber to have an on-board reference. If sensors could be found that would reach warm-up in 1 minute or less, power consumption could be reduced by a factor of ten or more.

2.6 Conclusions

Overall, the passive FD chamber technique is promising in both benchmarking and head-to-head tests relative to a Li-Cor LI-8100. The technique performs much as a typical dynamic chamber, and no significant new operational constraints were

identified during this study. Numerical modelling helped identify that diffusive through-flow potential (G) of the FD chamber (equivalent to pump volumetric flow in the traditional dynamic chamber method) was the most important operational parameter for measuring accurate efflux values.

Given the various field and laboratory tests described here, and the extensive 3-D modelling, the FD technique is perhaps better characterized than many existing chambers (static or dynamic). It is shown that the technique is theoretically valid and, not surprisingly, very similar to regular dynamic chambers which have been in use for many decades.

While accuracy and precision of FD dynamic chambers appear to be comparable to other techniques, the passive design offers the advantage of significantly reduced power consumption. FD chambers offer other potential advantages including simplified calibration (G is the only configurable/calibrated operational parameter), and flexibility as the technique can be extended to work with clear or opaque chambers, or adapted for use with other soil gases of interest. FD chambers are robust enough for further usage in field studies, but further FD empirical testing is probably justified in four areas: 1) to investigate potential venting/pressure considerations and examine whether additional compensatory vents are required ; 2) to define re-calibration intervals; 3) to establish fast and repeatable rapid-calibration devices for FD housings, and 4) to document performance and survivability in additional subnivean field studies and harsh environments.

Overall, the FD chamber technique is promising, and offers new possibilities to researchers in soil carbon cycle research.

Table 2.1: Range of simulations performed using the 3-D model, to assess error (observed flux / true flux) as a function of operational parameters. Changes in atmospheric diffusivity are meant to simulate non-diffusive surface boundary layer environments. This analysis was also performed for a range of accepted traditional static and dynamic efflux chambers, where FD fell in the middle of the pack. Results for the full comparative study will be documented in a separate manuscript.

Parameter	Range of Values	Increments
Collar length	0-20 cm	5
Diffusivity of FD chamber (D_{FD})	0.2-1 fractions of atmospheric D	5
Diffusivity of soil (D_s)	1x10^{-9} -1x10^{-5} m^{2}s^{-1}	5
Diffusivity of atmosphere (D_{atm})	1x10^{-5} -1x10^{-3} m^{2}s^{-1}	5

Table 2.2: Increase in C_{chamb}-C_{atm} for steady state chambers used in other studies. Although geometries are also a consideration, progressively larger values of C_{chamb}-C_{atm} indicate that larger chambers have a greater likelihood of inducing feedbacks in the soil, which result in lateral diffusion and under-reporting of flux.

Study	Area (m^2)	Volume (m^3)	Pump Rate (litres min^{-1})	Elevated CO_2 (ppm per 1 μmol $m^{-2}s^{-1}$)
FD (this study)	0.0020	0.0137	-	26-45
Gamnitzer et al. 2009	0.8300	0.6600	1.6000	694
Camarada et al. 2009	0.0314	0.0031	1.0000	42
Rochette et al. 1997	1.3273	0.2655	-	97
Bain et al., 2005	0.0500	0.0050	0.5000	134
Rayment and Jarvis, 1997	0.0616	0.0092	1.0000	82
Subke, 2002	0.0314	0.0025	1.0000	42
Kutch et al., 2001	0.0200	0.0028	1.0000	27

Table 2.3: Properties of the FD instrument used in the flux generator tests, with a Vaisala GMP 343 (0-2000 ppm) as the base sensor and a membrane arrangement that retains ∼26 ppm per 1 μmol $m^{-2}s^{-1}$ flux, depending on housing. Power consumption is estimated for hourly data collection, where the sensor is active for 15 minutes of every hour for warmup and measurement. For comparison, Li-Cor LI-8100 power consumption specification is ∼285 Watts/day. Accuracy and precision values for Li-Cor and similar instruments will vary, depending on user configuration.

Parameter	Value
Accuracy - Vaisala GMP343	2%
Precision - Vaisala GMP343	0.1 ppm
Accuracy - FD	2%
Precision - FD	0.0038 μmol $m^{-2}s^{-1}$
FD range	0-60 μmol $m^{-2}s^{-1}$
FD + FD_{ref} power consumption (25% duty)	10.8 Watts/day

Table 2.4: Analysis to identify the consequences of moving the atmospheric probe up and down in the surface boundary layer, using data from the Highland site where atmospheric boundary layer concentrations are measured continually in the first 200 cm of the atmosphere. One overnight and daytime period are shown.

Date	Sept 3 2010, 0200h	Sept 4, 2010, 1400h
Fit, z=0-100 cm	C_{atm}=568.49$z^{-0.093}$	C_{atm}=403.25$z^{-0.061}$
Fit R^2	0.96	0.94
C_{atm} z=sensor	489	366
C_{atm} z=-2.5 cm	522	381
C_{atm} z=+2.5 cm	471	357
C_{atm} z=+10 cm	442	342
F_{actual} z=sensor	5.30	3.90
F_{meas} z=-2.5 cm	4.00	3.27
F_{meas} z=+2.5 cm	6.02	4.26
F_{meas} z=+10 cm	7.40	4.85
F_{meas}/F_{actual} z=-2.5 cm	0.75	0.84
F_{meas}/F_{actual} z=+2.5 cm	1.14	1.09
F_{meas}/F_{actual} z=+10 cm	1.36	1.24

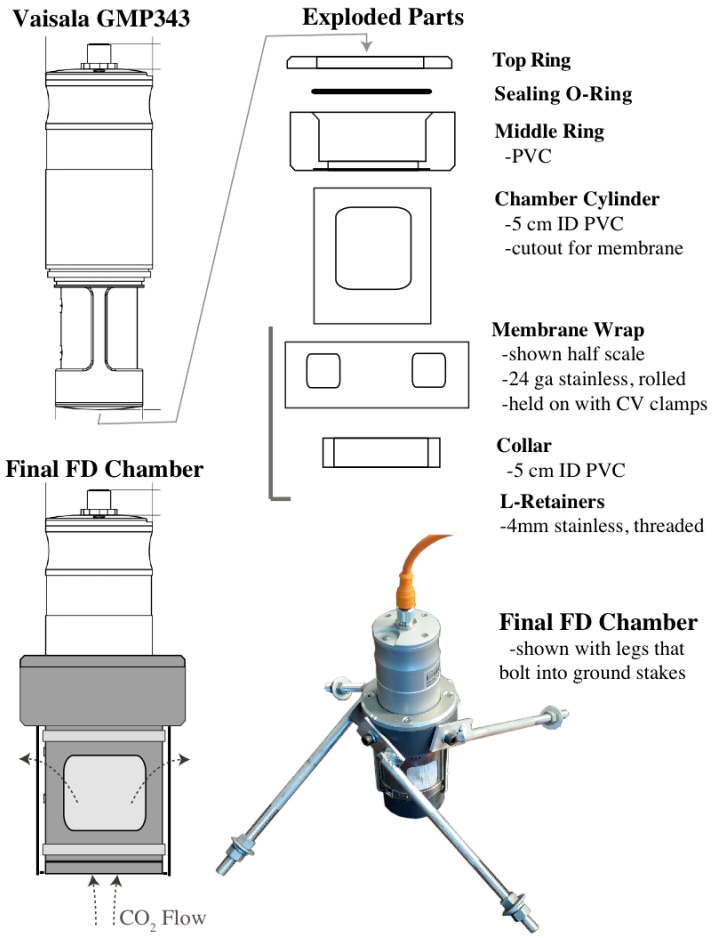

Figure 2.1: Schematic of Forced Diffusion Flux chambers tested in this study. Membranes not shown in exploded view. Reference (C_{atm}) setup is identical except that a thick impermeable rubber gasket is situated between the collar and cylinder in place of the usual Tyvek membrane. The typical G for the embodiment drawn here is $\sim$0.03886 $\pm$0.00364 owing to small differences in membranes, machining and assembly tolerances, etc.

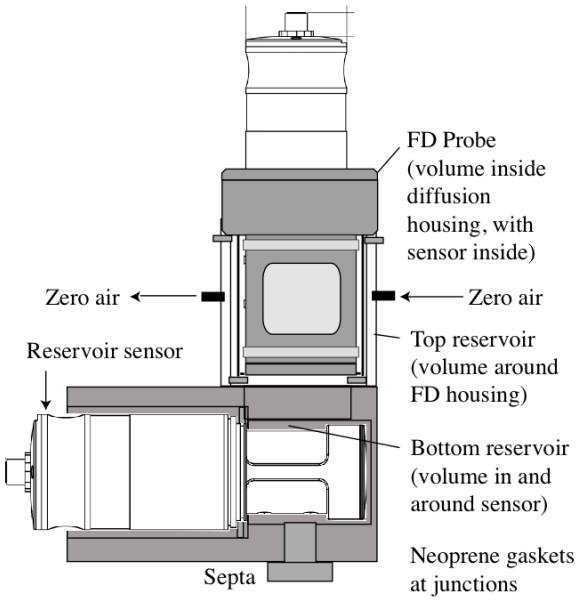

Figure 2.2: One-dimensional miniature flux generator device used for benchmarking in 1-D, and calibration of FD housings. The cavity around the FD housing is purged continually with N_2 at a flow rate of >200 sccm which is sufficient to minimize internal buildup of exhausting CO_2.

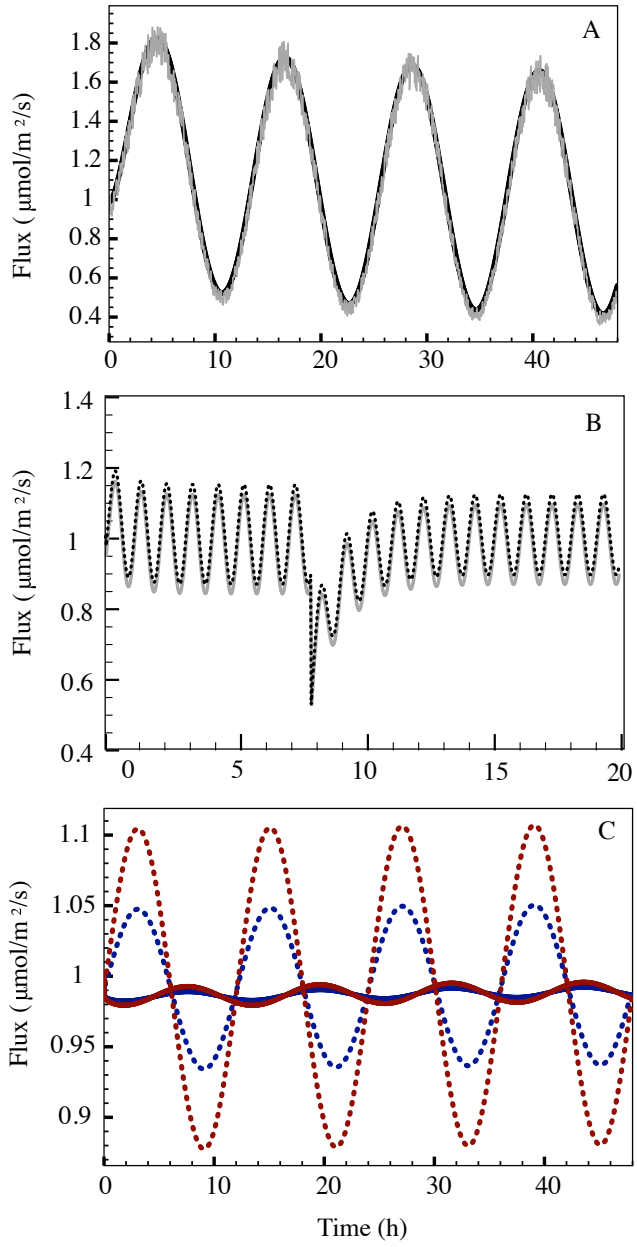

Figure 2.3: 1-D numerical model results. Panel A shows the sensitivity to concentration error, shown with 5% random error added to concentration data. Panel B shows true (black) and measured (grey) fluxes following a simulated step change in moisture, which causes a decreases in soil pore space and diffusivity of 0.05 $^{v}/_{v}$ and 8.26x10^{-7} m^{2}s^{s-1}, respectively. Panel C shows a FD chamber with and without atmospheric compensation in a time-variant atmosphere. The solid lines show two simulated atmospherically-corrected fluxes varying on 12 hour timescale, with slightly different amplitudes. The dotted lines represent the same timeseries without atmospheric correction. In both cases, the atmosphere is experiencing sinusoidal variation of ±75 ppm with the same 12hour period but a small temporal offset.

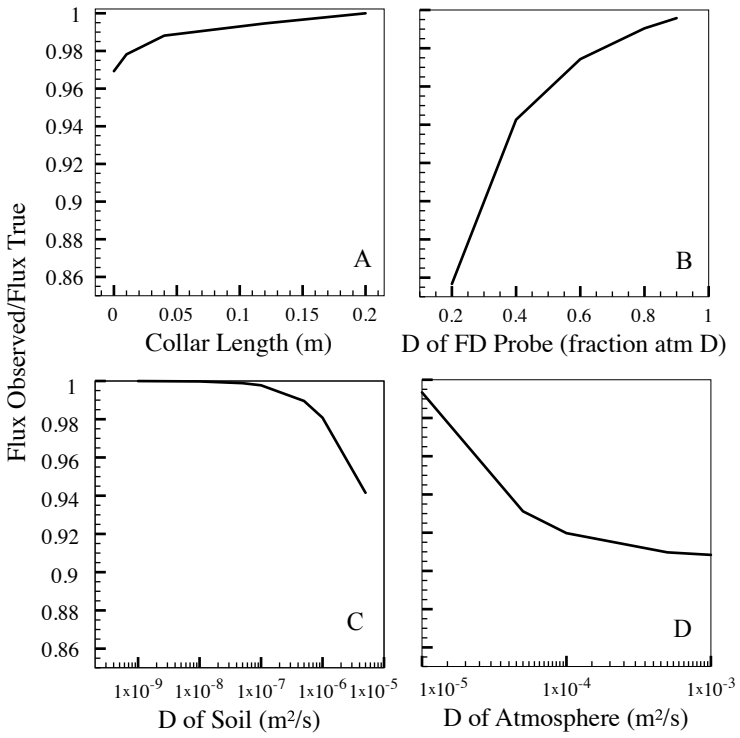

Figure 2.4: 3-D Numerical modeled flux error as a function of configurations and environments. These 3-D simulations allow lateral diffusion, and the FD technique is prone to small degrees of under-measurement of flux, particularly if the FD chamber has a very low diffusivity (D). Preliminary modelling of other instrument configurations (static chambers, dynamic chambers) suggests that these sensitivities should not be considered as unique to the FD technique.

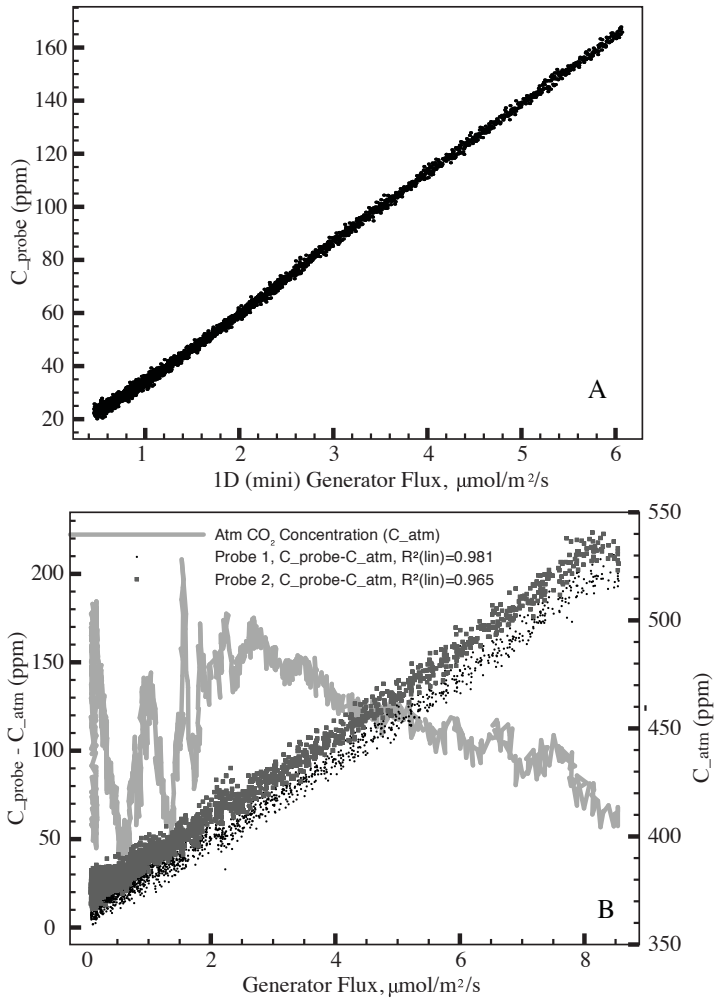

Figure 2.5: Panel A shows a 45-minute flux generator run using the miniature 1-D device. Concentrations in the FD chamber are plotted here against flux, showing the characteristically linear relationship. Deviations from linearity are most likely due to behaviour of Vaisala 343 sensors, as model data cannot reproduce this effect. Panel B shows one flux generator calibration run (24 hours long, 10 to 0.5 μmol/m^{2}s^{-1}) with two Vaisala 343-based FD soil FD chambers (C_{chamb}), and one Vaisala 343-based atmospheric FD chamber (C_{atm}) deployed on the synthetic soil surface in which lateral diffusion is allowed to take place. The C_{chamb}-C_{atm} difference and (G) is again linear despite widely variant C_{atm} values. Both panels show results which are typical of many dozen similar runs that have been performed to date.

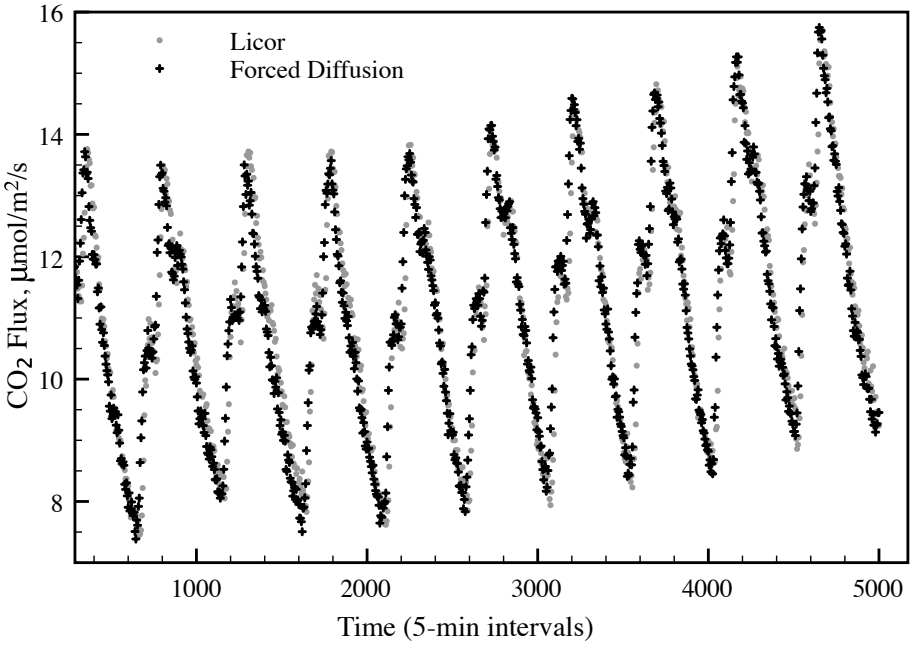

Figure 2.6: Comparison of a GMM-222 based FD FD chamber and a Li-Cor-8100 automated chamber, on mesocosm soils undergoing temperature change forced by heating cables controlled by a datalogger. Both instruments show very similar response over time, and linear regression yields an R^2 value of 0.901.

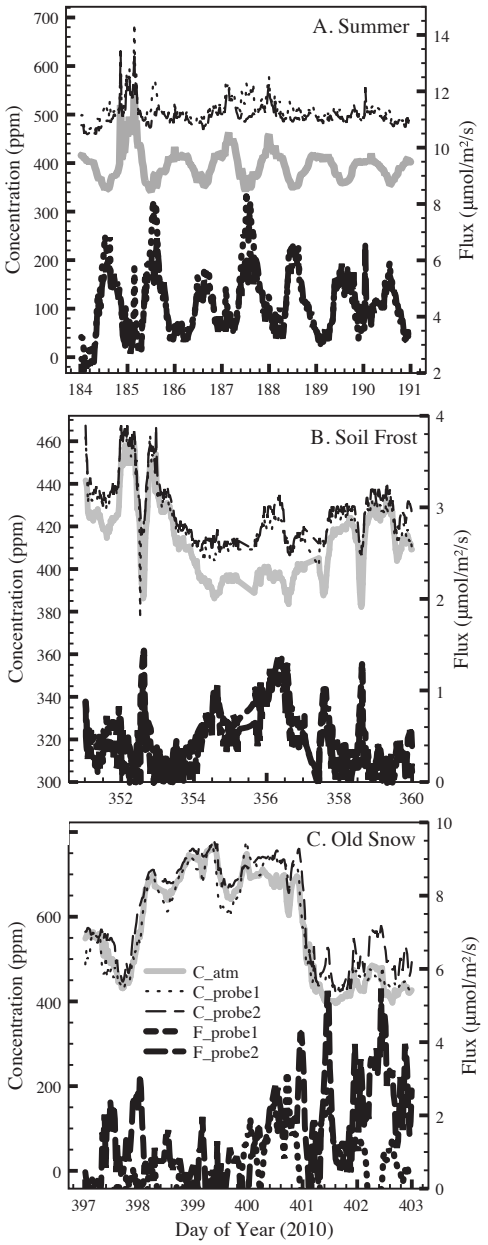

Figure 2.7: Field data from Woods Harbour, Nova Scotia, showing characteristic data for summer, soil frost, and old snow periods. In each case, fluxes and concentrations are shown for two FD chambers spaced 30 cm apart. The legend for all plots is shown in Panel C. Wide swings in lower boundary layer CO_2 concentrations obviously drive temporal variability in fluxes (particular in summer), which reinforces the need for an atmospheric reference sensor for accuracy.

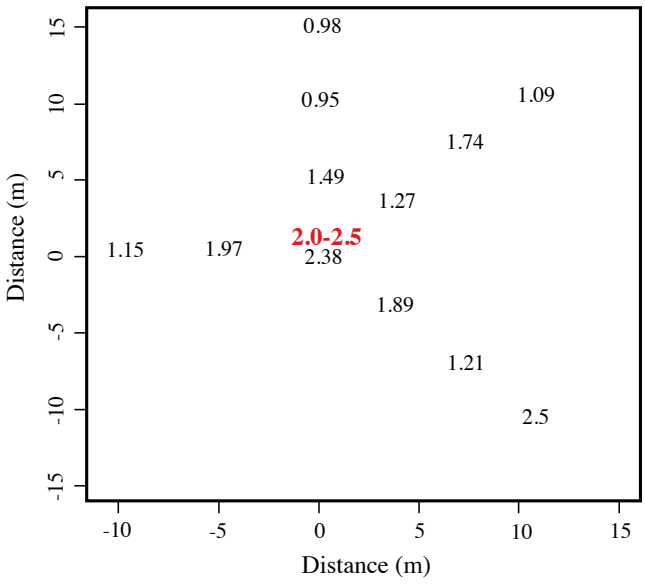

Figure 2.8: Example of spatial survey with Li-Cor LI-8100 and existing FD chambers, at the North Mountain site. During the time it took to conduct the Li-Cor survey, the FD chambers onsite were reading between 2.0 and 2.5 μmol/m^2/s, and the Li-Cor value in close proximity (30 cm) to the FD chambers matched up well in magnitude (2.38 μmol/m^2/s).

Chapter 3

Iso-FD: A Novel Method for Measuring the Isotopic Signature of Soil Flux

3.1 Preamble

This chapter describes the adaption of the FD technique, presented in Chapter 2, to the measurement of the isotopic composition of soil flux. Authorship on this manuscript is as follows: Nick Nickerson, Jocelyn Egan and Dave Risk. I was the principal investigator in this research and handled all of the writing, theory, and numerical modelling and also helped to perform the lab and field experiments with Jocelyn Egan. Dave Risk supervised this project. A version of this manuscript has been published in Soil Biology and Biochemistry in July, 2013 (Volume 62). Copyright permission for this publication can be found in Appendix E.

3.2 Abstract

Stable carbon isotopes have become a critical and often used tool in understanding ecological and physical processes affecting gas production and emissions in soil. While the insights gained using chamber based flux methods have been significant, it is known now that many of these chamber methods have an inherent bias that complicates the interpretation of their measurements. Here a new chamber method is presented that uses diffusive membranes to control CO_2 flow into and out of the chamber, and can measure the isotopic composition of soil flux without inducing a bias. Results from numerical modelling are presented, followed by laboratory calibration and field measurements using this new method coupled to a Cavity Ring Down Spectrometer (CRDS). Simulations, as well was lab and field results showed that the method is both robust over a range of environmental conditions and can be unbiased, unlike other chamber approaches. Finally, possibilities for future improvements and variations on the measurement approaches are discussed.

3.3 Introduction

Over the past two decades, the measurement of stable carbon (C) isotopes has become a critical tool in elucidating the biological and environmental controls on many of the pathways by which CO_2 can be produced and emitted from the soil (Ekblad and Högberg, 2001; Formanek and Ambus, 2004; Maseyk et al., 2009; Subke et al., 2009; Phillips et al., 2010). While field and laboratory work continues to advance the understanding of the biology, chemistry and physics of soil CO_2 processes, researchers are likely still overlooking or misinterpreting potentially critical scientific results from isotopic data due to methodological biases (Phillips et al., 2010; Nickerson and Risk, 2009b,c; Ohlsson, 2010; Gamnitzer et al., 2011).

Specifically, when measuring soil CO_2 efflux and its stable C isotopic signature, chamber methods such as static or dynamic chambers, may drive a potentially large bias because of non-steady state diffusion processes (Nickerson and Risk, 2009c). More importantly, these biases are likely to co-vary with environmental conditions (Nickerson and Risk, 2009c; Phillips et al., 2010), thereby confounding the interpretation of results further. These methodological biases have been documented and some solutions have been offered, such as modification of the historical chamber designs (Ohlsson, 2010) to minimize the bias and model fitting of chamber data to remove bias artifacts (Nickerson and Risk, 2009c; Gamnitzer et al., 2011). Although each of these approaches is likely to offer more reliable data, the ideal scenario would be to develop a new method of measurement that does not inherently have a bias.

Here, a steady-state method called Forced Diffusion (FD) (Risk et al., 2011), which is functionally similar to open chamber systems, was modified so that it could be used for measurement of isotopic fluxes. The hypothesis was that the steady state diffusion based chamber design should eliminate biases that are present in other chamber systems. The basic theory of the method is presented, as well as numerical modelling which helped us ensure that the method is theoretically robust under a host of diffusive conditions. FD chambers were then modified for use as Isotopic Forced Diffusion (Iso-FD) chambers, coupling them to the Picarro G1101-*i* Cavity Ring Down Spectrometer for measurements of CO_2 concentrations and isotopic signatures. The chamber design was tested against soil gas derived measurements of isotopic flux in the lab to validate the method and was subsequently deployed under field conditions

in a $\sim$ 20 year old Red Pine stand for comparison against the subsurface Keeling plot (see Appendix D2 for an expanded definition of the Keeling Plot) and gradient approaches.

3.4 Methods

3.4.1 Iso-FD Theory

Isotopic Forced Diffusion (Iso-FD) chambers are an isotopic variant of Forced Diffusion (FD) chambers presented in Risk et al. (2011). The chamber design is a logical extension of the typical dynamic chamber design (Rayment and Jarvis, 1997), except the outflow of accumulated soil gases is regulated by a diffusive membrane rather than mass flow. The chambers used in this study consist of a membrane-covered inlet in contact with the soil surface, and membrane covered outlets in contact with the surrounding atmosphere. For the FD chambers, the mass balance for bulk CO_2 measurements is:

$$V\frac{\delta C}{\delta t} = A_s F_{in} - A_a F_{out} \tag{3.1}$$

where V is the chamber volume, C is concentration, t is time, A_s is the area of the membrane in contact with the soil surface and A_a is the area of the membrane in contact with the atmosphere, F_{out} of the chamber can be thought of as the diffusive gradient across the membrane from the concentration in the chamber *C(t)* to the concentration in the atmosphere C_{atm}, which is dependent on both the path length of diffusion (L) and the diffusivity of the membrane material (D), as per Fick's Law. With these substitutions for F_{out}, the equation can be modified to:

$$V\frac{\delta C}{\delta t} = A_s F_{in} - A_a \frac{D}{L}\left(C(t) - C_{atm}\right) \tag{3.2}$$

Making the assumption of steady state diffusion through the chamber Equation 3.2 is reduced to:

$$F_{in} = \frac{A_a}{A_s}\frac{D}{L}\left(C_{FD} - C_{atm}\right) \tag{3.3}$$

Equation 3.3 describes the soil flux, where the atmospheric CO_2 concentration, C_{atm} is subtracted from the CO_2 concentration in the chamber, C_{FD}. Due to the natural variability in C_{atm}, it must also be monitored closely to avoid error in the final solution. To do this a separate, similarly designed chamber with a non-permeable bottom is

used to prevent soil gas from entering. This dummy chamber allows us to closely monitor changes in C_{atm} and correct for them in the final flux calculations.

In the case of isotopic flux, each of the carbon isotopologues of CO_2 can be treated as separate diffusing gases (Cerling et al., 1991), allowing us to write similar equations for both $^{12}CO_2$ and $^{13}CO_2$. By taking the ratio of the fluxes of each isotopologue the isotopic composition of soil flux is gained:

$$\frac{F_{in}^{^{13}C}}{F_{in}^{^{12}C}} = \frac{\frac{A_s}{A_a}\frac{D^{^{13}C}}{L}\left(C_{FD}^{^{13}C} - C_{atm}^{^{13}C}\right)}{\frac{A_s}{A_a}\frac{D^{^{12}C}}{L}\left(C_{FD}^{^{12}C} - C_{atm}^{^{12}C}\right)} \tag{3.4}$$

which can be simplified based on the understanding that 1) the area variables will cancel because the same chamber is used for each isotope, and 2) the path length (L) and diffusivity will reduce to the reciprocal of diffusion fractionation (1.0044) yielding the final Iso-FD solution:

$$\frac{F_{in}^{^{13}C}}{F_{in}^{^{12}C}} = \frac{1}{1.0044}\frac{\left(C_{FD}^{^{13}C} - C_{atm}^{^{13}C}\right)}{\left(C_{FD}^{^{12}C} - C_{atm}^{^{12}C}\right)} \tag{3.5}$$

Equation 3.5, of course, can be converted to del-notation for more convenient use.

3.4.2 Numerical Modelling

To ensure that the Iso-FD chambers do not suffer from any of the lateral diffusion artifacts present in other chamber systems they were modeled using a three-dimensional soil-atmosphere-chamber model, similar to the one used in Nickerson and Risk (2009b) and Nickerson and Risk (2009c). This new model (Creelman et al., 2013) has cubic grid geometry, making it more flexible to use both for varying soil properties and varying chamber sizes and geometries. In brief, the model transports gas between its six nearest-neighbour cells using Fick's Law:

$$F_{1,2} = -D_{1,2}\frac{\Delta C_{1,2}}{\Delta\left(i,j,k\right)_{1,2}} \tag{3.6}$$

where F is the flux between cells, $D_{1,2}$ is the intercell diffusivity constant, ΔC is the difference in the cell gas concentrations and Δ(i,j,k) is the three-dimensional difference in cell positions. After each time step, the concentrations in each cell are re-calculated taking into account relevant fluxes during the last time step. The model is modified from bulk CO_2 to modelling CO_2 isotopologues by the same process described in

Nickerson and Risk (2009b) Nickerson and Risk (2009b) and Nickerson and Risk (2009c) Nickerson and Risk (2009c). Previous work has shown that soil diffusivity, gas production rate and chamber collar depth to exert the most control over the bias caused by lateral diffusion. To this end steady state chamber concentrations and isotopic signatures were simulated for diffusivities and production rates spanning three orders of magnitude (D_{soil}: 1×10^{-8} - 5×10^{-6} m^2 s^{-1}; Production (P): 0.1 - 10 μmol m^{-2} s^{-1}) and collar lengths (ξ) from 0-8 cm long. A range of values (D: 1×10^{-7} - 5×10^{-6} m^2 s^{-1}) for the diffusivity of the Iso-FD chamber membrane (D term in Equation 3.3) were also simulated to examine the effect on the resulting isotopic flux estimates. The modeled and actual chamber had similar surface areas (Modeled: A_a=A_s=16 cm^2; Actual: A_a=20 cm^2, A_s=19 cm^2) although the volume of the modeled system was about half for computational reasons (Modeled: V=64 cm^3; Actual: V= 133 cm^3); however, this difference in V does not affect the final model results. For each combination of parameters (D_{soil}, P, ξ, D) the true isotopic flux of the modeled soil was compared to the flux estimated using the modeled Iso-FD chamber to estimate potential bias under the various conditions. The base model was also modified slightly to include a pump on the chamber, which draws air from the chamber for sampling and allows the same volume of air from the atmosphere above the chamber to enter and dilute the chamber concentration. This was a necessary model addition in order to test for pumping related biases in the case that the chamber air cannot be recirculated due to technical limitations, as is discussed in the following section.

3.4.3 Iso-FD Chamber Design & Isotopic Measurements

The Iso-FD chambers mirror the design of the Forced Diffusion (FD) chambers presented in Risk et al. (2011). The chambers are made from 5 cm internal diameter, 8 cm long sections of PVC tubing. On opposing sides of the PVC, two $\sim$ 10 cm^2 windows were cut to allow venting of gas to the atmosphere. The bottom (inlet) surface of the chamber, in contact with the soil, has an open surface area of $\sim$ 19 cm^2 while the top of the chamber is sealed with a PVC plug. Risk et al. (2011) Risk et al. (2011) provides detailed schematics and photos of the chamber design. For the Iso-FD chamber, the membrane material covering the inlet surface is a UV

resistant Tyvek (DuPont) and a Gore-Tex (W. L. Gore & Associates Inc., Newark, Delaware) membrane material covering the two opposing outlet surfaces. These two differing membranes (Diffusivity Tyvek > Diffusivity Gore-Tex) allow CO_2 to buildup to a sufficient concentration within the chamber so that isotopic measurements can be made with minimal error (discussed later). In theory, it is unnecessary to have a membrane on the inlet surface, as the diffusivity of CO_2 in free air is also greater than the diffusivity through the Gore-Tex membrane. However in practice the Tyvek bottom membrane helps exclude liquid water from the interior of the chamber as well as provides a barrier to potential mass flow from the soil pores into the chamber during sampling. Any mass flow events from the soil would violate the assumption of diffusive transport and thereby cause error in the Iso-FD estimates.

Isotopologue concentrations within the Iso-FD chamber are measured using a Cavity Ring Down Spectrometer (CRDS, Picarro G1101-*i*, Picarro Inc. Sunnyvale, California) connected to the top of the Iso-FD chamber via urethane tubing (Clippard Instrument Laboratory Inc., Cincinnati, Ohio). The chamber can operate in two different modes: 1) gas can be recirculated (or sampled in small quantities) to maintain the steady-state concentration within the chamber (as in Equation 3.2), or 2) gas can be drawn from the chamber with volume replacement via an atmospheric vent tube. Maintenance of pressure in the measurement cell of the Picarro G1101-*i* relies on a difference between inflow and outflow rates and because of this recirculation would cause undesired pressure changes in the Iso-FD chamber and likely lead to biased results because of chamber over/under pressurization. Air is instead drawn from the chamber and allow atmospheric air to flow in via a vent tube and replace air drawn by the G1101-*i* ($\sim$ 30 ml/min). This modifies the original mass balance equation (Eq. 3.2) to become:

$$V\frac{\delta C}{\delta t} = A_s F_{in} - A_a \frac{D}{L}\left(C(t) - C_{atm}\right) + \Gamma\left(C_{atm} - C(t)\right) \tag{3.7}$$

where Γ is the G1101-*i* pump draw rate (m^3/s). As a first-order estimate of the effect of pump draw and atmospheric air dilution on the final calculation of the isotopic flux Equation 3.6 is solved analytically assuming that F_{in} is constant. As the modeled chamber air is drawn by the G1101-*i* the concentration decays exponentially until it reaches an equilibrium value between the incoming atmospheric air and the soil flux through the diffusive portion chamber. Further analysis shows that for a fixed

total pumping time, regardless of whether the chamber reaches its new pump-driven equilibrium or not, the offset between the isotopic flux determined using the steady-state (recirculated) Iso-FD and the pump drawn Iso-FD is always a constant value regardless of the flux (F_{in}) rate or the isotopic signature of the flux. This estimated isotopic signature remains constant because, for a given constant pump rate, the same relative proportion of $^{12}CO_2$ and $^{13}CO_2$ is drawn from the chamber headspace. This allows us to determine a single offset value for a given chamber design and apply it to the Iso-FD solution (Eq. 3.5) to correct it for the pump effects. However, note that the analytical model assumption is that incoming flux (F_{in}) is constant during the pumping, which may not be the case in reality due to non-steady state effects. Because of this analytical model simplification, results are also presented using the numerical model, which further elucidate the relationship between pumping and potential biases and offsets.

3.4.4 Valving System

Picarros G1101-*i* CRDS analyzer is factory equipped with a single inlet port so in order to sample from multiple lines during experiments a custom valving system was constructed including eight two-way valves (EV-2M, Clippard Instrument Laboratory Inc., Cincinnati, Ohio) connected to a gas tight manifold. Two of these valves are dedicated to standard gases, while the other 6 were free to collect samples. The valves are fired using a Phidget Interface Kit 0/0/8 electronic relay (Phidgets Inc., Calgary, Alberta), which is connected to the Picarro G1101-*i* via a USB port and is commanded by a program written in Microsoft Visual Basic.

3.4.5 Lab Validation

To validate the Iso-FD technique in the lab custom built Flux Generator (FG) was used. The FG is functionally similar to that of Martin et al. (2004), using most of the same operational parameters and mass balance equations for calculating flux. Within the 234.23 L gas reservoir, a fan circulates injected gases at a fixed speed, mixing the whole volume in approximately 15 seconds. A 0.324 m^2 tray on top of the reservoir contains a homogenized soil of glass beads (22 cm deep, 50 % v/v $<$ 1mm diameter, 50 % v/v 1-4 mm diameter). Concentrations of CO_2 in the gas reservoir are

monitored continuously using a LiCor LI-820 infrared gas analyzer (IRGA). A four-port exhaust manifold and fan is situated over the tray to maintain the soil surface concentration near ambient levels, as described in Martin et al. (2004) Martin et al. (2004). A custom-designed LabVIEW interface and National Instruments Data Acquisition device automated the function of the FG (including CO_2 injections), performs calculations, and records data.

Within the FG glass bead soil two filtered sampling tubes were inserted, one near the top of the soil ($\sim$ 2-3 cm deep) and one near the bottom of the soil ($\sim$ 17-18 cm deep). These sampling tubes allow us to calculate the true isotopic flux leaving the FG instrument so that Iso-FD chambers can be calibrated for the pump offset and also to validate their ability to measure isotopic flux. Calculation of flux from these profile tubes uses the diffusion corrected two point Keeling plot approach, effectively the same as the atmospheric profile method used by Griffis et al. (2005) Griffis et al. (2005).

An Iso-FD chamber and a modified Iso-FD chamber for atmospheric measurement (bottom surface sealed) were situated on the surface of the glass bead soil. The two soil profile tubes, two chambers, two atmospheric tubes, and two standards were all sampled for 15 minutes duration ($\sim$ 450 mL of gas per sample) in the sequence shown in Figure 3.1, an example of the characteristic unprocessed data. The atmospheric (simply open to lab air) tubes were sampled between soil profile and chamber measurements to ensure the sampling pathway was purged of any residual gases from the previous measurements.

Laboratory trials of the Iso-FD method were performed by injecting CO_2 into the reservoir until the concentration reached 6000 ppm ($\sim$ 2L of pure CO_2 injected over 5-15 minutes), after which time the gas was allowed to diffuse freely through the glass bead soil and into the lab atmosphere. Each run lasted approximately 15 hours.

3.4.6 Field Trial

In September 2011, after lab validation, chambers were moved to a $\sim$ 20 year old plantation of Red Pine (*Pinus resinosa*) located in Heatherton, Nova Scotia (N 45° 33' 54", W 61° 46' 20"). Annual average rainfall for the region is 1100 mm/year with average monthly rainfalls in August of 92 mm and 101 mm in September. Annual

average temperature for the region is 7°C and average temperatures in August and September are 18.9 and 15.3, respectively.

For a period of approximately 3 days, the G1101-i was used to sample the two chambers as well was three horizontal soil gas well ($\sim$ 4,13,26 cm depth) that were installed at the site in May 2011. The gas well was constructed using 50 cm long sections of 1.3 cm inside diameter PVC tubing. Holes (1.0 cm diameter) were drilled on opposing sides along the length of the pipe at $\sim$ 4.5 cm intervals. The outsides of the wells were wrapped in Tyvek to exclude water from entering. A $\sim$ 10m long section of vinyl tubing ($\sim$ 3 mm inside diameter) was connected to the well via a barbed fitting to allow for sampling by the G1101-i.

Similar to the lab validation, the isotopic flux was calculated for the Iso-FD chambers (Equation 3.5) and compared them to the isotopic flux calculated via a subsurface Keeling plot approach. Two variants of the Keeling plot were used, the first uses the concentration and isotopic composition from shallowest subsurface gas well and the atmosphere to calculate the isotopic flux. The second includes concentrations and isotopic compositions from all three subsurface wells and the atmosphere. While the first, 2-point approach should give an estimate of the flux at the soil surface, the second 4-point approach offers a more integrated signal over the soil profile, in addition to being more statistically sound because of the increased number of points in the regression.

3.5 Results & Discussion

3.5.1 Numerical Simulations

Simulations of the Iso-FD technique under steady state conditions produced concentration and isotopic plumes directly below the chamber similar to those found using both static and dynamic chamber methods (Nickerson and Risk, 2009c), seen in Figure 3.2. However, in all simulations the predicted isotopic signature of flux using the Iso-FD method was very near the input value (Mean Deviation < 0.01‰) suggesting that while the concentrations and isotopic signatures in the subsurface change, leading to lateral diffusion, the soil to atmosphere diffusive isotopic flux remains stable during measurement despite the lateral diffusion impacts. This contrasts with the

results presented in Nickerson and Risk (2009c) Nickerson and Risk (2009c) regarding the functionally similar dynamic chamber method, which displayed significant error due to lateral diffusion. This non-biased quality of the Iso-FD method can be attributed to the diffusive (as opposed to advective for the typical dynamic chamber) nature of the exchange of CO_2 between the chamber and its surroundings. This allows the Iso-FD chamber to attain a new diffusive steady state during the measurement period that reflects the natural diffusive steady state and therefore allows the method to predict the true isotopic signature of flux, rather than a biased value as is recorded in the mass flow driven dynamic system.

The second set of simulations was performed to test the assumption of a constant offset under the second, pump-drawn, operational mode of the Iso-FD chamber. For a given Iso-FD membrane diffusivity, the pumping offsets (Figure 3.3) are relatively constant as the analytical solution (Eq. 3.6) predicted they should be. As soil diffusivity increases, the pump causes the offset to deviate due to non-steady state diffusion effects induced by the decrease in chamber concentration (Nickerson and Risk, 2009c). This soil diffusivity dependent deviation is strongest when the Iso-FD membrane has a low diffusivity and thus the concentration before pumping is highest and the change in concentration during pumping is highest. Note in Figure 3.3, that at very low membrane diffusivities the maximum pumping offset approaches the theoretical diffusive fractionation factor of 4.4 ‰. This end of the spectrum represents a chamber where most of the soil gas influx is being lost via pumping (advectively, with no fractionation) rather than across the Iso-FD diffusive membrane, so the chamber effectively becomes a standard dynamic chamber system (Rayment and Jarvis, 1997; Maseyk et al., 2009) with a small leak through the diffusive membrane. At the other end of the spectrum of membrane diffusivity, the chamber acts, as it theoretically should with no (or very little offset) and very little bias across the modeled soil diffusivity range. In this case the membrane diffusivity is much larger than the pump speed and the majority of the CO_2 flux is exiting the chamber diffusively.

3.5.2 Lab Validation

As was mentioned previously, two separate laboratory trials of the Iso-FD method were performed. Figure 3.4a shows the observed decay in $^{12}CO_2$ concentrations in

the glass bead soil, as measured by the soil profile tubes. To the right, in Figure 3.4b is the trajectory of soil profile isotopic composition during the same time period. Figure 3.4c shows the concurrent changes in the Iso-FD and atmospheric chamber $^{12}CO_2$ concentrations, with the isotopic signature of both chambers shown in Figure 3.4d.

Good correlation was observed between the true isotopic flux, calculated using the soil profile tubes, and the Iso-FD measured isotopic flux values, presented in Figure 3.5. Linear regression results yielded a slope of 0.956 (S.E.=0.0575) and y-intercept of -1.958 (S.E.=1.848) with an r^2 value of 0.9322. This suggests that the desired offset for this particular Iso-FD chamber design (and measurement length) is 1.958‰, however the regression standard error is quite high leading to a large amount of uncertainty in the estimate. This large spread in the potential intercept value (-3.806 to -0.110) is due in part to the variability in the data and the large distance to extrapolate the curve to the y-axis. This may be constrained better in future calibrations by using injection gases with several different isotopic signatures (around 0 ‰ or heavier), although since the offset value is constant through time for the same pump rate it will not affect the isotopic variability measured by the Iso-FD approach. Offset values calculated from individual data points average to 0.54 ‰ (S.E. = 0.14 ‰), which is likely a more reliable estimate than the extrapolated value from the regression. In both cases the experimental calculated offset is in the same direction as is predicted by the model, where the value observed in the Iso-FD has a consistently lighter isotopic signature than the true flux. Based on the results from the 3D modelling, these offset values suggest that the membrane has a modeled diffusivity on the order of 10^{-6} or 10^{-5}, suggesting that the pump offset over a full range of soil diffusivity may vary by $\sim$ 0.2-1.2 ‰ because of lateral diffusion effects (see Figure 3.3).

One of the main concerns when using pumps in chamber systems is the possibility for pressure driven advection to either limit or increase the flux of gases (Rayment and Jarvis, 1997). This is of particular concern when dealing with isotopes, as the type of transport (i.e. advective or diffusive) determines the transport fractionation and thus affects the isotope measurement. These laboratory trials were performed on a media (glass beads) that have both high diffusivity and permeability making

them particularly prone to advective biases. Despite this, no evidence of advection was apparent in the data, with all of the data collected during these two days falling on the diffusive mixing line for CO_2 stable isotopes. The lack of advection artifacts in this high-permeability system, suggests that it would be unlikely to see them in the field, however this assumption needs to be confirmed.

3.5.3 Field Trial

During the field trial, data from the Iso-FD tracked well with data from both the two-point and multi-point subsurface Keeling plots, shown in Figure 3.6. In most cases, departures from the relatively stable Iso-FD signatures (for example around day 265) are well correlated with sudden increases in CO_2 flux, as measured by a LiCOR LI-8100 located near the Iso-FD chamber (data not shown). It is also important to consider here, that the subsurface methods are measuring a more stable, time-integrated (because of diffusive processes) signal and therefore deviations seen in the Iso-FD data may in fact be high frequency changes in soil gas physics or microbial/root processes near the surface which do no last for a sufficient period of time to express themselves in the soil gas concentrations at depth (i.e. wind speed variation, rapid fluctuations in surface temperature). Additionally, note that the systematic difference in the two-point and multi-point subsurface data is likely due to a varying isotopic source signature with respect to depth, which could be a result of varying soil organic matter quality or rooting density variations. These field data are not shifted to take into account the offset caused by drawing air from the chamber, largely because of the uncertainty associated with the offset calculated during the Flux Generator testing. Assuming, however, the offset is similar to the estimated 0.54 ‰ the isotopic signature measured by the probes would fall between the root respired isotopic composition from the site (-27 ‰ $\pm$ 1.6 ‰, unpublished incubation data) and the fluxes measured using the subsurface Keeling plot which will tend to be biased toward deeper soil respiration rather than the very near surface where the bulk of the fine root mass is at this site ($\sim$ 60 % of fine root mass within the first 15 cm of soil is in the top 0-5 cm depth increment).

3.5.4 Uncertainty Analysis

While standard uncertainty analyses were used in the text while presenting the results, here the effect of methodological uncertainty is more generally explored. Please note here that these are uncertainties due to the measurement of the concentrations of isotopic species in instruments such as CRDS and IRMS, not biases due to the Iso-FD chambers, which were shown above to be theoretically free of methodological bias.

Error analyses shows that for the Iso-FD chambers, the most critical factor is the ratio between the $^{12}CO_2$ concentration in the Iso-FD chamber, and the atmospheric chamber (Chamber/Atmosphere; C2/C1). There is also a smaller error that is induced by difference between the isotopic signature in the chamber and the atmosphere (Chamber/Atmosphere; $\delta 2$-$\delta 1$), as this difference becomes small the error is minimized. Figure 3.7 shows the absolute probable error in the calculated isotopic flux value for C2/C1 and $\delta 2$-$\delta 1$ with 1 % and 5 % uncertainty in measured concentration values and 0.5 ‰ and 1.0 ‰ uncertainty in measured isotopic signatures (i.e. analytical uncertainty).

It is important to note that these errors in measuring isotopic fluxes are induced only by the differences between the Iso-FD chamber and atmospheric reference and not by the absolute concentration of CO_2 within the Iso-FD chamber. This contrasts with the bulk FD method (Risk et al., 2011), where increasing the chamber concentration significantly can lead to a bias in the measurement of bulk flux. In contrast with FD for bulk CO_2, the Iso-FD chamber concentration would ideally be made as high as possible to increase the difference between the Iso-FD chamber, and the atmospheric reference, in order to decrease the uncertainty in the measurement caused by gas analyses. However, this advice should be taken with caution, as the increase in Iso-FD chamber concentration may come at a cost (i.e. drastically increased subsurface CO_2 concentrations below the chamber may cause shifts in chemistry, for example by increasing acidity, or biology, for example if the microbial/fungal community contains CO_2 intolerant species). This trade-off between increased resolution and potential costs associated with the increase should be examined further in future studies using Iso-FD.

As a final note, using instruments such as the G1101-*i*, or any other CRDS/TDLAS,

generally allows better precision than is shown in Figure 3.6 because of the sheer number of samples that can be taken using these continuous systems. This should allow for more accurate Iso-FD results, even at low C2/C1 ratios. Despite this, as with any methodology, careful consideration of the uncertainty associated with the Iso-FD is critical in interpretation of the results.

3.5.5 Comparison with Other Chamber Types

During the model analysis, the recirculated Iso-FD technique showed no bias in the measurement of the isotopic composition of soil flux over the full range of model parameterization. Pump drawn Iso-FD results showed a diffusivity related bias, that depended on the Iso-FD membrane diffusivity and the soil diffusivity. For the current model of the Iso-FD this bias is estimated to be $\sim$ 0.2-1.24 ‰. Previous calculations using a similar 3D model have suggested that static Keeling plot based analysis are biased by up to 4.4 ‰ under similar model soil conditions, and other dynamic chamber systems range up to 7 ‰ (Nickerson and Risk, 2009c).

3.5.6 Sampling Method Modifications

While the isotopic sampling method presented in this manuscript provided good results, model results make it evident that the best sampling solution is to recirculate or quickly sample a small volume of air from the chamber, rather than drawing air continuously as with the test system. The continuous removal of air requires the determination of the isotopic offset value, which is cumbersome to calibrate and the Iso-FD chambers would otherwise be deployable without any calibrations. Small sample removal from the Iso-FD chambers could be done either by sampling chambers using pre-evacuated vials or by using a small sample TDLAS/CRDS method similar to Moyes et al. (2010a) Moyes et al. (2010a). Alternatively, a method whereby the G1101-i or other isotopic sampling device could be modified to recirculate the air without any shift in the pressure of the Iso-FD chamber would also provide data without the need to offset the values. At the time these experiments were performed, a reliable recirculation system was not available for the Picarro CRDS instruments, but this has recently become available and will likely lead to improved Iso-FD method in future work.

3.5.7 Chamber Design Considerations

The dual chamber design, where one chamber is used for atmospheric referencing, worked well in the lab and is likely to perform well in the field, at least in conditions where the atmosphere is laterally homogenous and the reference is placed close to the Iso-FD chamber. However in future designs of the chamber it may reduce error if the proximity of the atmospheric reference is maximized, possibly by integration of the reference and Iso-FD chambers in some manner (i.e. have a dual chamber reference/Iso-FD within a single physical unit). This would eliminate any possible error from laterally variant isotopic signature and/or atmospheric concentrations.

In order to use the chamber in its open configuration (i.e. drawing air) with systems such as the Campbell Scientific TGA100/TGA200 (Campbell Scientific Inc., Logan, Utah) which have a much higher flow rate than the G1101-*i*, the Iso-FD chambers would likely need a considerable size increase (both in volume and surface area). This size increase would allow these types of systems to draw a smaller proportion of the total chamber volume as well as increase the amount of soil flux entering the chamber, leaving a measurable difference between chamber and atmospheric air even at high flow.

3.6 Conclusions

While there are several future modifications that should be made to the Iso-FD chambers, including modifications to the calibration procedure, this manuscript has demonstrated that the chambers are both theoretically and practically robust for measuring the stable isotopic composition of soil CO_2 flux. This approach can obviously be applied to isotopologues other than $^{13}CO_2$ and $^{12}CO_2$, including radioactive isotopologues with long half-lives (i.e. ^{14}C), although each will have its own isotopologue specific transport characteristics that must be accounted for.

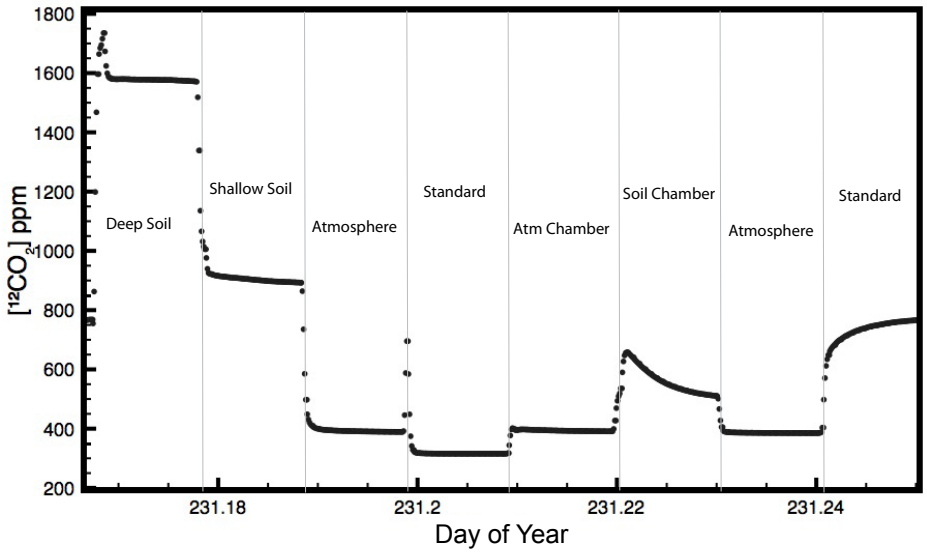

Figure 3.1: Characteristic data showing the CO_2 concentrations measured by the G1101-i as the valves switch. Visible transitions between sample types is caused by low gas flow rate and short lived analyzer/tubing memory effects.

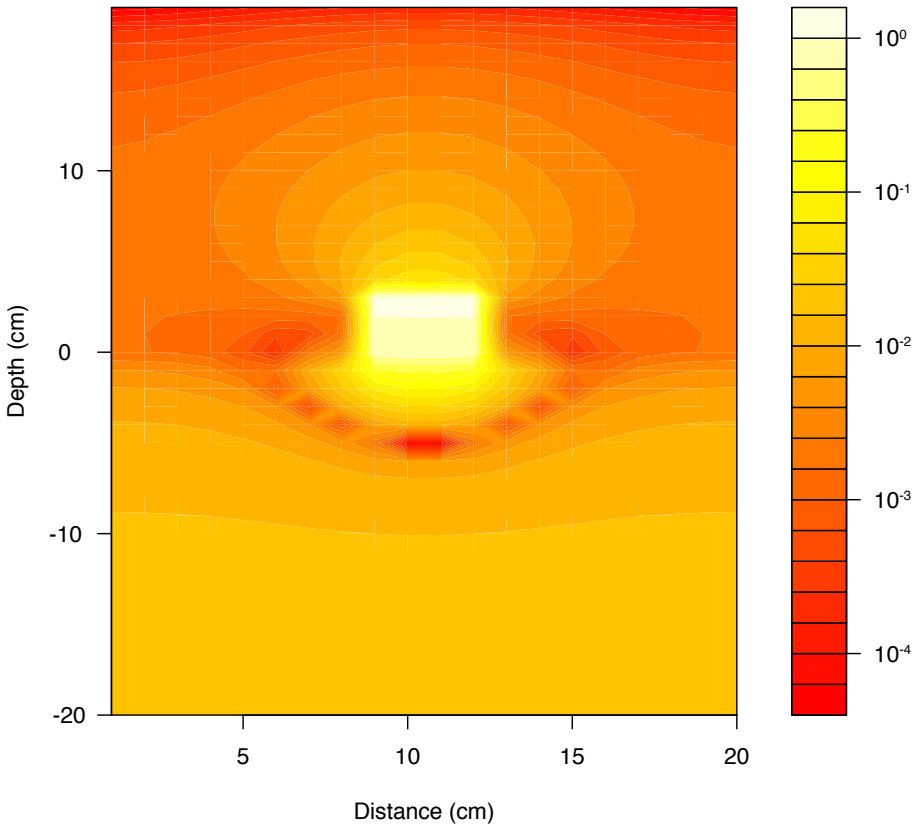

Figure 3.2: Contour plot of the isotopic deviance (difference between the steady state value with no Iso-FD chamber and the steady state value with chamber) as a function of depth and distance (with the chamber being the center of the modeled grid). Note that the isotopic deviance is in $\log_{10}$ scale to emphasize the effects. This model run was performed with a soil diffusivity of $1\text{x}10^{-6}$ m^2/s, isotopic deviance will increase with decreasing soil diffusivities.

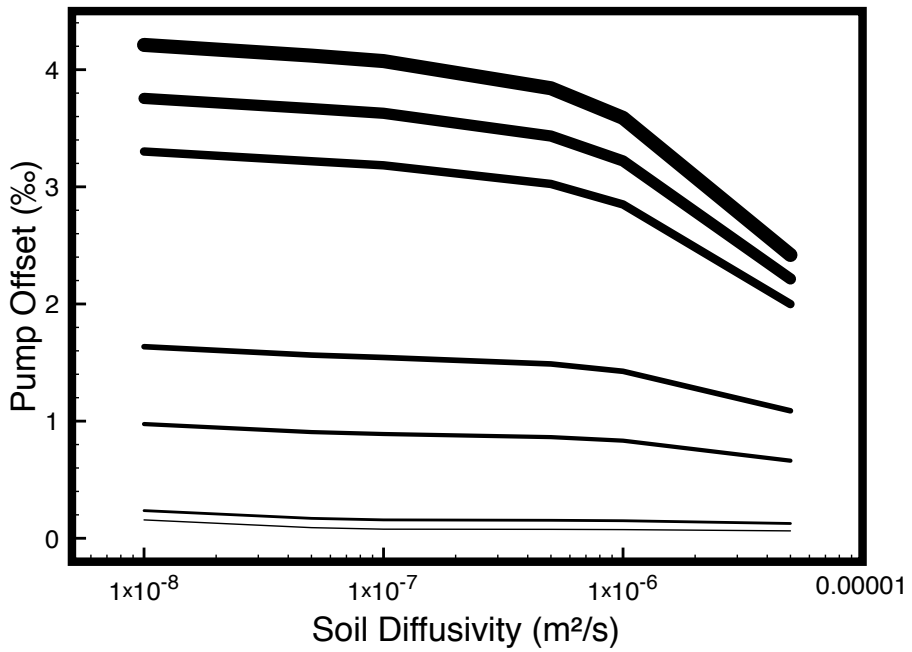

Figure 3.3: Pumping offset for Iso-FD chambers with varying membrane diffusivities on soils of various diffusivities. Thickness of lines represent membrane diffusivity with the thickest line being $1x10^{-7}$, $5x10^{-7}$, $1x10^{-6}$, $5x10^{-6}$, $1x10^{-5}$, $5x10^{-5}$ and $9x10^{-5}$ m^2/s for the thinnest line. As is evident, for slow diffusing Iso-FD membranes, the pumping offset can change considerably over varying soil diffusivities, however the membrane can be tuned by changing the fabric type or exposed surface area so that this bias is minimized.

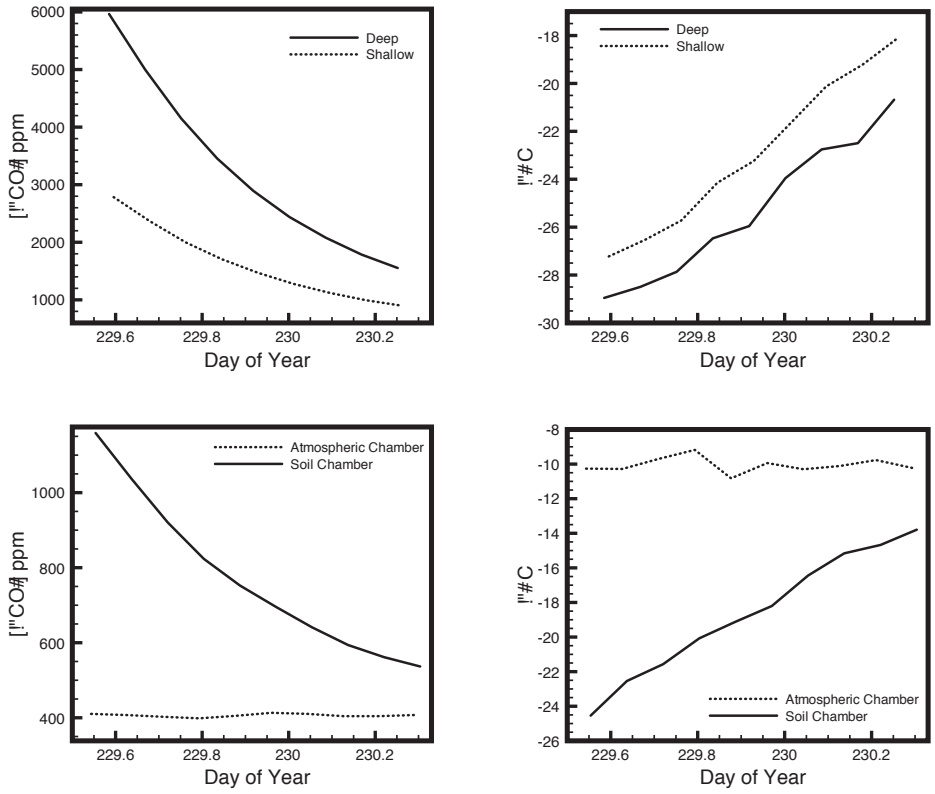

Figure 3.4: a) Decay in CO_2 concentrations in the within soil shallow and deep gas sampling tubes. b) Corresponding shifts in isotopic signature within the soil during the run. c) Concentrations measured within the atmospheric and Iso-FD chamber during the course of the experiment. d) Corresponding isotopic signatures within the chambers.

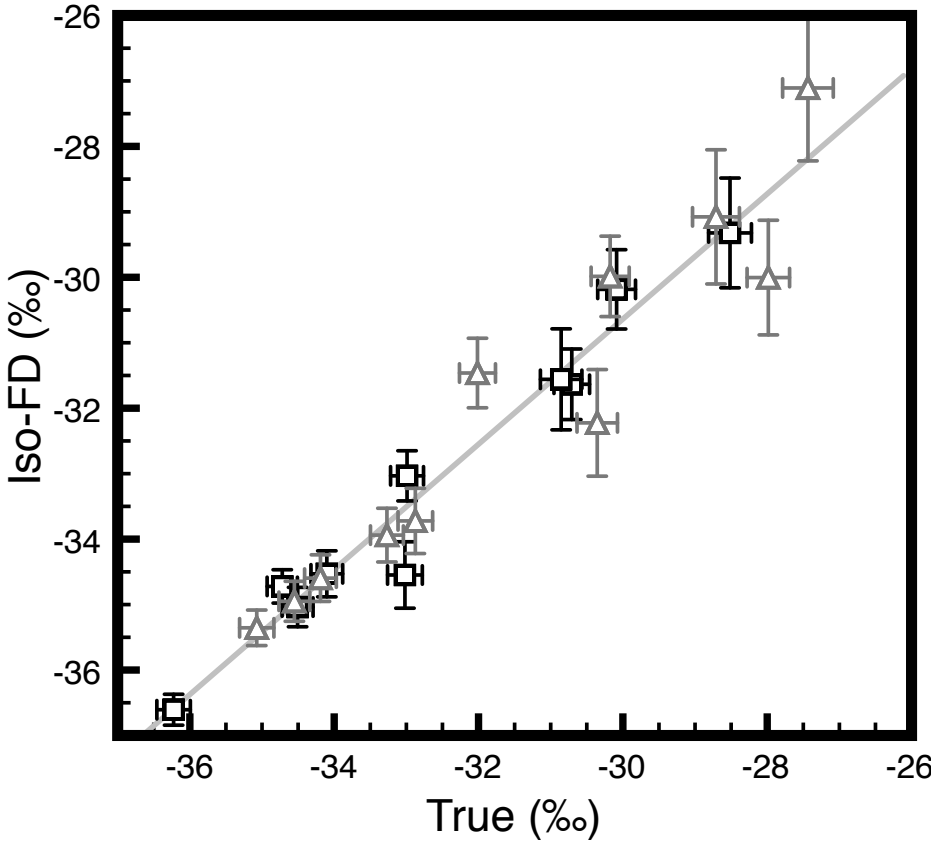

Figure 3.5: True isotopic signature of surface flux (calculated from the soil sampling tubes) verses Iso-FD measured isotopic signature of surface flux. Best-fit OLS line shown in grey, with a slope of 0.956 and y-intercept value of 1.916. Open squares represent sampling day 1, whereas open triangles represent sampling day 2. Error bars are calculated using standard analytical uncertainty analysis (see Discussion, Figure 3.6).

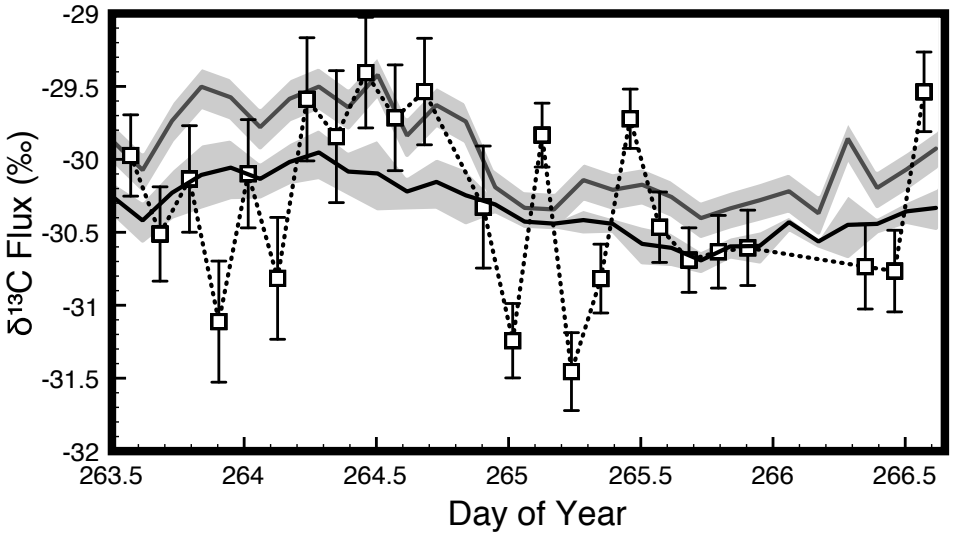

Figure 3.6: Field measurements of the isotopic composition of flux using the Iso-FD method (open squares), two-point subsurface Keeling plot (grey solid line) and multi-point subsurface Keeling plot (black line with intercept standard error shown in grey shading). Error for the two-point Keeling plot is calculated using standard uncertainty analysis. Keep in mind that the Iso-FD approach is likely to measure high frequency changes in isotopic flux cause by near-surface biological processes, whereas the Keeling plot approach records a much more stable time-integrated signature.

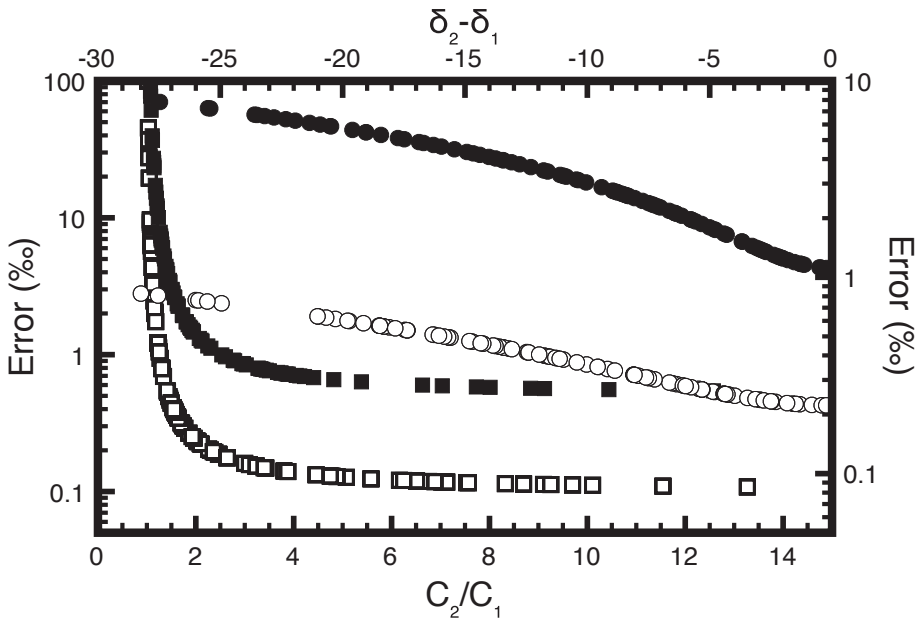

Figure 3.7: Probable uncertainty for 1 % (open squares) and 5 % (filled squares) standard deviations in CO_2 concentration measurements (left hand y-axis) and 0.5 ‰ (open circles) and 1 ‰ (closed circles) standard deviations in $\delta^{13}C$ measurements (right hand y-axis). The bottom x-axis represents the ratio of the Iso-FD chamber bulk CO_2 concentration (C_2) over the atmospheric reference bulk CO_2 concentration (C_1). The top x-axis shows the difference between the Iso-FD chamber isotopic signature ($\delta 2$) and the atmospheric reference isotopic signature ($\delta 1$).

Chapter 4

Subsurface Approaches for Measuring Soil CO_2 Isotopologue Flux: Theory and Application

4.1 Preamble

This chapter describes a diffusion-theory based method for estimating the isotopic signature of soil gas production and flux. Authorship on this manuscript is as follows: Nick Nickerson, Jocelyn Egan and Dave Risk. I was the principal investigator in this research and handled all of the writing, theory, and numerical modelling and also helped to perform the lab and field experiments with Jocelyn Egan. Dave Risk supervised this project. A version of this manuscript has been submitted to Journal of Geophysical Research: Biogeosciences and is currently in review.

4.2 Abstract

Measurements of the stable isotope composition of soil flux have many uses, from separating autotrophic and heterotrophic components of respiration to teasing apart information about gas transport physics. While soil flux chambers are typically used for these measurements, subsurface approaches are becoming more accessible with the introduction of field-deployable isotope analyzers. These subsurface measurements have the unique benefit of offering depth-resolved isotopologue flux data, which can help to disentangle the many soil respiration processes that occur throughout the soil profile. These methods are likely to grow in popularity in the coming years and a solid methodological basis needs to be formed in order for data collected in these subsurface studies to be interpreted properly. This manuscript explores the range of possible techniques that could be used for subsurface isotopologue gas interpretation and rigorously tests the assumptions and application of each approach using a combination of numerical modelling, laboratory experiments and field studies. These results suggest that methodological uncertainties arise due to poor assumptions

and mathematical instabilities but certain methods, particularly those based on diffusion physics, are able to cope with these uncertainties well and produce excellent depth-resolved isotopologue flux data.

4.3 Introduction

Measurement of the stable isotope composition of carbon dioxide (CO_2) has become an invaluable resource for understanding the biological and physical mechanisms that drive soil CO_2 dynamics (Cerling et al., 1991; Ekblad and Högberg, 2001; Subke et al., 2009; Gamnitzer et al., 2011). Isotopic data can be used for a variety of applications ranging from disentangling gas transport processes (Bowling and Massman, 2011) to tracing the links between aboveground and belowground carbon (C) allocation (Ekblad and Högberg, 2001). One of the more exciting prospects made possible by measurement of stable-C isotopologues of CO_2 is the potential to differentiate between autotrophic and heterotrophic CO_2 production, assuming each has a distinct source isotopic signature (Formanek and Ambus, 2004; Albanito et al., 2012). These distinct source signatures act as a fingerprint, allowing researchers to identify and account for CO_2 being produced by the individual components of the soil CO_2 system. Understanding of these individual components of soil respiration, and their relation to climate and soil properties, remains one of the more elusive problems in carbon cycle research (Davidson et al., 2006b).

To this end, a number of methods have been developed that researchers can employ to determine the isotopic composition of soil CO_2 fluxes. These methods generally fall into two categories, the first being surface flux chambers, and the second being sub-surface gas sampling. Flux chambers have been a staple device for the measurement of bulk CO_2 emissions from soil for many decades, and many of these chamber designs have been adapted to measurement of isotopologue flux (e.g. Subke et al. (2004); Ohlsson et al. (2005); Mora and Raich (2007); Maseyk et al. (2009)). Their prolific use is likely a result of the technical simplicity and cost-effective nature of the method, in addition to the ability to deliver reasonable estimates (Pumpanen et al., 2004; Ohlsson, 2010) of both bulk and isotopologue fluxes, without causing significant soil disturbance during installation and use.

Recent years have seen the increased use of sub-surface gas measurements to estimate the flux rates for bulk CO_2, largely due to improvements in CO_2 gas detection technologies (increased resolution, miniaturization), which allow for continuous measurement of soil pore space CO_2 concentrations (Tang et al., 2003; Xu et al., 2004; Barron-Gafford et al., 2010). With these subsurface approaches, researchers are able to estimate soil surface fluxes based on CO_2 gradient data, with the added benefit of being able to partition total flux with respect to depth, thereby allowing estimates of CO_2 production through the soil profile. As is the case with chamber methods, subsurface approaches have been adopted for use in CO_2 isotopologue studies (Pendall et al., 2001; Kayler et al., 2010; Moyes et al., 2010a; Bowling and Massman, 2011; Parent et al., 2013), but are still in their infancy for these applications. Subsurface gas sampling approaches may allow for investigation of the soil profile distribution of isotopic sources, and because of this they could be a very powerful tool for soil respiration research, providing complimentary isotopic data to chamber based studies. However, to use subsurface data to the highest of its abilities, the theoretical and methodological factors that may affect the accuracy and interpretation of data gained from the subsurface need to be examined.

Due to the recent adoption of subsurface techniques for CO_2 isotopologues, only a small amount of the potential of subsurface data has been tapped. For example, there are no studies that employ the flux gradient and production profile forms of Fick's laws, often used in bulk CO_2 research, for interpretation of isotopic data. Further, the Keeling plot approach has been used to interpret some subsurface isotopologue data to date (Pendall et al., 2001; Kayler et al., 2008), however, no work has proven that the Keeling plot is universally applicable for subsurface gas data. This is a particular concern due to the fact that the soil gas transport regime is generally considered to be diffusive, and Keeling plots have been shown to be non-linear in other diffusive systems (Nickerson and Risk, 2009b).

With the development of any new scientific methodology, there is the need to carefully test the reliability of the method, both under simplified theoretical conditions and in the system where it will be applied. Numerical and analytical modelling are often, or should be, the first hurdle that new methods must pass. Obviously it is critical for methods to be theoretically robust, not just for a special case of the

method application, but over all possible conditions. Carefully controlled laboratory experiments are a crucial next step in this process, as models are oversimplifications, and full-scale field studies are often overcomplicated by uncontrollable environmental and biological factors. Experimental methods allow the confirmation of theoretical results and also allow for the initial development of the physical embodiment of the methodological approach. Finally, the initial application of methods in the field allow for refinement of the more practical matters surrounding sampling in-situ, and can provide further method confirmation data, particularly when compared against currently accepted methods.

The purpose of this study is to examine the range of possible techniques that could be used for subsurface gas isotopologue interpretation, including the previously used Keeling plot method, and the isotopologue gradient and production profile approaches that are developed herein. These methods are rigorously tested using a combination of analytical modelling, laboratory experiments using an isotopologue flux generation system, and finally by deployment at a field site, where subsurface approaches were compared to one another.

4.4 Methods

4.4.1 Delta Notation

Isotopic compositions are commonly reported using delta notation. The delta value of a gas sample is calculated as follows:

$$\delta = \left(\frac{\left(\frac{[^{h}CO_2]}{[^{l}CO_2]} \right)}{R_{std}} - 1 \right) \times 1000 \tag{4.1}$$

where $[^{h}CO_2]$ and $[^{l}CO_2]$ are the concentrations of heavy and light CO_2 in the measured gas, respectively, and R_{std} is the ratio of $^{h}CO_2$ and $^{l}CO_2$ in the isotopic standard (Pee Dee Belemnite for stable carbon isotopologues of CO_2).

4.4.2 Subsurface Methods

Keeling Plot Approach

The Keeling plot is a stable C-CO_2 isotope specific variant of the general two end-member mixing model first developed for use in atmospheric CO_2 research (Keeling, 1958). The model assumes two distinct and constant sources of CO_2 isotopologues mixing within the soil profile. The first source is CO_2 from the atmosphere, diffusing into the soil profile, and the second source is CO_2 produced within the soil by autotrophic and heterotrophic organisms, diffusing to the atmosphere. Formally, the mixing model is as follows:

$$\delta_{obs} = \frac{A}{C_{obs}} + \delta_{rs} \tag{4.2}$$

where δ_{obs} is the observed (or measured) isotopic composition in the soil pore space, A is a fitting constant, C_{obs} is the measured bulk CO_2 concentration in the soil pore space and δ_{rs} is the diffusion-fractionated isotopic signature of respiration, the variable of interest. To obtain the value for δ_r, the isotopic signature of respiration, assuming strictly diffusive transport one must account for the 4.4‰ fractionation associated with gas diffusion through the soil matrix (Cerling et al., 1991; Davidson and Trumbore, 1995). This 4.4‰ fractionation must be subtracted from the Keeling plot estimate of δ_{rs} to derive the isotopic signature of respiration (Pendall et al., 2001). The Keeling plot model is implemented by regressing observed isotopic composition (δ_{obs}) against the reciprocal observed bulk CO_2 concentration ($1/C_{obs}$). The resulting y-intercept of the least-squares regression will give the value for δ_{rs} , which is corrected for diffusive fractionation to yield the isotopic composition of the soil respiration (Pendall et al., 2001; Ohlsson et al., 2005).

Gradient Method

The gradient method presented here is an isotopologue modification of the flux gradient approach for measuring bulk CO_2 effluxes (Risk et al., 2002a; Tang et al., 2003). Steady state (or non-steady state if one accounts for storage terms) diffusive transport of gas from one soil depth to the next (or from soil to the atmosphere) can be described using the one-dimensional form of Fick's First Law:

$$F(z) = D(z)\frac{\partial C(z)}{\partial z} \tag{4.3}$$

where F(z) is the flux density (μmol m^{-2} s^{-1}), D(z) is the soil diffusivity (m^2 s^{-1}) as a function of depth, z (m), and C(z) is the soil gas concentration (μmol m^{-3}).

Experimental evidence suggests that different stable isotopologues of the same gases (i.e. $^{12}CO_2$ and $^{13}CO_2$) diffuse independently with their own isotopologue specific concentration gradients and diffusivity rates (Cerling et al., 1991). Assuming this is true, Fick's Law can be applied to each isotopologue as follows:

$$F^l(z) = D^l(z)\frac{\partial C^l(z)}{\partial z}; F^h(z) = D^h(z)\frac{\partial C^h(z)}{\partial z} \tag{4.4}$$

where the superscripts l and h refer to the light and heavy isotopologues, respectively. Combination of the heavy and light versions of Fick's law (Eq. 4.4) allows for the calculation of the isotopic ratio of flux:

$$\frac{F^h(z)}{F^l(z)} = \frac{D^h(z)}{D^l(z)}\frac{\partial C^h(z)}{\partial z}\frac{\partial z}{\partial C^l(z)} \tag{4.5}$$

It is well known that in diffusive systems, the quotient of the diffusion coefficient of the heavy isotope over the diffusion coefficient of the lighter isotope yields the inverse of the kinetic fractionation factor (α; for CO_2 α=1.0044) (Cerling et al., 1991):

$$\frac{D^h(z)}{D^l(z)} = \frac{1}{\alpha} \tag{4.6}$$

Given this identity (Eq. 4.6), equation 4.5 can be discretized and simplified to yield:

$$\frac{F^h(z)}{F^l(z)} = \frac{1}{\alpha}\frac{\Delta C^h}{\Delta C^l} = \frac{1}{\alpha}\left[\frac{C^h_{z_2} - C^h_{z_1}}{C^l_{z_2} - C^l_{z_1}}\right] \tag{4.7}$$

where z_1 and z_2 are arbitrary depths in the diffusive medium (soil).

It should be noted that the relationship presented in Equation 4.7 is convenient for several reasons. First, there is no need to know the diffusion coefficient, which can be both difficult to measure and highly error prone. Second, the measurement of the gas concentrations can be performed from any arbitrary points z_2 and z_1 so long as the transport of gas between those two points is dominated by diffusion, which eliminates error due to the estimation of sampling depth. While it is not mathematically necessary for the difference between z_1 and z_2 to be small, in practice the larger the distance between the two measurement points the further the discretized form of Equation 4.7 is from the original, and more correct, continuous form given in

Equation 4.5. It is therefore desirable to difference points that are near each other, but a strict estimate on the proximity is not possible without information on the soil profile CO_2 concentrations and their derivatives. For example, if the soil CO_2 profile were linear then any two points in the profile could be used. However if the CO_2 profile is highly curvilinear then one must be more careful about choosing points. This concept will be clarified further in the results and discussion on the gradient method.

Production Profile Method

The production profile (PP) method can be considered as an extension of the gradient method, and is also used in bulk CO_2 research (Davidson and Trumbore, 1995; Risk et al., 2002a). Consider Fick's Second Law:

$$F(z) = D(z)\frac{\partial^2 C(z)}{\partial z^2} \tag{4.8}$$

To estimate gas production, P(z), at a given soil depth, the second order depth gradient of concentration (∂^2C(z)/∂z^2) at that depth and the soil gas diffusivity must be known. For isotopic measurements two similar equations can be written, one for the heavy isotopologue and one for the light isotopologue, from which the isotopic ratio of production can be determined by division.

If the equation is converted into its finite difference approximation one sees that the depth terms of the gradient cancel to leave a simple differencing of concentrations measured at several depths (z_1, z_2 and z_3): Similarly, the division cancels the diffusion coefficients to yield $1/\alpha$ (see Eq. 4.6).

$$\frac{P^h(z)}{P^l(z)} = \left(D^h\left(\frac{C^h_{z_3} - C^h_{z_2}}{z_3 - z_2} - \frac{C^h_{z_2} - C^h_{z_1}}{z_2 - z_1}\right)\right)\left(\frac{1}{D^l}\left(\frac{z_3 - z_2}{C^l_{z_3} - C^l_{z_2}} - \frac{z_2 - z_1}{C^l_{z_2} - C^l_{z_1}}\right)\right) \tag{4.9}$$

$$\frac{P^h(z)}{P^l(z)} = \frac{1}{\alpha}\left(\frac{C^h_{z_3} - 2C^h_{z_2} + C^h_{z_1}}{C^l_{z_3} - 2C^l_{z_2} + C^l_{z_1}}\right) \tag{4.10}$$

Equation 4.10 may be converted to delta notation if desired. This equation should yield the isotopic composition of production at the depth z_2, where z_2 is a point intermediate between z_1 and z_3. Again it is important to stress that with both the Gradient and Production Profile methods there is no need to know the diffusivity of the medium nor the depths from which the gas samples are taken because of the simplifications resulting from using isotopologue ratios.

4.4.3 Steady State Soil CO_2 Isotopologue Model

Under the assumption that the soil gas system is dominated by production by both heterotrophic and autotrophic sources and that gas transport is controlled by diffusion, the gas concentration within the soil profile can be calculated by solving the diffusion equation:

$$\theta \frac{\partial C}{\partial t} = \frac{\partial}{\partial z}\left(D(z,t)\frac{\partial C}{\partial z}\right) + P(z,t) \tag{4.11}$$

where θ is the soil air-filled pore space, C is the gas concentration, t is time, D(z,t) is the soil gas diffusivity as a function of depth (z) and time, and P(z,t) is the biological production function, which is also a function of depth and time. Making the simplifying assumptions that the soil gas system is in steady state (∂C/∂t=0), and that the soil gas diffusivity is constant with depth (D(z)=D), the equation can be rearranged to solve for soil gas concentration:

$$\frac{\partial^2 C}{\partial z^2} = \frac{-P(z)}{D} \tag{4.12}$$

where P(z) is the non-time dependent production function. Many researchers have observed an approximately exponential relationship between CO_2 production and depth (i.e. Davidson and Trumbore (1995), that is:

$$P(z) = \frac{P_0}{\lambda} e^{-z/n} \tag{4.13}$$

where P_0 is the total respiration rate, integrated over all depth, η is the e-folding depth, or the depth at which production is reduced to 1/e of its value at z=0 and λ is a parameter that constrains all production to occur over soil depths 0 to L, where L is some arbitrary depth at which production and diffusion of CO_2 stops (e.g. water table):

$$\lambda = \eta - \eta e^{-L/n} \tag{4.14}$$

Combination of equations 4.12 and 4.13 allows for integration of the steady state diffusion equation:

$$\frac{\partial^2 C}{\partial z^2} = -\frac{P_0}{D\lambda} e^{-z/n} \tag{4.15}$$

which is subject to the following boundary conditions:

$$C(z=0) = C_{atm} \tag{4.16}$$

$$\left.\frac{\partial C}{\partial z}\right|_{z=L} = 0 \tag{4.17}$$

After integration and application of the boundary conditions one arrives at the final steady state solution for the concentration of CO_2 as a function of depth:

$$C(z) = -\frac{\eta P_0}{D\lambda}(\eta e^{-z/\eta} + z e^{-L/\eta} - \eta) + C_{atm} \tag{4.18}$$

Here a common assumption that the bulk CO_2 solution (Eq. 4.18) describes the concentration of $^{12}CO_2$ is made. A further assumption is that $^{13}CO_2$ is an independent species of CO_2, with its own characteristic diffusion and production rate (Cerling et al., 1991). Under this assumption the second steady state equation can be written:

$$\frac{\partial^2 \chi}{\partial z^2} = \left(-\frac{P_0}{D_\chi \lambda} e^{-z/n}\right)(R_d e^{-z/\sigma} + R_b) \tag{4.19}$$

Where Chi (χ) is the $^{13}CO_2$ concentration, D_χ is the $^{13}CO_2$ diffusion coefficient, R_d is the difference in the ratio of $^{13}CO_2/^{12}CO_2$ production between depth 0 and L, R_b is the ratio of $^{13}CO_2/^{12}CO_2$ production at depth L and σ is the e-folding depth of the $^{13}CO_2/^{12}CO_2$ production ratio (i.e. how quickly the $^{13}CO_2/^{12}CO_2$ production ratio changes with depth). Integration of Eq. 4.19 and application of the boundary conditions stated in Eq. 4.16 and 4.17 yields the steady state solution for the concentration of $^{13}CO_2$ with depth:

$$\chi(z) = \frac{\eta P_0}{D_\chi \lambda(\eta+\sigma)}\left(\left(e^{-z\left(\frac{\eta+\sigma}{\eta\sigma}\right)}\left(\frac{-\eta\sigma^2 R_d}{\eta+\sigma} - R_b(\eta^2+\eta\sigma)e^{z/\sigma}\right) - z e^{-L\left(\frac{1}{\eta}+\frac{1}{\sigma}\right)}\right.\right.$$
$$\left.\left.(R_d\sigma + R_b(\eta+\sigma)e^{L/\sigma})\right) - \frac{-\eta\sigma^2 R_d}{\eta+\sigma} - R_b(\eta^2+\eta\sigma)\right) + C_{atm}R_{atm} \tag{4.20}$$

At this point the isotopic composition of soil profile CO_2 can be determined by the division of χ(z) and C(z) (Eqs. 20 & 18, respectively) and application of the delta notation.

4.4.4 Model Parameter Ranges and Data Generation

For model testing of the three sub-surface methods steady state soil CO_2 and isotopic signatures were simulated for a range of conditions that would be expected in the field. Listed in Table 1 are the parameter names and ranges used in the simulations. Unless performing a specific parameter sensitivity analysis, parameters were randomly

sampled within these ranges so that a range of possible soil conditions could be covered without performing a time-intensive iterative parameter search over the whole parameter space. Equations 4.18 and 4.20 were solved using a Perl script under the Macintosh OS X operating system. Calculations for the Keeling, Gradient and Production Profile methods were also preformed in Perl.

4.4.5 Laboratory and Field Testing

Laboratory Tests

To test the proposed subsurface methods in a carefully controlled environment a Flux Generator (FG) apparatus (Martin et al., 2004) was used. The FG consists of a glass bead soil ($\sim$17 cm deep, 0.234 m^2 surface area) that rests on top of a 234.23 L reservoir. Pure CO_2 is injected into the reservoir until the desired concentration is reached, and the reservoir gas is then allowed to flux diffusively from the synthetic soil. The flux of bulk CO_2 and CO_2 isotopologues can then be calculated using the measured decay timeseries data from the FG apparatus (Martin et al., 2004). Within the synthetic soil two subsurface sampling tubes were installed (perforated vinyl tubing) with an additional sampling tube resting on the soil surface. These tubes were connected to the G1101-i valving system (see Section 2.5.3) for sampling during the reservoir decay. The decay in reservoir concentration was also modeled using a finite-difference algorithm (see Nickerson and Risk (2009a) to ensure that the FG system was behaving diffusively and to provide a common reference isoflux for comparison to the subsurface approaches. Unfortunately only the Keeling and gradient approaches could be tested on this apparatus, as the Production Profile method requires that CO_2 be produced within the soil profile (the second order derivative of concentration must be greater than zero).

Field Tests

Ultimately these methods will be applied in-situ, and while it is not the ideal environment for methodological testing, field deployments often reveal methodological complications that were otherwise unapparent in controlled test environments. The

purpose of these field experiments was to compare the three methods in an uncontrolled setting, and to evaluate the uncertainty associated with using each method in a natural environment (errors due to instrumental set-up and natural noise in subsurface signals).

The field site is a ∼20 year old plantation of Red Pine (Pinus resinosa) located in Heatherton, Nova Scotia (N 45° 33' 54", W 61° 46' 20"). Annual average rainfall for the region is 1100 mm/year with average monthly rainfalls in August of 92 mm and 101 mm in September, which were the two months over which the field experiment spanned. Annual average temperature for the region is 7 °C and average temperatures in August and September are 18.9 °C and 15.3 °C, respectively. The soil in the region is classified as a moderate to well drained Orthic Humo-Ferric Podzol, although there is limited horizonation at this site due to relatively recent (ca. 30 years ago) tillage on the property.

Two soil pits were excavated in May 2011 to 50 cm depth, approximately 15 meters away from each other. These two soil pits were on separate treatment plots in the same forest stand. One plot was completely intact whereas the second had undergone tree-girdling approximately one year earlier in order to cut off supply of photosynthates to the roots. Gas wells were constructed using 50 cm long sections of 1.3 cm inside diameter PVC pipe. Holes (1.0 cm diameter) were drilled on opposing sides along the length of the pipe at ∼4.5 cm intervals. The outside of the pipe section was wrapped in Tyvek® building material (polyethylene membrane, DuPont) to exclude water from entering the gas well. Three (3) sections of larger diameter (1.8 cm ID) pipe were installed in the side of the soil pit at depths ranging between 4 and 28 cm (installation at approximately 5, 15 and 25 cm but these depths varied due to soil conditions) to allow for insertion of gas wells into the soil without damaging the membrane material. Each of the three larger pipes were drilled with opposing 1.0 cm diameter holes as well, so when then smaller diameter Tyvek wrapped tubing was inserted into the larger diameter tubing, the holes were aligned. An ∼10m long section of vinyl tubing was connected to each of the gas wells and the soil pit was filled. A similar Tyvek wrapped tube was also laid on the soil surface to sample the near surface atmospheric gas. Gas concentration and isotopic composition measurements were gathered from these pre-installed gas-sampling tubes over an approximately 8-day period occurring

between September 18 and 27, 2011.

Isotopic Measurements

To sample gases in the lab and field Picarro G1101-i Cavity Ring Down Spectrometer was used (hereafter referred to as the G1101-i) and coupled to a custom designed valving system (6 sample valves) to allow for routing more than one sample port into the G1101-i. Gases were sampled by approximately 15 minutes of continuous pumping (∼25 mL/min flow rate) from the soil-gas sampling tubes, using the analyzers vacuum pump. Two standards were supplied (∼312 ppm [-9.6‰], 760 ppm [-27.8‰]) to the G1101-i every 2 hours to allow for correction of the isotopic composition and CO_2 concentrations. The raw data was post-processed to use only the last 30 points before the valve switch, roughly 3-4 minutes of data, and average them to a single value (typical standard deviations are ∼1-3 ppm and ∼0.05-0.15‰). Since the G1101-i is only rated to ∼4000 ppm CO_2 (personal communication, Aaron Van Pelt, Picarro Inc.), prior to sampling standards tests were performed to confirm that the G1101-i would maintain linearity in the expected soil gas concentration range, 0-10,000 ppm. Results were good, with r^2 values of 1.00 and 0.92 (n=8) for concentration and isotopic composition, respectively. Note that while linearity was maintained over the full range, the slope of the fit was not equal to one. This multiplier was corrected for in the data reported in this manuscript, using both field and laboratory standard data.

Prior to deployment a simple laboratory experiment was performed on an inert soil (crushed automotive glass) with a known pore-space CO_2 concentration in order to evaluate the effects of sample drawing on the measured soil CO_2 concentrations and isotopic compositions. No bias in the measurements was found for sample draw times of up to 30 minutes (data not shown). Based on these results, gas was sampled for 15-minute periods during laboratory and field experiments to avoid any potential sample draw related issues while allowing the G1101-i enough measurement time to produce stable CO_2 concentration and isotopic composition measurements.

4.5 Results and Discussion

4.5.1 Model - Keeling Plot Approach

In published studies where the subsurface Keeling plot approach has been used (i.e. Pendall et al. (2001)), it is common to use as many sampling points over the soil column as is practical, to get more robust fit statistics for the regression. Due to this practice, it should be noted that the resulting Keeling plot intercept should represent an integrated estimate of the isotopic signature of production over the depth interval from which the data were collected, after accounting for the 4.4‰ offset associated with diffusion. In the following Steady State Soil CO_2 Isotopologue Model runs, soil profile CO_2 concentrations and isotopic compositions were simulated from a depth of z=0 m to z=1 m in increments of 1 cm, yielding 101 data points for each Keeling plot regression, unless otherwise noted. In the case of using the full soil profile, the typical assumption is that the Keeling plot estimate of δ_r should be exactly equal to the isotopic ratio of surface flux. To check for biases in the Keeling plot δ_r estimates, the soil flux isotopic ratio was calculated (by differentiation and solution of Equations 4.18 and 4.20 for z=0) for each Steady State Soil CO_2 Isotopologue Model run and compared it to the regression-estimated δ_r.

For 1000 randomly sampled parameter combinations (parameter ranges listed in Table 1) the mean bias in the Keeling plot estimate of δ_r was found to be 0.09‰ with a standard deviation of 1.38‰. The maximum and minimum observed errors were 4.12‰ and -3.74‰, respectively. The errors for these 1000 runs were approximately normally distributed, with the histogram shown in Figure 4.1. Sensitivity analyses were also ran for each Steady State Soil CO_2 Isotopologue Model parameter with respect to Keeling plot bias. The results of these sensitivity analyses are shown in Figure 4.2. Most parameters had some effect on bias, with the minimum effects seen in changing the values of C_{atm} and R_{atm}. Maximum errors were observed when the difference between the isotopic signature of CO_2 produced at the bottom of the soil profile and the top of the soil profile were maximized. Positive differences in R_d ($R_d \propto \delta_{top}$ - δ_{bott}) resulted in positive bias in the Keeling plot estimate and negative values in R_d resulted in negative Keeling plot bias. The core reason for the observed biases in the Keeling plots was non-linearity created by depth-dependent isotopic signatures of

production. In the case that isotopic signature was constant through the soil profile, the Keeling plot was perfectly linear with no bias (assuming no error in the data). Please note that the Steady State Soil CO_2 Isotopologue Model parameters used in the sensitivity test are characteristic of the higher end of the bias shown in Figure 4.1. These were chosen to clearly show the sensitivity of each parameter for demonstrative purposes. In many situations, where the bias is closer to the mean shown in Figure 4.1, these sensitivities will be significantly dampened but it is still expected that they will maintain their characteristic curvatures.

To make these Steady State Soil CO_2 Isotopologue Model results more transferrable to field-based studies, 1000 additional simulations were ran where the sampling depth interval was increased to every 10 cm, and the deepest sample was at 50 cm (half the soil profile length). This resulted in six (including z=0) measurements of soil CO_2 concentrations and $\delta^{13}C$. Mean bias in the Keeling plot estimate of δ_r was 0.13‰ with a standard deviation of 1.13‰. The maximum and minimum observed errors were 3.70‰ and -3.13‰, respectively. Noise was then added to the data to simulate environmental variability and measurement uncertainty. Both a low noise (S.D.=0.1‰ for δ_{obs}, S.D.=1% of reading for C_{obs}) and a high noise (S.D.=0.5‰ for δ_{obs}, S.D.=5% of reading for C_{obs}) were simulated. The increase in the standard deviation of the errors from no error (1.13‰), to low (1.20‰) and high error (1.23‰) scenarios was negligible compared to the error caused by non-linearity in the subsurface Keeling plots.

4.5.2 Model - Gradient Approach

First, as a point of clarification, the Gradient Approach provides estimates of isotopologue flux and not isotopologue production. Under the assumption of steady state diffusive conditions, the isotopologue flux across the soil-atmosphere boundary is equal to the integrated isotopologue production from the whole soil profile. However, it is not necessarily the case that the isotopologue flux at any depth be equal to the isotopologe production rate, as the flux is influenced by concentrations and isotopic ratios of gas in the soil profile. Isotopologue production can be calculated using the PP method, discussed in section 3.3.

For the gradient method 1000 random parameter combinations were sampled to

arrive at initial bias estimates. In this case bias is defined as the average difference over the soil profile of the Steady State Soil CO_2 Isotopologue Model calculated isotopic composition of flux minus the estimated isotopic composition flux using the gradient method. Gradient estimates of the isotopic flux composition were calculated using sampling intervals of 1 cm. Samples were excluded where the difference in the $^{12}CO_2$ concentrations between two successive sampling depths was <10 μmol m^{-3} because the reciprocal form of the $^{12}CO_2$ concentrations in the gradient equation (Eq. 4.7) causes amplification of any error inherent in ΔC_l. The gradient method offered good estimates of the isotopic composition of flux with depth, with a mean isotopic bias of 0‰ and a standard deviation of 0.0017‰. This reported bias is within the rounding error of the calculations and should likely be treated, for all intents and purposes, as being zero bias.

It would be impractical, if not impossible, to sample at 1 cm increments in the field, so an additional 1000 simulations were ran where the sampling increment was reduced to 10 cm and measured to 50 cm total soil depth. This lower limit on depth was chosen to avoid differencing small CO_2 gradients that occur deep in the soil profile which amplify uncertainty in estimates of isotopologue flux, discussed above and in further detail in Section 3.4. In this case the resulting bias was still centered around zero, with a mean of -0.0040‰ and a larger standard deviation of 0.0972‰. The increased bias in this case was essentisally due to estimating the derivative using a larger secant line between sampling points separated by 10 cm rather than 1 cm. Most of the bias occurred in regions where the CO_2 isotopologue depth gradients were changing quickly, leading to a misestimate by the discretized form of Eq. 4.17 (again, essentially the problem of moving from tangent to secant lines). A sample of the Steady State Soil CO_2 Isotopologue Model calculated isotopic flux and isotopic flux calculated using the gradient method with depth increments of 1 cm and 10 cm is shown in Figure 4.4.

4.5.3 Model - Production Profile Approach

In contrast to the Keeling plot and gradient methods, which provide estimates of isotopic flux, the production profile (PP) method provides depth-dependent results for the isotopic signature of CO_2 production within each soil layer. To test the

reliability of the method the values estimated with the PP method were compared to the prescribed Steady State Soil CO_2 Isotopologue Model values over the same depth interval. To arrive at a single number for the deviation between prescribed and PP values the absolute deviations between prescribed and PP over the full soil profile were summed and then divided by the number of sampling depths.

The first simulation again consisted of 1000 randomly chose parameter sets. The PP isotopic composition was calculated at 1 cm intervals throughout the 1m long simulated soil column. In some simulations, after a certain soil depth the gradient of CO_2 in the soil approached zero, and because of the lack of gradient the isotopic signature of production was not able to be calculated. This was addressed by adding an additional constraint in the Steady State Soil CO_2 Isotopologue Model: only using CO_2 and isotopic signatures up to the point where the concentration difference between two consecutive soil depths is $\geq$10 μmol m^{-3}.

The PP method offered very good estimates of the isotopic signature of production over the full soil depth, with a mean bias of 0.002‰ and a standard deviation of 0.005‰. These reported bias values are within the potential numerical error in the calculations. A sensitivity analysis was also preformed on each of the Steady State Soil CO_2 Isotopologue Model parameters using the PP method, but once again the error was negligible in all modeled results.

An additional 1000 simulations were run with the sampling interval modified to every 10 cm, similar to the Keeling plot and gradient data, to get a more realistic idea of the PP method performance in the field. In general the error increased during these runs with the mean error being 0.12‰ and the standard deviation being 0.19‰. The distribution of the error was similar with 878 out of 1000 measurements in the 0-0.2‰ bin, 70 measurements in the 0.2-0.4‰ bin, and errors >1.0‰ occurring in less than 2% of the simulations. The reason for the increased error in these coarse sampling interval runs stems largely from trying to estimate the derivative of the continuous concentration function using secant lines rather than tangent lines. As the sampling interval decreases, the results will converge on the true results (as was observed in the 1 cm interval runs), but as the interval increases, so should the error in the estimated vs. true values. It can therefore be assumed that in settings where there are steep depth gradients in CO_2 production or suspected isotopic composition,

the sampling interval should be made as fine as possible to minimize these biases.

4.5.4 Error Analysis (PP and Gradient)

Error in the Keeling plot method has been treated extensively in other research (i.e. Pataki et al. (2008)), so in this section focus is on the two Fick's Law-based methods.

Uncertainty analysis was performed (propagation of uncertainty using the partial derivative method applied to equations 4.7 and 4.10) by examining the probable errors in the flux gradient estimate that would be associated with two error rates, a low rate being 1% error in concentration measurement and 0.1‰ error in isotopic measurement, and a high rate being 5% error in concentration measurement and 0.5‰ error in isotopic measurement. For the gradient method, the error in estimated $\delta^{13}C$ of flux scales strongly with the ratio of C_2 to C_1 (see Figure 4.5a and Equation 4.7). Essentially for concentration values that are very similar (small gradients), the measurement error is large relative to the soil CO_2 gradient, and drives the error rate up. The error in the gradient calculation is reduced to the error in measurement as the ratio of C_2 to C_1 becomes large. Contrastingly, as the difference between the isotopic composition at C_2 (δ_2) and C_1 (δ_1) becomes larger, so does the error (also shown in Figure 4.5a).

Similarly, probable errors inherent in the PP method were evaluated with the same error rates as above. For PP (Figure 4.5b), the error scaled strongly with the second order gradient in concentration (i.e. as the gradient in concentration becomes linear the error is larger). Further, errors are large when the quotients of the isotopologue gradients in the soil are small, decreasing to a minimum and then increasing slightly as the isotopologue gradient quotient becomes larger. Unfortunately, the uncertainties are not as simple to interpret in the PP case as the gradient approach, but the errors can be calculated easily from the uncertainty equations for a given experimental or field setup.

4.5.5 Laboratory Results

Finite-difference calculations indicated that both the concentrations and isotopic composition within the FG synthetic soil were evolving as would be expected under diffusive conditions. Regressions of finite-difference modeled CO_2 vs. measured CO_2

had slopes not significantly different than one and r^2 values greater than 0.97. There was a slight bias for the model concentrations to decay at a slightly different rate than the measured concentrations (slopes for modeled vs. measured were 1.06 1.08), but this deviation is quite small and is likely the result of heterogeneous diffusion coefficients within the synthetic soil, combined with unknown initial conditions for the modeled soil.

Comparisons of the measured Keeling plot and Gradient isotopologue fluxes with modeled flux showed good correspondence. For the Keeling plot the regression of modeled vs. measured isotopic composition of flux yielded a slope of 0.93 with a standard error of 0.065 (r^2=0.96). For the Gradient method two results exist for isotopic flux compositions, the flux between the deep and shallow (D-S) soil sampling tubes, and the flux between the shallow sampling tube and the atmosphere (S-A). For the D-S flux, regressions yielded a slope of 0.96 (S.E.=0.11; r^2=0.91) and 0.91 (S.E.=0.061; r^2=0.97) for the S-A flux. There is also good correspondence between the three methods, with Keeling vs. D-S and S-A slopes of 1.04 (S.E.=0.069; r^2=0.97) and 0.97 (S.E.=0.041; r^2=0.99), respectively and a D-S vs. S-A slope of 0.88 (S.E.=0.097; r^2=0.91). In all cases the slope was not significantly different from 1 nor was the y-intercept significantly different from 0‰ ($p<0.01$). Please note that the PP approach could not be tested on this apparatus because no production occurs within the synthetic soil and therefore the second order derivative of concentration is equal to zero.

4.5.6 Field Results

During September, 2011, approximately three days of subsurface isotopic data were collected from the girdled site (Julian Days 261-263) and three days of data from the intact site (Julian Days 264-266). The raw time series measurements of CO_2 concentrations and isotopic composition at the two sites are shown in Figure 4.6.

Figure 4.7 presents a time series of soil $\delta^{13}CO_2$ flux calculated with the Keeling plot and Gradient methods (data from the PP method are presented in Fig. 4.9). The intact site displayed an average soil respiration signature of -30.3‰, estimated by the Keeling plot approach, and -30.0‰, -30.4‰ and -30.6‰ for the three Gradient approach depths (G1 shallowest, G2 - middle and G3 - deepest, respectively). The

girdled site had a similar average of -30.7‰, estimated by the Keeling plot approach, and -30.4‰, -30.9‰ and -24.8‰ for the three Gradient approach depths (G1, G2 and G3, respectively). Note that the standard deviation for G3 was quite high (-11.0‰) owing to the fact the concentration gradients deep in the soil were small and therefore measurement errors become larger (as was discussed in Section 3.4). For comparison, isotopic measurements of bulk soil organic matter from the same region range between about -28‰ to -26‰ over the first 50 cm soil depth (Risk et al., 2009) and it is not uncommon to observe biochemical fractionation during respiration of several per mil (Moyes et al., 2010).

The only notable event in the time series happens at around Julian Day 262.1, where a large spike occurs in the isotopic composition of flux at G2 concurrent with a small depletion in the isotopic flux recorded in G1 (Figure 4.7). These deviations appear to be related to a rain event that likely decreased soil diffusivity in the top few cm of soil leading to a buildup of CO_2 in the soil profile. These short time-scale dynamics therefore do not likely reflect a change in the isotopic signature of production, but rather a transient, non-steady state change in the isotopic composition of flux. The spikes are not present in isotopic fluxes calculated with the other methods, but this is not wholly unexpected. For the Keeling plot method, the rain related changes in signature is likely overprinted by the fact that the Keeling plot represents the integration of flux at all depths, and therefore is not likely to pick up events happening on smaller spatial scales. The PP method (discussed further below, shown in Figure 4.9) also did not pick up these observed deviations, but the method is also intended to detect changes in the isotopic signature of production, which are not expected to change due to physical disturbances to the gas transport regime.

While there appears to be some variation in the signature of flux with depth using the gradient approach, the Keeling plot intercept values themselves are unable to show this because they represent a depth averaged isotopic flux composition estimate. It was clear from the modelling results, however, that if the isotopic signature of production (and thus surface flux, under steady state conditions) changes with depth, then the Keeling plot would display curvature. Keeling plot residuals were isolated from the data, displayed in Figure 4.8, to see if this phenomenon could be observed. The figure shows that the residuals from both sites display a curvature (grey lines

are spline interpolations to make it easier to follow the data) that is consistent with what is expected from the modeled results.

Finally, the PP approach was used to estimate the isotopic signature of production in the soil profile two PP points, PP1 (shallow) and PP2 (deep), shown in Figure 4.9. Unfortunately, as was predicted in the error analyses for this method, the error due to analytical uncertainty overpowers the environmental signal, and leads to a high uncertainty in PP estimates of isotopologue production rates.

4.6 Summary and Recommendations

4.6.1 Summary Comparison of Theoretical, Lab and Field Data

Theoretical data showed that the Keeling plot approach was likely to deviate from the true isotopic flux composition values in situations where the stable isotopic signature of production varied as a function of depth. In contrast, the gradient and PP approaches did not suffer from this bias, as they allow separate treatment of each depth interval, and therefore captured this depth dependent variability. However, the gradient and PP approach suffer when the depth increment between measurements becomes too coarse, and therefore does not allow for accurate estimation of the derivate of the CO_2 isotopologue profile. While it was not attempted here, this could possibly be counteracted by using measurements that are then interpolated to finer depth intervals using fitting functions, although this is likely to introduce its own complications as the fits may not capture the true shape of the profile.

During the lab testing of the Keeling plot and gradient methods on the FG apparatus good correspondence was found between finite-difference calculations of $\delta^{13}CO_2$ flux, and estimates with the Gradient and Keeling methods. One notable result was a slightly worse performance (compared to model results) for methods where near-surface concentration and isotopic compositions were used in calculations (Keeling plot and S-A gradient). This is likely due to either non-diffusive processes operating near the experimental soil surface (i.e. advection) or because of high-resolution temporal changes in the atmospheric isotopic composition and CO_2 concentrations.

Field results for the Keeling plot displayed a curvature consistent with the predicted curvature associated with depth varying CO_2 isotopologue production.

While the curvature in these field results is only slight, allowing a reasonable estimate of the depth-integrated signature of isotopologue flux using the method, Keeling plots from other sites with strong production gradients may be affected more significantly. Curvature related error will be further exacerbated by the reality that the highest density of points in the Keeling plot are likely to occur at small values of $1/CO_2$, biasing the linear fit toward deeper isotopologue compositions and eliminating any evidence of high-temporal resolution changes near the soil surface. The Gradient method performed well against the Keeling plot approach in the field, mirroring what was seen in the lab experiments, but with minor deviations due to the depth variation in isotopologue production and/or event-driven changes in the gas diffusion regime. The PP approach seemed to provide reasonable estimates for isotopic signatures of production, but as is evident from the uncertainty analysis, the amplification in error is much too large given the current instrument resolution and the relatively weak second-order CO_2 gradients at this field site. Where second-order gradients are significantly stronger, the PP approach may perform better and yield useful information about depth variation in isotopologue production.

4.6.2 Davidson's δ_J Method

While the δ_J method of Davidson and Trumbore (1995) was not formally considered in the analysis and results, some conclusions can be drawn about the method based on the results shown in the Keeling plot and Gradient method sections. It is first important to note that the δ_J method is derived assuming steady-state conditions, like all other methods presented in this manuscript. Davidson′s derivation of the δ_J method is a special case of the Keeling plot (or the Gradient approach), where only two points are used in the calculation of isotopologue flux. By design, the δ_J method always uses the atmospheric concentration and isotopic composition as one set of its constraining variables. The second set is chosen by the user to be the concentration and isotopic composition at any arbitrary depth in the soil profile. Again, because the δ_J method is a special case of the Keeling plot, it can therefore be expected to display similar biases and sensitivities as those presented in Section 3.1 and Figures 4.1 and 4.2. For the δ_J method these biases are likely to be slightly different than the Keeling plot estimated biases because the Keeling plots analyzed in section 3.1 have

significantly larger data densities (n>>2) and therefore the linear regression will tend to be biased more toward the region where data density is highest (for example, in Figure 4.3 most of the linear regression would be biased to the domain of 1/[CO_2] ¡ 5e-4 ppm-1).

4.6.3 Considerations for Field Measurements

Several recommendations can be made on the placement of soil gas sampling tubes or wells given the various constraints and errors inherent in each method presented in this manuscript.

For the Keeling plot method it is important to choose sampling depths in such a way that the Keeling plot is not artificially biased due to higher data density on the near-zero end of the 1/[CO_2] domain. This statistical bias (unrelated to the non-linearity bias shown in section 3.1) occurs as a result of the strong increase in CO_2 concentration in the shallow soil, which is generally followed by a leveling-off of CO_2 concentrations in the deeper soil, often observed in field studies (Davidson and Trumbore, 1995; Breecker et al., 2012). For Keeling plot data, it is therefore important that users choose sampling depths such that the data will have an even spacing on the 1/[CO_2] axis of the Keeling plot, and such that no region of the 1/[CO_2] domain has a significantly higher data density than any other region. This could be done in post-processing (i.e. by excluding data points from the Keeling plot data set) or it may be accomplished in the field, given a reasonable a-priori estimate of what the soil CO_2 gradient looks like.

For example if the CO_2 concentration with depth were to resemble an exponential function, users might consider placing a large percentage of their soil sampling tubes or probes near the surface, and the remaining sampling could be done at depth. The exact placement of these sampling tubes is difficult to prescribe, but a rough estimate could be obtained by integration of the CO_2 concentration profile and normalizing this integral to 100% (or 1). Then by integrating over specific depth intervals, for example 0-5 cm, users could determine how much of the integral lies in that region, compared to the 100% total. For example, assume that 40% of the integral lies in the 0-5cm region, and that a possible 10 sampling tubes/wells can be deployed with depth in the soil, then 4 out of those 10 tubes should go in the top 5 cm of the soil,

if possible given size constraints and other logistical concerns.

For the gradient method, similar approach to the Keeling plot method would be advocated. Here the best results, with the least error, are obtained when the point-to-point soil CO_2 concentrations are quite different (i.e. when the gradient is strong). The procedure for locating sampling tubes would therefore be similar to that outlined above, where the majority of the gas sampling tubes/well should be placed near the surface, with fewer at depth where CO_2 gradients are generally quite small. Again, the approach for the PP method would be similar, although somewhat more complex as users would need to define regions where the second order gradient (curvature in the CO_2 profile) was large. This may not be as straight forward as in the first two cases, and would likely require more detailed information about the soil profile than can be assumed without previous measurements. The optimization of sampling depths PP approach may therefore be best done in post-processing.

While these guidelines presented here will likely serve reasonably in most cases, the placement of gas sampling tubes/wells and analysis of field data is complex. Care should be taken to ensure that the measurements and analysis procedures are suitable on a case-by-case basis.

4.7 Conclusions

These theoretical, lab, and field results show that all three methods are robust for specific applications. The least error-prone of all of the methods, considering both calculation uncertainty and bias due to incorrect assumptions (i.e. linearity of model, steady state conditions), is the Flux Gradient approach. This approach offers both low uncertainty compared to the PP method and is able to resolve depth dependent isotopic signatures, unlike the Keeling plot that instead provides a depth-integrated signature. Given current analytical uncertainty, it is unlikely that the PP methods will provide good results except in cases where isotopic source signatures are very different (i.e. C3-C4 transitional systems or labeled soils). Future improvement in the accuracy and precision of laser based field techniques may allow the PP method to be applied more widely. Finally, the Keeling plot method is statistically robust when the soil has a relatively homogenous isotopic source signature with depth. However when this assumption is violated an inherent bias is observed in the mixing model

that may skew results. The Keeling plot provides a depth-integrated signature, which may be useful in some circumstances, but will be a hindrance in studies where the signatures are expected to vary with depth.

Bear in mind that the treatment of each of these subsurface techniques assumes that soil CO_2 concentrations are at or near steady state. Luckily, the concentration and stable isotope measurements during the field study were relatively stable, but this may not always be the case, and any non-steady state diffusion will cause a bias in all three methods. This potential non-steady state bias should always be considered when dealing with isotopic data, as it can cause significant deviation from the true isotopic signatures. Fortunately, for the gradient and production profile methods, non-steady state versions of the diffusion equation may be used to compensate for these effects (see Parent et al. (2013); Goffin et al. (2014)), however care should be taken as these non-steady state approaches are more complicated and have inherent errors associated with the determination of pore space and soil gas diffusivity.

Table 4.1: Parameter ranges for production damping depth (η), isotopic production damping depth (σ), atmospheric CO_2 concentration (C_{atm}), atmospheric $^{12}CO_2/^{13}CO_2$ ratio (R_{atm}, expressed in delta notation for ease of interpretation), soil total CO_2 production rate (P_0), soil diffusivity (D), difference in isotopic signature of production between the top and bottom of the soil profile (R_d) and isotopic signature at the bottom of the soil profile (R_b).

Parameter	Range (units)
η	0.01-0.5 (m)
σ	0.01-0.5 (m)
C_{atm}	250-750 (ppm)
R_{atm}	(-3)-(-13) (‰)
P_0	0.1-10 (μmol m^{-2} s^{-1})
D	10^{-5}-10^{-10} (m^2 s^{-1})
R_d	[-19]-20 (‰)
R_b	[-14]-[-34] (‰)

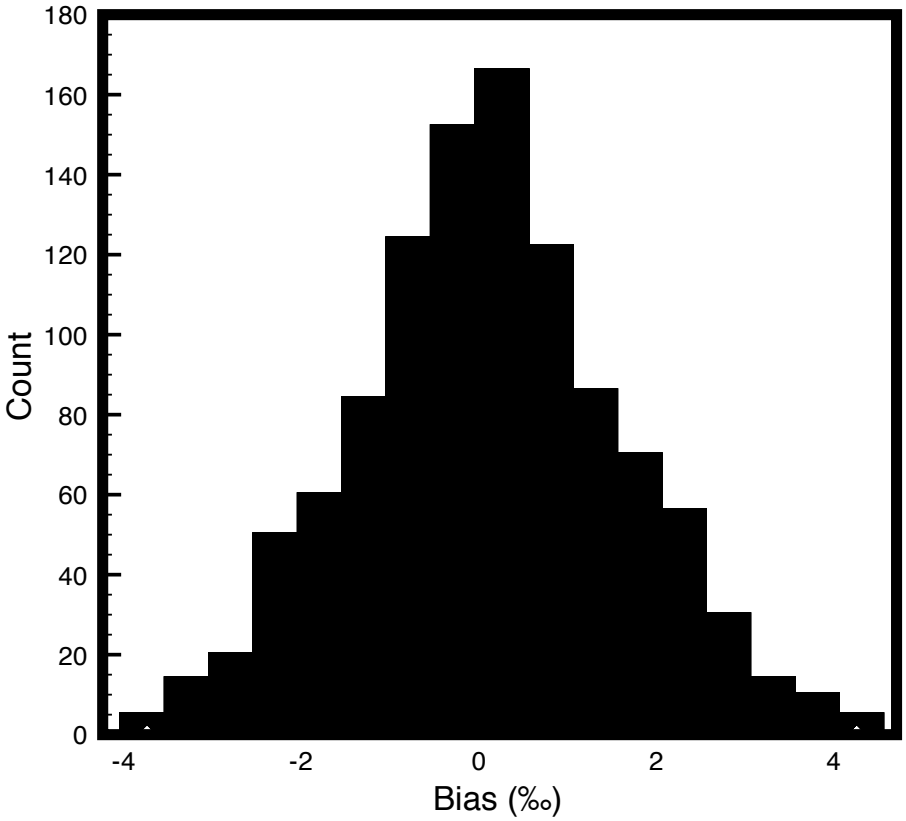

Figure 4.1: Histogram of Keeling plot bias for 1000 randomly sampled parameter sets. Mean bias is 0.09‰ with a standard deviation of 1.38‰.

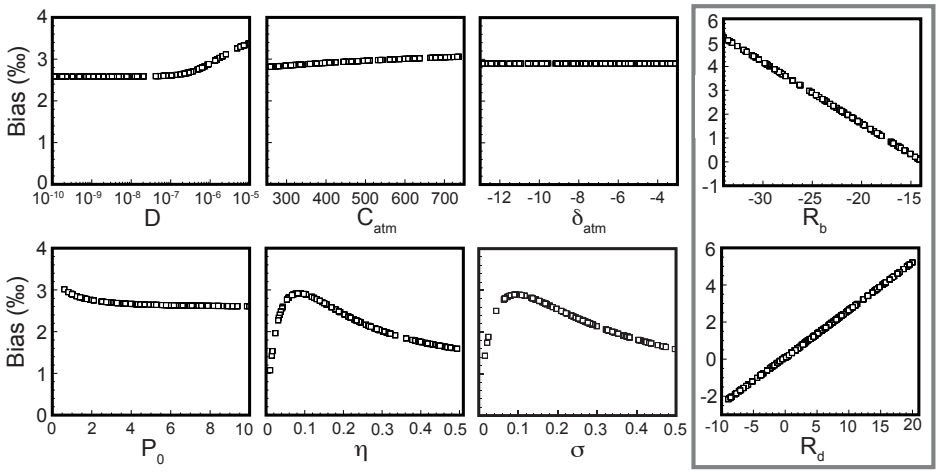

Figure 4.2: Sensitivity analyses for Keeling plot bias. Except for the parameter on the x-axis in each plot, all other values were fixed as follows: D=1×10^{-6} m^2 s^{-1}; C_{atm}=380 ppm; δ_{atm}=-8‰; R_b=-25‰; R_d=11‰ (both expressed in delta notation for ease of reading); P_0=1 μmol m^{-2} s^{-1}; η=0.1 m; σ=0.1 m. R_b and R_d are set inside of the grey box to draw attention to the fact that the axes are different from the other plots. Please note that the model parameters used in the sensitivity test are characteristic of the higher end of the bias shown in Figure 4.1 and with different model parameter sets the sensitivity magnitudes will be dampened.

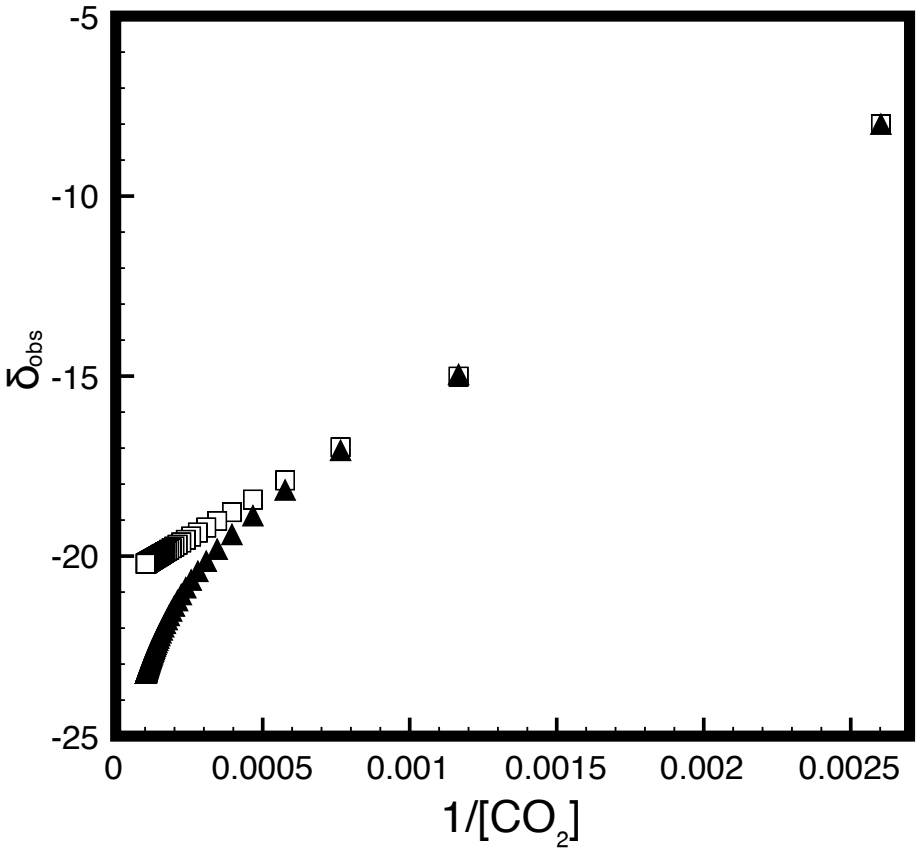

Figure 4.3: Keeling plots for a linear and non-linear case with δ_{obs} in units of ‰ and $1/[CO_2]$ in units of 1/ppm. For both simulations D=5×10^{-6} m^2 s^{-1}; C_{atm}=380 ppm; δ_{atm}=-8‰; P_0=1 μmol m^{-2} s^{-1}; η=0.2 m; σ=0.1 m. For the curve shown in square symbols R_b=-25‰ and R_d=0‰ and the Keeling plot bias is negligible. For the curve shown in triangular symbols R_b=-25‰ and R_d=16‰ and the Keeling plot bias is 3.35‰. Clearly the change in isotopic signature with depth causes non-linearity in the Keeling plot.

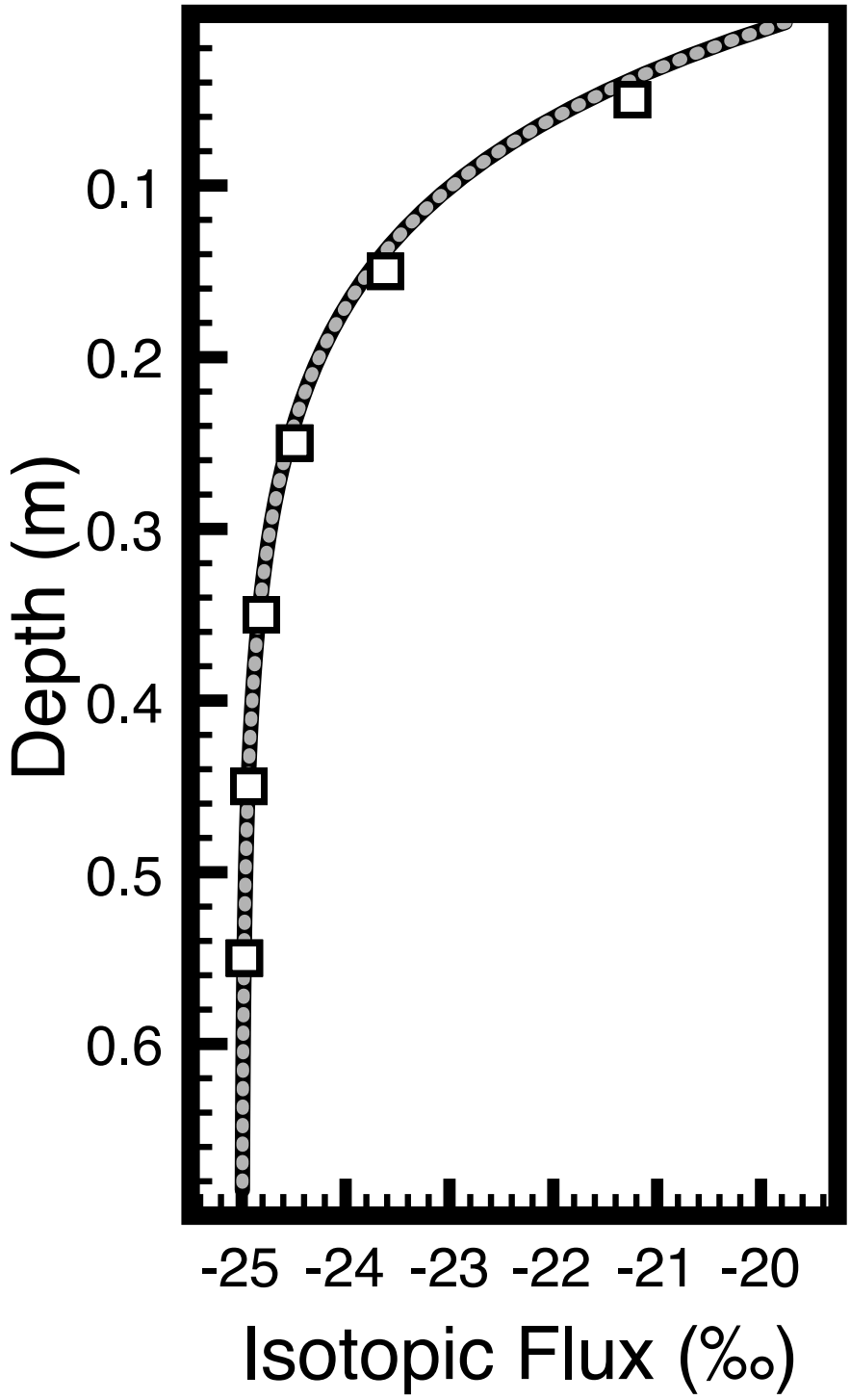

Figure 4.4: Example figure for isotopic flux (‰) estimated using the gradient approach with sampling intervals of 1 cm (gray dashed line) and 10 cm (squares). For comparison the true isotopic flux is shown as the solid black line.

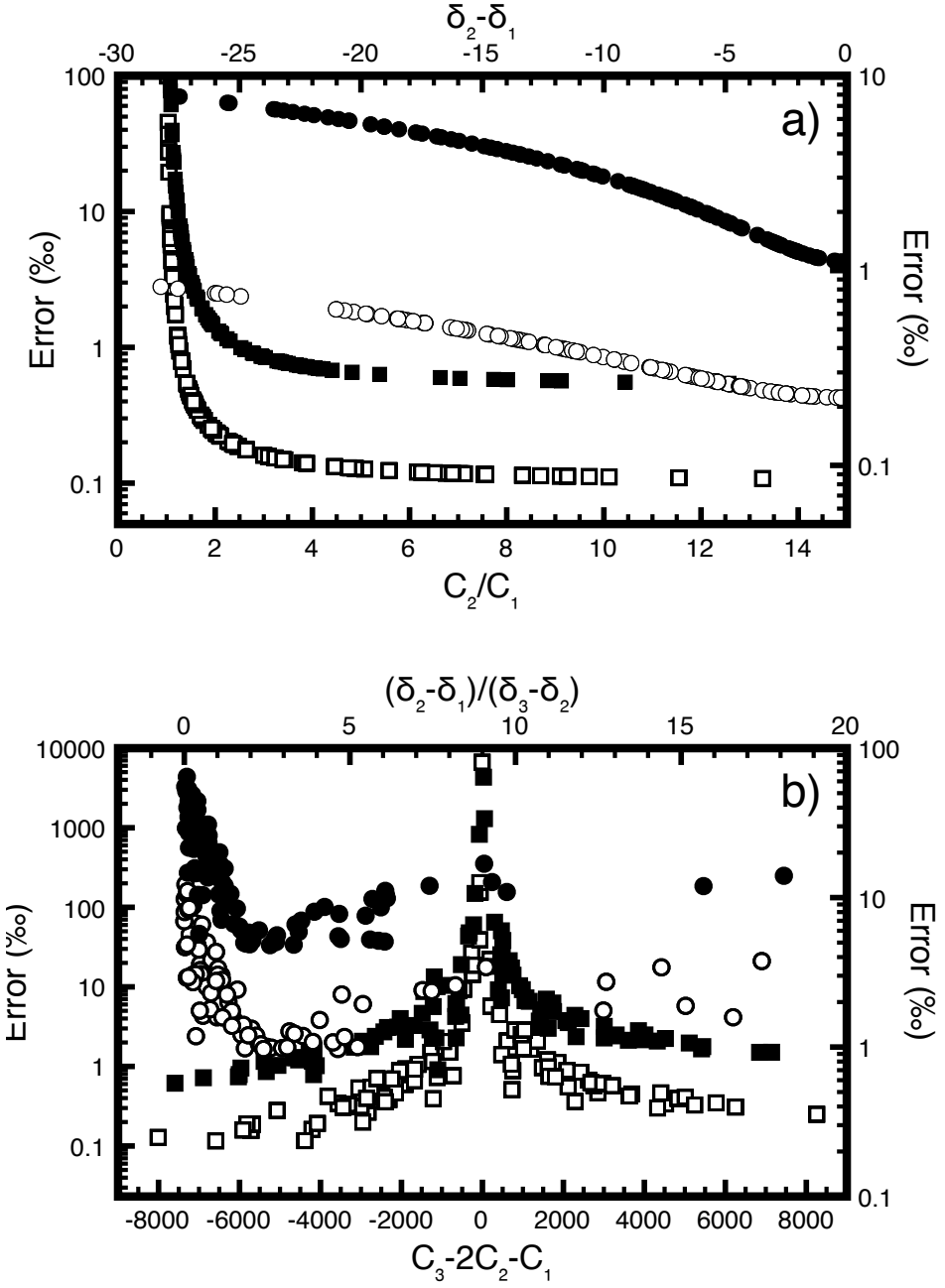

Figure 4.5: a) Error in estimated isotopic signature (‰) for the gradient method for measurement errors (standard deviations of reading) of 1% CO_2 and 0.1‰ $\delta^{13}C$ (open symbols) and 5% CO_2 and 0.5‰ $\delta^{13}C$ (closed symbols). Square symbols show the error rate for different ratios of C_2 to C_1 (left y-axis) and circles show the error rate for varying differences between δ_2 and δ_1 (right y-axis). b) Error in estimated isotopic signature (‰) for the production profile (PP) method for measurement errors (standard deviations of reading) of 1% CO_2 and 0.1‰ (open symbols) and 5% CO_2 and 0.5‰ (closed symbols). Note that because of the form of the equation, as the second order gradient converges to zero the error is asymptotic to infinity.

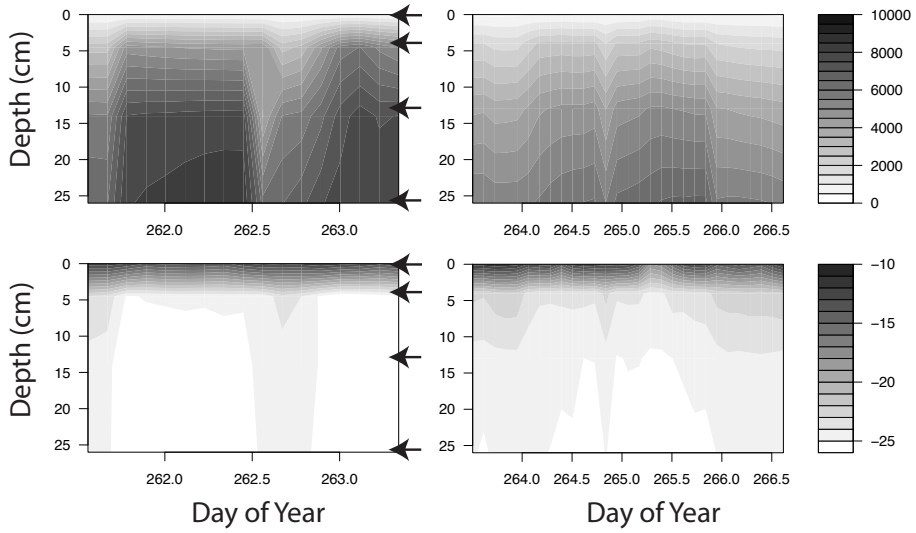

Figure 4.6: Contour plots of soil CO_2 concentration (top row, ppm) and isotopic composition (bottom row, ‰) for the girdled (left column) and intact sites (right column). Approximate locations of the 4 subsurface sampling tubes are show on the plots with arrows although this varied slightly between the two sites.

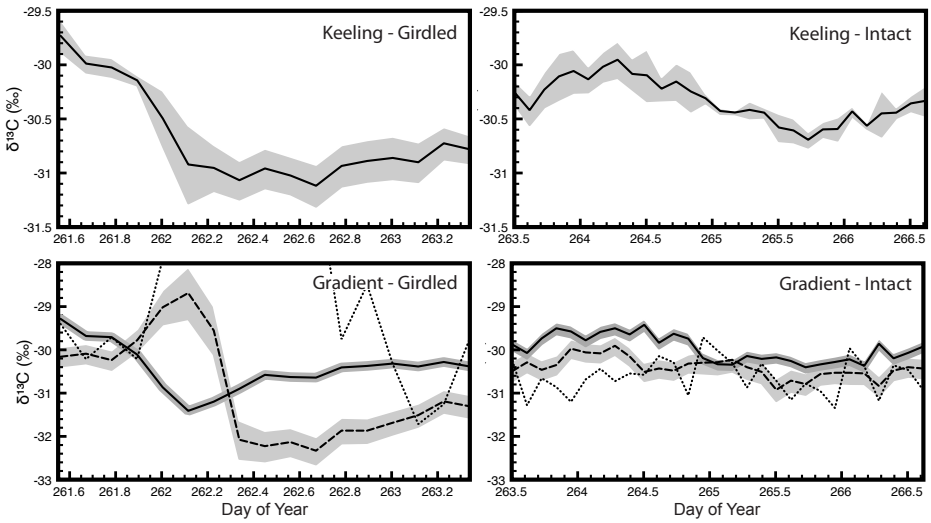

Figure 4.7: Keeling plot intercepts (top row) and gradient estimates (bottom row) of the CO_2 isotopologue flux signature form the girdled (left column) and intact (right column) sites. For the gradient approach, the solid line is G1, the shallowest set of gas wells, the long dashed line is the middle set of wells (G2) and the dotted lined is the deepest set of wells (G3). Error is shown in shaded regions, for the Keeling plot error is expressed as the standard error of the intercept estimate using OLS, for the gradient measurements the error is calculated using uncertainty analysis.

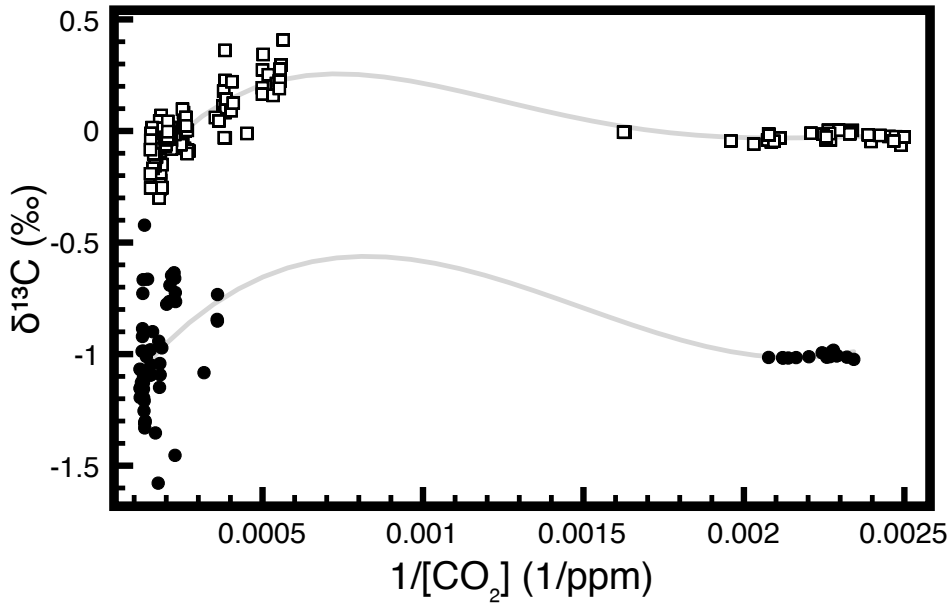

Figure 4.8: Keeling plot residuals for the intact (open squares) and girdled (closed circles) sites. Note the distinct curvature, likely driven by a non-constant isotopic signature of production with depth. For clarity, the data from the girdled site has been shifted down a constant -1‰.

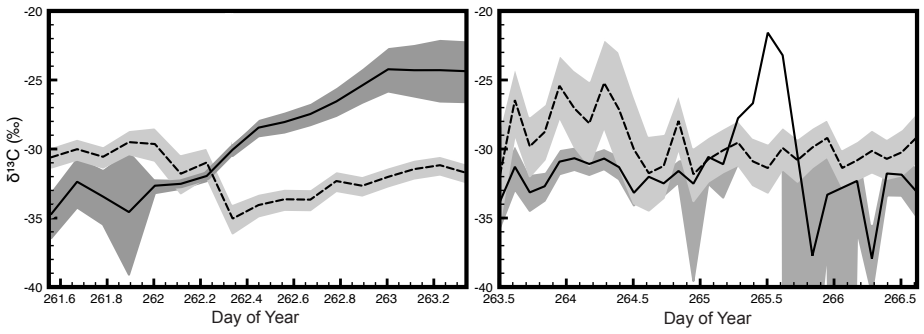

Figure 4.9: Production profile estimates for the girdled (left) and intact (right) sites at both PP1 (shallowest, solid line) and PP2 (deepest, dashed line). Error bounds were calculated using uncertainty analysis and for the intact sites, the bounds were removed from the spike around Julian Day 265.5 for plot scaling purposes.

Chapter 5

A Numerical Examination of $^{14}CO_2$ Chamber Methodologies for Measuring Fluxes at the Soil Surface

5.1 Preamble

This chapter describes a three-dimensional model analysis of several commonly used chamber methods for measuring the radiocarbon content of soil respiration. Authorship is as follows: Jocelyn Egan, Nick Nickerson, Claire Phillips and Dave Risk. Jocelyn Egan is lead author on this manuscript, however we each contributed equally to the research. Jocelyn wrote the bulk of the manuscript and performed some analyses on the model data. I was responsible for the model development, data collection and interpretation as well as the error analyses. Claire Phillips and Dave Risk both served as supervisors to this work. A version of this manuscript has been submitted to Radiocarbon and is currently in review.

5.2 Abstract

Radiocarbon is an exceptionally useful tool for studying soil-respired CO_2, providing information about soil turnover rates, depths of production and the biological sources of production through partitioning. Unfortunately, little work has been done to thoroughly investigate the possibility of inherent biases present in current measurement techniques, like those present in $\delta^{13}CO_2$ methodologies, caused by disturbances to the soil's natural diffusive regime. This study investigates the degree of bias present in four radiocarbon sampling chamber methods using a three-dimensional numerical soil-atmosphere model. The four chambers were tested numerically with varying $\Delta^{14}C$ and $\delta^{13}C$ of production, collar lengths, soil biological productivity rates, and soil diffusivities. The static and Iso-FD chambers showed almost no isotopic measurement bias, significantly outperforming dynamic chambers which demonstrated biases exceeding ±200‰ across all modeled scenarios. The study

also showed that ^{13}C and ^{14}C diffusive fractionation are not a constant multiple of one another, but that the $\delta^{13}C$ correction still works in diffusive scenarios because changes to $^{13}C/^{12}C$ diffusive fractionation are not large enough to impact measured $\Delta^{14}C$ values during chamber equilibration.

5.3 Introduction

The radioactive isotope of carbon (^{14}C) is an exceptionally useful tool for studying soil-respired CO_2, providing information about the biological sources of production through partitioning (Gaudinski et al., 2000; Trumbore, 2000; Hahn et al., 2006; Schuur and Trumbore, 2006; Hicks-Pries et al., 2013). In recent years many studies have utilized partitioning techniques, both physical and isotopic, as tools for separating sources of soil respiration, to understand how soil respiration sources may be affected by the future changing climate (Hanson et al., 2000; Högberg et al., 2001; Bhupinderpal-Singh et al., 2003; Lee et al., 2003; Kuzyakov, 2006; Moyes et al., 2010b; Bond-Lamberty et al., 2011; Drake et al., 2012; Gomez-Casanovas et al., 2012; Risk et al., 2012). Source partitioning with isotopes has an advantage over physical partitioning as it typically involves less disturbance than physical partitioning. However, in natural abundance isotopic partitioning studies, radiocarbon can be more useful than $\delta^{13}C$. The difference between autotrophic and heterotrophic $\delta^{13}C$ signatures of soil-respired CO_2 is only few permil (‰) (except in C3-C4 vegetation shifted studies), whereas there can be a much larger separation between $\Delta^{14}C$ source signatures, especially in systems where slow decomposition or long-term storage accentuate isotopic differences (Trumbore, 2006). A peak in atmospheric $\Delta^{14}C$ signatures in 1963 caused by nuclear weapons testing has allowed researchers to utilise this ^{14}C as a tracer to distinguish whether carbon substrates were utilized pre- or post-bomb, because post-bomb signatures are distinctive given their relative ^{14}C enrichment (Levin and Hesshaimer, 2000). Autotrophic respiration consumes new carbon, so its radiocarbon signature will reflect current atmospheric $^{14}CO_2$ signatures, whereas heterotrophic signatures will reflect the age of the substrates that the heterotrophs consume, which can very new or quite old (Gaudinski et al., 2000; Phillips et al., 2013).

Despite the potential utility of $^{14}CO_2$ as a tool for investigating soil-respired CO_2, little work has been done to thoroughly investigate the possibility of biases

inherent to existing measurement techniques, because high cost of analysis naturally drives researchers to focus effort on the ecological aspect of studies, rather than error/uncertainty testing. In the case of $\delta^{13}C$, Cerling et al. (1991) demonstrated that although mass differences in ^{12}C and ^{13}C isotopologues cause ^{12}C to diffuse 1.0044 times faster through the soil, if the soil is at a diffusive steady-state, the $\delta^{13}C$ of production should match the $\delta^{13}C$ of surface flux. Soils are, however, rarely at a diffusive steady-state, and research looking at $\delta^{13}C$ has shown that non-steady-state transport fractionations can be induced by soil transport (Nickerson and Risk, 2009a; Moyes et al., 2010b) and headspace sampling (Ohlsson, 2010), where non steady-state chambers can induce a bias of 4 ‰ and steady-state chambers up to 15 ‰ caused by lateral diffusion (Nickerson and Risk, 2009c). The magnitude of these biases could potentially overprint the $\delta^{13}CO_2$ signatures of biological flux (Kayler et al., 2010; Phillips et al., 2010; Moyes et al., 2010b), making partitioning difficult. These time-dependent fractionations ("dynamic fractionations"; Nickerson and Risk (2009a)) will also be present and will potentially cause biases when attempting to measure $^{14}CO_2$, because like $^{13}CO_2$, $^{14}CO_2$ has a different diffusion coefficient than $^{12}CO_2$, diffusing 1.0088 times slower (Wang et al., 1994) . Currently, to calculate $\Delta^{14}C$, researchers use $\delta^{13}C$ to correct for potential steady-state mass dependent fractionations (Stuvier and Polach, 1977). The $\delta^{13}C$ correction will not account for dynamic fractionations however, because the assumption that ^{14}C fractionation is a constant multiple of ^{13}C fractionation may not hold in typical measurement conditions where the soils are rarely at steady-state. It will therefore be of interest to the radiocarbon community to know if steady-state and non steady-state chamber methods used to measure $\Delta^{14}C$ of soil-respired CO_2 induce bias in a similar magnitude to those of $\delta^{13}C$.

In order for researchers to understand bias that may have been induced by $^{14}CO_2$ chamber methodologies in past studies, and to help decide which chamber method is the most robust for future studies, a three-dimensional numerical soil-atmosphere model was used to simulate soil-atmosphere-chamber exchange of CO_2 isotopologues, including $^{14}CO_2$, to compare isotopic signatures measured by various chamber methods to the natural steady-state. The effect of chamber-specific methods, such as pump speed, stable isotopic signature calculations and mixing model type, were also considered to determine the effect of these on the final estimates of stable

and radioactive isotopic signature. Additionally, the effects of equilibration on the change in the $\Delta^{14}C$ of soil flux was examined, and the amount by which $^{13}CO_2$ and $^{14}CO_2$ fractionation factors differ from one another during chamber equilibration. This was done in order to understand whether a biased stable isotopic value for flux used as a correction in the calculation of $\Delta^{14}C$ will affect the results. Predictions are that the static and dynamic chambers will induce more bias measuring $\Delta^{14}C$ of flux than they do for $\delta^{13}C$, as the diffusive fractionation factor for $^{14}CO_2$ is larger, and furthermore because additional error could be related to the $\delta^{13}C$ correction in a dynamic environment (Stuvier and Polach, 1977).

5.4 Methods

5.4.1 Soil-Atmosphere Model

A three-dimensional coupled soil-atmosphere-chamber model was used to explore biases inherent in current $^{14}CO_2$ chamber methodologies. The model simulates CO_2 produced in the soil, diffusion to the atmosphere and in some cases into a chamber set on the surface of the modeled soil. Model physics and structure are further described in Creelman et al. (2013).

Each carbon isotopologue of CO_2 ($^{12}CO_2$, $^{13}CO_2$ and $^{14}CO_2$) is treated separately with its own specific atmospheric concentration, production and diffusion rate. In the case of $^{14}CO_2$ it is assumed that radioactive decay is negligible over the timescale of the measurements (Cerling et al., 1991; Wang et al., 1994). This method produces model runs for each isotopologue where the resulting concentrations and fluxes of each isotopic species are used to calculate total CO_2, $\delta^{13}C$ and $\Delta^{14}C$ signatures of the soil CO_2 and surface flux at each time step.

Simulations were performed using a range of soil production rates, soil diffusivity coefficients, chamber collar lengths and $\delta^{13}C$ and $\Delta^{14}C$ signatures of biological production (Table 4.1). In all model scenarios the $\delta^{13}C$ and $\Delta^{14}C$ of the atmosphere were 8.8 ‰ and 100 ‰, respectively, which are in the range of most typical environments.

5.4.2 Calculation of Isotopic Signatures

The model output calculates isotopic signatures using del notation. δ^{13}C is presented in ‰ as:

$$\delta^{13}C = \left(\frac{R_s}{R_{std}} - 1\right) \times 1000 \tag{5.1}$$

where R_s is the $^{13}C/^{12}C$ ratio of the sample and R_{std} is the $^{13}C/^{12}C$ ratio of the PDB standard. Δ^{14}C is also presented in ‰ using the value of fraction modern (FM) of the sample:

$$\Delta^{14}C = (FM - 1) \times 1000 \tag{5.2}$$

FM is calculated using A_s, the measured activity of the sample, where the model outputs a $^{14}C/^{12}C$ ratio and A_{abs}, which is equivalent to A_s to the fourth decimal place (Southon, 2011). A_{abs} is the measured activity of the oxalic acid standard, with a model parameterization value of $1.2511e^{-12}$, where A_{abs} is 0.95 times the activity of the oxalic acid standard in 1950, corrected to a δ^{13}C of -19‰ (Stuvier and Polach, 1977):

$$FM = \frac{\left(\frac{A_s}{A_{abs}}\right)\left(1 - \frac{25}{1000}\right)^2}{\left(1 + \frac{\delta^{13}C_s}{1000}\right)^2} \tag{5.3}$$

where $\delta^{13}C_s$ is the δ^{13}C signature of the sample, and 25 is the sample activity corrected for δ^{13}C isotopic fractionation.

5.4.3 Chamber Descriptions

Four chambers were chosen from past studies, for testing in the model environment, and these chambers are described below, but also represented graphically in Figure 5.1. All calculations to determine chamber δ^{13}C and Δ^{14}C from the model output were performed using the equations provided in the original studies. All results were converted to Δ^{14}C notation in cases where the results were calculated in per cent modern or fraction modern to facilitate comparison of the results between different chambers.

Dynamic Chambers

Dynamic chambers are a type of steady-state chamber often employed in soil flux studies, including radiocarbon studies. They theoretically minimize alteration to the

soil CO_2 concentration gradient by flowing atmospheric air or a CO_2 free gas through the chamber, which decreases the headspace concentration in order to maintain chamber concentrations closer to the surrounding atmosphere (Rayment and Jarvis, 1997). Two dynamic chambers were chosen to model. Chamber A has a volume of $\sim$ 11.5 L and is based on the chamber presented in Gaudinski et al. (2000). It utilized a pump with a constant flow rate of 0.5 L/min, and soda lime column to decrease the headspace concentration, regardless of the soil flux value at the time of measurement, just before diverting the flow path into a molecular sieve trap to collect 2 mg C for radiocarbon analysis. For modelling purposes it was assumed that the soda lime and molecular trap were perfectly efficient at removing CO_2 from the air stream, and further, that there was no isotopic fractionation associated with either process. Stable isotopic (δ^{13}C) signatures of surface flux were used to correct the Δ^{14}C of the headspace for mass-dependent fractionation and for incomplete stripping of atmospheric CO_2 during the trapping period using the following equation:

$$X = \frac{\delta^{13}C_{measured} - \delta^{13}C_{soil}}{\delta^{13}C_{atmosphere} - \delta^{13}C_{soil}} \tag{5.4}$$

where X is the fraction of remnant atmospheric air in the sample, $\delta^{13}C_{atmosphere}$ is the atmospheric δ^{13}C signature and $\delta^{13}C_{soil}$ is the δ^{13}C signature of soil respiration. Δ^{14}C is then calculated as:

$$\Delta^{14}C_{soil} = \frac{\Delta^{14}C_{measured} - X \times \Delta^{14}C_{atmosphere}}{1 - X} \tag{5.5}$$

Chamber B differs from Chamber A by using an infrared gas analyser in-line with the pump to determine the flux rate into the headspace prior to CO_2 scrubbing. The pump speed was adjusted to match the soil flux rate, thereby maintaining near natural steady-state conditions in the chamber (Schuur and Trumbore, 2006). The same equations for X and $\Delta^{14}C_{soil}$ that were used for Chamber A were also used for Chamber B. The modeled volume (11.5 L) and surface area (0.058 m^2) of Chamber B were based on the values used in Schuur and Trumbore (2006).

Static Chamber

Static chambers are a type of non-steady-state chamber in which CO_2 from soil is allowed to accumulate without interference in the chamber headspace. In the case

of ^{14}C sampling, after the accumulation period, a molecular sieve trap or sampling flask captures gas from the headspace. For modelling scenarios, the static chamber, Chamber C, is based on the one presented by Hahn et al. (2006). The chamber was deployed for 30 minutes to allow CO_2 accumulation in the headspace before sampling, thereby ensuring that enough CO_2 is captured in the sampling flask for Δ^{14}C analysis. Isotopic signatures (δ^{13}C and Δ^{14}C) of flux were calculated using a standard 2-source mixing model:

$$\delta^{13}C_{respired} = \frac{\delta^{13}C_{chamber} \times [CO_2]_{chamber} - \delta^{13}C_{freeair} \times [CO_2]_{freeair}}{[CO_2]_{chamber} - [CO_2]_{freeair}} \tag{5.6}$$

where $\delta^{13}C_{respired}$ is the stable isotopic signature of respired CO_2, $\delta^{13}C_{chamber}$ and $[CO_2]_{chamber}$ are the stable isotopic signature and CO_2 concentration of chamber air, respectively, and , $\delta^{13}C_{freeair}$ and $[CO_2]_{freeair}$ are the stable isotopic signature and CO_2 concentration of the free air (near-surface atmosphere). A similar equation can be constructed to calculate the chamber estimate respired radiocarbon activity, which can then be converted to Δ^{14}C signature (Hahn et al., 2006).

Isotopic-Forced Diffusion Chamber

The Isotopic-Forced Diffusion (Iso-FD) chamber is similar in design to a dynamic chamber, but rather than mass outflow, the air exchange between the chamber and atmosphere is regulated by a diffusive membrane (Figure 5.1D). This chamber design has been tested as a tool for sampling $\delta^{13}CO_2$ (Nickerson et al., 2013) and is based on the Forced Diffusion (FD) bulk CO_2 flux chamber presented by Risk et al. (2011). Here its theoretical performance for Δ^{14}C sampling was evaluated (Chamber D). The principle of FD operation is to restrict exchange between the chamber and the atmosphere passively using membranes of known diffusivities. The offset in CO_2 concentration and isotopic abundance between the chamber and the surrounding atmosphere can then be related to soil flux rate and composition. Membranes of particular diffusivities and panel surface areas were chosen for the specific chamber geometry, in order to obtain the ideal amount of CO_2 build-up in the chamber for measurements with the smallest error (Creelman et al., 2013). As is the case with dynamic chamber, FD chamber interior concentrations are an intermediate between the atmosphere and soil, so the technique uses an atmospheric reference chamber,

which has no soil inlet, alongside the FD chamber, to correct for changes in the atmospheric concentrations in the mass balance equation. For this configuration, both the chamber and atmospheric reference were coupled to molecular sieve traps. Δ^{14}C signatures were calculated from the model output for this chamber using the following equation, modified from that presented in Nickerson et al. (2013):

$$\frac{F_{in}^{14C}}{F_{in}^{12C}} = \frac{1}{1.0088} \frac{\left(C_{FD}^{14C} - C_{atm}^{14C}\right)}{\left(C_{FD}^{12C} - C_{atm}^{12C}\right)} \tag{5.7}$$

where $F_{in}^{14C}/F_{in}^{12C}$ is equivalent to A_s and can be represented in del notation with equations 5.2 and 5.3, 1.0088 is the diffusive fractionation factor for $^{14}CO_2$ (Wang et al., 1994), and C_{FD} and C_{atm} are the concentrations of each isotopologue present in the Iso-FD chamber and atmospheric reference chamber. Again, for consistency the modeled volume and surface area of the chamber were 11.5 L and 0.058 m^2, respectively.

5.4.4 Error Analysis

Propagation of uncertainty (error) was calculated for the chambers using the standard partial derivative form (Ku, 1966):

$$s_f = \sqrt{\left(\frac{\partial f}{\partial x}\right)^2 s_x^2 + \left(\frac{\partial f}{\partial y}\right)^2 s_y^2 + \left(\frac{\partial f}{\partial z}\right)^2 s_z^2 + ...} \tag{5.8}$$

where s_f is the absolute error in the function f, which is composed of the variables x, y, z, and so on, each with variable specific uncertainty s_x, s_y, s_z. For the specific equations used for each chamber see Appendices A and B.

5.5 Results & Discussion

5.5.1 Dynamic Chambers (A and B)

Simulations of Chamber A, which used a constant pump speed of 0.5 L/min, showed that headspace CO_2 concentrations could differ substantially from the atmosphere unless the soil flux rates were well-matched to the CO_2 scrubbing rates. Assuming steady-state concentrations at the soil surface were initially in the range of $\sim$ 380-1000 ppm CO_2, using a constant pump speed of 0.5 L/min, the optimal soil flux

rate into the chamber should be 2-6 μmol m^{-2} s^{-1} in order to maintain steady-state concentrations. When soil flux rates fall in this range, the simulation results showed ^{14}C errors were at their lowest (Figure 5.2A). This suggested that the main driver of error for Chamber A is the constant pump rate, which is unable to maintain a near steady-state concentration in the chamber during measurement, when fluxes are too low or too high to match the rate of CO_2 removal.

$\Delta^{14}CO_2$ errors were exacerbated when Chamber A was placed on virtual porous soils, and where flux rates were low (Figure 5.2A). This was due to a combination of over-pumping and lateral diffusion, a problem which is exacerbated in soils of high soil diffusivity. In low diffusivity soils, however, the chamber performed relatively well because of the limited feedback between the chamber and the soil, which created an effective 1D diffusion pathway eliminating lateral diffusion errors. Results from simulations with varying soil collar depth helped support the interpretation that lateral diffusion contributed to ^{14}C measurement errors. When the collar depth was increased at fixed levels of diffusivity and production, $\Delta^{14}C$ errors decreased linearly (data not shown).

The apparent ^{14}C errors associated with Chamber A were also affected by similarity in isotopic values of soil CO_2 production and atmospheric CO_2. This increase in bias arose because of the chamber based errors in the estimate of X (Eq. 5.4). Any error in the chamber estimate becomes amplified because the two $\delta^{13}C$ values are differenced in the denominator of the calculation. As the $\delta^{13}C$ signature of production became more enriched, overestimates in $\Delta^{14}C$ began to appear in lower porosity soils (i.e. soils with higher moisture/bulk density). Similarly, biases also became larger in porous soils with low biological productivity (Figure 5.2A).

When the specified $\Delta^{14}CO_2$ of production in the model was more enriched, in porous soils with low fluxes, the chamber-measured signatures were more depleted than they should have been. When the signatures of production were more depleted, the chamber yielded more enriched values than it should have (Figure 5.3A). Near the point where soil production and atmospheric $\Delta^{14}CO_2$ were similar, the error in measurement was minimized. This minimized error was likely an apparent minima caused by the lack of distinction between source and ambient $\Delta^{14}CO_2$ signatures.

For chamber B, in which pump speed was regulated to hold CO_2 at a constant

concentration, modeled errors varied with soil porosity and productivity. In soils with high diffusivity, $\Delta^{14}CO_2$ was slightly underestimated, and slightly overestimated in soils with low diffusivities and low biological production rates. The adjustment of the pump speed to the ambient atmospheric concentration led to the maintenance of near steady-state concentrations in the chamber during the measurement period, with some deviation from the true steady-state caused by soil diffusivity (and therefore soil collar length) and the slight stratification of the model atmosphere, causing the slight over- and underestimates.

Similar to the Chamber A results, if the $\delta^{13}C$ signature of production and atmosphere were considerably different, $\Delta^{14}CO_2$ deviations from true isotopic value occurred in soils with low productivity. However, as the $\delta^{13}C$ signature of production approached that of the atmosphere (more enriched), deviations similarly became apparent in highly productive soils as well (Figure 5.2B). In soils when the $\Delta^{14}CO_2$ of production was depleted relative to the atmosphere, Chamber B gave slight overestimates of $\Delta^{14}CO_2$. If the $\Delta^{14}CO_2$ of production were to be enriched more than the range of the model simulations, the chamber would produce slight underestimates across all diffusivities, again in soils with lower productivity (Figure 5.3B).

Error analysis performed on Chamber A and B provided further explanation for deviations in isotopic signature when the inputted isotopic signature of production was similar to that of the atmosphere.

Uncertainty estimates for the dynamic chambers consist of two necessary calculations, the first of which is the uncertainty in X, the fraction of remaining atmospheric air in the chamber. Uncertainty in X is largely driven by the difference between $\delta^{13}C_{atm}$ and $\delta^{13}C_{soil}$ (the denominator in Equation 5.4), where large differences between the two values minimize the error. Shown in Figure 5.4(a) are uncertainty estimates in X (unitless) as a function of $\delta^{13}C_{atm}$ and $\delta^{13}C_{soil}$ for measurement errors of 0.1‰ (open squares) in all of the variables in Equation 5.4, and 0.3 ‰ measurement error in $\delta^{13}C_{atmosphere}$ and $\delta^{13}C_{measured}$ and 1.0 ‰ measurement error in $\delta^{13}C_{soil}$ (circles).

Figure 5.4(b) shows the subsequent $\Delta^{14}C_{soil}$ uncertainty estimates as a function of X for measurement errors of 10 ‰ in $\Delta^{14}C_{measured}$ and $\Delta^{14}C_{atmosphere}$, and error in X of 0.01, displayed in the open squares. While the value of X drives the largest uncertainty

in the estimate of $\Delta^{14}C_{soil}$, the spread in the uncertainty data at a given X value is linearly related to the absolute difference between $\Delta^{14}C_{measured}$ and $\Delta^{14}C_{atmosphere}$. Also shown is the uncertainty for measurement errors of 50 ‰ in $\Delta^{14}C_{measured}$ and $\Delta^{14}C_{atmosphere}$, and error in X of 0.1 (grey circles).

Based on the uncertainty analysis, measurements of $\Delta^{14}C$ done with a dynamic chamber can be made with much more certainty in scenarios where the atmosphere values of $\delta^{13}C$ and $\Delta^{14}C$ are different (5 ‰ in the case $\delta^{13}C$) from the $\delta^{13}C$ and $\Delta^{14}C$ of the soil.

As demonstrated through the comparison of Chambers A and B in Figures 5.2 and 5.3, Chamber B performed consistently better than Chamber A, in all simulated scenarios. This increased performance can be attributed to maintenance of near steady-state conditions through the adjustment of pump speed. With a constant pump speed there is an optimal range of flux rates when Chamber A can perform well, but it is less applicable than Chamber B across a large range of soil conditions.

5.5.2 Static Chamber

Previous numerical modelling by Nickerson and Risk (2009c) showed a bias towards underestimation of $\delta^{13}CO_2$ using static chamber designs. The combination of a strong concentration gradient between the soil and chamber, and diffusive fractionation caused $^{12}CO_2$ to accumulate in the chamber before $^{13}CO_2$, and tended to make the signature of the chamber headspace more negative than the equilibrium condition, as $^{13}CO_2$ caught up (please refer to Figure 3 of Nickerson and Risk (2009b)). One expects to see similar results when this type of chamber is used to measure $^{14}CO_2$, but this was not observed (Fig. 5.4). In fact, the static chamber design (Chamber C) performed very well over the whole range of soil conditions, with the deviation from the true isotopic signature of $\Delta^{14}CO_2$ flux being in the numerical error bounds of the model ($\sim$ 1 ‰ $\Delta^{14}CO_2$).

Based on subsequent analytical modelling of the chamber isotopic signatures (data not shown), it seems that the marginally increased fractionation factor for $^{14}CO_2$ (1.0044 for $^{13}CO_2$ and 1.0088 for $^{14}CO_2$) is balanced by a very low $\Delta^{14}CO_2$ concentration gradient, leading to a smooth transition from atmospheric to respired isotopic signatures for $\Delta^{14}CO_2$. When the fractionation factor was increased in the

analytical model, the non-linear mixing behaviour that was noted in the $\delta^{13}CO_2$ simulations became evident in the $\Delta^{14}CO_2$ results. Similarly, if the fractionation factor was held at 1.0088, but the absolute abundance of $^{14}CO_2$ increased, with $^{12}CO_2$ and $^{13}CO_2$ staying the same, (and thus the gradients between soil and atmosphere became larger) the non-linear mixing behaviour also became evident.

Figure 5.5 shows the probable uncertainty for the static chamber. It assumes two error rates, the first with a measurement error of 10 ‰ (5 ‰ AMS error and 5 ‰ sampling and extraction error; (Phillips et al., 2013)) in $\Delta^{14}C$ signatures and 1 % in bulk gas concentrations (open squares), and the second with measurement errors of 50 ‰ in $\Delta^{14}C$ signatures, and 5 % in bulk gas concentrations (open circles). Most of the uncertainty in the estimation of the radiocarbon fluxes with this chamber comes from the ratio of the final (C2) and initial concentrations (C1). Like the dynamic chambers, measurements made with the static chamber can be done with more certainty when the final chamber measurements are at least twice the value of the initial chamber measurements.

5.5.3 Isotopic-Forced Diffusion Chamber

In all simulations with the Iso-FD chamber, the predicted isotopic signature of flux was very near the prescribed value. Similar to the static chamber results, the Iso-FD results were within the numerical error bounds of the model ($\sim$ 1 ‰ $\Delta^{14}CO_2$). The accuracy of this chamber can be attributed to the fact that a diffusive steady-state was maintained during the measurement period, avoiding isotopic disequilibrium created by other chamber designs. Simulations showed similar behaviour with $\Delta^{14}CO_2$ as for the $\delta^{13}CO_2$ embodiment of this chamber in Nickerson et al. (2013), where a slight build-up of concentration in the chamber headspace produced concentration and isotopic plumes directly below the chamber. However, despite these plumes sampling errors were negligible.

Assuming the fractionation factor for the Iso-FD calculations is constant and known, the uncertainty for the Iso-FD chamber takes the same form as the static chamber and uses the same calculation variables (Figure 5.5). For the Iso-FD chamber, most of the uncertainty in the estimation of the radiocarbon fluxes comes from the ratio of concentration measurements in soil chamber and atmospheric

chamber measurements, which can be thought of as equivalent to the ratio of the final (C2) and initial concentrations (C1) for the static chamber. As was the case with the dynamic chambers and static chamber, measurements made with Iso-FD chambers have more certainty when the soil chamber concentration measurements are at least twice the value of the atmospheric chamber measurements.

5.5.4 Other Considerations

There are also some other possible biases that should be considered, which are not included in the model. The simulated soil in the model is at steady-state. It has a constant biological production, soil diffusivity and isotopic signatures of production through depth, so no non steady-state (NSS) effects (Nickerson and Risk, 2009a) are included in the results. A non-uniform soil with varying diffusivities and production rates through depth, would provide different model results than the uniform modeled soil (Venterea and Baker, 2008). Nickerson and Risk (2009a) and Moyes et al. (2010b) demonstrated the effects of dynamic fractionations, where soil features and processes such as biological production, diffusivity, pore space and atmospheric concentrations, which have temporal variation, will induce NSS transport conditions that lead to transient changes in the isotopic composition of the soil CO_2 flux. The main driving force behind this is the difference in the diffusion rate between CO_2 isotopologues, which will be slightly amplified when considering $^{14}CO_2$ due to its increased mass. The measured values could therefore be further biased on top of the potential biased induced by the chamber method. Despite the counterbalance of low ^{14}C concentration gradients shown in the case of the static chamber, these dynamic fractionation effects should be investigated further in order to ensure that they are not causing bias.

The model also assumes that the method used to sample from the chamber, molecular sieve trap or sampling flask, is completely efficient and causes no fractionations. $\Delta^{14}C$ static chamber methods can include a capillary tube that attaches a sampling flask to the chamber (Hahn et al., 2006). This method could cause a potential fractionation, where the lighter isotopologue, $^{12}CO_2$, would travel faster than $^{14}CO_2$ through the capillary tube, so the resulting mixture in the sampling flask could potentially be more depleted than the mixture in the chamber headspace. It would be ideal to obtain a quick sample from the chamber, for example, by attaching the sampling flask under

vacuum to the chamber and sucking up 1 L of sample immediately. This configuration would be similar to how the model simulates sampling from the chamber and would work well for the two-point mixing model used for static chambers (Hahn et al., 2006). Another issue not addressed in the model surrounding the static chamber and Iso-FD chamber methods is the possible stratification of the chamber headspace gas because of the lack of mixing. In the case of the static chamber, concentration stratification as well as the capillary tube used in the Hahn et al. (2006) chamber, fractionation could lead to an even greater bias in the captured gas in the sampling flask, where the gas traveling along the tube is not well mixed. For the Iso-FD chamber, there could also be problems with using molecular sieve traps, because as CO_2 is removed from the chamber headspace, it decreases the concentration in the chamber, causing the chamber to no longer be at steady-state. In the case of dynamic chambers, if the soda lime trap and molecular sieve trap have different trapping efficiencies, then the expected advantage of having a truer steady-state, will not be met. If the soda lime and molecular sieve traps also fractionate ^{14}C, then the already biased results found in this study will be further biased.

Although the Iso-FD and static chambers perform well under all simulated conditions in the numerical model, there are some other things that needed to be considered. The two samples needed for these chambers (soil or final chamber measurement, and atmosphere or initial chamber measurement) have to be different enough from one another, to keep the error rate within an acceptable range (Figure 5.6). For the Iso-FD chamber this means choosing an appropriate membrane and for the static chamber this means leaving the chamber deployed for a long enough period of time. Therefore, in scenarios where the soil chamber or final concentrations and the atmospheric chamber or initial chamber concentrations are quite similar, these chambers would not be ideal.

The $\delta^{13}C$ correction used to account for potential steady-state mass-dependent fractionations in $\Delta^{14}C$ assumes that $^{14}CO_2$ and $^{13}CO_2$ diffusive fractionation are a constant multiple of one another. Figure 5.6 (a & b) demonstrates that this assumption is incorrect. In a time series view of chamber equilibration (Figure 5.6a), $^{14}C/^{12}C$ does not behave in the same way as $^{13}C/^{12}C$ (lateral diffusion), except for when the radiocarbon signatures of production and atmosphere are equal (50 ‰

in this case). In Figure 5.6b, chamber equilibration mixing lines of $^{14}C/^{12}C$ and $^{13}C/^{12}C$ demonstrate whether a difference in mixing behaviour between the stable and radioactive isotopes exists. A hook in the line signifies a different mixing behaviour for ^{13}C and ^{14}C, whereas a straight line means the mixing behaviour is the same for both isotopes. Despite the differences in mixing behaviours between the isotopes (fractionation no longer a constant multiple), the changes to the fractionation factor multiple between the two isotopes does not change enough for lateral diffusion biases in the stable isotope to have an impact on the radiocarbon result.

5.6 Conclusions

These model simulations provided insights that were unexpected. The static chamber has low theoretical sampling errors, where it was expected to induce a greater bias than dynamic chambers, like in the case of $\delta^{13}C$ (Nickerson and Risk, 2009c). Based on the simulation results, the static chamber and Iso-FD chamber performed the best under all soil conditions, but other considerations should be made when choosing a sampling method, including aspects not included in the model simulations, such as the choice between molecular sieve traps or sampling flasks, the cost, and the length of time needed to sample the chamber. This modelling exercise also showed that the assumption that stable and radiocarbon isotopic diffusion fractionations are a constant multiple of one another through time is not universally true, especially under non-steady state conditions. The $\delta^{13}C$ correction still stands because the changes to the diffusive fractionation during equilibration are not large enough to impact $\Delta^{14}C$, but researchers should still be cautious, and this should be investigated further for non steady-state soil conditions.

Table 5.1: The ranges of model parameters input for the $\Delta^{14}CO_2$ chamber simulations.

Variable	**Ranges**
Diffusivity (m^2/sec)	10^{-8}, 5x10^{-8}, 10^{-7}, 5x10^{-7}, 10^{-6}, 5x10^{-6}
Productivity (μmol/m^2/sec)	0.1, 1, 5
Collar Length (cm)	0, 2, 4, 8
δ^{13}C of production (‰)	-30, -20, -15
Δ^{14}C of production (‰)	-500, -200, 0, 200, 500

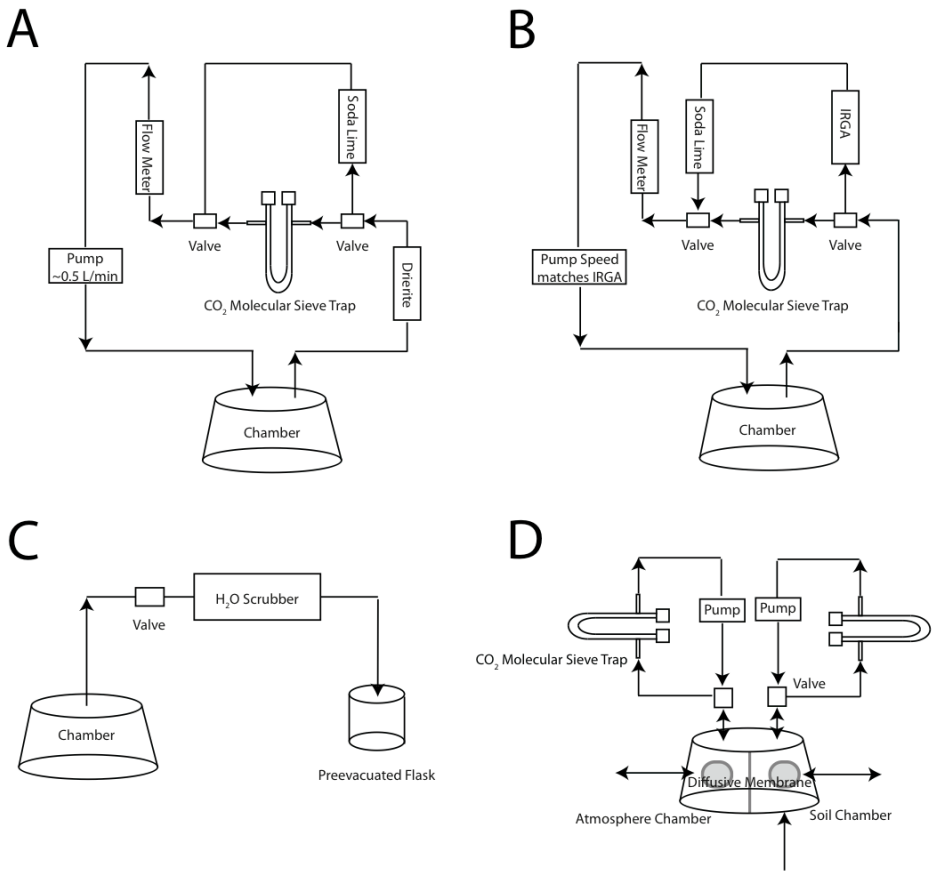

Figure 5.1: The four chambers that were modeled. A) A dynamic chamber with a pump speed set to 0.5 L/min (Gaudinski et al., 2000). B) A dynamic chamber with a pump speed that matches the soil flux rate (Schuur and Trumbore, 2006). C) A static chamber where CO_2 accumulates for 30 minutes prior to sampling (Hahn et al., 2006). D) A diffusion driven dynamic chamber, which is based on the Isotopic Forced Diffusion (Iso-FD) design for a $\delta^{13}C$ chamber presented in Nickerson et al. (2013).

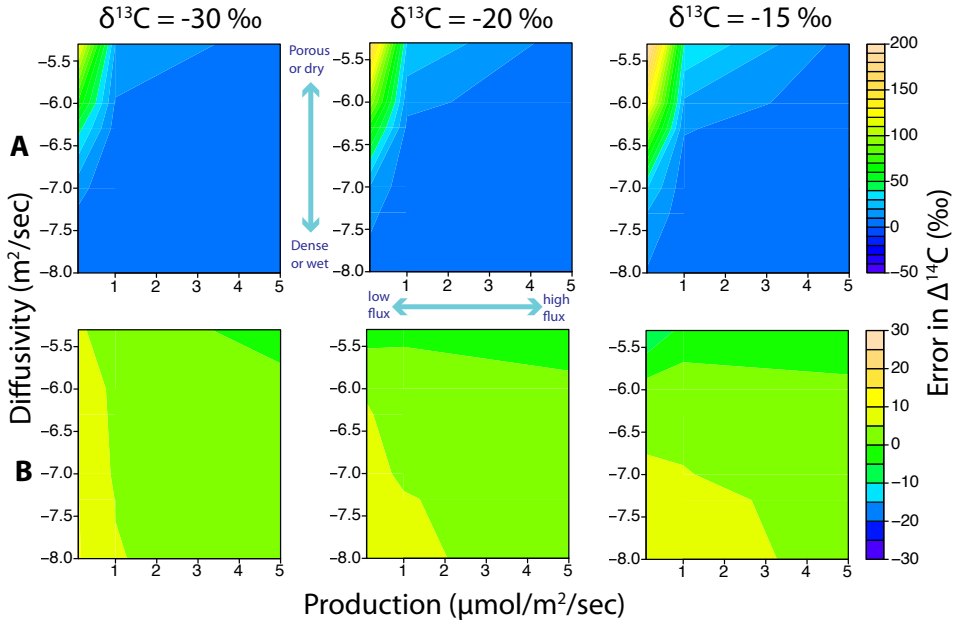

Figure 5.2: Contour plots of model output error of Δ^{14}C (‰) of Chamber A (panel A) and Chamber B (panel B) with a simulated Δ^{14}C of production of - 200 ‰, collar length of 2 cm, and δ^{13}C of production of - 30 ‰, - 20 ‰ and -15 ‰ in columns 1, 2 and 3, respectively. Soil production (μmol/m^2/sec) is on the x axis and log of soil diffusivity (m^2/sec) on the y axis. Note scale differences between Chamber A and Chamber B.

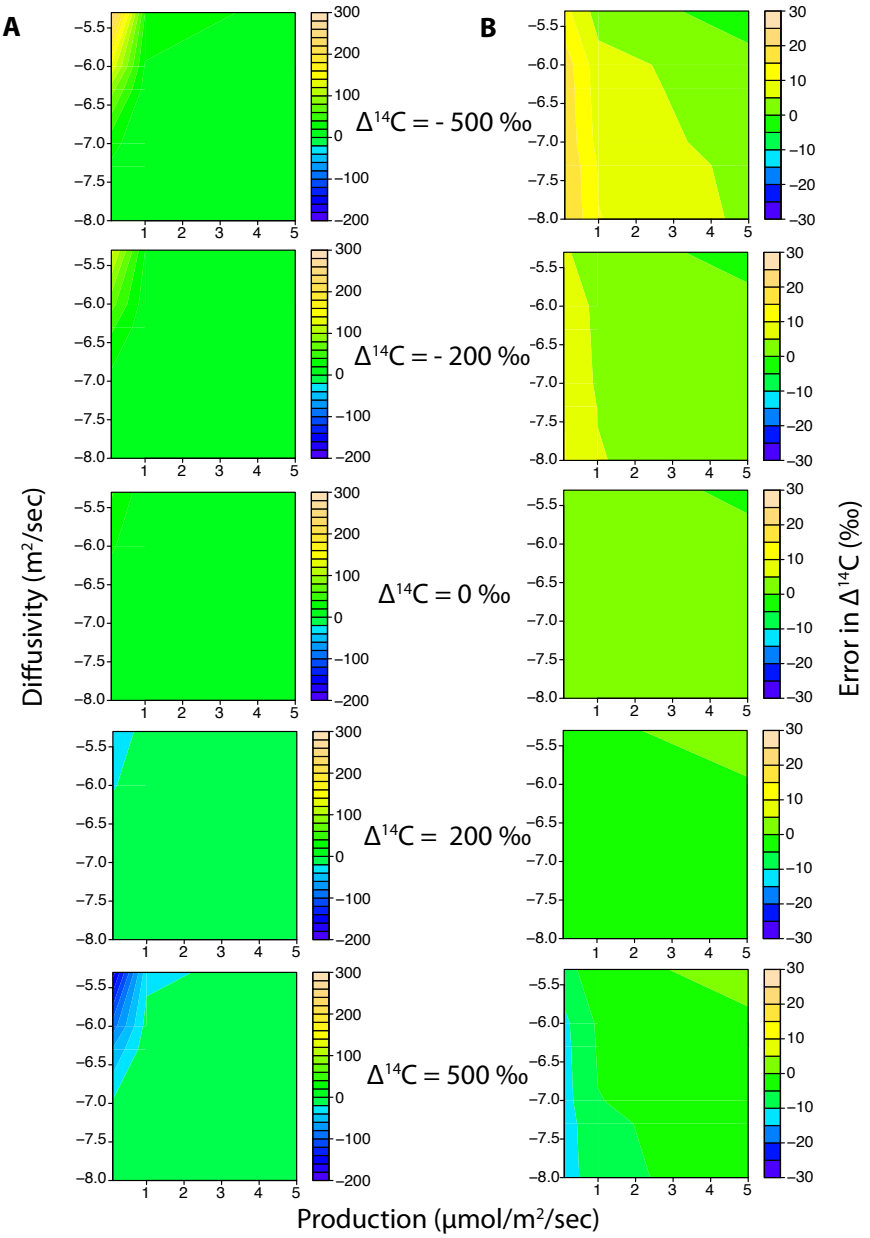

Figure 5.3: Contour plots of model output error of $\Delta^{14}C$ (‰) of Chamber A (column A) and Chamber B (column B) with a simulated $\delta^{13}C$ of production of - 30 ‰, collar length of 2 cm, and $\Delta^{14}C$ of production of - 500 ‰, - 200 ‰, 0 ‰, 200 ‰ and 500 ‰ in rows 1, 2, 3, 4 and 5 respectively. Soil production (μmol/m^2/sec) is on the x axis and log of soil diffusivity (m^2/sec) on the y axis. Note scale differences between Chamber A and Chamber B.

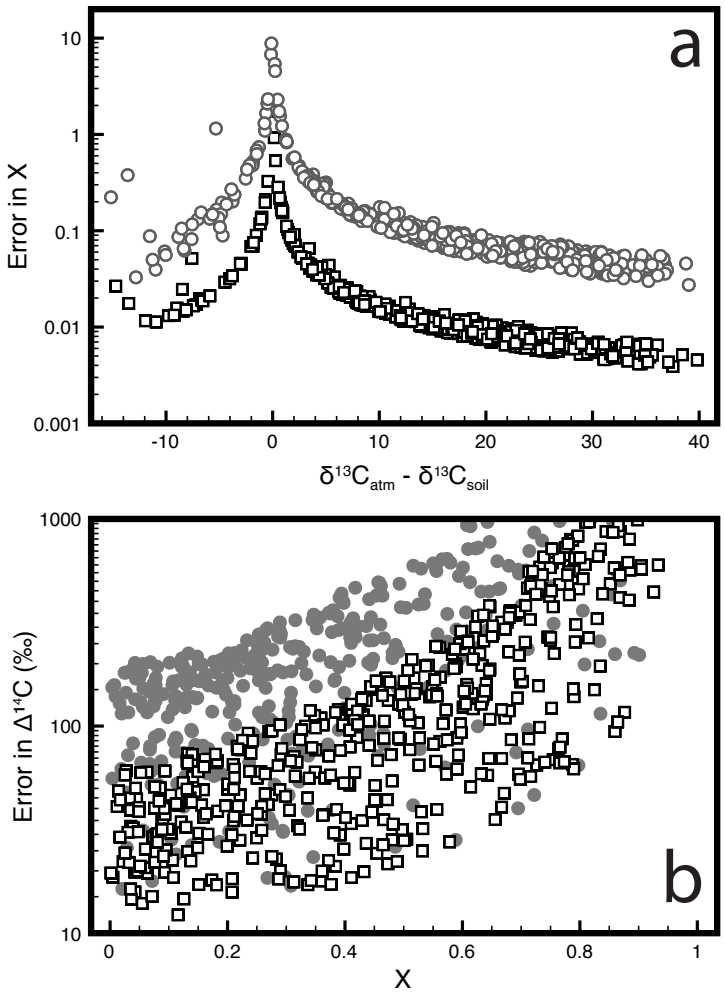

Figure 5.4: Uncertainty estimates for the dynamic chambers. (a) Uncertainty estimates in X (unit less) as a function of $\delta^{13}C_{atm}$ and $\delta^{13}C_{soil}$ for measurement errors of 0.1‰ in all of the variables in Equation 5.4 (open squares), and 0.3 ‰ measurement error in $\delta^{13}C_{atmosphere}$ and $\delta^{13}C_{measured}$ and 1.0 ‰ measurement error in $\delta^{13}C_{soil}$ (circles). (b) $\Delta^{14}C_{soil}$ uncertainty estimates as a function of X for measurement errors of 10 ‰ in $\Delta^{14}C_{measured}$ and $\Delta^{14}C_{atmosphere}$, and error in X of 0.01 (open squares), and the uncertainty for measurement errors of 50 ‰ in $\Delta^{14}C_{measured}$ and $\Delta^{14}C_{atmosphere}$, and error in X of 0.1 (grey circles).

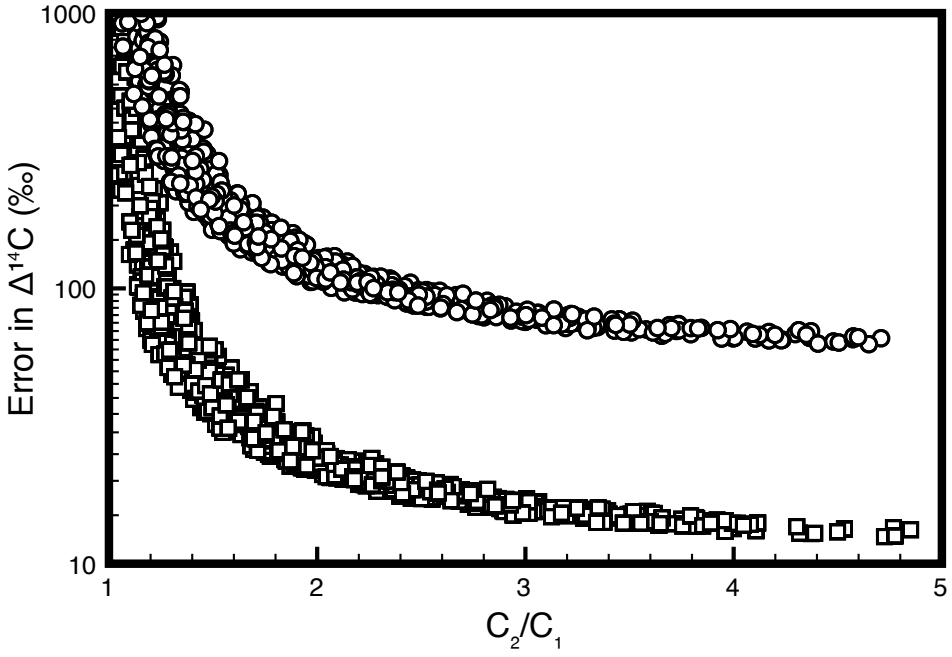

Figure 5.5: The probable uncertainty for static and Iso-FD chambers assuming two error rates, the first with a measurement error of 10 ‰ in Δ^{14}C signatures, and 1 % in bulk gas concentrations (open squares), and the second with measurement errors of 50 ‰ in Δ^{14}C signatures, and 5 % in bulk gas concentrations (open circles). C1 and C2 are the initial and final concentrations for the static chamber, or for the Iso-FD chamber, they are equivalent to the atmospheric chamber and soil chamber measurements.

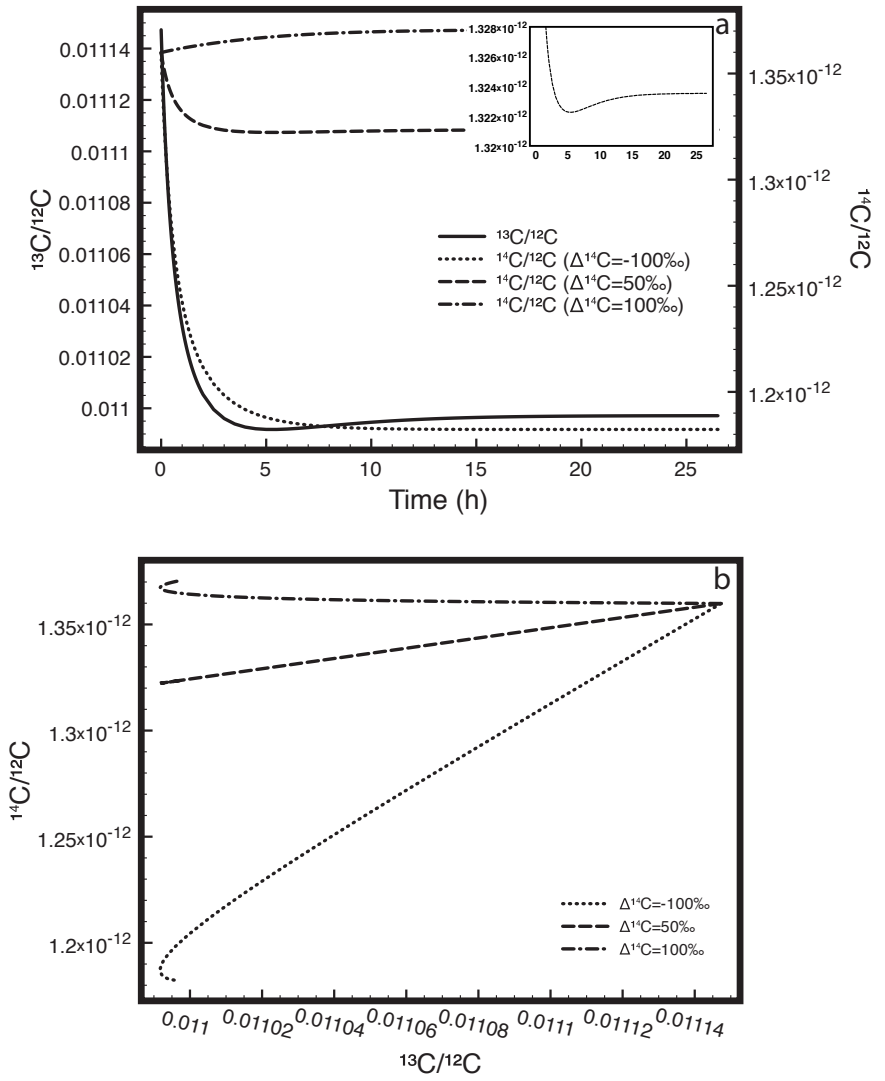

Figure 5.6: (a) Time series of chamber equilibration for stable carbon and radiocarbon ratios. Note that the $^{13}C/^{12}C$ ratio overshoots the equilibrium value between 2 and 10 hours due to lateral diffusion. This behavior is not present in the radiocarbon ratios except for when the radiocarbon signature of production and the radiocarbon signature of the atmosphere (50 ‰ for this model simulation) are equal. The insert is a y-axis zoom of the $\Delta^{14}C$ 50 ‰ line to display the overshooting behaviour. (b) Radiocarbon and stable carbon ratio mixing lines during chamber equilibration for three $\Delta^{14}C$ signatures. A hook in the line signifies a different mixing behaviour for ^{13}C and ^{14}C, whereas a straight line means the mixing behaviour is the same for both isotopes.

Chapter 6

Interpreting Diel Hysteresis Between Soil Respiration and Temperature

6.1 Preamble

This chapter presents a model analysis showing how diel hysteresis patterns, observed by many researchers during field based measurements, are likely a result of lags between soil temperature and soil CO_2 efflux. Authorship on this paper is as follows: Claire Phillips, Nick Nickerson, Dave Risk and Barbara Bond. Claire Phillips was the principal investigator in this work and was responsible for running the model and writing the bulk of the manuscript. I co-developed the theory, computational model and helped to interpret the results. Dave Risk and Barbara Bond both had supervisory roles in this work. This manuscript was published in Global Change Biology in January, 2011 (Volume 17, Issue 1). Copyright permission for this publication can be found in Appendix E.

6.2 Abstract

Increasing use of automated soil respiration chambers in recent years has demonstrated complex diel relationships between soil respiration and temperature that are not apparent from less frequent measurements. Soil surface flux is often lagged from soil temperature by several hours, which results in semielliptical hysteresis loops when surface flux is plotted as a function of soil temperature. Both biological and physical explanations have been suggested for hysteresis patterns, and there is currently no consensus on their causes or how such data should be analyzed to interpret the sensitivity of respiration to temperature. A one-dimensional soil CO_2 and heat transport model based on physical first principles was used to demonstrate a theoretical basis for lags between surface flux and soil temperatures. Using numerical simulations, it is demonstrated that diel phase lags between surface flux and soil temperature can

result from heat and CO_2 transport processes alone. While factors other than temperature that vary on a diel basis, such as carbon substrate supply and atmospheric CO_2 concentration, can additionally alter lag times and hysteresis patterns to varying degrees, physical transport processes alone are sufficient to create hysteresis. Therefore, the existence of hysteresis does not necessarily indicate soil respiration is influenced by photosynthetic carbon supply. It is also demonstrated how lags can cause errors in Q_{10} values calculated from regressions of surface flux and soil temperature measured at a single depth. Furthermore, synchronizing surface flux and soil temperature to account for transport-related lags generally does not improve Q_{10} estimation. In order to calculate the sensitivity of soil respiration to temperature, approaches that account for the gradients in temperature and production existing within the soil are most useful. The consideration of heat and CO_2 transport processes is a requirement to correctly interpret diel soil respiration patterns.

6.3 Introduction

Soil respiration, which is often the largest flux of CO_2 leaving terrestrial ecosystems (Ryan and Law, 2005; Jassal et al., 2007; Gaumont-Guay et al., 2008), is likely to be an important determinant of ecosystem carbon balance under future climate scenarios. The temperature sensitivity of soil respiration is one of the more basic characteristics that ecologists would like to quantify in order to predict fluxes in changing environments. However, regressions between soil respiration and temperature often have relationships that do not agree with theoretical models, such as the commonly used Arrhenius or vant Hoff type expressions (see Davidson et al. (2006b) for a detailed discussion). Models based on simple reaction kinetics do not capture the biological and physical complexities of soil systems, including heat and gas transport dynamics (Risk et al., 2002a; Pumpanen et al., 2003; Davidson et al., 2006a; Pavelka et al., 2007). While there is much agreement that more sophisticated, mechanistic models are required to describe and predict soil respiration, many suggestions have focused on improving descriptions of biological production (Trumbore, 2006; Carbone and Vargas, 2008), and the complexities of soil physical processes have not received the same level of attention.

In recent years, automated soil respiration chambers have gained widespread

use, providing temporally dense sets that reveal complex relationships between soil respiration and temperature that are not apparent with less frequent survey measurements. Many researchers who analyze data from automated chambers have observed diel hysteresis, evidenced by semielliptical shapes in regression plots of soil temperature and soil respiration (see examples in Riveros-Iregui et al. (2007); Bahn et al. (2008); Carbone and Vargas (2008). These ellipses result from phase lags between the diel signals of soil temperature and soil respiration, but there is no consensus on what causes phase lags, or how best to analyze lagged data in order to determine the temperature sensitivity of soil respiration (Pavelka et al., 2007; Graf et al., 2008; Gaumont-Guay et al., 2008).

Two main lines of reasoning have been proposed to explain the origins of phase lags. The first is the covariate argument, that environmental factors which oscillate out of phase with soil temperature, such as carbon supply from recent photosynthate, modify CO_2 emissions (Tang et al., 2005a; Stoy et al., 2007; Vargas and Allen, 2008; Kuzyakov and Gavrichkova, 2010). The second is the heat transport argument, that soil temperature measured at an arbitrary depth is out of sync with surface efflux, due to shifts in the phase and amplitude of soil temperature with depth (Pavelka et al., 2007; Graf et al., 2008). This argument is based on the fact that soil CO_2 production in an integrated response a to nonuniform temperature profile, so temperatures measured at discrete soil depths are likely to differ in both magnitude and phase from the average temperature forcing soil CO_2 production. The covariate and heat-transport explanations are not mutually exclusive, and both factors are likely to play important roles in diel soil respiration dynamics. An additional factor that has not been discussed extensively is that gas diffusion through soil imposes a lag between the time of CO_2 production at depth and release from the soil surface.

An excellent example of how these potential explanations can act simultaneously is the multiple influences that soil moisture can have on diel soil respiration patterns. Lags between soil respiration and temperature, and the semielliptical forms produced when these variables are plotted against each other, have been shown to vary seasonally with soil moisture (Tang et al., 2005a; Riveros-Iregui et al., 2007; Carbone and Vargas, 2008; Vargas and Allen, 2008). All of the processes mentioned above - substrate supply, heat transport, and CO_2 diffusion - are influenced by soil

moisture and can provide partial explanations for seasonal changes in diel hysteresis. Additionally, hysteresis patterns can also change day-to-day under conditions where soil moisture is fairly constant, and so diel influences from factors not wholly related to moisture should also be considered, such as photosynthetic carbon supply (Liu et al., 2006; Bahn et al., 2009), and disturbances such as atmospheric turbulence (Flechard et al., 2007).

Having multiple drivers which vary on a diel basis complicates the goal of measuring the temperature sensitivity of respiration in situ. Determining the temperature response of surface flux requires first disentangling the effects of temperature from other diel environmental drivers, and second, relating surface flux rates to nonuniform CO_2 production and temperature profiles. This study aimed to provide a conceptual framework and a modelling tool for addressing both parts of this process.

To evaluate the influences of temperature on surface flux in the absence of any other controlling factors, the theoretical diel relationship between soil temperature and surface flux resulting from purely physical transport processes was determined. Using basic principles of gas diffusion and heat transport, the expected lag times and hysteresis patterns between soil temperature and surface flux were simulated. A series of sensitivity analyses were then performed to determine the impacts on lag times of variations in soil physical factors, such as thermal diffusivity and gas diffusivity, and environmental factors, such as air temperature variation. To show the challenges and possibilities for distinguishing temperature from other diel signals, increasingly complex field scenarios were simulated, modelling simultaneous changes in temperature and other environmental variables, including atmospheric CO_2 and carbon substrate supply. These simulations demonstrate how both physical and biological drivers might influence hysteresis patterns under field conditions.

To understand how transport processes impact calculations of the temperature sensitivity of soil respiration, simulations to examine the accuracy of Q_{10} values (see Appendix D1 for a description of the Q_{10} concept) calculated from regressions of surface flux and soil temperature were also used. Several shortcomings at diel timescales were identified with this commonly used regression approach and potential alternatives are suggested.

6.4 Methods

6.4.1 Model Description

The one-dimensional soil CO_2 transport model described by Nickerson and Risk (2009a) was modified so that it had the following functionality: (1) a CO_2 transport component governed by Fick's First law of diffusion, (2) a heat transport component that shifts and dampens oscillating air temperatures with increasing soil depth, and (3) a simple CO_2 production function that adjusts production rate in each soil layer by the depth and temperature of the layer. The modeled environment assumes a well-mixed atmospheric boundary layer and a soil profile of length L (m) that is divided into 100 uniform layers. Each layer has specific values for total porosity, volumetric water content, and air-filled porosity. Air-filled porosity is used in turn to calculate both gas diffusivity (D_{CO_2}) and thermal diffusivity (D_T), based on empirical relationships from the literature (details below). D_{CO_2} and D_T, along with CO_2 and temperature gradients, determine the rate of CO_2 and heat transport, respectively. For the purposes of these instructive simulations, soil physical properties and diffusivities were assumed to be constant throughout the soil profile. The CO_2 transport component of the model allows gas exchange between neighbouring soil layers following concentration gradients. Flux rates between layers are determined with the discrete, one-dimensional form of Fick's First Law:

$$F_{ij} = D_{ij}\frac{\Delta C_{ij}}{\Delta z_{ij}} \tag{6.1}$$

where D_{ij} is the effective CO_2 diffusion coefficient between two soil layers (layer i and layer j), ΔC_{ij} is the difference in layer CO_2 concentrations (μmol m^{-3}), and Δz_{ij} is the difference in the depths (m) of the two layers. Temperature corrections for diffusivity are calculated for each layer at each model time step (1 s) as follows:

$$D_i = D_0\left(\frac{T_i}{T_0}\right)^{1.75} \tag{6.2}$$

where D_0 is soil diffusivity at reference temperature T_0 (273 K) and T_i is the ambient temperature (K) of layer i. At each model time step, a new CO_2 concentration in each layer (C_i) is calculated as function of the layer depth:

$$C_i(z,t) = \frac{C_i(z,t-1)\theta \cdot L/N + F(z-1) - F(z) + \gamma(z)}{\theta \cdot L/N} \tag{6.3}$$

where C_i(z, t-1) is the layer concentration at the previous time step, θ is the soil air-filled pore space, F(z-1) is flux from the layer below (which is generally positive, representing a flux in, but the sign depends on concentration gradients), F(z) is the flux from the present layer, γ(z) is layer CO_2 production (μmol m^{-3} s^{-1}), L is the total depth of the soil column and N is the total number of soil layers. Unless otherwise noted, biological CO_2 production decreases with soil depth according to the following exponential function (Nickerson and Risk, 2009a):

$$\gamma(z, T_{ave}) = \frac{\Gamma_0}{\sum_{z=0}^{L} exp\left(\frac{-z}{d_p}\right)} exp\left(\frac{-z}{d_p}\right) \tag{6.4}$$

where T_{ave} is the average temperature of the atmosphere and profile, Γ_0 is total basal soil production at the average temperature (μmol m^{-3} s^{-1}), z is the layer depth, and d_p is the exponential folding layer, or the layer at which the proportion of total soil production remaining is 1/e (0.37). By manipulating d_p, CO_2 production can be confined mostly to shallow soil layers, or spread more evenly across the soil profile. A basal value for total soil CO_2 production is defined by the user and partitioned with Eqn (4) to give layer-specific basal production. At each time step, layer production is adjusted in response to the current layer soil temperature T(z,T) using a modified vant Hoff relationship:

$$\gamma(z, T) = \gamma(z, T_{ave}) \times Q_{10}{}^{((T(z,t)-T_{ave})/10)} \tag{6.5}$$

The heat transport component of the model approximates air and soil temperature as sinusoidal curves (Hillel, 1998), where soil temperature is shifted and damped from the air temperature curve as a function of depth:

$$T(0, t) = T_{ave} + A_0 sin(\omega t) \tag{6.6}$$

$$T(z, t) = T_{ave} + A_0[sin(\omega t - z/d_T)]e^{-z/d_T} \tag{6.7}$$

where T(0,t) is the temperature at the soil surface (z=0), A_0 is the amplitude of the surface temperature fluctuation (1/2 of the total daily range), and ω is the radial frequency, which converts time to radians. For a sine wave oscillating on a period of 1 day (86,400s), ω = 2/86,400. The constant d_T is the thermal damping depth, and

is defined as the depth at which temperature amplitude decreases to the fraction 1/e. Thermal damping depth (m) is related to thermal diffusivity (D_T) as follows:

$$d_T = \sqrt{2D_T/\omega} \tag{6.8}$$

One should note that the two parameters in the heat transport equations which are impacted by environment are diel air temperature amplitude (A_0), and thermal diffusivity (D_T).

6.4.2 Model Implementation

Simulations were performed to examine (1) the impacts of model parameters on lag times and hysteresis patterns and (2) how lags affect calculation of soil respiration temperature sensitivity. A set of default soil physical and environmental conditions were defined for simulations (Table 1), based on measurements of a sandy loam soil from the HJ Andrews Experimental Forest in the western Cascades of Oregon, USA (44.21N, 122.21W). Further description of the site and soil is provided by Pypker et al. (2008). Default environmental conditions are characteristic of early summer. For sensitivity analyses, each of these parameters was varied across a large range of realistic values. Soil depth was modeled as 100cm for all scenarios.

Realistic values for D_{CO_2} at different soil moisture contents were modeled using the relationship described by Moldrup et al. (2000), which expresses soil gas diffusivity as a function of air-filled porosity and soil moisture release characteristics:

$$D_P = D_0 \times (2\epsilon_{100}^3 + 0.04\epsilon_{100}) \left(\frac{\epsilon}{\epsilon_{100}}\right)^{2+3/b} \tag{6.9}$$

where D_P is soil gas diffusivity, D_0 is gas diffusivity in free air (1.39×10^{-5} m^2 s^{-1} for CO_2 at 273K and 1 atm), ϵ is the ambient air-filled porosity, ϵ_{100} is the air-filled porosity at -100cm H_2O tension (~10 kPa), and b is the slope from a log plot relating volumetric water content to soil water potential. Coefficients determined from 12 intact soil cores taken from the HJ Andrews Experimental Forest were used. Moisture-release coefficients were determined by treating cores on pressure plates at pressures ranging from 10 to 50 kPa.

To parameterize D_T at different moisture levels, a published dataset for a sandy-loam soil of D_T measurements from intact soil cores across air-filled porosities ranging

0-0.60 (Ochsner et al., 2001) was used. To interpolate between measured porosities the data were fit with a second-order polynomial.

Simulations were initiated with a spin-up period for modeled CO_2 flux to stabilize. The spin-up period was deemed sufficiently long when daily maximum soil surface flux values were constant for at least 5 consecutive model days. To minimize spin-up time, simulations were initialized with the steady-state solution proposed by Cerling et al. (1991) for a uniform profile. The model was solved by Euler integration with a computation time step for all simulations of 1 s, and model output was recorded every 300 s.

Two synthetic tests were conducted to examine the performance of the CO_2 transport component under steady-state and transient conditions. The steady-state test served to assess numerical errors associated with discretizing the soil profile into layers. This test entailed modelling uniform production profiles across a range of gas diffusivities, and comparing the modeled concentration profiles to Cerling's steady-state solution. Soil concentration errors due to discretization were found to be <0.5% across all diffusivity levels. The transient test examined time lag errors related to iterating the model in discrete time steps. CO_2 concentration was varied at the upper boundary layer (atmosphere) as a sinusoidal wave, and compared the phase lags between peak CO_2 concentrations in the atmosphere and soil with the theoretical phase lag described by (Beltrami, 1996):

$$\delta = \frac{z}{2}\sqrt{\frac{\tau}{\pi \times D_{CO_2}}} \tag{6.10}$$

where δ is the phase lag (s), z is soil depth (m), τ is the period over which atmospheric CO_2 oscillates (1 day or 86 400 s), and D_{CO_2} is the effective CO_2 diffusivity of soil ($m^2\ s^{-1}$).

6.4.3 Comparison of apparent and actual Q_{10} values

These results examined how varying model parameters affected calculation of Q_{10} values with a widely used regression approach, which relates the natural logarithm of surface flux to soil temperature at an arbitrary depth (Pavelka et al., 2007):

$$ln(R) = \alpha T + \beta \tag{6.11}$$

where R is surface flux, T is soil temperature, and α and β are coefficients estimated from linear least squares regression. The Q_{10} of surface flux was calculated as:

$$Q_{10} = e^{10\alpha} \tag{6.12}$$

These Q_{10} values from post hoc calculations are termed apparent Q_{10} values to contrast them with the input Q_{10} used to parameterize the model (generally 2.0). It should be noted that in these simulations a small amount of diel variation in surface flux resulted from the temperature sensitivity of CO_2 diffusivity [Eqn (2)], rather than from the temperature sensitivity of CO_2 production. The variation in surface flux resulting from the temperature sensitivity of D_{CO_2} was negligible, however, accounting for o $< \pm 1\%$ change in respiration when temperature was varied ± 15°C over a 24 h period (see Appendix C for more details).

6.5 Results

6.5.1 Impacts of Transport-Related Lags on Regressions of Surface Flux and Soil Temperature

Owing to the attenuation and phase shift of soil temperatures with increasing depth, the relationship between modeled surface flux and soil temperature varied with soil temperature measurement depth (Fig. 6.1). Plots of surface flux against soil temperature produced hysteresis loops which changed in three respects with increasing depth: their rotational direction (see arrows in Fig. 6.1), their roundness or narrowness (minor radius), and the orientation of their principal axes. All three of these qualities were functions of the lag time between surface flux and soil temperature. At depths where soil temperature reached a daily maximum before surface flux (e.g. at soil depths above 5 cm in Fig. 6.1), hysteresis loops rotated clockwise, while at deeper depths where soil temperatures peaked after surface efflux, the loops rotated counter clockwise.

The narrowness, or minor radius, of hysteresis loops, as well as the orientation, can be described as functions of lag time using principles of harmonic motions. As adapted from Beltrami (1996), two sine waves that are offset by a lag give the equation

of an ellipse when superimposed perpendicularly:

$$R = R_A \frac{T}{T_A} cos(\delta) + R_A \sqrt{\left(1 - \frac{T^2}{T_A}\right)} sin(\delta) \tag{6.13}$$

where R_A and T_A are the amplitudes of respiration rate and temperature, respectively, R and T are instantaneous respiration rate and temperature, respectively, and δ is the lag, or the difference in phase between the temperature and respiration waves (expressed in radians). When the lag is a full period (equivalent to 0 or 24h), the expression of an ellipse simplifies to a straight line with positive slope. For a 1/2 period (12 h), the expression simplifies to a straight line with negative slope. For lags of 1/4 period (6 h), the result will be a horizontal ellipse. The results show it is possible to observe any of these orientations within a soil profile. Lags up to and exceeding 24 h occurred for deep reference soil temperatures, particularly at low thermal diffusivities, which slow propagation of temperature through the soil. With a reference soil temperature at 30 cm depth, lags exceeded a full 24 h period when values of D_T became $<2\times10^{-7}$ m^2 s^{-1}.

Even at soil depths where there was no time lag between temperature and surface flux, regressions did not produce close estimates of respiration temperature sensitivity. For the example in Fig. 6.1, surface flux was nearly synchronized with 5 cm soil temperature and little hysteresis was apparent. However, the least squares estimate of Q_{10} was 1.53, which is substantially smaller than the actual Q_{10} of 2.0 used to parameterize the model, shown in gray. The closest approximation of the input Q_{10} occurred at 15cm depth, despite pronounced hysteresis at this depth. This depth also is not associated with an area where most production occurs. The production profile for this simulation declined exponentially with depth, with more than two-thirds of CO_2 production occurring above 10 cm (d_p=10 cm). There was no discrete soil depth where temperature was synchronized with surface flux and approximated the correct Q_{10} value.

It was found that in general, the strength of correlation (R^2) between surface flux and soil temperature measured at an arbitrary depth was strongly influenced by transport-related lags (Fig. 6.2a), and R^2 was a poor statistic for predicting what soil depth would return an accurate Q_{10} (Fig. 6.2b). To examine the influence of lag time on R^2 and Q_{10} values estimated from regressions of surface flux and soil temperature,

thermal diffusivity was varied in the model, which as described below was the model parameter with the largest impact on lag time (Fig. 6.4a). Regressions between surface flux and soil temperature were then examined using reference depths of 5, 10, 15, and 20 cm. R^2 was found to have a predictable and regular relationship with lag time, regardless of the reference temperature depth (Fig. 6.2a). R^2 peaked at 0 and 12 h lag, which is the when the expression for an ellipse simplifies to a straight line, and reached a minimum at 6 and 18h lag, which is when the expression produces a horizontal ellipse. As described above [Eqn (13)], the narrowness, or minor radius of hysteresis loops can be described as a function of lag time, and as hysteresis loops become more round the strength of correlation decreases, and as they become more narrow the strength of correlation increases.

The apparent Q_{10} values calculated from regressions were also related to lag time, but the form of the relationship was different from the form of the R^2 relationship (Fig. 6.2b). As a result, the conditions providing the highest R^2 values did not produce the most accurate Q_{10} values. The most accurate Q_{10} estimates coincided with conditions which produced lag times of 34 h, and corresponded with a wide range of R^2 values. The Q_{10} and lag relationship differed slightly for each reference depth because the slope of least squares regression, and therefore the Q_{10}, is also influenced by the amplitude of soil temperature variation at the reference soil depth [Eqn (13)].

Attempting to remove the lag by shifting surface flux data to be in-phase with soil temperature data before calculating the regression did not systematically improve estimates of Q_{10} values (Fig. 6.2c). Calculated Q_{10} values increased exponentially with the magnitude of the phase adjustment. For adjustments exceeding a few hours, this approach produced Q_{10} values many times greater than the Q_{10} used to parameterize the model. This indicates that knowing the lag time that is due to heat and gas transport does not readily help to determine meaningful Q_{10} values. Even after adjusting for transport-related lags, the problem remains that no single reference soil depth consistently approximates the average temperature across the whole soil production profile.

These examples demonstrate that it is best to consider temperatures across the production profile to understand temperaturerespiration relationships; however, for practical purposes, temperature measurements in field studies are often restricted to

one or a few discrete soil depths. In order to strengthen conceptual links between processes that take place across the entire soil production profile, and patterns that may be observed in field data, for the remainder of this article most results are shown using an arbitrary soil temperature depth of 10 cm. Also, because the simulations use an exponential relationship between temperature and CO_2 production, the time offsets between daily maximum respiration and temperature differ slightly from the time offsets between minimum values. For simplicity, lag times between maxima are reported, and it is noted when trends differ for lag times between minima.

6.5.2 Sensitivity of Lag Time to Thermal Diffusivity

Thermal diffusivity (D_T) influenced the speed with which changes in air temperature propagated through soil, and the depth to which diel variations in air temperature were detectable (Fig. 6.3). As D_T was increased in the model, changes in air temperature propagated through soil more quickly, which shortened lags between soil temperatures and surface flux. Variations in D_T had a larger effect on lag times than any other single factor that was examined, although the effect was nonlinear (Fig. 6.4a). Lag times varied sixfold for values of D_T within the range of 1-10^{-7} m^2 s^{-1}, which is the approximate range for mineral soils experiencing normal field moisture levels (Ochsner et al., 2001). Lag times increased substantially for lower D_T values in the range of 1-10^{-8} m^2 s^{-1}, which corresponds with the range for organic soils (Hillel, 1998).

6.5.3 Sensitivity to CO_2 Diffusivity, Production Depth

In contrast to D_T, large changes in simulated D_{CO_2} had a relatively small effect on lags between surface flux and soil temperature (Fig. 6.4a), but D_{CO_2} nevertheless had unique and complex impacts that are important for interpreting temperaturerespiration relationships. Lags were found to occur not only between surface flux and soil temperature, but also between soil CO_2 concentrations and temperature measured at the same depth (Fig. 6.5a). zLags between soil CO_2 and temperature at the same depth were particularly pronounced at low D_{CO_2} . Low gas diffusivity increased the residence time of soil CO_2, causing delayed responses in CO_2 concentration to soil temperature changes. While lags between CO_2 concentration and soil temperature

decreased as D_{CO_2} was increased in the model, lags between surface flux and soil temperature sometimes showed the opposite response. D_{CO_2} impacts on surface flux lags depended on both the distribution of CO_2 production, and the depth of the reference soil temperature. When production was concentrated near the surface (Fig. 6.5b), the phase of the surface flux sine wave shifted closer to the waves of near-surface temperatures as D_{CO_2} increased, but also shifted farther away from the waves of deep soil temperatures. At reference soil depths near the surface, lags between surface flux and soil temperature decreased with increasing D_{CO_2} , but at deeper reference depths lags increased. In contrast, when CO_2 production was uniformly distributed throughout the soil (Fig. 6.5c), a greater proportion of CO_2 came from deep soil layers, and increasing D_{CO_2} caused the phase of the surface flux sine wave to shift closer to deep soil temperatures and to shift farther from air and near-surface temperature.

The sensitivity of lags to variations in production depth when D_{CO_2} was held constant was also explored. Figure 6.4a shows changes in the depth of CO_2 production with respect to the exponential folding depth, d_p, where a higher d_p indicates production is spread more evenly across the soil profile and a lower d_p indicates production is confined more to the shallow subsurface. Changes in production within the shallow subsurface (e.g. an increase in d_p from 5-10 cm) had greater impacts on lag time than changes in production deeper within the soil (e.g. an increase in d_p from 60 to 70 cm), because most diel variability in soil temperature occurred at shallow depths. Even at very high D_T, diel temperature oscillations occurred primarily within the top few centimetres of soil. For example, for the maximum D_T plotted in Fig. 6.4a (D_T=9×10^{-7} m^2 s^{-1}), temperature amplitude decreases to approximately one-third by 16cm depth. CO_2 production deep in the soil profile varied little throughout the day because it experienced a relatively constant temperature environment, so increasing production from deep soil did little to shift diel respiration oscillations.

6.5.4 Sensitivity to Basal Respiration Rate and Other Environmental Variables

Further sensitivity analysis revealed the general principle that variables which caused nonuniform changes in temperature or respiration across the soil profile tended to impact lag times. For example, changing the diel amplitude of air temperature (A_0)

tended to impact lags by altering temperature variation at shallow soil depths to a greater extent than deeper soil depths. Also, changing the temperature sensitivity of CO_2 production by altering Q_{10} in the model affected lags by altering the proportional contribution from soils of different temperatures (Fig. 6.4b). See also Appendix C. In contrast, increases in the basal CO_2 production rate did not influence lags. Changing basal production rate alone did not alter the proportional contribution from each soil layer to surface flux.

6.5.5 Effects of Soil Moisture on Phase Lags

To model the physical effects of soil moisture on lags, both D_T and D_{CO_2} were allowed to vary simultaneously as functions of air-filled porosity (Fig. 6.6a and b). D_T and D_{CO_2} have different relationships with soil moisture: heat propagates more quickly through water than through air-filled pore spaces, whereas CO_2 propagates more quickly through air-filled pores than through water. As simulated soil moisture was decreased, this caused an increase in D_{CO_2} and a decrease in D_T, but both had the same effect of increasing lag time between surface flux and 10 cm soil temperature (Fig. 6.6a), for reasons described above. As the lag time between surface flux and 10 cm soil temperature increased under dry conditions, hysteresis loops also became less linear and more elliptical in shape.

To demonstrate some of the potential impacts of moisture on biological activity, an additional level of complexity was added to the moisture simulation by decreasing basal CO_2 production rate as a linear function of soil dryness (Fig. 6.6c and d). While this simple linear approximation may not be realistic for very high soil moistures, it is likely to represent respiration responses to drier soil moisture conditions. As soil moisture was decreased in the model, the diel amplitude of surface flux decreased, and hysteresis appeared to become more linear and horizontal (Fig. 6.6d). This occurred as a result of the magnitude and daily range of respiration changing, rather than a change in the orientation of the ellipses. Lags, which control the shape and orientation of hysteresis loops, remained unaffected by altered production rates (Fig. 6.6c). As mentioned above, simulated changes in basal production rate alone did not affect lag times unless the distribution of production was also changed.

6.5.6 Diel Variation in Atmospheric CO_2

Concentrations of atmospheric CO_2 within and near plant canopies often vary on a diel basis, due to plant gas exchange taking up CO_2 during the day and releasing CO_2 at night (Liu et al., 2006). Diel oscillations in atmospheric CO_2 were simulated as a sinusoidal wave with a daily range of 50 ppm. Data from the HJ Andrews Experimental Forest indicated that daily minimum CO_2 concentration at the soil surface may be lagged from maximum temperature by as much as ± 5 h, so it was hypothesized that diel changes in atmospheric CO_2 could modify surface flux and contribute to diel hysteresis between surface flux and temperature. Simulations indicated, however, that atmospheric CO_2 has a negligible effect on flux rates, particularly when compared with effects of temperature variation. When air and soil temperature were held constant, varying atmospheric CO_2 alone changed surface flux rates by $<0.5\%$. In contrast, when diel temperatures varied even moderately, CO_2 production required little temperature sensitivity to swamp the effects of atmospheric CO_2 variations.

6.5.7 Changing Substrate Supply

Several lines of evidence have indicated close links between canopy carbon supply and soil respiration rates, including phloem girdling studies (Högberg et al., 2001; Tedeschi et al., 2006), studies across natural gradients of root activity (Tang et al., 2005b), lag analyses between canopy variables and soil respired $\delta^{13}CO_2$ (Fessenden and Ehleringer, 2003; McDowell et al., 2004; Ekblad et al., 2005; Kodoma et al., 2008), and isotopic labeling studies of photosynthate (Hogberg et al., 2008; Bahn et al., 2009). Simulations were performed to show the potential impacts of diel variations in subsurface photosynthate supply on hysteresis in the respiration vs. temperature relationship. There is much uncertainty regarding the specifics of phloem loading to roots and how much respiration responds to fluctuations in carbon supply, and a simple approach of modelling diel variation in photosynthate supply as a linear function of photosynthetic active radiation (PAR) was used, increasing basal soil CO_2 production rate from 1.5 μmol m^2 s^{-1} at night to 3 μmol m^2 s^{-1} in response to peak PAR over a 12 h photoperiod (Fig. 6.7a). As phloem transport may delay the supply of carbon substrates belowground, a range of time offsets between peak

PAR and peak subsurface photosynthate supply (626 h) were also simulated. Some studies have suggested lags in soil respiration responses of less than a day (Tang et al., 2005b), while others have suggested lags ranging 18 days (Högberg et al., 2001; McDowell et al., 2004; Mencuccini and Holtta, 2010); however, for illustrative purposes this analysis focused on potential short-term responses to photosynthesis over the course of approximately 1 day. Because the timing and magnitude of impacts from photosynthetic carbon supply are likely to vary substantially (Kuzyakov and Gavrichkova, 2010), the goal was to emphasize only the gross patterns that could result from the combined influences from photosynthetic carbon supply and physical transport processes.

Diel variations in substrate supply substantially modified surface flux and produced hysteresis relationships with complex shapes (Fig. 6.7b). Although the shapes were quite variable depending on the timing of peak substrate supply, there were some consistencies among the curves that may be useful for interpreting field data. The hysteresis loops were consistently flatter on the bottom, corresponding with periods when PAR-dependent substrate supply ceased and respiration responded only to soil temperature. For large time offsets between substrate supply and soil temperature, soil respiration also exhibited double peaks over the course of the day, peaking once in response to maximum carbon supply and again in response to maximum temperature (Fig. 6.7a).

6.6 Discussion

The heat and CO_2 transport model described here demonstrates that purely physical drivers can have strong influences on diel dynamics of surface flux, and if transport-related lags are not accounted for, these influences may obfuscate the interpretation of the temperature sensitivity of soil respiration. Interpreting diel dynamics has two distinct but related challenges, discussed below: first, distinguishing the effects of temperature variation from other factors, and second, determining the temperature sensitivity of respiration given nonuniform soil temperature and production profiles.

6.6.1 Effects of Soil Moisture

Soil moisture can have multiple biological and physical influences on soil respiration, making it challenging to distinguish temperature and non-temperature influences on soil respiration across moisture conditions. Potential impacts of moisture on diel respiration dynamics both with and without biological responses to moisture were examined. When only soil physical processes were represented in the model, decreasing soil moisture caused phase lags between surface flux and soil temperature to increase, and also caused diel hysteresis to become more pronounced (Fig. 6.6a and b). These purely physical trends are consistent with field observations in several studies. Under oak canopies, Tang et al. (2005b) observed increasing lag times between surface flux and soil temperature at 8 cm depth as soils dried, although they attributed the lag to the influence of tree photosynthesis on respiration of the rhizosphere rather than to gas and temperature transport processes (discussed more below). Similarly, in mixed conifer forests (Vargas and Allen, 2008) and in shrub ecosystems (Carbone et al., 2008), the periods of most pronounced diel hysteresis coincided with the driest parts of the growing season.

The results from the these field studies seem to conflict with findings of Riveros-Iregui et al. (2007), who observed less pronounced hysteresis between soil CO_2 concentrations and temperature at 20cm depth as soil dried. However, transport-related lags could occur not only between surface flux and soil temperature, but also in the type of measurements made by Riveros-Iregui et al. (2007), between CO_2 concentrations and soil temperatures measured at the same depth (Fig. 6.5a). Lags between soil CO_2 and temperature at the same depth consistently decreased as D_{CO_2} was increased in the model, opposite of how lags between surface flux and shallow soil temperatures behaved (Fig. 6.5b). In addition, results showed a potential biological explanation for decreased hysteresis with drying. When CO_2 production declined at low moistures, the magnitude and diel range of surface flux and subsurface concentrations decreased (Fig. 6.6c and d), which caused hysteresis to appear less pronounced and more linear at low moisture.

These examples demonstrate the difficulty of teasing apart moisture-dependent biological and physical processes that are potential drivers of diel respiration patterns. For example, it would be logical to interpret an increase in lag between surface flux

and soil temperature as the soil dries as a product of substrate limitations (Carbone et al., 2008). Substrate limitations are indeed coupled with soil moisture, since low moisture can reduce canopy production and allocation of photosynthate belowground (Irvine et al., 2002, 2005), and also reduce diffusion of carbon substrates through soil (Davidson et al., 2006b). But increasing lags can also result from moisture influences on D_T and D_{CO_2} (Fig. 6.6a), so it is unlikely that changes in lag times and diel hysteresis would be due to substrate limitations alone. Similarly, declines in the amplitude and apparent temperature sensitivity of surface flux with decreasing soil moisture have been attributed to reduced substrate supply, although heat transport effects produce similar results (Fig. 6.6b).

6.6.2 Detecting Effects of Factors Other than Temperature on Diel Surface Flux Patterns

Numerical simulations provide a theoretical limit to the impact of soil physical processes on lag times. Phase lags between surface flux and a reference temperature at 10cm depth were found to be between 1 and 4h for mineral soils across a wide range of soil physical and environmental conditions (Figs 4 and 6). Lag times greater than this may be indicative of other biological factors influencing soil respiration. For example, Tang et al. (2005b), found an approximately four hour lag between soil surface flux and temperature at 8 cm depth under an oak tree canopy, and no lag in an adjacent area of dead annual grasses. This large difference in lag times is unlikely to be a result of physical processes alone, since soil temperature data indicate D_T was similar in the two locations. As Tang et al. (2005b) concluded, photosynthetic carbon supply may have influenced the different diel patterns in these two locations.

Asymmetrical time series or hysteresis patterns also provide a tool for detecting impacts of environmental factors other than temperature. The simulations of diel changes in substrate supply (Fig. 6.7) demonstrated that asymmetrical hysteresis patterns can develop in response to processes that are limited to a portion of the day only, such as photosynthesis. This example also demonstrated that double peaks can form in diel time series of surface flux when peak carbon supply is offset by a long period from peak temperature. Carbone et al. (2008) also observed daily double peaks in field measurements of shrub and grassland ecosystems, particularly during

parts of the growing season when soil respiration was most active. Asymmetrical diel patterns such as these cannot be accounted for by temperature alone and must be attributed to influences from more than one factor.

At a minimum, by measuring both air and soil temperature, or still better, measuring soil temperature at more than one depth, one can calculate soil thermal diffusivity to obtain a rough estimate of theoretical lags between soil temperature and surface flux due to heat transport. The time difference between peak temperatures measured at several soil depths can be used to constrain D_T (Beltrami, 1996), which was shown to influence expected lag times more than any other single factor examined. Even without more detailed information on other parameters, an estimate of D_T can provide a rough approximation of expected lag times (e.g. Fig. 6.4). Because soil moisture has a large influence on D_T, such estimates may be particularly helpful for researchers trying to account for changes in diel respiration-temperature relationships over a range of moisture conditions.

The heat and gas transport model used in this study can be extended to simulate field studies, and may provide an approach to tease apart influences of temperature from other factors that have diel periodicity. Detailed environmental data and soil physical parameters are required to drive the model; however, such data are becoming increasingly available. The transport equations are limited, however, to conditions where soil heat transport is dominated by conduction and CO_2 transport is dominated by diffusion. More complex transport functions would be required to simulate heat transport in flows of soil water, or to simulate mass flow of CO_2 in response to pressure gradients. The model also emphasizes physical processes, and was less rigorous for representing biological relationships. The approach for simulating diel variation in photosynthetic carbon supply was simplistic compared to the vegetation-specific model of phloem transport by Mencuccini and Holtta (2010), but could be readily coupled to such plant physiological models.

6.6.3 Impacts of Diel Dynamics on Interpretation of Temperature Sensitivity

A related issue to distinguishing temperature and non- temperature respiration responses is describing the temperature sensitivity of soil respiration from diel

datasets. Without any change to the true temperature sensitivity of soil respiration, phase lags can alter the orientation of regressions between surface flux and soil temperature, and impact least squares fits to the data. The fact that the apparent temperature sensitivity of soil respiration differs depending on the depth where temperature is measured has been described by others (Pavelka et al., 2007; Graf et al., 2008). Less widely appreciated, perhaps, is the fact that Q_{10} estimates are related to the orientation of hysteresis loops, and can themselves be described as functions of lag times [Eqn (13) and Fig. 6.2].

There are several inherent problems with estimating respiration temperature sensitivity by regressing surface flux and soil temperature. The first problem is identifying an appropriate soil temperature reference depth, because R^2 relates primarily to how close the phases of surface flux and soil temperature are to one another (Fig. 6.2a), and does not predict the depth which returns the most accurate Q_{10} value. Furthermore, the depth where soil temperature produces the most accurate Q_{10} can be below the portion of the soil profile where most CO_2 production occurs (Fig. 6.1). Neither the depth where R^2 is highest nor the depth where apparent Q_{10} is most accurate have mechanistic significance, they are coincidentally associated with phase lags that produce interesting ellipses when surface flux and soil temperature are plotted perpendicularly. Using transport models, it may be possible to predict the depth that produces the most accurate Q_{10} value. Graf et al. (2008) attempted this approach to determine the depth where Q_{10} should be measured, using a physical model of soil respiration similar to the one presented here. In simulations spanning several model years, they examined the sensitivity of Q_{10} uncertainty to soil physical and environmental parameters. Their simulations demonstrated two important points that are consistent with the results from diel simulations: that shallow depths underestimate Q_{10} values, and that the depth of maximum correlation between surface flux and soil temperature is different than the depth returning the input Q_{10}. These results suggest that transport effects do not only create analysis challenges in diel datasets, but at longer timescales as well.

The underlying problem with estimating temperature sensitivity from surface flux is that surface flux is an integrated response to temperature across the soil profile, not just to soil temperatures at a single depth. (Reichstein et al., 2005) presented a

potential alternative for estimating soil respiration Q_{10} values, by using a statistical model that represents surface flux as the summation of multiple fluxes from different depths, and includes soil temperature measured at each depth. Using temperatures from two depths, the authors were able to explain more than 95% of the diel variation in surface flux data, as compared with only 80% when using soil temperature from a single depth. The multiple-source model also calculated higher Q_{10} values than a single-source model. Results from this study and Graf et al. (2008) indicate Q_{10} values are generally underestimated with a single, shallow reference temperature, so the dual source model may estimate Q_{10} more accurately.

An alternative approach used by (Risk et al., 2008a) involved quantifying CO_2 production within the soil profile, and estimating temperature sensitivity by comparing production and temperature at the same depth. Fluxes within the soil can be determined from changes in CO_2 concentration over time. Soil profiling systems that are well-suited to this approach are becoming more widespread, and future work should further assess the potential for this approach and its limitations under non-steady-state conditions.

Even these alternative approaches are not immune, however, to influences from environmental variables other than temperature. Given that factors other than temperature are likely to influence diel patterns of soil respiration under field conditions, caution is recommended in interpreting any apparent relationship between soil respiration and temperature at diel timescales as a true measure of temperature sensitivity.

In conclusion, high-frequency soil respiration measurements have important potential for identifying influences from multiple environmental factors. However, heat and gas transport creates lags between surface flux and soil temperature that can easily be misinterpreted and obscure the direct impacts of temperature. Analysis approaches that represent surface flux as the summation of fluxes across a nonuniform soil profile may provide a means for handling transport-related lags and more accurately determining the temperature sensitivity of soil respiration.

Table 6.1: Default parameters used for model simulations. Deviations from these values are noted in the text or figures.

Parameter	Default Value
Soil Porosity	0.65 (v/v)
Air Filled Porosity (Θ)	0.35 (v/v)
Thermal Diffusivity (D_T)	6.41 $\times 10^{-7}$ m^2 s^{-1}
Gas Diffusivity (D_{CO_2})	1.29 $\times 10^{-6}$ m^2 s^{-1}
Production exponential folding depth (d_p)	10 cm
Q_{10}	2
Average air and soil temperature (T_{ave})	15 °C
Air temperature amplitude (A_0)	7.5 °C
Total basal CO_2 production	1.5 μmol m^{-2} s^{-1}
Atmospheric CO_2	385 ppm

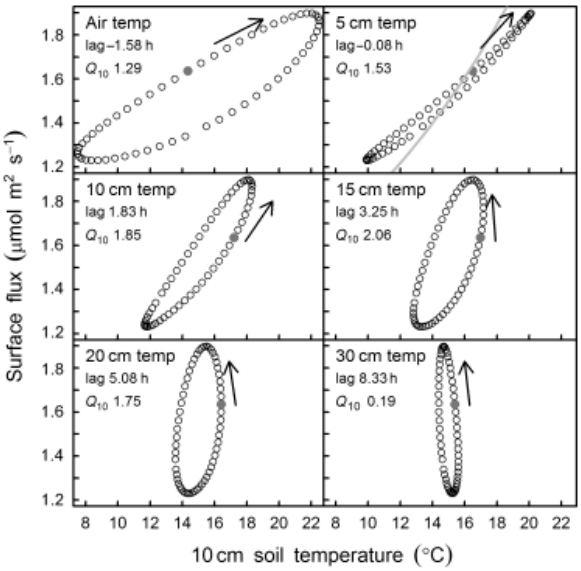

Figure 6.1: Diel hysteresis between surface flux and soil temperature at several depths, and apparent Q_{10} values calculated from least squares regression (see text for details). Solid points show time = 12 h and arrows indicate the direction of hysteresis over time. Gray line represents the fitted mean that would produce an apparent Q_{10} equal to the input value of 2. D_T=5$\times 10^{-7}$ m^2 s^{-1} (same data as bottom panel of Fig. 6.3). Negative lags indicate surface flux reaching a maximum before temperature whereas positive lags indicate temperature peaking first.

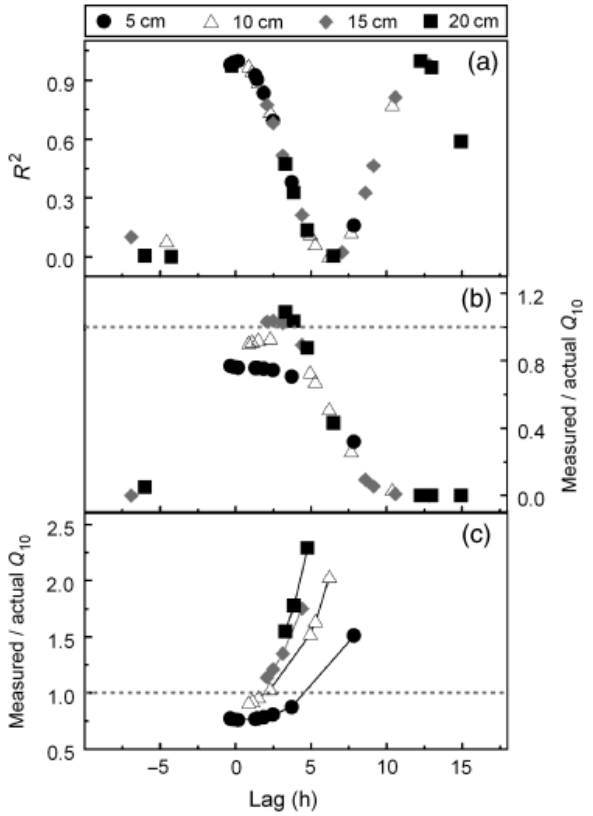

Figure 6.2: Impact of phase lags on R^2 and apparent Q_{10} calculated from regressions of surface flux and soil temperature. (a) R^2 for regressions with soil temperature at reference depths of 5 cm (circle), 10cm (trangle), 15cm (diamond), and 20cm (square). Lag time was varied by changing thermal diffusivity from 1×10^{-8} to 9×10^{-7} m^2 s^{-1}, as in Fig. 6.4a. (b) Apparent Q_{10} as a function of phase lag, normalized by the actual Q_{10} used to parameterize the model. (c) Same as (b), but surface flux data was shifted to be in-phase with soil temperature before calculating apparent Q_{10}. Apparent Q_{10} approached infinity with increasing phase lag, so only normalized values <2.5 are shown for clarity.

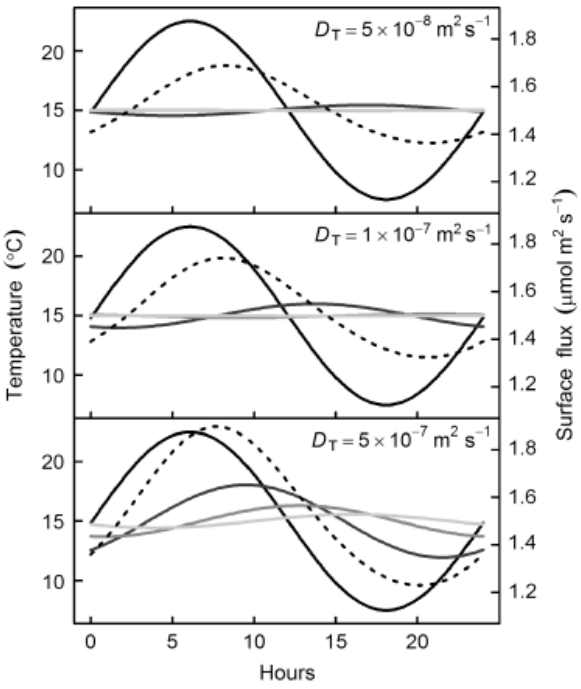

Figure 6.3: Effect of thermal diffusivity, D_T, on soil temperatures at several depths (solid lines) and surface CO_2 flux (dotted line). Soil temperature depths from darkest to lightest are: soil surface, 10, 20, and 30cm depth. See Table 1 for values of other input parameters.

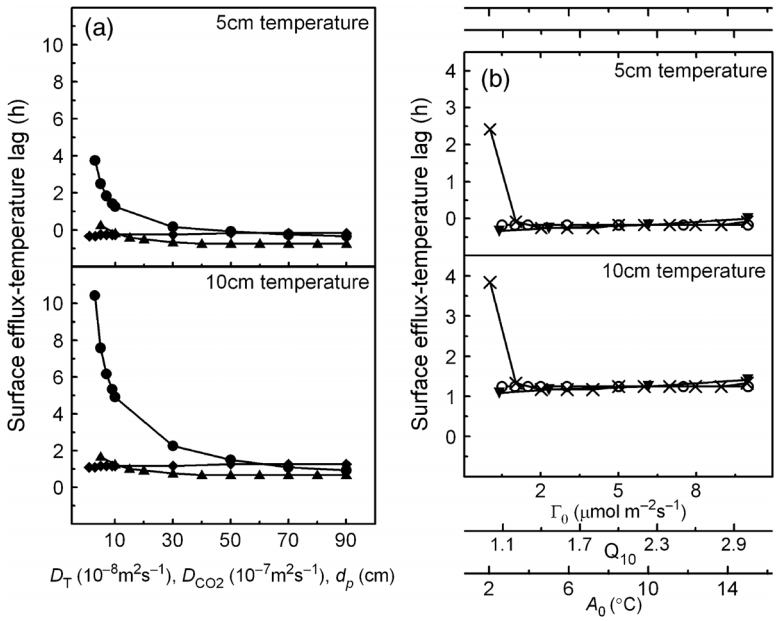

Figure 6.4: Sensitivity of lag time to soil and environmental parameters. (a) Thermal diffusivity, D_T (circle); CO_2 diffusivity, D_{CO_2} (diamond); and exponential folding depth for CO_2 production, d_p (triangle). (b) Basal total CO_2 production, Γ_0 (open circle); Q_{10} temperature sensitivity (cross); and diel air temperature amplitude, A_0 (triangle).

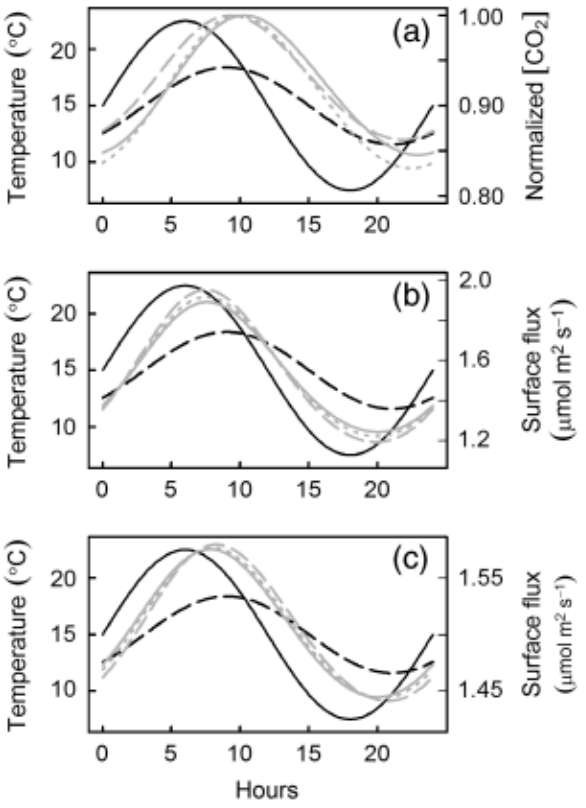

Figure 6.5: Effect of CO_2 diffusivity on soil CO_2 concentrations and surface fluxes. (a) CO_2 concentration at 10 cm depth for three levels of D_{CO_2}: 5×10^{-7} (solid gray), 1×10^{-6} (dotted gray), 5×10^{-6} (dashed gray). Air temperature (solid black) and 10 cm soil temperature (dashed black) are also shown. (b) Same as (a) except gray lines represent surface CO_2 flux. (c) Same as (b) except CO_2 production was uniformly distributed across soil profile, rather than decreasing exponentially with depth.

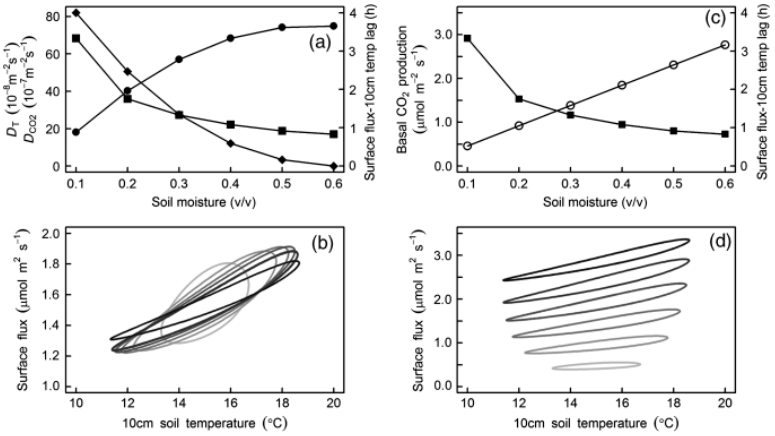

Figure 6.6: Potential responses of soil respiration to diel changes in photosynthate supply. (a) Diel changes in photosynthetic active radiation (PAR) (dashed black), air temperature (dashed gray), 10cm soil temperature (solid gray), and surface CO_2 flux (solid black). In this example, subsurface carbon supply peaked 16 h after PAR. (b) Hysteresis between surface flux and 10 cm soil temperature for various offsets between peak PAR and peak subsurface carbon supply: 16 h offset [solid black, same as in (a)], 20 h offset (dashed dark gray), and 26 h offset (dot-dashed light gray).

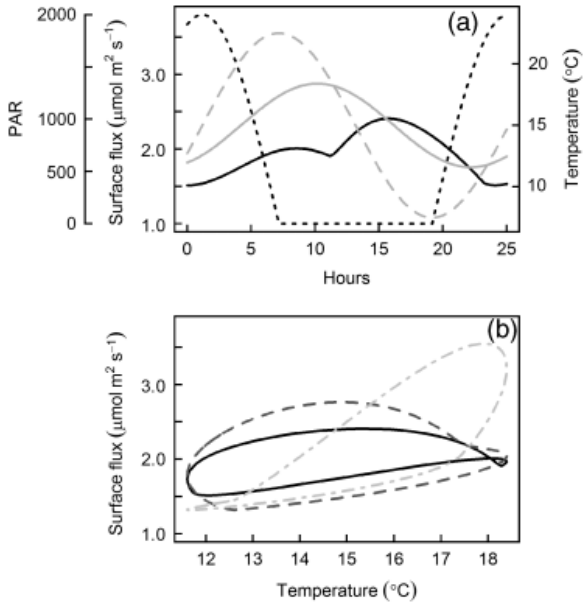

Figure 6.7: (a) Effect of moisture on thermal diffusivity (circle), CO_2 diffusivity (diamond), and the lag time between surface flux and 10cm soil temperature (square) for a uniform sandy-loam soil. (b) Surface flux hysteresis for moisture-dependent conditions shown in (a). From lightest to darkest: 5%, 15%, 25%, 35%, 45%, and 55% water content (v/v). (c) Changes in total basal CO_2 production (open circle) were added to simulations, but had no effect on lag times (square). (d) Corresponding surface flux hysteresis. From lightest to darkest: 5-55% water content (v/v), as in (b).

Chapter 7

Using Production Weighted Heat to Disentangle the Environmental Sensitivities of Soil Respiration

7.1 Preamble

This chapter presents a ground-up theoretical analysis of the interpretation of the temperature sensitivity of soil respiration, with the intention of avoiding some of the pitfalls discussed in the previous chapter. Authorship on this manuscript is as follows: Nick Nickerson, Claire Phillips, Jon Martin and Dave Risk. I developed the theory and performed the modelling and data interpretation and wrote the bulk of the manuscript. Claire Phillips worked with me on the initial theory and some of the analyses of the data. Jon Martin provided field data from a previous publication to test the theory on, and provided feedback on the manuscript in general. Dave Risk was supervisor to this work. The chapter is currently in preparation for submission to Journal of Geophysical Research - Biogeosciences.

7.2 Abstract

Balances between carbon emission from soil respiration and uptake by photosynthesis play an important role in regulating global climate. While the processes that govern photosynthesis are well understood, the understanding of soil respiration is lacking and researchers pay little attention to the physical aspects of the soil which may have a significant influence on the understanding of respiration measurements. Traditional approaches for interpretation of soil respiration data have been shown to produce poor results, in some cases as a consequence of not considering soil physical processes, such as heat transport, in the data interpretation. We take a ground-up theoretical approach that considers the effect of heat transport on soil respiration data. Results indicate that much of the soil-physics driven biases in soil respiration data interpretation can be eliminated by consideration of soil heat

transport, in particular by calculating the weighted average soil heat otherwise known as production weighted heat (H_{pw}). This H_{pw} analytical approach is applied to simulated soil respiration data as well as an extensive field data set which each demonstrate its improvement over the status-quo and potential drawbacks. Future extension of this approach to interpreting field data will likely take the form of more complex numerical optimization, which will cope better with less-idealized experimental field data sets.

7.3 Introduction

It has long been recognized that an incomplete knowledge of the biological, chemical and physical complexities of the soil system hampers our ability to accurately model soil respiration, and thus the ability to accurately predict the future impact of these emissions on the earth's climate system (Kirschbaum, 1995; Trumbore et al., 1996; Schlesinger and Andrews, 2000; Davidson et al., 2000, 2006b; Knorr et al., 2005) . While many researchers have focused on understanding the essential biological processes (Schimel and Weintraub, 2003; Davidson et al., 2012), fewer have dedicated time to understanding the associated soil physics, which ultimately influence the supply of substrate, as well as govern the heat, moisture and gas transport processes that are crucial to the function of these biological systems (Graf et al., 2008; Subke and Bahn, 2010; Phillips et al., 2011).

Biochemical temperature sensitivity, which may control up to 80% of the variation in heterotrophic soil respiration (Lloyd and Taylor, 1994; Davidson et al., 1998), is unfortunately one of the most difficult climate forcings to understand $in-situ$. In part, this difficulty stems from uncertainties in the timings and magnitudes of nutrient and substrate supply (Stoy et al., 2007; Martin et al., 2012), but is also in part caused by the poor understanding or neglect of heat and gas transport within the soil. A prime example of this is the prevalent use of a single temperature measurement at an arbitrary depth within the soil profile to estimate temperature-respiration relationships (Graf et al., 2008; Phillips et al., 2011). While this method may work in laboratory experiments where the soil temperature is homogeneous and could offer a reasonable first-order approximation for the form of the relationship $in-situ$, it does not take into account the reality that the temperature throughout the soil profile is

heterogeneous in both space and time as a result of heat transfer processes. Recently, with the introduction of respiration measurement techniques with high temporal resolution (Savage et al., 2008), this heterogeneity problem has risen into clearer view, largely because these heat and gas transport related complications are considerably more apparent in short term observations (i.e. diel). Recent research has shown that heat and gas transport in the soil are, at least in part, responsible for hysteresis loops that have been noted in multiple diel temperature-respiration studies to date (Carbone and Vargas, 2008; Carbone et al., 2008; Vargas and Allen, 2008a; Phillips et al., 2011).

If single-depth temperature measurements are not the ideal regressor then what should be used for soil respiration studies? Considering the problem from a soil-profile standpoint, it is understood that hetereotrophic organisms are distributed with depth in the soil (the actual distribution does not matter for now) (Davidson et al., 2006a; Tang et al., 2003, 2005a). Similarly, temperature fluctuations in the atmosphere propagate through the soil, with the amplitude of the signal decreasing with depth, and signal phase shifting linearly (i.e. peak soil temperature at depth z_1 occurs before peak soil temperature depth z_2, assuming $z_1<z_2$) (Beltrami, 1996; Smerdon et al., 2009). So each depth interval of heterotophic activity experiences a damped and phase shifted temperature signal that drives respiration. Soil flux, measured at the soil surface, is the sum of respiratory activity at all soil depths. Logically it follows that an appropriate regressor for soil respiration measurements is the sum of soil temperature over all depths, or the soil heat. The heat metric has been proposed before by Risk et al. (2002b), who showed that the soil heat method out performed the single-temperature metric in terms of goodness-of-fit using soil CO_2 gradient data, however there have been few studies that have since used soil heat or considered its applicability to soil respiration studies. Hypotheses for this work are that soil heat is: 1) The mathematically appropriate regressor and, 2) Will out perform any single-depth soil temperature for estimating biochemical temperature sensitivity.

While the most direct approach to test these hypotheses would be to take $in-situ$ measurements, there is unfortunately no a priori knowledge about what the environmental responses should be, nor is there a method to separate the effect

of temperature sensitivity from other covarying environmental factors (Martin et al., 2012). Modeled soil systems offer a pseudoreality in which to understand some of the more fundamental aspects of soil respiration. Here the basic theory behind heterotrophic soil respiration processes is presented, with a focus on temperature response, and from this the appropriate soil heat-based regressor is drawn, which is termed production weighted heat (H_{pw}). Using a numerically-modeled soil system, that includes both heat and gas transport, we test the applicability of H_{pw} under a variety of model conditions. Finally, the H_{pw} method was applied to a portion of a comprehensive soil respiration and temperature data set that spans more than 100 days of uninterrupted measurement.(Martin et al., 2012).

7.4 Theory

Consider an idealized soil in which CO_2 is produced (P) as a function of both depth (z) and temperature (T):

$$P(z,T) = \Gamma(z)\Psi(T(z)) \tag{7.1}$$

where Γ(z) is the distribution of production with depth at a fixed temperature and Ψ(T(z)) is the temperature function which modifies Γ(z) (i.e. Ψ(T(z)) may be the Q_{10} function).

Starting with the most basic case, one can assume that each depth in the soil profile produces CO_2 at the same rate such that Γ(z)=K, where K is some constant. Similarly one can assume that the response of production to temperature is linear, such that:

$$\Psi(T(z)) = \nu T(z) \tag{7.2}$$

where ν is the slope of the linear function that defines the temperature sensitivity of respiration. These assumptions yield the CO_2 production function:

$$P_l(z,T) = K\nu T(z) \tag{7.3}$$

Assuming that all CO_2 produced in the soil profile exits the soil via the soil surface instantaneously (neglecting gas diffusion for now), the surface flux can be determined by integration of Eq. 7.2:

$$F = K\nu \int_{z=0}^{z_{max}} T(z)dz \tag{7.4}$$

where z=0 is the soil surface and z_{max} is the maximum depth to which CO_2 is produced. This example is somewhat trivial since it is easily seen that to regain the temperature sensitivity, ν, one must divide surface flux by the product of K and depth integrated temperature (or alternatively, regress flux against the product of K and depth integrated temperature), but it provides motive for use of the same approach with more complicated production functions.

Expanding from this simple case, multiple studies have found that the distribution of CO_2 production with depth is approximately exponential (Risk et al., 2002a,b; Davidson and Trumbore, 1995; Davidson et al., 2006a), with CO_2 production decreasing with increasing depth because of changing substrate supply, expressed as:

$$\Gamma(z) = Ae^{-z/d_p} \tag{7.5}$$

where A is some constant that describes the respiration magnitude and D_p is the e-folding depth of production (63% of respiration occurs above the e-folding depth and 37% below).

Similarly for Ψ(T(z)), many field and laboratory studies have found an exponential relationship between temperature and CO_2 production, commonly expressed using the Q_{10} relationship (Davidson et al., 2006b):

$$\Psi(T(z)) = \Psi_{ref} Q_{10}^{\frac{T(z)-T_{ref}}{10}} \tag{7.6}$$

where Ψ_{ref} is the respiration rate at the reference temperature (T_{ref}).

Combining Equations 7.2 and 7.3 yields the specific production function (P_s(z,T)):

$$P_s(z,T) = \beta e^{-z/d_p} \left(Q_{10}^{\frac{T(z)-T_{ref}}{10}} \right) \tag{7.7}$$

where β is a constant that combines A and Ψ_{ref}. Integration of the above equation with respect to depth gives the surface flux of CO_2. Unfortunately there is no closed form solution to this integral for arbitrary T(z), which means a specific T(z) function must be assumed to continue with the derivation. For simplicity the analytical solution for a sinusoidal temperature propagating through the soil was chosen (Hillel, 1982; Beltrami, 1996):

$$T(z) = T_0 + \Delta T sin(\omega t - z d_T) e^{-z d_T} \tag{7.8}$$

where T_0 is the mean temperature, ΔT is the amplitude of the sinusoidal temperature swings, ω is the angular frequency of the sinusoid, t is time and d_T is the thermal damping depth, defined as:

$$d_T = \sqrt{\frac{\omega}{2\kappa_T}} \tag{7.9}$$

where κ_T is the thermal diffusivity. It should be noted that for the solution given in Eq. 7.8, sums of solutions are also solutions, in other words, multiple terms may be added to the equation to describe two or more oscillation frequencies (i.e., daily and yearly). Substitution of Eq. 7.6 into Eq. 7.4 yields a specific function for T(z) which means the integral of Eq. 7.4 can be evaluated. In this case however, the double exponential in the Q_{10} function does not yield an analytical solution to the equation, but rather the integral must be numerically computed.

In the original simple example, where Γ(z) was constant with depth, the temperature sensitivity was regained by dividing by the depth integrated temperature (see Equation 7.4) because at constant temperature each soil depth contributes equally to the total efflux. In the new, more complex model, each depth does not contribute equally and this must be accounted for by finding the integral temperature weighted by the normalized production function:

$$H_{pw} = \int_{z=0}^{z_{max}} T(z)\beta_n e^{-z/d_p} dz \tag{7.10}$$

where β_n is the normalized equivalent of β. For the reminder of this manuscript, Eq. 7.10 will be referred to as the production weighted heat, or H_{pw}. Again by extension of the result for the linear case (Eq. 7.4) to this more complicated system it is hypothesized that the true temperature sensitivity should be given by regressing flux against H_{pw}.

7.5 Methods

7.5.1 Model

Model Implementation

As was mentioned in section 2 these equations must be integrated numerically. To test the hypothesis that the temperature sensitivity should be given by regressing

flux against H_{pw}, a numerical integration code was written to solve surface flux (F) and H_{pw} using Reimann summation with z-steps of 5×10^{-4} m. These data were then regressed using the R Nonlinear Least Squares (NLS) function to yield estimates of Q_{10} assuming an exponential relationship between F and H_{pw} of the form:

$$F = B_1(Q_{10}^*)^{\frac{H_{pw}}{10}} \tag{7.11}$$

where B_1 is some parameter that expresses the basal respiration rate and Q_{10}^* is the NLS estimated value for the true Q_{10}.

Before integrating Equations 7.7 (which implicitly includes Eq. 7.8 and 7.9) and 7.10, a range of possible parameters were defined and within that range randomly sampled sets of parameters to arrive at final solutions to the integrals. These parameter ranges are listed in Table 1, below. Note that two modes of oscillation are included in the temperature functions (Eq. 7.8 and 7.9), one that represents the yearly temperature oscillation (denoted with subscript y) and one that represents the daily temperature variation (denoted with subscript d). Parameters that were fixed at a single value included the Q_{10} (Q_{10}=2) and basal surface flux (F=1 at a homogeneous soil temperature of 0 °C, although the distribution of production in the subsurface will vary depending on d_p). In order to avoid confusion, when the results of this analytical (but numerically integrated) model are presented, it will be referred to as the Base Model.

Diffusion Model

While the theory presented previously outlines considerations of gas production and thermal dependence, soil gas transport was neglected in these solutions. To examine the potential effects of gas diffusivity regimes, a numerical one-dimensional soil gas diffusion model was used. Briefly, the diffusion model contained exactly the same production and heat transport equations as were presented in the Theory section above, but once gas was produced it was transported via Fick's law from the depth of production to the soil surface where it was emitted as surface flux. For a more detailed overview of the diffusion model, please see Nickerson and Risk (2009a) or Phillips et al. (2011).

7.5.2 Field Data

Field Site

Field data was collected from a mature Ponderosa pine forest in the Deschutes National Forest, OR, USA (44.452 N, 121.557W, 1253 m), part of the Ameriflux network of eddy covariance flux sites (Ameriflux site code: USME-2). Soil respiration was measured within 100 m of the eddy flux tower using a LI-COR LI-8100 and LI-8150 multiplexer unit. Four chambers were multiplied to the system, C1 was 0.6 m from a mature ponderosa pine tree, C2 and C3 were interspersed in bitterbrush and trees and were 1.2 and 1.8 m from the base of the nearest tree, respectively, and C4 was isolated from trees (3.4 m from the base of the nearest tree) in a bitterbrush clearing. Soil respiration was logger hourly, with a 3-minute measurement cycle (including a 30s dead band and 30s purge between chambers). Soil meteorological data were collected using standard AmeriFlux guidelines (http://public.ornl.gov/ameriflux/). Soil temperature was measured using thermocouples at 2, 3, 8, 16, 32 and 64 cm depths. Volumetric soil moisture was measured at 10, 20, 30, 50, 70, 100, 130 and 160 cm depths using three Envirosmart probes (Sentek Sensor Technologies, Stepney, SA, Australia). Data were logged every 30min using a Campbell Scientific 10x logger (Campbell Scientific Inc., Logan, UT, USA). Data from this site has been presented and analyzed previously in Martin et al. (2012).

7.6 Results & Discussion

7.6.1 Base Model

To initially test the hypothesis that production weighted heat is an appropriate regressor to estimate Q_{10} 140 random-parameter realizations of one year of soil flux and temperature data were simulated. The resulting flux data were then regressed against H_{pw} to yield estimates of Q_{10}. Using the full year of data, the mean estimate for these 140 realizations was $Q_{10}^{*} = 2.01$ (σ=0.01). Shown in Figure 7.1(a) is an example of one of these simulations, including time series for surface flux, soil heat content (simply the integral of temperature with respect to depth) and H_{pw}. Figure 7.1(b) shows the resulting Flux vs. H_{pw} curve for the time series data in Figure 7.1(a). For comparison Q_{10} was also calculated by the traditional method, using an

arbitrarily chosen measurement of soil temperature at 5 cm. The resulting mean Q_{10} estimate was 1.83 (σ=0.14), with the distribution of Q_{10} estimates over all 140 runs shown in Figure 7.2(a).

Estimation of Q_{10} using diel timescale data, a period over which it has generally been difficult to estimate temperature sensitivity because of hysteresis effects (see Phillips et al. (2011)), was also considered. Diel regressions using H_{pw} also yielded excellent results for the value of Q^*_{10}, with the mean value for 70 randomly sampled simulations being Q^*_{10}=2.00 (σ=0.01). Again, for comparison Q^*_{10} was calculated for the same set of simulations assuming an arbitrary temperature measurement depth of 5 cm and found a mean Q^*_{10}=1.69 (σ=0.20), with the distribution of Q^*_{10} shown in Figure 7.2(b).

These base model simulations yielded excellent results for Q_{10} estimates, both on annual and diurnal time scales. When compared to the standard method of using an arbitrary measurement depth for estimation of Q_{10} the H_{pw} method provides much more closely constrained estimates over all model conditions. Of course, the resulting distribution for the arbitrary case will change depending on which depth is chosen for the temperature measurement (Graf et al., 2008), but in all cases the H_{pw} method should perform better because it is not biased by the diffusion of heat into the subsurface.

7.6.2 Non-Uniform Q_{10}

It is, of course, unreasonable to assume that Q_{10} in the field will be homogeneous with respect to depth. Given this, the theory presented in Section 2.1 was modified to accommodate a linear Q_{10} distribution:

$$Q_{10}^{lin}(z) = \left(\frac{Q_{10}^{bot} - Q_{10}^{top}}{z_{max}} \right) z + Q_{10}^{top} \tag{7.12}$$

where Q_{10}^{top} is the Q_{10} value at the soil surface and Q_{10}^{bot} is the Q_{10} value at the soil base, z=z_{max}.

Simulations and subsequent regressions produced values for Q_{10} which were intermediate between Q_{10}^{bot} and Q_{10}^{top}. In this case, since the total soil CO_2 production is measured as surface flux, the resulting Q_{10} estimates should represent the average

Q_{10} for all CO_2 produced in the soil profile. This can be expressed as follows:

$$Q_{10}^{avg} = \int_{z=0}^{z_{max}} \beta_n e^{-z/d_p} \left(\left(\frac{Q_{10}^{bot} - Q_{10}^{top}}{z_{max}} \right) z + Q_{10}^{top} \right) dz \tag{7.13}$$

where Q_{10}^{avg} is the production weighted average Q_{10} value.

Figure 7.3 shows the resultant Q_{10} estimates for 50 random parameter sets with the expected value (Eq. 7.13) on the x-axis of the chart. In general, the estimated Q_{10} values were less than the expected values with the average deviation (Q_{dev}) being around -0.1 (Q_{10}^{avg} - Q_{10}^{*}).

Sensitivity analysis with this more complicated linear Q_{10} model revealed several parameter sensitivities, seen in Figure 7.4. First, the relationship between Q_{dev} and both yearly and daily temperature amplitude is shown in Figure 7.4(a). It becomes clear that as the daily amplitude approaches zero so does the deviation from the Q_{10}^{avg} value, suggesting that the source of error is the diel temperature cycles. Similarly as the yearly temperature amplitude approaches zero the error increases, again suggesting that the diel signal is biasing the Q_{10} estimate. Bias sensitivities also occurred for the damping depth parameter, shown in Figure 7.4(b), and the thermal diffusivity (Figure 7.4(c)). In both cases it is assumed the magnitude of the diel signal is responsible for the misestimate of Q_{10}, but the other parameters exacerbate the problem to a small degree. Several of the more biased model runs were examined to confirm the hypothesis that diel signals caused these biases. In essence, what was found is that when the daily signal is significant compared to the yearly signal, a diel hysteresis effect is created, caused by the varying Q_{10} with depth. This diel hysteresis causes the regression to become biased, as it does in typical flux vs. temperature data (Phillips et al., 2011), and also in temperature vs. temperature data in heat diffusion analyses (Smerdon et al., 2009). Further analysis of the bias using homogenous temperature profiles in the modeled soil showed that the heterogenous Q_{10} with depth used in these model simulations also causes the final output (that is the flux and H_{pw} data which are regressed) to have a slight bias away from being perfectly exponential, which also accounts for a portion of the bias seen in the sensitivity tests above. If the values of Q_{10}^{bot} and Q_{10}^{top} are set equal to each other (homogeneous Q_{10}), this non-perfect exponential bias is eliminated.

7.6.3 Gas Diffusion Model

While gas diffusion is not likely to be the main source of hysteresis in traditional flux vs. temperature data (Phillips et al., 2011), it should still have some effect on the surface flux signal as it controls the rate of CO_2 transport from the subsurface. This suggests that it should also affect the estimated Q_{10} gained using the production weighted heat (H_{pw}). To examine the gas diffusion influence, a series of numerical simulations were run with varying soil air-filled pore space and gas diffusivities, listed in Table 2.

Results from these simulations were predictable, in that regressions of flux vs. H_{pw} at high gas diffusivities yielded good results for estimated Q_{10}, when considering the full year of flux data (Figure 7.5). As gas diffusivities decreased, and the time for CO_2 to diffuse from the site of production to the surface increased, the performance of the H_{pw} regressions suffered. Decreases in the gas diffusivity cause increased hysteresis effects on both a diel and yearly scale, although the diel effects should be larger considering the characteristic gas diffusion times should be on the order of hours to days (Phillips et al., 2011). Because of this, the effect of LOESS smoothing (Locally Weighted Scatterplot Smoothing) the data to eliminate daily cycles was examined (also shown in Figure 7.5), however the LOESS procedure did not significantly improve the estimate of Q_{10} because of the supra-diel diffusion hysteresis effects. The resulting relationship between gas diffusivity and Q_{10}^* for the parameter set used in these simulations (see Table 2 caption) is shown in Figure 7.6. The shape (i.e. exponential rise to max) of the relationship is expected to hold under other parameter combinations, although the exact values for Q_{10}^* will be distinct for each parameter combination.

The diel H_{pw} estimates of Q_{10} in the gas diffusivity runs were also examined. As was expected, diel estimates of Q_{10} were biased more heavily by gas diffusion than yearly estimates with the closest to true Q_{10} value being 1.81 (σ=0.01) at the largest effective diffusivity of 8.63×10^{-6} m^2 s^{-1} (shown in Figure 7.6(b)). The time series data for dial Q_{10} as a function of the day of year (DOY) shows a periodic behaviour in the Q_{10} signal with the maximum and minimum values of Q_{10} preceding the maximum and minimum annual values for air temperature and soil heat. Again, for comparison, in each of the gas-diffusion runs the Q_{10} was calculated assuming

an arbitrary temperature measurement depth of 5 cm. This data is shown both in Figures 7.6a,b for comparison to the H_{pw} estimated Q_{10} values.

7.6.4 Estimating Production Weighted Heat (H_{pw})

Analysis and consideration of this model data has shown that two distinct problems arise when trying to estimate H_{pw} using data collected in laboratory or field experiments: 1) Estimating the soil temperature depth profile through time, and; 2) Estimating the shape of the production profile.

Estimating the soil heat profile can be done in several ways. Perhaps the most straight forward is by direct measurement of the soil temperature at many soil depths. It is difficult to estimate the spatial density at which this must be done to yield accurate heat content estimates, and for H_{pw} the density of measurement also depends on the production profile shape. For example if a large percentage of flux is produced in the top 2-3 cm of soil, then the thermistor density there would have to be considerably higher than deeper in the soil profile. Methods based on fibre optic temperature sensors may be the most likely candidates for the direct measurement method (Selker et al., 2006), although the spatial resolution of distributed fibre optic systems is not yet refined to the required resolution for this heat profile application. Current limitations using traditional thermistor based approaches lie largely in the size of equipment and accurate positioning in the soil profile relative to the soil surface.

Alternatively, the soil temperatures could be measured at discrete depth intervals and then interpolated or fitted using a physically based thermal transfer model (Beltrami, 2001). This approach allows interpolation at as fine a scale as the user defines, but obviously suffers from other problems related to model parameterization and simplified heat transport physics. For the model approach it is critical that field sites are set up such that the skin temperature, that is the temperature at the soil atmosphere interface, is accurately estimated as this can often be considerably different that the surface air temperature due to direct radiation and latent heat effects (Smerdon et al., 2004). Additionally, at least two (preferably many more) in soil sensors are required to estimate the second order derivative of the heat profile for model parameterization and fitting purposes.

Secondly, and more critical to estimating the value of H_{pw} is the estimation

of the shape of the production profile, as it can strongly modify the production-weighted heat content. The only real methods to do this are via the flux gradient approaches (Risk et al., 2002a,b; Tang et al., 2003, 2005a), where the soil pore space gas concentrations and gas diffusivities are used to estimate production over discrete depth intervals. To obtain the required density of points it would be relatively easy to interpolate over this profile with a fitting function, be it a polynomial, spline or any other characteristic function. The major difficulty comes in estimating the soil gas diffusivity, which is the least certain parameter in the flux gradient approach and can therefore significantly skew results if mis-estimated. Several methods for estimating diffusivity are available, including mathematical models (McCarthy et al., 1995; Moldrup et al., 2000), inversion of data (Koehler et al., 2010), and direct measurement (Risk et al., 2008b).

7.6.5 Field Data

Again, while field data is not the ideal way to prove a methodological approach, it is ultimately where the approach will be applied and provide benefit to the understanding of soil respiration processes. Using measured temperatures at the site as constraints, the soil profile temperatures were modeled using a standard 1D conductive heat transport model (1 cm model layers). A good correspondence between modeled and measured soil temperatures was found with slopes of modeled vs measured soil temperatures of 0.99 (r^2=0.95) and 0.86 (r^2=0.92) for 8 and 32 cm soil depths, respectively. These modeled temperatures were then integrated to obtain estimates of the soil heat content for the calculation of H_{pw}. It was assumed that the production profile at the site was exponential, having the same form as Equation 7.5. Multiple H_{pw} realizations were calculated by allowing the e-folding depth of production to vary between 1-100 cm in 1 cm increments. Each H_{pw} estimate was then regressed against soil flux from each chamber (C1, C2, C3, C4) and chose the H_{pw} estimate that provided the highest Pearson correlation coefficient as the correct estimate of H_{pw} at the site. This regression method was tested against the model data presented in the previous section and was reliable at reproducing the correct damping depth to within 1 cm (i.e. the resolution of the fitting algorithm). Gaseous diffusion contributions to H_{pw} estimates for this site were assumed to be negligible,

as the diffusion coefficients at the site have be previously estimated to be quite high (4.5×10^{-6} to 1.8×10^{-5} m^2 s^{-1}) (Martin et al., 2012).

Estimates of *e*-folding depth at the site ranged from 0.21 m to 0.11 m, yielding Q_{10} estimates ranging from 1.68 to 2.33 and basal respiration (T=0°C) estimates ranging from 0.66-1.92 (Figure 7.7). Sites that were closest to trees typically had higher basal respiration values but there was no significant correlation between basal respiration and distance from nearest tree. Distance to the nearest tree and *e*-folding depth were negatively correlated (r^2=0.69; slope p-value=0.11) suggesting that more respiration is occurring near the surface of the soil as the distance from trees is increased, likely due to a decrease in the proportion of root respiration in total soil respiration. Calculation of Q_{10} using production weighted heat, in its current form, assumes no autotrophic components because autotrophic respiration is likely responsive to aboveground conditions that are not included in the H_{pw} formulation (although the case could be made that if the autotrophic component was responsive to soil temperature at discrete depths the H_{pw} approach could work). Initial results (and field placement) suggest chamber 4 is likely the least influenced by autotrophic respiration and therefore it will be the focus for the remainder of the analysis.

Comparing time series of soil moisture and flux events it was noted that there were several occasions where flux was increased significantly by moisture pulses (e.g. Birch effect, Jarvis et al. (2006)). These data were hand filtered (removing obvious moisture-flux spikes) to determine if the H_{pw} regressions improved in the absence of moisture effects. The result was a slightly deeper damping depth for respiration (0.14 m), slightly inflated Q_{10} value of 2.53 and decreased basal respiration (0.54 μmol m^{-2} s^{-1}). The correlation coefficient improved from 0.67 to 0.74 in the moisture filtered case. Despite the removal of the large majority of data that appeared to be affected by moisture pulses, there was still considerable spread of data during the warmest periods recorded in the data set. Most of this spread seems to result from data collected in July, where temperatures were high and fluxes were at their peak. Despite similar temperature ranges occurring later in the summer, a steadily decreasing soil moisture content appears to be affecting the temperature response of flux (Figure 7.8). This result suggests that there is, not surprisingly, some component of the modeled flux vs. temperature relationship that is controlled by soil water content which is currently

not embodied in the H_{pw} formulation.

7.7 Recommendations & Conclusions

Estimation of the temperature sensitivity of heterotrophic respiration can be improved through the use of the H_{pw} approach. Not only does the approach yield more accurate estimates of modeled temperature sensitivity, it is also arguably the most theoretically robust analytical temperature-flux model available. There are still complications to the use of the method, including estimating of the soil heat using field data, constraining the shape of the biological CO_2 production profile, including the effects of gas diffusivity and the impact of soil moisture, and complications related to the presence of autotrophic activity in the data (which is not included in the current model because of the aboveground influences on autotrophic respiration). Obviously one does not expect the current analytical model to be able to cope with all of these issues, and thus it is presented as a "second-order" approach to the problem of estimating the environmental sensitivities of respiration. Ultimately the most useful methods will include a combination of the H_{pw} approach and process-based descriptions of the other physical and biological soil processes that control surface flux. This approach could eventually take the form of a fully-coupled model where parameterization is accomplished via field measurements and computational inversion algorithms (i.e. Metropolis Monte Carlo). This more flexible model structure will also likely be more cross applicable to field conditions ranging from desert to rainforest, assuming of course the physics and biology are accurately described.

Table 7.1: Equation parameters and parameter ranges used in integrations of Eq. 7.7 and 7.10.

Parameter	Range
D_T	1 - 900 $\times 10^{-8}$ m^2 s^{-1}
d_p	0.01 - 0.40 m
T_0	0-20 °C
ΔT_y	2-20 °C
ΔT_d	2-15 °C

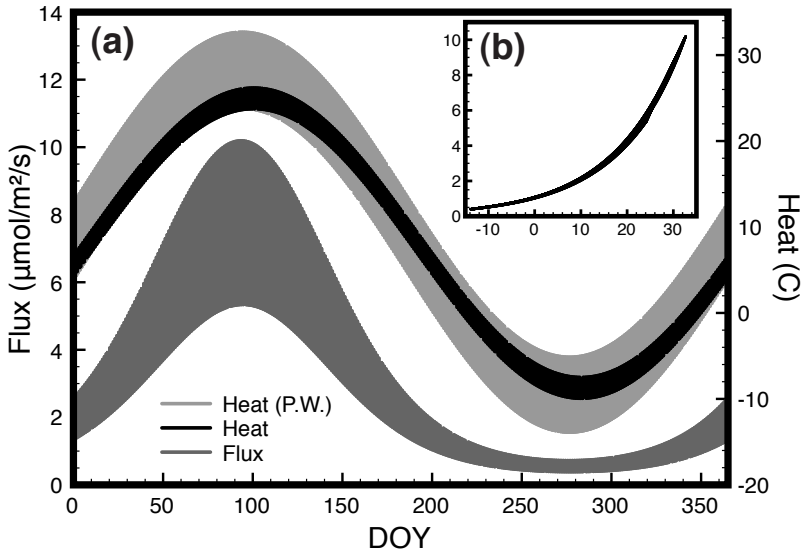

Figure 7.1: (a) Time series plot for surface flux, production weighted heat and unweighted soil heat content. Note that the production weighting shifts the heat curve back to correlate in time with flux leading to a non-hysteretic regression. (b) Final flux (y-axis; μmol m^{-2} s^{-1}) vs. H_{pw} (x-axis; °C) relationship for the time series data shown in (a).

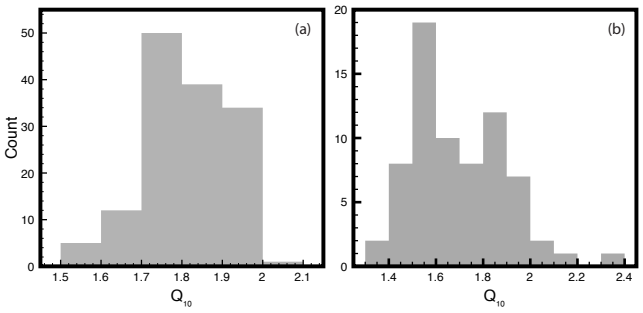

Figure 7.2: Distribution of yearly (a) and diel (b) Q_{10} estimates for an arbitrary temperature measurement depth of 5 cm.

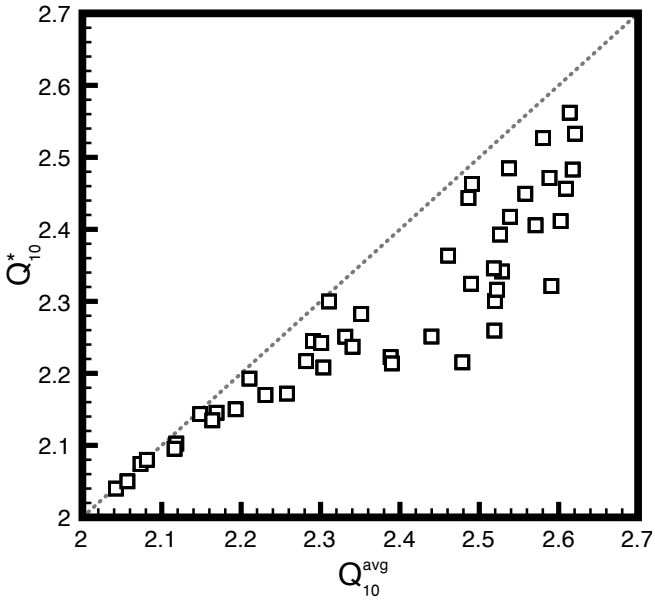

Figure 7.3: Comparison of expected (Q_{10}^{avg}) and regression estimated (Q_{10}^{*}) values for a linear Q_{10} profile with respect to depth (Eq. 7.12). Data were generated by random assignment of model parameters within the range specified in Table 1. In the linear Q_{10} vs. depth function, Q_{10} values at the soil surface (Q_{10}^{top}) and at depth (Q_{10}^{bot}) were assigned randomly with values between 2 and 3.

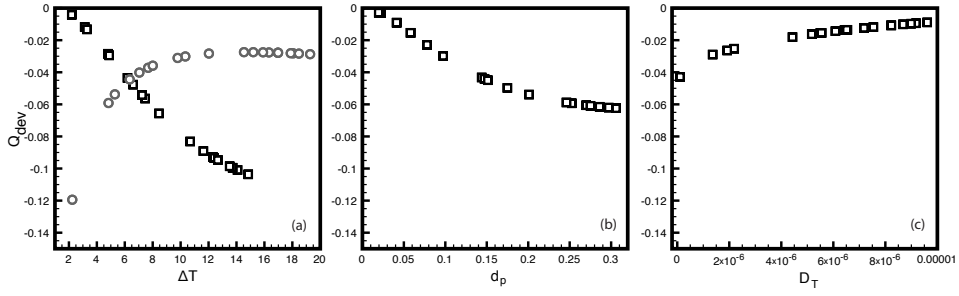

Figure 7.4: Sensitivity of the Q_{10} deviation (Q_{dev}) to yearly (grey circles) and daily (black squares) temperature amplitudes, damping depth (d_p), and thermal diffusivity (D_T). Data were generated by random assignment of model parameters within the range specified in Table 1.

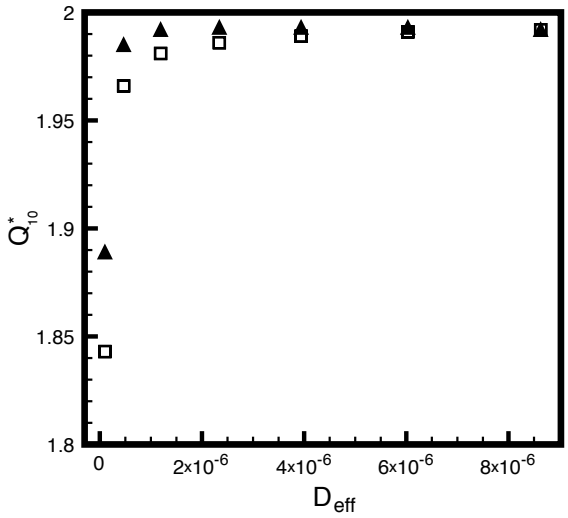

Figure 7.5: Estimates of Q_{10} with soil gas diffusion considering yearly data with 24h LOESS smoothing (triangles) and without LOESS smoothing (squares). Effective diffusivity (D_{eff}) in units of $m^2\ s^{-1}$.

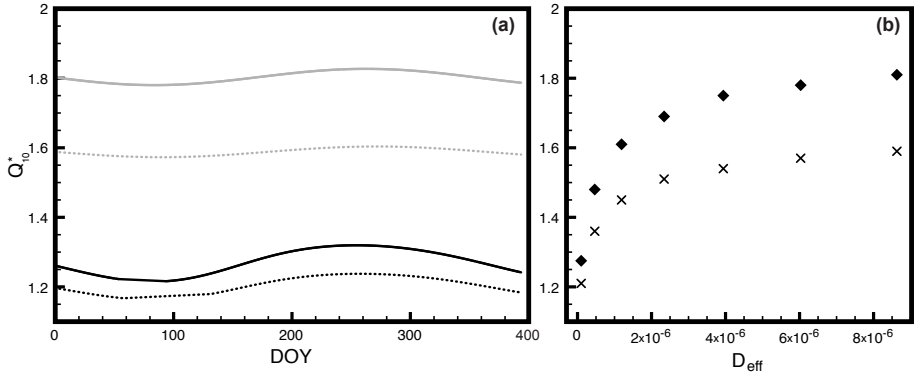

Figure 7.6: (a) Timeseries of Q_{10} estimates for low diffusivity (black lines, D_{eff}=9.94×10^{-8} $m^2\ s^{-1}$) and high diffusivity (gray lines, D_{eff}=8.63×10^{-6} $m^2\ s^{-1}$) for both the H_{pw} (solid line) and standard approach (T_{5cm}, dotted line). (b) Estimated Q_{10} over a range of diffusivities for the H_{pw} (diamonds) and standard approach (T_{5cm}, crosses).

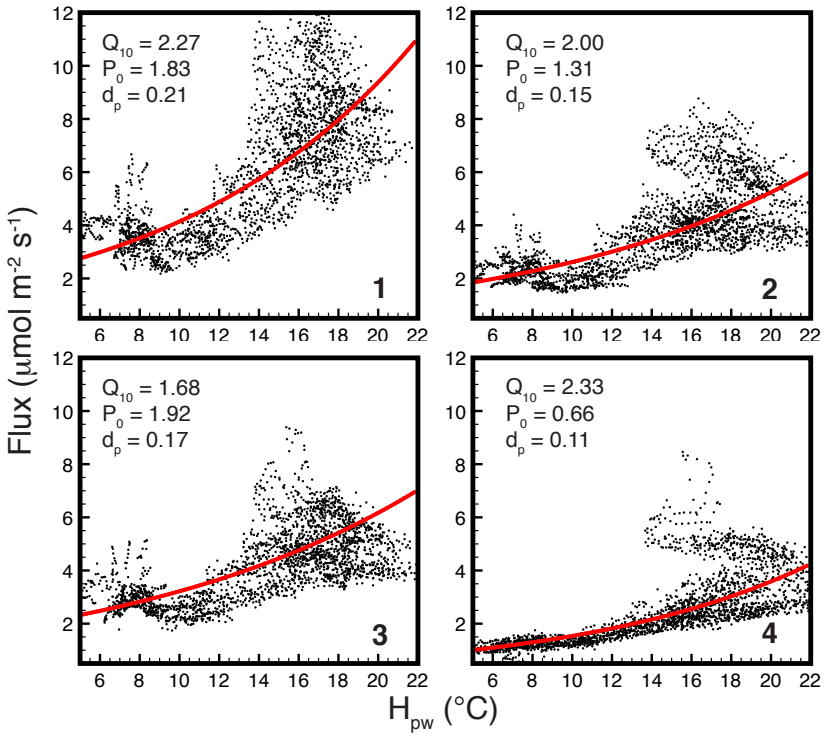

Figure 7.7: Soil flux vs. H_{pw} estimates for the 4 chambers deployed at the Deschutes National Forest field site. Chamber 1 had the closest tree proximity (0.6 m), followed by Chamber 2, 3 and finally Chamber 4 which had the highest distance from trees at 3.4m. The relatively good fit of the data in Chamber 4 is attributed to the decreased presence of autotrophic respiration in the total respiration measurements.

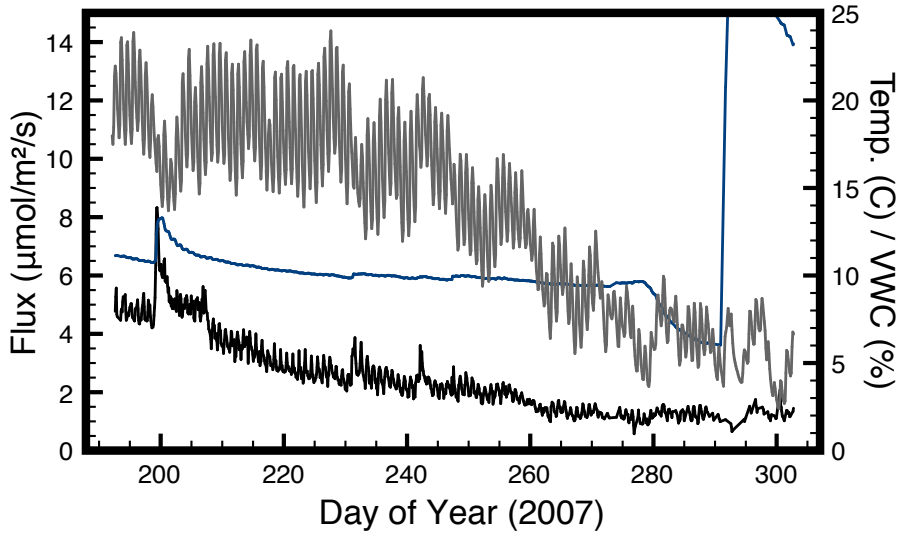

Figure 7.8: Timeseries of soil flux (black line), soil temperature (8 cm, grey line) and soil VWC (10 cm, blue line) which clearly demonstrates the effect that soil moisture is having on the measured flux time series which is affecting the performance of the H_{pw} regressor.

Chapter 8

Challenges in Determining the Environmental Sensitivity of Soil Respiration: Data Interpretation and the Role of Isotopic Data

8.1 Preamble

This chapter presents a conceptual model for data interpretation based on the research presented in other chapters of this thesis and discusses the future uses of isotopic data in soil respiration modelling. I am the primary author on the manuscript and have performed all analysis and writing. Dave Risk is supervisor of this work. This chapter has not been published, but is intended for journal submission at a later date.

8.2 Abstract

Some soil respiration studies suggest that physical controls on the soil influence the measurement and interpretation of soil respiration data as much or more than biological drivers. Inclusion of complex physical and biological processes in soil respiration models requires a move away from statistical approaches using simple equations and toward process-based models that incorporate complex system behaviours. However, these process-based modelling approaches require a higher degree of parameterization and significantly more measured field data as model constraints. Here a concept termed "Soil Process Detail" is presented that relates a model′s complexity to the amount of information required to produce reliable and accurate model results. This framework clearly shows the utility of process-based models but also accounts for the tradeoff between model realism and supplementary information requirements. Finally, the role of soil gas isotopologue measurements in informing process-based models is also discussed. These isotopic measurements hold the key to increasing model information and better constraining model results.

8.3 Introduction

Atmospheric concentrations of greenhouse gases (GHGs) play an extremely important role in regulating Earth's climate system (IPCC, 2001). Carbon dioxide (CO_2), which is produced primarily by aerobic respiration and consumed by photosynthetic activity, is arguably the most well studied GHG to date. While it is agreed that the processes underlying photosynthetic uptake of CO_2 by plants are well understood, much of the literature suggests that a process-based understanding of soil respiration is lacking (Davidson et al., 2006b). Researchers have made many great strides toward understanding the fundamental soil biology and ecology (Schimel and Weintraub, 2003; Tang et al., 2005a; Risk et al., 2008a; Davidson et al., 2012), developing robust methodologies for measuring GHG exchanges (Davidson et al., 2002; Subke et al., 2004; Livingston et al., 2005; Senevirathna et al., 2007; Risk et al., 2008b), and adopting more complex mathematical techniques for analysis and predictive modelling (Pumpanen et al., 2003; Reichstein et al., 2005; Ryan and Law, 2005; Livingston et al., 2005; Graf et al., 2008). To date, much of this research has focused on the biological properties of the soil system, as the soil organisms are ultimately the producers of CO_2. However, there are many physical processes that control the transport of decomposable substrate (Davidson et al., 2012), nutrient supply (Schimel and Weintraub, 2003), the local-environment (i.e. temperature and moisture) (Xu et al., 2004; Wei et al., 2010; Falloon et al., 2011; Moyano et al., 2012; Suseela et al., 2012) as well as the eventual emission of the produced gas to the atmosphere (i.e. diffusion and advection) (McCarthy et al., 1995; Moldrup et al., 2000; Kayler et al., 2010; Bowling and Massman, 2011). While researchers acknowledge these complexities they have not, until recently, received as much attention as the biological aspects.

These physical considerations affect the fundamental soil system dynamics, and therefore impact the measurement and interpretation of soil respiration data (Livingston et al., 2005; Phillips et al., 2010, 2011). Recognizing the importance of soil physics in soil respiration studies is one step toward developing more robust models that can be used to predict soil respiration dynamics across space and through time. However, the inclusion of these physical processes, as well as more complex biological processes, in soil respiration models requires a move away from statistical approaches

using simple equations and toward process-based models that can incorporate complex system behaviours. These process-based modelling approaches require a higher degree of parameterization using measured field data in order to function properly. Here, we present two concepts that could increase the ease and accuracy of future modelling efforts, which are not normally considered. The first concept is that of Soil Process Detail, or the relevancy of constraining information to models that aim to estimate soil parameters and future behaviour. The second concept is that of isotopic data integration.

Soil Process Detail relates a model′s complexity to the amount of information required to produce reliable and accurate model results. This conceptual framework is intended to help researchers better understand how increases in model complexity need to be matched with an increased amount of information used for model parameterization. Ultimately process-based approaches will lead to more robust, more transferrable models but without consideration of Soil Process Detail, process-based models are likely to produced biased results leading to misinterpretation and misunderstanding of soil respiration dynamics. This being said, even when models are well formulated, they must be fed relevant data in order to appropriately constrain parameters and produce robust results. As a follow-up to the concept of Soil Process Detail, the application of isotopic data to challenges in understanding soil respiration is discussed. While isotopic tracing of C through the soil system has been commonplace for many years (Cerling et al., 1991; Amundson et al., 1998; Rochette et al., 1999; Högberg et al., 2001; Formanek and Ambus, 2004), the relatively recent development of accurate, high-resolution, field-deployable laser-based techniques is opening up new avenues of research that are particularly exciting for soil respiration modelling. In these models, isotopic data can be used to further constrain model parameters to offer a more robust understanding of soil respiration at the process level than can be achieved using bulk gas emissions data alone.

The balance of this manuscript will introduce and provide examples of how increasing Soil Process Detail can help to further constrain models, and will discuss the possible avenues through which isotopic data might be integrated into process based models in order to improve their overall predictive ability.

8.4 Soil Respiration Modelling & Soil Process Detail

8.4.1 Background

In their 2006 paper, Davidson et al. note that the majority of currently used soil respiration models still rely on chemical thermodynamics equations developed in the 19th century (Arrhenius, 1889; van't Hoff, 1898), or modifications thereof. While theoretically the underlying chemical reactions which eventually lead to respiration should follow these classical thermodynamics equations, there is the obvious caveat that the biological systems are significantly more complex and rely on numerous internal and external processes to mediate respiration. This complexity has been recognized for many years and the recent significant increase in data temporal density and quality has further highlighted the need for more complex models to describe the wealth of new data (Richardson et al., 2006b; Davidson et al., 2012). For reference, Table 1 presents a brief overview of some commonly used respiration models and the predictive variables included in their formulation.

These respiration models can be broadly split into two categories; empirical/statistical models (e.g. Linear, Polynomial, Fourier) and process based models (e.g. Q_{10}, Lloyd and Taylor, Enzyme Kinetics). In general, the statistical models are quite robust for reproducing site and measurement period specific data patterns and gap filling procedures but are perhaps less useful for prediction of future respiration. This is largely because the model environmental sensitivities that are critical for predictive reasons are generally poorly formulated or convoluted into other variables. An excellent example of this convolution is the use of Julian Day in the Neural Network Model (H, Table 1), which could be a proxy for temperature, substrate supply, phenology and a host of other time-variant parameters. On the other hand, process based models of respiration are likely to offer far greater predictive value being more robust through time and across space (more transferrable) because of their bottom-up approach and the inclusion of observable thermodynamics and enzyme reactions. This makes them less likely to break down when being used to extrapolate into future climates and also makes process based models the ideal approach for better understanding the nature of and interactions between heterotrophic and autotrophic respiration processes in-situ, both at short and long time scales.

However, even if we assume that process based models are the most robust approach for interpreting and extrapolating respiration data, it should be recognized that there are multiple dimensions to the problem of model selection or formulation. Arguably as important as the problem of biological model selection is the choice of the level of detail to include for non-biological soil processes, for example soil temperature, moisture or gas diffusion. From here on, we will use the term Soil Process Detail (SPD) to refer to the level of information used in the description of the driving (independent) variables for the biological respiration model. We will also refer to biological respiration models on a continuum from empirical to process based; again assuming well parameterized process based models are the optimum.

These two definitions allow us to construct a conceptual phase-space that can be used to evaluate the utility (which we will loosely define as the predictive power, or predictive ability) of a model. Model utility relates to a models ability to accurately describe actual biological, chemical and physical processes and thus its ability to extrapolate (predict) soil respiration measurement across space and time. To place this in context, consider the well-known Q_{10} model for respiration (Figure 1). This model has a relatively low SPD as it is only a function of temperature, and traditionally only a single arbitrary temperature measurement is used as input. In contrast, at the same point on the empirical-to-process-based axis of Figure 1, sits the Linear Combination Q_{10} model proposed by (Reichstein et al., 2005); but, this model has a higher SPD because it allows for input of the soil temperature at multiple depths, creating a fuller description of the soil physical environment. Still further up the Soil Process Detail axis sits the Production Weighted Heat approach of (Nickerson et al., 2014) which allows for a complete description of the soil temperature profile, converging on the maximum information line of Figure 1 and arguably providing a more realistic SPD than the biological model (assuming the Q_{10} model is a simplified version of real respiration processes). Note that as we moved up along the SPD axis of the plot toward the maximum information line we crossed into a new utility tier indicating the model will likely have better predictive power.

Consider for example the Dual Arrhenius and Michaelis-Menten (DAMM) model proposed by Davidson et al. (2012) in which soil temperature, moisture and soil pore space characteristics are implicit to the model structure. In order to accurately

employ this model in-situ, there should be full and accurate descriptions of the soil temperature, moisture and pore space (air-filled, water-filled and total) as a function of both depth and time in order to minimize error in the predicted model environmental sensitivities and therefore maximize the predictive ability of the model. If this full description is not present, the model will fall into a lower utility category, even though it is on the higher end of the process-based portion of the scale. On the other hand, it is much easier for this model to move up through utility tiers because the utility gradient is steepest on the process-based end of the phase-space (i.e. only a few measurements of soil temperature, pore space, etc. would allow the DAMM model to easily surpass a statistical model in utility).

While the idea of Soil Process Detail may still be somewhat abstract, in the following section, we will show a practical example of the importance of increasing the Soil Process Detail for allowing accurate estimation of biological environmental sensitivities. Accurately estimating these sensitivities, or model parameters, is critical to ensuring that utility is maximized. Without accurate estimates, models will not have predictive power over time, nor will they be transferrable from location to location.

8.4.2 Soil Process Detail - A Practical Example

The importance of sufficient SPD can be most directly demonstrated through analysis of simulated respiration data, which offers a controllable pseudo-reality in which to test the concept. In this simulation, we assume the soil is a many-layered system with layer specific temperatures and CO_2 production rate (Phillips et al., 2011). Determination of the total soil production is achieved by numerical integration of the layer specific production equations. We make several assumptions about the behaviour of the biological respiration, first that it follows a Q_{10} behavior (Model D in Table 1), second that it is distributed exponentially with depth and, third that the Q_{10} parameter is depth invariant (Phillips et al., 2011). To evaluate the effect of various simulation parameters on each of the approaches presented below, we analyzed 90 randomized instances of the model, allowing for a reasonably accurate statistical evaluation of each approach under varying climate and soil conditions. Further detail on the simulations, including the randomized parameter approach, can be found in

Nickerson et al. (2014) and (Phillips et al., 2011).

Conveniently, as was mentioned in the discussion above, there are three methods (D,I,K, Table 1) that use Q_{10} descriptions of biological processes (i.e. have the same value on the empirical to process based scale) but differ in the level of Soil Process Detail (SPD) used in the method formulations. This allows us to evaluate the importance of increasing soil level detail directly, without convolution by variant biological behaviours.

Frequently researchers use the standard Q_{10} formulation (Model D, Table 1, Figure 1) with regression approaches to correlate air or soil temperature at a single arbitrary depth with soil respiration (usually both parameters are measured at the same temporal frequency). The Q_{10} model parameter estimates can be determined either by linearization of the function and subsequent linear regression, or by non-linear regression approaches. In this example we have processed simulated soil respiration data (90 randomized instances) with the Q_{10} function by linearization and regression of the transformed flux vs. soil temperature measured at various arbitrary depths. Shown in Figure 2 are the resulting estimates for Q_{10} using arbitrary soil temperatures as the independent variable in the Q_{10} regressions. Note first that no soil depth accurately predicts the modeled Q_{10} in all model instances (i.e. the histograms have a significant standard deviation in all cases). In some cases the correct Q_{10} is included within the spread of the histogram. This is expected to happen, as was shown by Graf et al. (2008), and results from an optimal selection of temperature depth such that the true Q_{10} is recovered. This optimum is predictable, given knowledge of the soil production profile and thermal regime but this approach offers a heuristic method of Q_{10} determination only (Phillips et al., 2011), and furthermore one that will change with changes in soil conditions that affect the CO_2 production and thermal conductivity.

Moving along the Soil Process Detail scale, we next demonstrate the ability of the linear combination Q_{10} approach proposed by Reichstein et al. (2005) to predict an accurate Q_{10}. The form of this equation is presented in Table 1 (Linear Combination Q_{10}) and the parameter estimates can be determined by non-linear regression approaches. We applied this approach to the same set of 90 model instances used above, increasing the number of temperatures used from one (which should

yield the same result as the standard regression approach, Figure 3) to a total of 6 temperatures distributed from 0 cm to 32 cm in the soil (0.00 m, 0.02 m, 0.04 m, 0.08 m, 0.16 m, 0.32 m). Note that after 6 independent variables were included in the regression equation, the solution became over parameterized and would not converge (i.e. the data do not provide enough information to the model for a unique set of parameters to be realized). As the number of soil temperatures included in the model was increased, the Reichstein et al. (2005) approach showed a gradual convergence on the true Q_{10}, and a tightening of the distribution.

Interestingly, simultaneous with the Q_{10} convergence in the Reichstein et al. (2005) approach, we also note a loosening of the models ability to accurately predict the basal respiration (θ_1, θ_3, ... θ_{2i+1}, Table 1, Equation I) rate of the soil layers. Despite the fact that the simulation was parameterized with an exponential basal production vs. depth function, the Reichstein approach showed no systematic improvement in the prediction of the depth-dependent basal respiration estimates (Rn, Model I, Table 1). Fitting algorithm-driven adjustments (related to the numerical approach used in non-linear curve fitting) in the basal respiration estimates appeared to occur in an attempt to match the phase of respiration with the phase of the combined temperature data, as the number of temperatures used in the model increased. Note that Reichstein et al. (2005) had predicted this would happen with the model, as it is fully expected based solely on the mathematical curve-fitting approach. Even though the Reichstein et al. (2005) approach was unable to accurately estimate basal respiration rates, it continued to offer increasingly good estimates of Q_{10} with increasing Soil Process Detail (i.e. increasing number of temperatures included in the regression), as was expected based on the SPD conceptual framework outlined earlier. Readers should be aware that the simulations used here do not include error in the results, and thus the maximum number of soil depths that could be included before the model became ill-constrained is probably much higher than could be obtained using in-situ soil respiration and temperature data.

Finally, using the same set of 90 simulation instances, we tested the hypothesis that a continuing increase in Soil Process Detail would further enhance the stability and accuracy of the Q_{10} estimate by using the (Nickerson et al., 2013) production weighted heat approach. Perhaps not surprisingly, in a simulation where soil

temperatures are the only driving factor, the model which included the most complete description of the soil temperature profile in both space and time also yielded the most accurate Q_{10} estimates (Figure 4). Further analysis of the data set showed no sensitivities to any of the model input parameters and confirmed that the variation (σ=0.003) observed in the histogram in Figure 4 can be accounted for by numerical rounding errors in the simulation and subsequent fitting procedures.

8.4.3 Summary

Improving biological modelling of soil respiration, in particular moving toward process-based models of biological systems, is key in better understanding soil respiration. That being said, an improvement in the biological description of the system should be complimented by a similar improvement in the physical description of the system.

Computational tools are now at a stage where they can be used with relative ease to model these more complex systems, as is evidenced by the recent surge of complex model-data fusion, and these computational tools require sufficient SPD to adequately constrain parameters. While environmental measurements and interpolation of theses measurements using physical models (i.e. numerical heat transport and water transport models) helps increase SPD, eventually a limit will be reached where measurements of bulk trace gas emissions will no longer contain adequate information.

In this instance, isotopic tools can be used to augment these bulk trace gas flux measurements and help enhance the predictive power of soil respiration models. In the next section we will briefly discuss these isotopic methods, why the time is ripe to move towards more isotopic measurements in soil science and how they have helped and can continue to help inform the next generation of process based soil respiration models.

8.5 The New Role of Isotopic Data

Measurement and analysis of bulk greenhouse gas data has significantly enhanced our understanding of the fundamental biological, chemical and environmental processes controlling soil respiration. However, there are many questions that bulk gas measurements cannot answer because of the limited amount of information they

contain. Researchers have routinely used isotopic data to answer these more probing questions for several decades now, with excellent results (Cerling et al., 1991; Högberg et al., 2001; Formanek and Ambus, 2004; Bahn et al., 2009; Phillips et al., 2010; Albanito et al., 2012; Goffin et al., 2014). Isotopic studies are relatively sparse compared to bulk gas studies due to the overhead imposed by sampling for and measurement using Isotope Ratio Mass Spectrometry (IRMS). However, a new generation of spectroscopic instruments is offering the ability to measure isotopic gases in-situ with high-temporal resolution, which is opening up many new doors for soil respiration research (Midwood and Millard, 2011). We strongly believe that these high-resolution high-accuracy isotopic measurements are the next step in enhancing our process based understanding of soil respiration, both from heterotrophic and autotrophic organisms.

From a biological perspective, perhaps the most exciting prospect offered by the measurement of isotopes is the potential to separate autotrophic and heterotrophic respiration in-situ and with minimal disturbance to the natural system (Subke et al., 2006). Researchers have routinely used isotopic techniques to partition soil respiration into individual components (Formanek and Ambus, 2004; Albanito et al., 2012). In general this is made possible either by the natural difference in the isotopic signature of CO_2 respired by autotrophic and heterotrophic organisms (caused by differing biochemical processes) or by applying an isotopic label, either to the soil organic matter pool or canopy atmosphere which propagates through the atmosphere-plant-soil system creating distinctive isotopic signatures for each respiration source (Subke et al., 2009). The application of high-resolution, high-accuracy laser based systems in these partitioning studies promises excellent results. For example, the ability to detect changes in isotopic signature on timescales of minutes to hours is unprecedented in partitioning studies, which in many cases are fortunate to have a single measurement on a daily basis. This opens a whole avenue of research studying diurnal timescale changes in the proportions of autotrophic and heterotrophic respiration, caused by availability of light, vapour pressure deficit and a host of other covarying environmental drivers. The ability to detect changes in bulk gases at these timescales arguably caused a paradigm shift in the understanding and interpretation of bulk CO_2 respiration (Riveros-Iregui et al., 2007; Carbone and

Vargas, 2008; Risk and Kellman, 2008; Phillips et al., 2011), so it is not unreasonable to speculate that the same will be true of our understanding of short timescale isotopic processes.

On a similar thread, these laser-based systems have recently been applied to collect and analyze subsurface (soil pore) gases in order to construct a depth-resolved understanding of soil processes (Parent et al., 2013; Goffin et al., 2014). This type of research has been done for many years in bulk CO_2 research using solid-state CO_2 sensors (Tang et al., 2003; Xu et al., 2004). What is most compelling about these new subsurface methods is the potential to use them in conjunction with natural abundance or tracer techniques to partition heterotrophic and autotrophic respiration as a function of time and depth in the soil, in an attempt to correlate the various respiratory sources with variables such as rooting density or soil organic matter content (Goffin et al., 2014). These depth-dependent measurements are a critical input for process-based models that include diffusive processes and other time-lags between production of CO_2 in the subsurface and its eventual emission into the atmosphere which have generally been neglected (Nickerson and Risk, 2009a; Subke et al., 2009). The inclusion of depth-resolved isotopic partitioning data in additional bulk gas measurements is a critical next step in better understanding respiratory lags in the soil and accurately representing them in ecosystem model structure.

From a soil physics perspective, the measurement of isotopes brings an interesting new possibility to the table. For many years, researchers have been concerned about the potential for natural and artificially-induced advection of soil gases in environments where high wind and highly variable pressure gradients exist (Hutchinson and Livingston, 2001; Takle et al., 2004; Massman, 2006; Reicosky et al., 2008). These advective gas fluxes cause significant bias in measurements of soil gas fluxes, which are often assumed to happen under strictly diffusive conditions. Until recently these events were either tracked using differential pressure sensing equipment, or went largely unnoticed. Recent work by Bowling and Massman (2011) shows the potential for isotopic data to detect these advection events. Because advective transport does not fractionate against heavy isotopes (but diffusion does) one can use isotopic data to detect and quantify the effects of advection on total soil gas transport. While this is useful in all environments, it is of particular interest to researchers working in

snow-covered regions, where advective movement of CO_2 may represent a significant portion of the winter and annual CO_2 fluxes (Massman, 2006; Bowling and Massman, 2011).

While these isotopic studies are extremely interesting from an experimental standpoint what is more exciting is the potential for these measurements to help constrain soil respiration models. As was mentioned, the measurement of bulk gas fluxes when augmented with soil process data, such as temperature and moisture contents and transport, provide important constraints of soil respiration model parameters. However, a critical missing component in constraining these models is the timing, magnitude and source location (e.g. depth) of heterotrophic and autotrophic respiration in the soil profile and how this gas is eventually transported from the soil to the atmosphere. The current lack of this information from the field observations and experiments means that modellers must make various assumptions that may or may not be true of the soil system thereby hampering our ability to fully understand the processes that drive soil respiration from both major components.

8.6 Conclusions

While it is likely that biological descriptions of respiration processes will continue to evolve over the coming years, there is a strong need for the soil physics and mathematical interpretive framework to evolve alongside. Without this tandem development our process-based understanding of soil respiration process will always be lacking. Consideration of Soil Process Detail when formulating and implementing process-based models will ultimately help reduce or exclude biased results that may lead to poor interpretation or misunderstanding of soil respiration processes. From a field and laboratory measurement perspective, one of the most critical next steps to improving both the biological and physical understanding of soil respiration processes is to utilize isotopic data to its fullest extent. By combining process-based approaches with isotopic data, researchers will have the ability to probe the dynamics of soil respiration with more detail and accuracy than can be accomplished using bulk gas measurements alone.

Table 8.1: Respiration models commonly used by researchers, as modified from Richardson et al. (2006). Model parameters, θ_1, . . . θ_n, differ among models. T refers to a measured temperature variable, either T_{air} or T_{soil}. T_{ref} is a fixed reference temperature, usually 10°C. JDπ is the Julian Day (JD) expressed in radians (=2π × JD/366). SWC is soil water content, in % by volume.

Model	Formula	Reference
[A] Linear	$\theta_1+\theta_2 T$	Wofsy et al. (1993)
[B] Polynomial	$\theta_1+\theta_2 T+\theta_3 T^2$	Wofsy et al. (1993)
[C] Arrhenius	$\theta_1+\exp\left[\left(\frac{\theta_2}{283.15R}\right)\left(1-\frac{283.15}{T}\right)\right]$	Lloyd and Taylor (1994)
[D] Q_{10}	$\theta_1 \times \theta_2{}^{(T-T_{ref})/10}$	Black et al. (1996)
[DS] Q_{10}-S: T=T_{soil}		
[DA] Q_{10}-S: T=T_{air}		
[D1] Q_{10}-vTemp: Temperature Varying Q_{10}		
[D2] Q_{10}-vTime: Time Varying Q_{10}	$\theta_1[\theta_2 + \theta_3 sin(JD_\pi) + \theta_4 cos(JD_\pi)]^{(T-T_{ref})/10}$	
[D3] Q_{10}-Gresp: SWC Modulated	$\theta_1 \times \theta_2{}^{(T-T_{ref})/10} \times \frac{SWC}{SWC+\theta_3} \times \frac{\theta_4}{SWC+\theta_4}$	Carlyle and Ba Than (1988)
[E] Lloyd and Taylor	$\theta_1+\exp\left(\frac{\theta_2}{T+273.15-\theta_3}\right)$	Lloyd and Taylor (1994)
[Er] Lloyd and Taylor-Rest: Restricted Form	$\theta_1+\exp\left(\frac{-308.56}{T+46.02}\right)$	Lloyd and Taylor (1994)
[F] Logistic	$\frac{\theta_1}{1+exp(\theta_2+\theta_3 T)}$	Barr et al. (2002)
[G] Fourier	$\theta_1+\theta_2 sin(JD_\pi)+\theta_3 cos(JD_\pi)+...$	Hollinger et al. (2004)
[H] Neural Network	$f(T_{soil}, T_{air}, JD_\pi, SWC, ...)$	Hagen et al. (2006)
[I] Linear Combination Q_{10}	$\theta_1 \times \theta_2{}^{(T-T_{ref})/10} + \theta_3 \times \theta_4{}^{(T-T_{ref})/10} + ...$	Reichstein et al. (2005)
[J] Enzyme Kinetics	$V_{max} \times \frac{[S_x]}{kM_{S_x}+[S_x]} \times \frac{[O_2]}{kM_{O_2}+[O_2]}$	Davidson et al. (2012)
[K] Production Weighted Heat	$\theta_1 \times \theta_2{}^{\int (T(z)-T_{ref})/10}$	Nickerson et al. (2014)

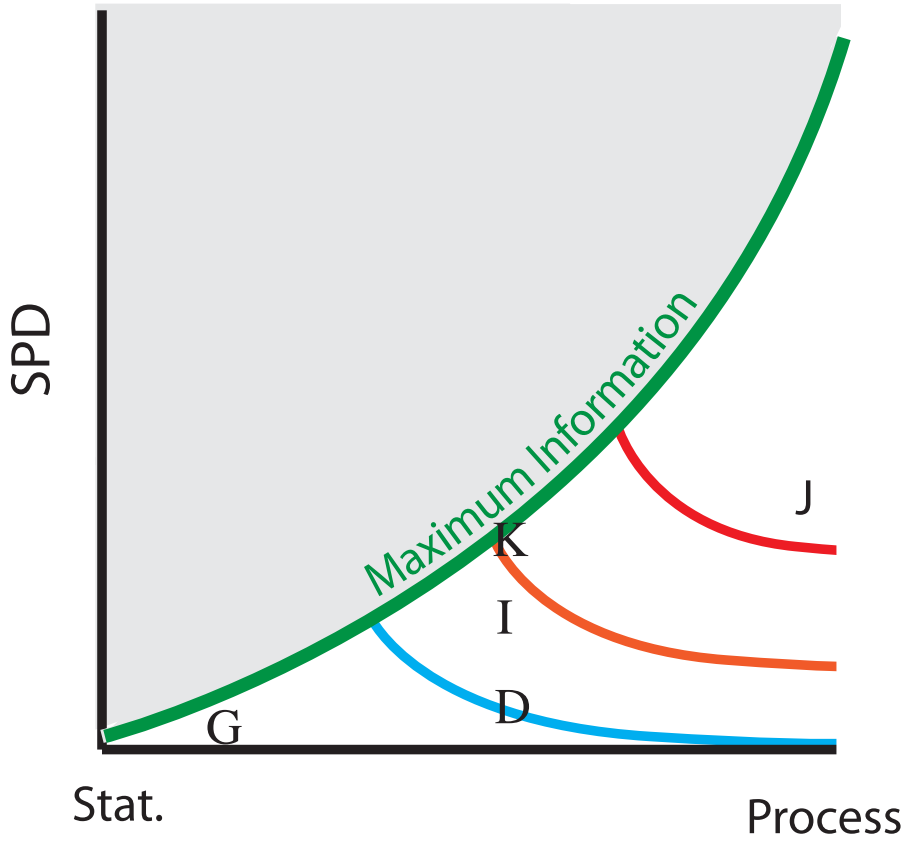

Figure 8.1: Conceptual framework for the optimization of Soil Process Detail (SPD) populated with several commonly used soil respiration models from Table 1. No models SPD can ever exceed the maximum information line, which is defined by the number of soil processes included in the model structure (for example the Q_{10} model (D, Table 1) only considers soil temperature, so when soil temperature is fully described in space and time the model will reach the maximum information line). Contours indicate increasing model utility (with increasing redness), defined as the predictive power, or predictive ability of a model.

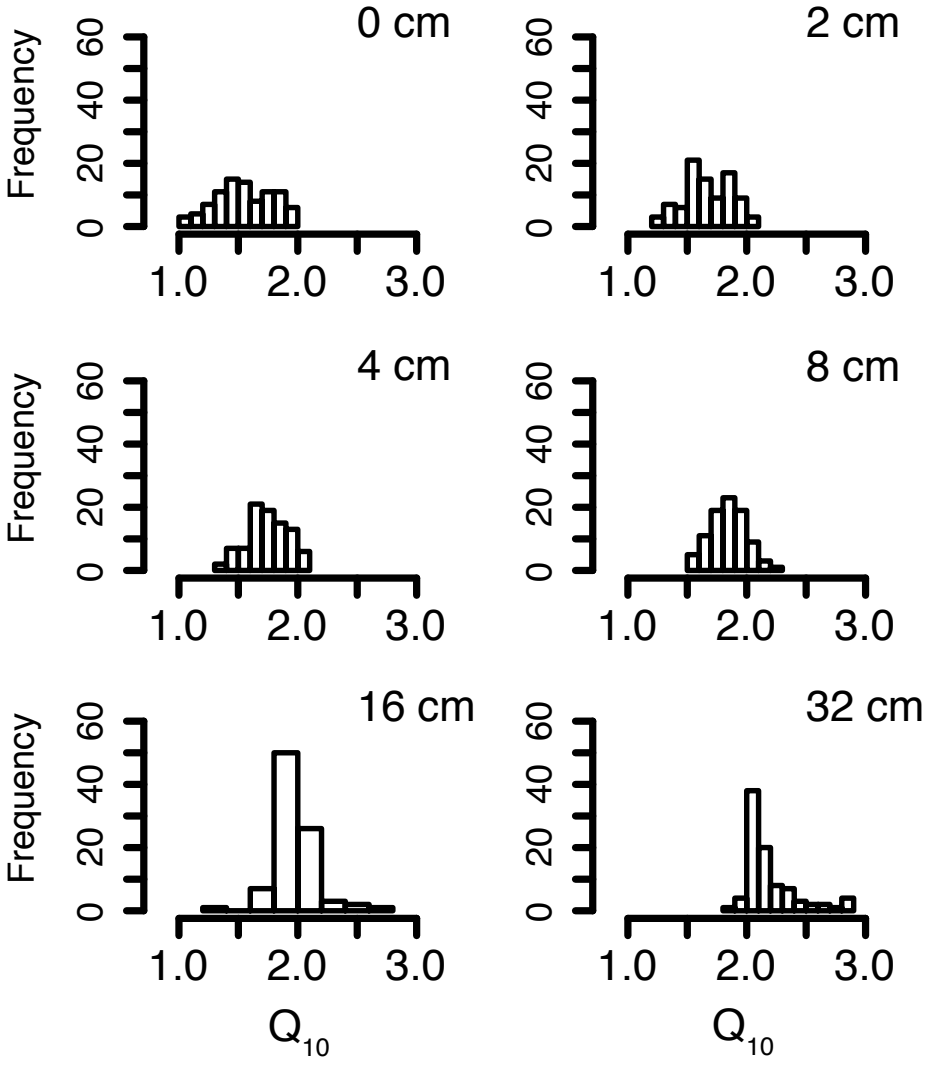

Figure 8.2: Estimates of the Q_{10} temperature sensitivity (actual Q_{10}=2.0) of soil respiration for 90 random simulation instances for six arbitrary temperature measurement depths. Note that these simulations show an optimum depth of 16 cm, consistent with the work of Graf et al. (2008), but this optimum is not stable at all soil parameter combinations, as is evident based on the large spread in the Q_{10} distribution.

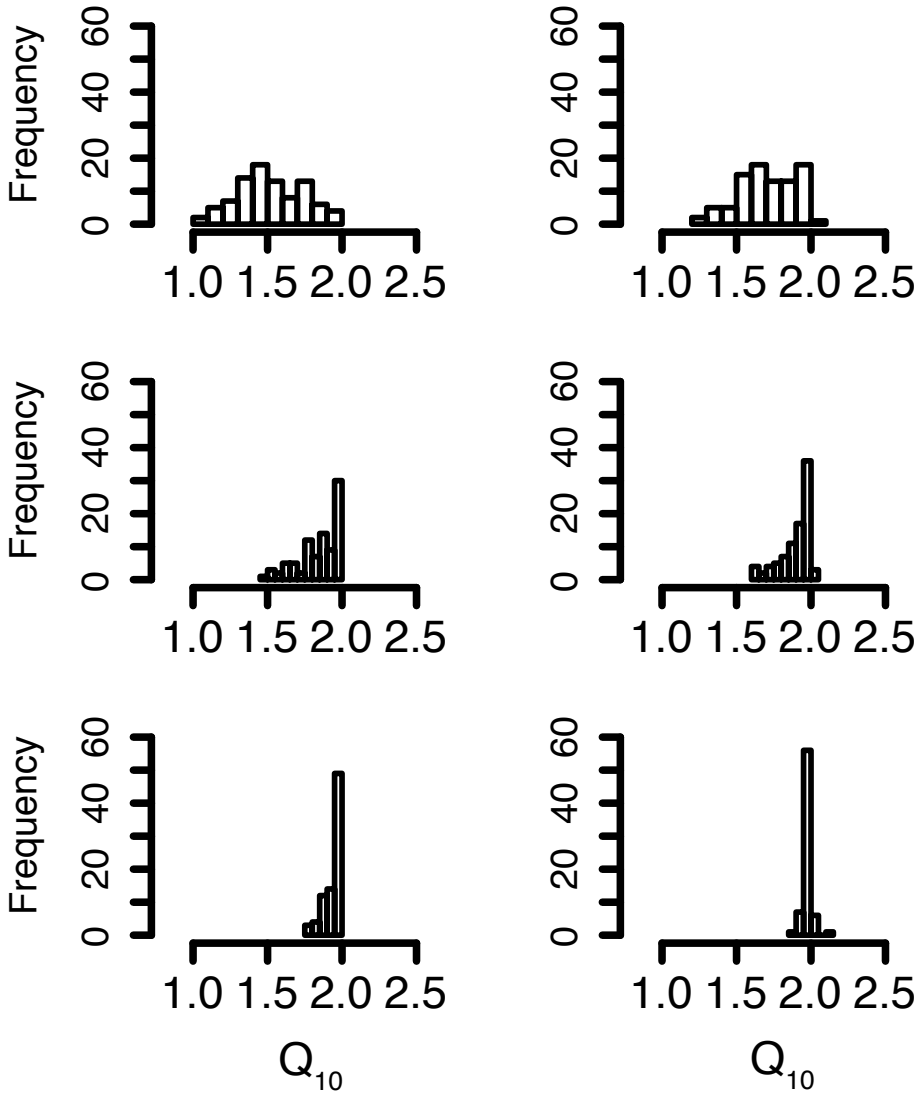

Figure 8.3: Estimates of the Q_{10} temperature sensitivity (actual Q_{10}=2.0) of soil respiration for 90 random simulation instances for linear combinations of up to 6 soil temperature measurement depths using the Reichstein et al. (2005) model. As the number of soil depths used in the model increases the estimated Q_{10} converges to the actual Q_{10}, however as the model grows so does the potential for over fitting.

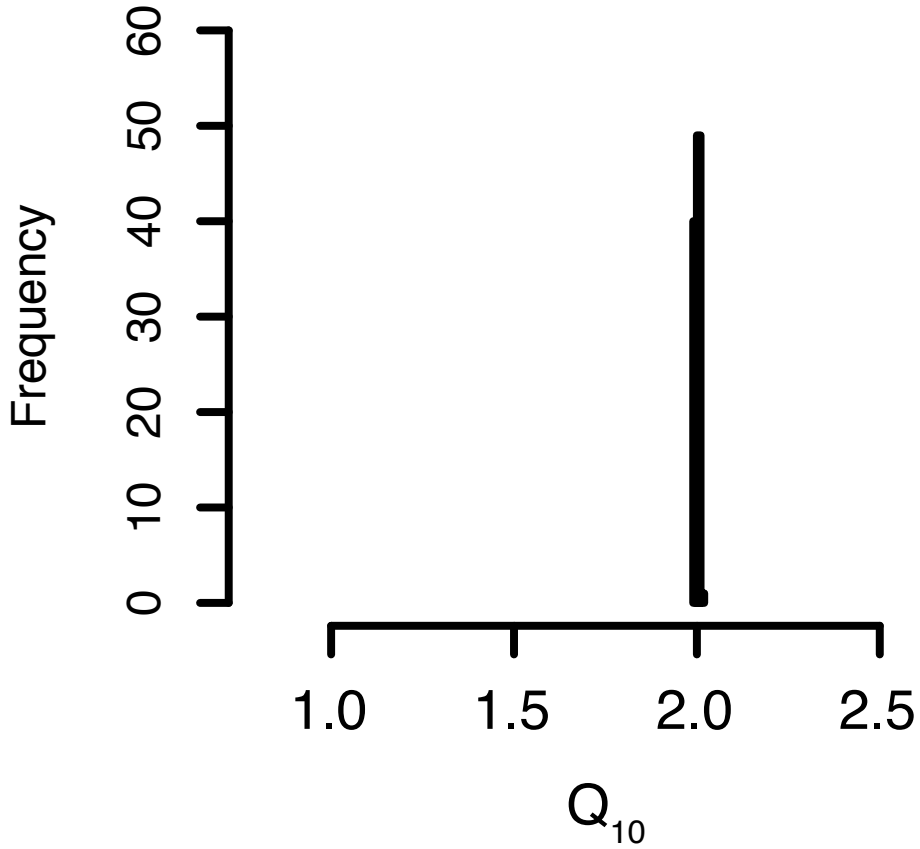

Figure 8.4: Estimates of the Q_{10} temperature sensitivity (actual Q_{10}=2.0) of soil respiration for 90 random simulation instances for the Production Weighted Heat approach of Nickerson et al. (2014). Note that the variation in the histogram can be accounted for by rounding errors in the simulation and fitting algorithms.

Chapter 9

Conclusions

9.1 Conclusions

This thesis aimed to evaluate the impact that physical considerations - mainly heat and gas transport - have on the study of GHG emissions, with a focus on CO_2 and its carbon isotopologues. This goal was accomplished in two distinct parts, the first looking mainly at methodologies that are likely to become widely-used in the near future, and the second looking at using novel methods to avoid problems inherent in soil GHG emissions interpretation and modelling.

In this thesis several new measurement methods were developed for the soil respiration research community that emphasize high-temporal resolution and the reduction of bias in measurements of soil respiration and isotopologue fluxes. High-temporal resolution datasets have become more commonplace over the past decade, and have been extremely important in understanding soil respiration and in particular short time-scale respiration processes. Methods such as Forced Diffusion (FD) and subsurface approaches will hopefully allow more researchers to gather high-frequency measurements and further develop our understanding of soil respiration at these short timescales where individual soil processes and environmental responses are most apparent. Similarly, while robust new methods for soil respiration studies are important, it is also critical to understand both the new and old methods in detail to ensure that no biases or systematic errors are present in data gathered by these methods. The analysis of methods for systematic biases was an integral part of this thesis, and will hopefully guide others in their selection and study of respiration measurement methods. Finally, much of the methods related research focussed on measuring isotopologue fluxes from the soil, and this is for good reason. Natural abundance and tracer isotopic studies are powerful tools for understanding ecosystem processes in greater detail, but the differences in isotopic signature for the various soil processes can often be quite small. This makes identification and correction for method related

bias extremely important. Ultimately these isotopologue measurements will allow researchers to take the process-based understanding of soil respiration processes to the next level, but this transition will be severely-hampered by methodological problems if careful consideration is not taken in isotopologue applications.

While measurement methods are extremely important, the ultimate goal of soil respiration studies is to develop a process-based understanding of the soil system, and the processes that lead to soil gas emissions. It was not until recently, with the application of high-resolution measurement techniques, that researchers began to obviously see the effect that soil physics was having on soil respiration data interpretation. Even then these effects were not clear to many researchers, who often used soil biology to explain many behaviours that are likely physical in nature. The use of physically based models in this thesis helped us show clearly the impacts that soil physical processes may be having on soil respiration data, and thus its interpretation. These simple models are able to explain many behaviours observed in laboratory and field based studies of soil respiration, and provide an excellent building block for the future study of soil respiration. Ultimately researchers want to understand the biology behind soil respiration, and stripping away these physical layers will be crucial in that understanding. The production weighted heat approach was the beginning of that process, but it is clear that more complex methods will need to be developed to finish the task. There is a strong need now to move toward other interpretative methods. Analytical and statistical approaches for soil respiration interpretation and modelling offer a good first order estimate in many cases, but to truly understand soil processes more complex numerical process-based models are needed. The soil respiration research community has taken steps in this direction, with ever increasing interest in model-data fusion approaches and numerical modelling. Much of the research presented in this thesis regarding heat and gas diffusion is likely to help form the base-level of these models.

Finally, soil physics was a major focus of this thesis and the complex physical nature of the soil system means that there are many windows of opportunity ahead. Even within the relatively narrow window of gas and heat diffusion that was studied here there are many processes that were unconsidered, for example direct radiation, self heating of soil by biological activity, aqueous gas diffusion and coupled diffusion

processes. Other physical aspects such as water transport (both by percolation and evapotranspiration) and soil structure considerations (horizonation, pore distributions, fracture networks, soil aggregates, clay content, mineral distribution) will also undoubtedly be important in future process-based models of soil respiration. While the thesis may be biased to understanding the soil physics, it is also undeniably important to continue to carefully study the soil biology and chemistry carefully as well. Because of the tight linkages between all soil processes, only a combined approach using all three aspects of the soil can be expected to yield the desired process-based understanding of soils.

9.2 Future Directions

While I have considered many methodological approaches in this thesis, there are many more which require further understanding and likely still many things to understand about the methods developed and presented herein. I strongly believe that this understanding should be informed by theoretical, laboratory and field-based approaches. Each approach has its strengths and weaknesses, and it is only though the combination of all three that researchers can hope to reveal all of the nuances of a method and evaluate its applicability for scientific research. While the availability of many methods is useful for tackling complex problems, there is also an increasing need to focus on data quality control and quality assurance, which can be complicated by the many-methods approach to soil respiration monitoring. Ultimately a balance has to be struck between the practicalities of field research and the need for comparable and accurate data sets for meta-analyses and respiration modelling.

For soil respiration modelling and interpretation, it will be important in future research to consider the soil physics but also to consider the purpose of the modelling. I would like to see a move away from statistical modelling to process-based models, because these process-based models are ultimately more robust across both space and time. This robustness will also help us understand fundamental differences in the biology, physics and chemistry from ecosystem to ecosystem. For example if a process based model that is well-suited to boreal forests is applied to a tropical ecosystem and fails, then it will be relatively easier to pull apart the model processes and see which assumptions are being violated. This move towards process based

models will also need a better understanding of the soil physics. In this thesis I have unfortunately only scratched the surface of the complex physical processes that occur in the soil system. If this research were continued, the first new topics I would like to address are: 1) Including the effects of soil moisture in the models presented in this thesis; 2) Implementing algorithms for model optimization and testing the improved model against field data from various regions, and; 3) Continuing to work on the understanding and application of isotopic methods as these are likely to lead to an increased ability to optimize soil respiration models.

Appendix A

A Numerical Examination of $^{14}CO_2$ Chamber Methodologies for Measuring Fluxes at the Soil Surface

A.1 Dynamic Chambers

For each of the dynamic chambers, the relative proportion of atmospheric CO_2 in the chamber compared to soil flux is calculated as:

$$X = \frac{\delta^{13}C_{measured} - \delta^{13}C_{soil}}{\delta^{13}C_{atmosphere} - \delta^{13}C_{soil}} \tag{A.1}$$

where X is the fraction of remnant atmospheric air in the sample, $\delta^{13}C_{atmosphere}$ is the atmospheric $\delta^{13}C$ signature and $\delta^{13}C_{soil}$ is the $\delta^{13}C$ signature of soil respiration. The uncertainty in the calculation of X can be formulated as follows:

$$s_X = \sqrt{\left(\frac{\partial X}{\partial(\delta^{13}C_{measured})}\right)^2 s^2_{\delta^{13}C_{measured}} + \left(\frac{\partial X}{\partial(\delta^{13}C_{atmosphere})}\right)^2 s^2_{\delta^{13}C_{atmosphere}} + \left(\frac{\partial X}{\partial(\delta^{13}C_{soil})}\right)^2 s^2_{\delta^{13}C_{soil}}} \tag{A.2}$$

And the individual partial derivatives can be calculated from Eq. A1:

$$\frac{\partial X}{\partial(\delta^{13}C_{measured})} = \frac{1}{\delta^{13}C_{atmosphere} - \delta^{13}C_{soil}} \tag{A.3}$$

$$\frac{\partial X}{\partial(\delta^{13}C_{atmosphere})} = \frac{\delta^{13}C_{measured} - \delta^{13}C_{soil}}{(\delta^{13}C_{atmosphere} - \delta^{13}C_{soil})^2} \tag{A.4}$$

$$\frac{\partial X}{\partial(\delta^{13}C_{atmosphere})} = \frac{1}{\delta^{13}C_{atmosphere} - \delta^{13}C_{soil}} + \frac{\delta^{13}C_{measured} - \delta^{13}C_{soil}}{(\delta^{13}C_{atmosphere} - \delta^{13}C_{soil})^2} \tag{A.5}$$

The uncertainty in the estimated $\Delta^{14}C$ signature can then be calculated by partial differentiation of Equation A6:

$$\Delta^{14}C_{soil} = \frac{\Delta^{14}C_{measured} - X \times \Delta^{14}C_{atmosphere}}{1 - X} \tag{A.6}$$

Where the relevant uncertainty terms are:

$$s_{\Delta^{14}C_{soil}} = \sqrt{\left(\frac{\partial \Delta^{14}C_{soil}}{\partial(\Delta^{14}C_{measured})}\right)^2 s^2_{\Delta^{14}C_{measured}} + \left(\frac{\partial \Delta^{14}C_{soil}}{\partial(\Delta^{14}C_{atmosphere})}\right)^2 s^2_{\Delta^{14}C_{atmosphere}} + \left(\frac{\partial \Delta^{14}C_{soil}}{\partial(X)}\right)^2 s^2_X} \tag{A.7}$$

And the individual partial derivatives are as follows:

$$\frac{\partial \Delta^{14}C_{soil}}{\partial(\Delta^{14}C_{measured})} = \frac{1}{(1 - X)^2} \tag{A.8}$$

$$\frac{\partial \Delta^{14}C_{soil}}{\partial(\Delta^{14}C_{atmosphere})} = \frac{X}{(1 - X)^2} \tag{A.9}$$

$$\frac{\partial \Delta^{14}C_{soil}}{\partial(X)} = \frac{\Delta^{14}C_{atmosphere}}{1 - X} + \frac{\Delta^{14}C_{measured} - X\Delta^{14}C_{atmosphere}}{(1 - X)^2} \tag{A.10}$$

Appendix B

A Numerical Examination of $^{14}CO_2$ Chamber Methodologies for Measuring Fluxes at the Soil Surface

B.1 Static Chamber and Iso-FD

Both the static chamber and the Iso-FD chamber rely on the same mixing model to calculate the respired $\Delta^{14}C$ signature . For comparison we have included equation B1 and B2 that describe the mixing in the static and Iso-FD chambers, respectively:

$$A_{respired} = \frac{A_{chamber} \times [CO_2]_{chamber} - A_{free\,air} \times [CO_2]_{free\,air}}{[CO_2]_{chamber} - [CO_2]_{free\,air}} \tag{B.1}$$

$$\frac{F_{in}^{^{14}C}}{F_{in}^{^{12}C}} = \left(\frac{1}{\alpha}\right)\left(\frac{C_{FD}^{^{14}C} - C_{atm}^{^{14}C}}{C_{FD}^{^{12}C} - C_{atm}^{^{12}C}}\right) = \left(\frac{1}{\alpha}\right)\left(\frac{A_{FD}C_{FD}^{^{12}C} - A_{atm}C_{atm}^{^{12}C}}{C_{FD}^{^{12}C} - C_{atm}^{^{12}C}}\right) \tag{B.2}$$

The uncertainty in either equation is therefore formulated as:

$$s_{SC,FD} = \sqrt{\left(\frac{\partial(SC,FD)}{\partial(A_{SC,FD})}\right)^2 s_{A_{SC,FD}}^2 + \left(\frac{\partial(SC,FD)}{\partial(A_{atm})}\right)^2 s_{A_{atm}}^2 + \left(\frac{\partial(SC,FD)}{\partial(C_{SC,FD}^{^{12}C})}\right)^2 s_{C_{SC,FD}^{^{12}C}}^2 + \left(\frac{\partial(SC,FD)}{\partial(C_{atm}^{^{12}C})}\right)^2 s_{C_{atm}^{^{12}C}}^2} \tag{B.3}$$

Where the partial derivatives for each term are:

$$\frac{\partial(SC,FD)}{\partial(A_{SC,FD})} = \frac{\alpha^{-1}C_{atm}^{12C}}{C_{SC,FD}^{12C} - C_{atm}^{12C}} \tag{B.4}$$

$$\frac{\partial(SC,FD)}{\partial(A_{atm})} = \frac{\alpha^{-1}C_{SC,FD}^{12C}}{C_{SC,FD}^{12C} - C_{atm}^{12C}} \tag{B.5}$$

$$\frac{\partial(SC,FD)}{\partial(C_{SC,FD}^{12C})} = \frac{\alpha^{-1}A_{SC,FD}}{C_{SC,FD}^{12C} - C_{atm}^{12C}} - \frac{\alpha^{-1}(A_{SC,FD}C_{SC,FD}^{12C} - A_{atm}C_{atm}^{12C})}{(C_{SC,FD}^{12C} - C_{atm}^{12C})^2} \tag{B.6}$$

$$\frac{\partial(SC,FD)}{\partial(C_{atm}^{12C})} = \frac{\alpha^{-1}A_{atm}}{C_{SC,FD}^{12C} - C_{atm}^{12C}} + \frac{\alpha^{-1}(A_{SC,FD}C_{SC,FD}^{12C} - A_{atm}C_{atm}^{12C})}{(C_{SC,FD}^{12C} - C_{atm}^{12C})^2} \tag{B.7}$$

Appendix C

Interpreting Diel Hysteresis Between Soil Respiration and Temperature

This supporting information provides an expanded explanation of the impacts of diel temperature range and Q_{10} on phase lags between surface flux and soil temperature.

As the diel air temperature variation (A_0) was increased in the model, shallow soil depths experienced bigger variations in temperature than deep soil layers, since temperature oscillations damped with depth. Furthermore, high temperatures had a greater effect on CO_2 production than low temperatures, due to the exponential relationship between CO_2 production and temperature. The combination of higher temperature maxima at shallow depths and greater sensitivity of production to high temperatures resulted in shallow depths contributing proportionately more CO_2 to surface flux than deep soil layers as A_0 was increased in the model. As a consequence, it was also observed that peak surface flux shifted closer to peak temperatures measured at soil depths of 5cm and less. While lags between surface flux and shallow soil temperatures decreased with larger values of A_0, lags between peak surface flux and deeper soil temperatures (10cm and deeper) increased, because deeper soil layers

contributed proportionately less CO_2 to surface flux (Figure C.1). In contrast, lag times between daily minimum surface flux and minimum soil temperature tended to exhibit the reverse trend. Shallow soil layers experienced more extreme minimum values with increasing values of A_0, and contributed proportionately less CO_2 to surface flux than deeper soil layers at temperature minimums.

Based on these observations, one might also expect that increasing the sensitivity of CO_2 production to temperature would have similar effects as increasing A_0: decreasing the lag between peak surface flux and near-surface temperatures (5 cm and less), and increasing the lag between peak surface flux and deeper soil temperatures (10 cm and greater). THe simulations supported this prediction in part (Figure C.2); however, changing Q_{10} did not produce a monotonic change in lag time. The lag between surface flux and 10 cm soil temperature initially decreased between Q_{10} values 1-1.4, before increasing slightly between Q_{10} values 1.4-3. For Q_{10} values close to 1 (production has little temperature sensitivity), surface flux exhibited a small amount of temperature sensitivity due to temperature dependence of the D_{CO_2} parameter. At fairly low Q_{10} values, however, these small changes in D_{CO_2} were obscured by temperature-dependent changes in production.

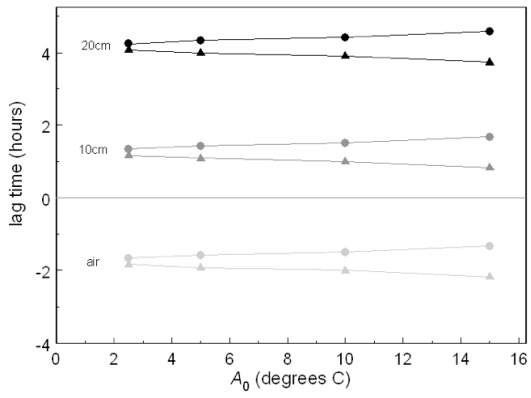

Figure C.1: Effect of A_0 on lag times between surface flux and temperature at the soil surface, and at 10cm and 20cm depth. Circles show lag times between the daily maxima of surface flux and temperature. Triangles show lag times between the daily minima of surface flux and temperature. Negative lag times (between surface flux and air temperature) indicate a peak in temperature prior to a surface flux, and positive lag times (for 10 and 20 cm temperature measurement depths) indicate a peak in temperature after surface flux.

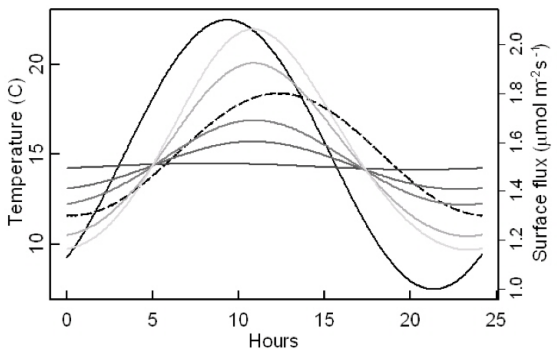

Figure C.2: Time series for surface flux at several Q_{10} values, in comparison to air and soil temperatures. Air temperature (black), 10 cm soil temperature (dashed black), and surface CO_2 flux for various Q_{10} values (grey lines). Q_{10} values from dark to light grey: 1, 1.2,1.4, 2, 2.4.

Appendix D

Expanded Definitions of Commonly Used Concepts

D.1 Q_{10} Temperature Sensitivity

The parameter Q_{10} is a multiplier used to describe the increase in a reaction rate (e.g. the increase in soil respiration) given a 10K change in temperature. For example if a biological respiration system has a Q_{10} equal to 2, the rate of respiration will double for every 10K rise in temperature. The functional form for the Q_{10} equation and its variants can be found in Table 8.1. The concept of Q_{10} comes from chemical thermodynamics and is functionally equivalent to the Arrhenius equation (Arrhenius, 1889).

D.2 Keeling Plot, Keeling Intercept

The Keeling Plot and Keeling Intercept are C-isotope specific forms of a generalized two end-member mixing model introduced by C.D. Keeling (Keeling, 1958). The approach assumes there are two sources of CO_2 that are mixing in the environment in question. The background, usually atmospheric CO_2, mixes with the second source,

typically respiratory:

$$C_M = C_B + C_S \tag{D.1}$$

where C_M is the total concentration of the mixture, C_B is the concentration of the background source and C_S is the concentration of the second source in the mixture.

As this concentration mixing occurs, the isotopic composition of the mixture is described as:

$$\delta_M C_M = \delta_B C_B + \delta_S C_S \tag{D.2}$$

where δ_M is the isotopic signature of the mix, δ_B is the isotopic signature of the background and δ_S is the isotopic signature of the source. The equations are combined to estimate δ_S, the source isotopic signature, based on prior knowledge of the background and measurements of the mixture between source and background:

$$\delta_M = C_B(\delta_B - \delta_S)(1/C_M) + \delta_S \tag{D.3}$$

Based on Equation D3, we can see now that linear regression of δ_M (y-axis) against $1/C_M$ (x-axis) will yield δ_S (the y-intercept of the linear regression). This y-intercept is referred to as the Keeling Intercept or Keeling Plot Intercept. The graph which shows the linear fit between δ_M and $1/C_M$ is referred to as the Keeling Plot.

Appendix E

Copyright Permissions

E.1 Forced Diffusion Soil Flux: A New Technique for Continuous Monitoring of Soil Gas Flux

Copyright release for the manuscript "Forced Diffusion Soil Flux: A New Technique for Continuous Monitoring of Soil Gas Flux" is presented on the following page.

From: "Butler, Verity - Chichester" <vbutler@wiley.com>
Subject: FW: Copyright release for PhD thesis
Date: 26 February, 2014 8:32:54 AM AST
To: Nick Nickerson <nnickers@stfx.ca>
Cc: "gcb@life.illinois.edu" <gcb@life.illinois.edu>, "Clark, Felicity - Oxford" <fclark@wiley.com>

2 Attachments, 32 KB

Dear Nick,

Thank you for your email request. We do not sign forms such as the one you have attached. Please find our gratis thesis grant below.

Permission is granted for you to use the material requested for your thesis/dissertation subject to the usual acknowledgements and on the understanding that you will reapply for permission if you wish to distribute or publish your thesis/dissertation commercially.

Permission is granted solely for use in conjunction with the thesis, and the article may not be posted online separately.

Any third party material is expressly excluded from this permission. If any material appears within the article with credit to another source, authorisation from that source must be obtained.

Best Wishes,

Verity Butler
Permissions Co-ordinator

Wiley
The Atrium, Southern Gate
Chichester, PO19 8SQ
UK
www.wiley.com
vbutler@wiley.com

WILEY

-------- Original Message --------
Subject: Copyright release for PhD thesis
Date: Mon, 17 Feb 2014 18:54:23 -0400
From: Nick Nickerson <nnickers@stfx.ca>
To:gcb@life.uiuc.edu

Hi,

I am sending you a PDF for copyright release of an article published in Global Change Biology for my Ph D thesis. If you could email it or fax it back to me (1.902.466.6889, Attn: Nick Nickerson) I would app reciate it.

Please let me know if you have any questions, or if I can be of assistance.

E.2 Iso-FD: A Novel Method for Measuring the Isotopic Signature of Soil Flux

Copyright release for the manuscript "Iso-FD: A Novel Method for Measuring the Isotopic Signature of Soil Flux" is presented on the following page.

ELSEVIER LICENSE
TERMS AND CONDITIONS

Mar 11, 2014

This is a License Agreement between Nick R Nickerson ("You") and Elsevier ("Elsevier") provided by Copyright Clearance Center ("CCC"). The license consists of your order details, the terms and conditions provided by Elsevier, and the payment terms and conditions.

All payments must be made in full to CCC. For payment instructions, please see information listed at the bottom of this form.

Supplier	Elsevier Limited The Boulevard,Langford Lane Kidlington,Oxford,OX5 1GB,UK
Registered Company Number	1982084
Customer name	Nick R Nickerson
Customer address	1 Research Drive
	Halifax, NS B2Y 4M9
License number	3345921286814
License date	Mar 11, 2014
Licensed content publisher	Elsevier
Licensed content publication	Soil Biology and Biochemistry
Licensed content title	Iso-FD: A novel method for measuring the isotopic signature of surface flux
Licensed content author	Nick Nickerson,Jocelyn Egan,Dave Risk
Licensed content date	July 2013
Licensed content volume number	62
Licensed content issue number	
Number of pages	8
Start Page	99
End Page	106
Type of Use	reuse in a thesis/dissertation
Intended publisher of new work	other
Portion	full article
Format	both print and electronic
Are you the author of this Elsevier article?	Yes

Will you be translating?	No
Title of your thesis/dissertation	ENHANCING THE MEASUREMENT, INTERPRETATION AND UNDERSTANDING OF SOIL RESPIRATION THROUGH APPLICATION OF PHYSICAL PRINCIPLES
Expected completion date	Apr 2014
Estimated size (number of pages)	250
Elsevier VAT number	GB 494 6272 12
Permissions price	0.00 USD
VAT/Local Sales Tax	0.00 USD / 0.00 GBP
Total	0.00 USD
Terms and Conditions	

INTRODUCTION

1. The publisher for this copyrighted material is Elsevier. Byclicking "accept" in connection with completing this licensingtransaction, you agree that the following terms and conditions apply to thistransaction (along with the Billing and Payment terms and conditionsestablished by Copyright Clearance Center, Inc. ("CCC"), at the timethat you opened your Rightslink account and that are available at any time at http://myaccount.copyright.com).

GENERAL TERMS

2. Elsevier hereby grants you permission to reproduce the aforementionedmaterial subject to the terms and conditions indicated.

3. Acknowledgement: If any part of the material to be used (for example,figures) has appeared in our publication with credit or acknowledgement toanother source, permission must also be sought from that source. If suchpermission is not obtained then that material may not be included in yourpublication/copies. Suitable acknowledgement to the source must be made, eitheras a footnote or in a reference list at the end of your publication, asfollows:

“Reprinted from Publication title, Vol /edition number, Author(s), Title ofarticle / title of chapter, Pages No., Copyright (Year), with permission fromElsevier [OR APPLICABLE SOCIETY COPYRIGHT OWNER].” Also Lancet special credit -“Reprinted from The Lancet, Vol. number, Author(s), Title of article, PagesNo., Copyright (Year), with permission from Elsevier.”

4. Reproduction of this material is confined to the purpose and/or media forwhich permission is hereby given.

5. Altering/Modifying Material: Not Permitted. However figures andillustrations may be altered/adapted minimally to serve your work. Any otherabbreviations, additions, deletions and/or any other alterations shall be madeonly with prior written authorization of Elsevier Ltd. (Please contact Elsevierat permissions@elsevier.com)

6. If the permission fee for the requested use of our material is waived inthis instance, please be advised that your future requests for Elseviermaterials may attract a fee.

7. Reservation of Rights: Publisher reserves all rights not specificallygranted in the combination of (i) the license details provided by you andaccepted in the course of this licensing transaction, (ii) these terms andconditions and (iii) CCC's Billing and Payment terms and conditions.

8. License Contingent Upon Payment: While you may exercise the rightslicensed immediately upon issuance of the license at the end of the licensingprocess for the transaction, provided that you have disclosed complete andaccurate details of your proposed use, no license is finally effective unlessand until full payment is received from you (either by publisher or by CCC) asprovided in CCC's Billing and Payment terms and conditions. If fullpayment is not received on a timely basis, then any license preliminarilygranted shall be deemed automatically revoked and shall be void as if nevergranted. Further, in the event that you breach any of these terms andconditions or any of CCC's Billing and Payment terms and conditions, thelicense is automatically revoked and shall be void as if never granted. Use of materials as described in a revoked license, as well as any use of thematerials beyond the scope of an unrevoked license, may constitute copyrightinfringement and publisher reserves the right to take any and all action toprotect its copyright in the materials.

9. Warranties: Publisher makes no representations or warranties with respectto the licensed material.

10. Indemnity: You hereby indemnify and agree to hold harmless publisher andCCC, and their respective officers, directors, employees and agents, from andagainst any and all claims arising out of your use of the licensed materialother than as specifically authorized pursuant to this license.

11. No Transfer of License: This license is personal to you and may not besublicensed, assigned, or transferred by you to any other person withoutpublisher's written permission.

12. No Amendment Except in Writing: This license may not be amended exceptin a writing signed by both parties (or, in the case of publisher, by CCC onpublisher's behalf).

13. Objection to Contrary Terms: Publisher hereby objects to any termscontained in any purchase order, acknowledgment, check endorsement or otherwriting prepared by you, which terms are inconsistent with these terms andconditions or CCC's Billing and Payment terms and conditions. These termsand conditions, together with CCC's Billing and Payment terms and conditions(which are incorporated herein), comprise the entire agreement between you andpublisher (and CCC) concerning this licensing transaction. In the eventof any conflict between your obligations established by these terms andconditions and those established by CCC's Billing and Payment terms andconditions, these terms and conditions shall control.

14. Revocation: Elsevier or Copyright Clearance Center may deny thepermissions described in this License at their sole discretion, for any reasonor no reason, with a full refund payable to you. Notice of such denialwill be made using the contact information provided by you. Failure toreceive such notice will not alter or invalidate the denial. In no eventwill Elsevier or Copyright Clearance Center be responsible or liable for anycosts, expenses or damage incurred by you as a result of a denial of yourpermission request, other than a refund of the amount(s) paid by you toElsevier and/or Copyright Clearance Center for denied permissions.

LIMITED LICENSE

The following terms and conditions apply only to specific license types:

15. **Translation**: This permission is granted fornon-exclusive world **English** rights only unless yourlicense was granted for translation rights. If you licensed translation rightsyou may only translate this content into the languages you requested. Aprofessional translator must perform all translations and reproduce the contentword for word preserving the integrity of the article. If this license is tore-use 1 or 2 figures then permission is granted for non-exclusive world rightsin all languages.

16. **Posting licensed content on any Website**: The followingterms and conditions apply as follows: Licensing material from an Elsevierjournal: All content posted to the web site must maintain the copyright informationline on the bottom of each image; A hyper-text must be included to the Homepageof the journal from which you are licensing at http://www.sciencedirect.com/science/journal/xxxxx orthe Elsevier homepage for books at http://www.elsevier.com; CentralStorage: This license does not include permission for a scanned version of thematerial to be stored in a central repository such as that provided byHeron/XanEdu.

Licensing material from an Elsevier book: A hyper-text link must be includedto the Elsevier homepage at http://www.elsevier.com . Allcontent posted to the web site must maintain the copyright information line onthe bottom of each image.

Posting licensed content on Electronic reserve: In addition to the above the following clausesare applicable: The web site must be password-protected and made available onlyto bona fide students registered on a relevant course. This permission isgranted for 1 year only. You may obtain a new license for future websiteposting.

For journal authors: the following clauses are applicable inaddition to the above: Permission granted is limited to the author acceptedmanuscript version* of your paper.

***Accepted Author Manuscript (AAM) Definition:** An accepted authormanuscript (AAM) is the author's version of the manuscript of an article thathas been accepted for publication and which may include any author-incorporatedchanges suggested through the processes of submission processing, peer review,and editor-author communications. AAMs do not include other publishervalue-added contributions such as copy-editing, formatting, technicalenhancements and (if relevant) pagination.

You are not allowed to download and post the published journal article (whetherPDF or HTML, proof or final version), nor may you scan the printed edition tocreate an electronic version. A hyper-text must be included to the Homepage ofthe journal from which you are licensing at http://www.sciencedirect.com/science/journal/xxxxx. As part of our normal production process, you will receive an e-mail noticewhen your article appears on Elsevier's online service ScienceDirect(www.sciencedirect.com). That e-mail will include the article's Digital ObjectIdentifier (DOI). This number provides the electronic link to the publishedarticle and should be included in the posting of your personal version. We askthat you wait until you receive this e-mail and have the DOI to do any posting.

Posting to a repository: Authorsmay post their AAM immediately to their employer's institutional repository forinternal use only and may make their manuscript publically available after thejournal-specific embargo period has ended.

Please also refer to Elsevier'sArticle Posting Policy for further information.

18. **For book authors** the following clauses are applicable in addition tothe above: Authors are permitted to place a briefsummary of their work online only.. You are notallowed to download and post the published electronic version of your chapter,nor may you scan the printed edition to create an electronic version. Posting to a repository: Authors arepermitted to post a summary of their chapter only in their institution'srepository.

20. **Thesis/Dissertation**: If your license is for use in athesis/dissertation your thesis may be submitted to your institution in eitherprint or electronic form. Should your thesis be published commercially, pleasereapply for permission. These requirements include permission for the Libraryand Archives of Canada to supply single copies, on demand, of the completethesis and include permission for UMI to supply single copies, on demand, ofthe complete thesis. Should your thesis be published commercially, pleasereapply for permission.

Elsevier Open Access Terms andConditions

Elsevier publishes Open Access articles in both its Open Access journals andvia its Open Access articles option in subscription journals.

Authors publishing in an Open Access journal or who choose to make theirarticle Open Access in an Elsevier subscription journal select one of thefollowing Creative Commons user licenses, which define how a reader may reusetheir work: Creative Commons Attribution License (CC BY), Creative CommonsAttribution – Non Commercial - ShareAlike (CC BY NCSA) and Creative Commons Attribution – Non Commercial – No Derivatives (CC BYNC ND)

Terms & Conditions applicable toall Elsevier Open Access articles:

Any reuse of the article must not represent the author as endorsing theadaptation of the article nor should the article be modified in such a way asto damage the author's honour or reputation.

The author(s) must be appropriately credited.

If any part of the material to be used (for example, figures) has appearedin our publication with credit or acknowledgement to another source it is theresponsibility of the user to ensure their reuse complies with the terms andconditions determined by the rights holder.

Additional Terms & Conditionsapplicable to each Creative Commons user license:

CC BY: You may distribute andcopy the article, create extracts, abstracts, and other revised versions,adaptations or derivative works of or from an article (such as a translation),to include in a collective work (such as an anthology), to text or data minethe article, including for commercial purposes without permission from Elsevier

CC BY NC SA: For non-commercialpurposes you may distribute and copy the article, create extracts, abstractsand other revised versions, adaptations or derivative works of or from anarticle (such as a translation), to include in a collective work (such as ananthology), to text and data mine the article and license new adaptations or creationsunder identical terms without permission from Elsevier

CC BY NC ND: For non-commercialpurposes you may distribute and copy the article and include it in a collectivework (such as an anthology), provided you do not alter or modify the article,without permission from Elsevier

Any commercial reuse of Open Access articles published with a CC BY NC SA or CC BY NC NDlicense requires permission from Elsevier and will be subject to a fee.

Commercial reuse includes:

- Promotional purposes (advertising or marketing)
- Commercial exploitation (e.g. a product forsale or loan)
- Systematic distribution (for a fee or free ofcharge)

Please refer to Elsevier'sOpen Access Policy for further information.

21. **Other Conditions**:

v1.7

If you would like to pay for this license now, please remit this license along with your payment made payable to "COPYRIGHT CLEARANCE CENTER" otherwise you will be invoiced within 48 hours of the license date. Payment should be in the form of a check or money order referencing your account number and this invoice number RLNK501247788.
Once you receive your invoice for this order, you may pay your invoice by credit card. Please follow instructions provided at that time.

Make Payment To:
Copyright Clearance Center
Dept 001
P.O. Box 843006
Boston, MA 02284-3006

For suggestions or comments regarding this order, contact RightsLink Customer Support: customercare@copyright.com or +1-877-622-5543 (toll free in the US) or +1-978-646-2777.

Gratis licenses (referencing $0 in the Total field) are free. Please retain this printable license for your reference. No payment is required.

E.3 Interpreting Diel Hysteresis Between Soil Respiration and Temperature

Copyright release for the manuscript "Interpreting Diel Hysteresis Between Soil Respiration and Temperature" is presented on the following page.

February 17, 2014

Global Change Biology
Dr. S. Long
University of Illinois
Urbana, IL, USA

I am preparing my PhD thesis for submission to the Faculty of Graduate Studies at Dalhousie University, Halifax, Nova Scotia, Canada. I am seeking your permission to include a manuscript version of the following paper(s) as a chapter in the thesis:

Phillips, C.L., Nickerson, N., Risk, D., Bond, B. (2011) Interpreting diel hysteresis between soil respiration and temperature. Global Change Biology, 17(1): 515-527

Canadian graduate theses are reproduced by the Library and Archives of Canada (formerly National Library of Canada) through a non-exclusive, world-wide license to reproduce, loan, distribute, or sell theses. I am also seeking your permission for the material described above to be reproduced and distributed by the LAC(NLC). Further details about the LAC(NLC) thesis program are available on the LAC(NLC) website (www.nlc-bnc.ca).

Full publication details and a copy of this permission letter will be included in the thesis.

Yours sincerely,

Nick Nickerson

Permission is granted for:

a) the inclusion of the material described above in your thesis.

b) for the material described above to be included in the copy of your thesis that is sent to the Library and Archives of Canada (formerly National Library of Canada) for reproduction and distribution.

Name: SHEIK SAJID AR Title: Term Coord.

Signature: [redacted] Date: 2/21/14.

No rights are granted to use content that appears in the Work with credit to another source.

Bibliography

Albanito, F., McAllister, J.L., Cescatti, A., Smith, P., Robinson, D., 2012. Dual-chamber measurements of $\delta^{13}C$ of soil-respired CO_2 partitioned using a field-based three end-member model. Soil Biology and Biochemistry 47, 106-115.

Amundson, R., L. Stern, T. Baisden, Wang, Y., 1998. The isotopic composition of soil and soil-respired CO_2, Geoderma 82, 83-114.

Arrhenius, S., 1889. Uber die Reaktionsgeschwindigkeit bei der Inversion von Rohrzucker durch Sauren. Zeitschrift fur Physik Chemie 4, 226-248.

Bahn, M., Rodeghiero, M., Anderson-Dunn, M. et al., 2008. Soil respiration in European grasslands in relation to climate and assimilate supply. Ecosystems 11, 1352-1367.

Bahn, M., Schmitt, M., Siegwolf, R., Richter, A., Bruggemann, N., 2009. Does photosynthesis affect grassland soil-respired CO_2 and its carbon isotope composition on a diurnal timescale? New Phytologist 182, 451-460.

Barr, A.G., Griffis, T.J., Black, T.A., Lee, X., Staebler, R.M., Fuentes, J.D., Chen, Z., Morgenstern, K., 2002. Comparing the carbon budgets of boreal and temperate deciduous forest stands. Canadian Journal of Forest Research 32, 813-822.

Barron-Gafford, G.A., Scott, R.L., Jenerette, G.D., Huxman, T.E., 2010. The relative controls of temperature, soil moisture, and plant functional group on soil CO_2 efflux at diel, seasonal, and annual scales. Journal of Geophysical Research 116, 2156-2202.

Beltrami, H., 1996. Active distortion of annual air/soil thermal orbits, Permafrost and Periglacial Processes 7, 101-110.

Beltrami, H., 2001. On the relationship between ground temperature histories and meteorological records: a report on the Pomquet station, Global and Planetary Change 29(3-4), 327-348.

Bhupinderpal-Singh, Nordgren, A., Lofvenius, M.O., Högberg, M.N., Mellander P-E., Högberg, P., 2003. Tree root and soil heterotrophic respiration as revealed by girdling of boreal Scots pine forest: extending observations beyond the first year, Plant, Cell and Environment 26, 1287-1296.

Bjorkman, M.P., Morgner, E., Cooper, E., Elberling, B., Klemedtsson, L., Bjork, R.G., 2010. Winter carbon dioxide effluxes from Arctic ecosystems: An overview and comparison of methodologies. Global Biogeochemical Cycles 24, GB3010.

Black, T.A., Den Hartog, G., Neumann, H.H., Blanken, P.D., Yang, P.C., Russell, C., Nesic, Z., Lee, X., Chen, S.G., Staebler, R., Novak, M.D., 1996. Annual cycles of water vapour and carbon dioxide fluxes in and above a boreal aspen forest. Global Change Biology 2, 219-229.

Bond-Lamberty, B., Thomson, A., 2010a. Temperature-associated increases in the global soil respiration record. Nature 464, 579-582.

Bond-Lamberty, B., Thomson, A., 2010b. A global database of soil respiration data, Biogeosciences 7, 1915-1926.

Bond-Lamberty, B., Bronson, D., Bladyka, E., Gower, S.T., 2011. A comparison of trenched plot techniques for partitioning soil respiration. Soil Biology and Biochemistry 43, 2108-2114.

Bowling, D.R., Massman, W.J., 2011. Persistent wind-induced enhancement of diffusive CO_2 transport in a mountain forest snowpack. Journal of Geophysical Research 116, G04006.

Breecker, D.O., Payne, A.E., Quade, J., Banner, J.L., Ball, C.E., Meyer, K.W., Cowan, B.D., 2012. The sources and sinks of CO_2 in caves under mixed woodland and grassland vegetation. Geochimica et Cosmochimica Acta 96, 230-246.

Carbone, M.S. Vargas, R., 2008. Automated soil respiration measurements: new information, opportunities and challenges. New Phytologist 177, 295-297.

Carbone, M.S., Winston G.C., Trumbore, S.E., 2008. Soil respiration in perennial grass and shrub ecosystems: linking environmental controls with plant and microbial sources on seasonal and diel timescales. Journal of Geophysical Research 113, G02022.

Carlyle, J.C., Ba Than, U., 1988. Abiotic controls of soil respiration beneath an eighteen-year-old Pinus radiata stand in south-eastern Australian Journal of Ecology 76, 654-662.

Cerling, T. E., Solomon, D. K., Quade, J., Bowman, J.R., 1991. On the isotopic composition of carbon in soil carbon-dioxide. Geochimica et Cosmochimica Acta 55, 3403-3405.

Creelman, C., Nickerson, N., Risk, D., 2013. Quantifying lateral diffusion error in soil CO_2 respiration instruments using numerical modeling, Soil Science Society of America Journal, 77: 699-708.

Davidson, E.A., Trumbore, S.E., 1995. Gas diffusivity and production of CO_2 in deep soils of the eastern Amazon, Tellus 47B, 550-565.

Davidson, E.A., Belk, E., Boone, R.D., 1998. Soil water content and temperature as independent or confounded factors controlling soil respiration in a temperate mixed hardwood forest. Global Change Biology 4, 217-227.

Davidson, E. A., Trumbore, S. E., Amundson, R., 2000. Soil warming and organic carbon content, Nature 408, 789-790.

Davidson, E.A., Savage,K., Verchot,L.V., and Navarro,R.I., 2010. Minimizing artifacts and biases in chamber-based measurements of soil respiration. Agriculture and Forest Meteorology 113, 21-37.

Davidson, E.A., Savage, K.E., Trumbore, S.E., Borken, W., 2006. Vertical partitioning of CO_2 within a temperate forest soil. Global Change Biology 12, 944-956.

Davidson, E.A., Janssens, I., Luo, Y., 2006. On the variability of respiration in terrestrial ecosystems: moving beyond Q_{10}. Global Change Biology, 12, 154-164.

Davidson, E.A., Janssens, I.A., 2006. Temperature sensitivity of soil carbon decomposition and feedbacks to climate change. Nature 440, 165-173.

Davidson, E. A., Samanta, S., Caramori, S.S., Savage, K., 2012. The Dual Arrhenius and Michaelis-Menten kinetics model for decomposition of soil organic matter at hourly to seasonal timescales. Global Change Biology, 18, 371-384.

Drake, J.E., Oishi, A.C., Giasson, M.-A., Oren, R., Johnsen, K.H., Finzi, A.C., 2012. Trenching reduces soil heterotrophic activity in a loblolly pine (Pinus taeda) forest exposed to elevated atmospheric [CO_2] and N fertilization. Agricultural and Forest Meteorology 165, 43-52.

Elberling, B., Brandt, K.K., 2003. Uncoupling of microbial CO_2 production and release in frozen soil and its implications for field studies of arctic C cycling. Soil Biology & Biochemistry 35, 263-272.

Ekblad, A., Högberg, P., 2001. Natural abundance of ^{13}C in CO_2 respired from forest soils reveals speed of link between tree photosynthesis and root respiration, Oecologia, 127, 305-308.

Ekblad, A., Bostrom, B., Holm, A., Comstdet, D., 2005. Forest soil respiration rate and $\delta^{13}C$ is regulated by recent above ground weather conditions. Oecologia, 143, 136142.

Falloon, P., Jones, C.D., Ades, M., Paul, K., 2011. Direct soil moisture controls of future global soil carbon changes: An important source of uncertainty. Global Biogeochemical Cycles 25, GB3010.

Fessenden, J.E., Ehleringer J.R., 2003. Temporal variation in $\delta^{13}C$ of ecosystem respiration in the Pacific Northwest: links to moisture stress. Oecologia, 136, 129-136.

Flechard, C.R., Neftel, A., Jocher, M., Ammann, C., Leifeld, J., Fuhrer, J., 2007. Temporal changes in soil pore space CO_2 concentration and storage under permanent grassland. Agricultural and Forest Meteorology, 142, 66-84.

Formanek, P., Ambus, P., 2004. Assessing the use of $\delta^{13}C$ natural abundance in separation of root and microbial respiration in a Danish beech (Fagus sylvatica L.) forest. Rapid Communications in Mass Spectrometry, 18, 897-902.

Gamnitzer, U., Schaufele, R., Schnyder, H., 2009. Observing ^{13}C labelling kinetics in CO_2 respired by a temperate grassland ecosystem. New Phytologist 184, 376-386.

Gamnitzer, U., Moyes, A.B., Bowling, D.R., Schnyder, H., 2011. Measuring and modeling the isotopic composition of soil respiration: insights from a grassland experiment, Biogeosciences 8, 1333-1350.

Gaudinski, J.B., Trumbore, S.E., Davidson, E.A., Zheng, S., 2000. Soil carbon cycling in a temperate forest: radiocarbon-based estimates of residence times, sequestration rates and partitioning fluxes. Biogeochemistry 51(1), 33-69.

Gaumont-Guay, D., Black, A., Mccaughey, H., Barr, A.G., Krishnan, P., Jassal, R.S., Nesic, Z., 2008. Soil CO_2 efflux in contrasting boreal deciduous and coniferous stands and its contribution to the ecosystem carbon balance. Global Change Biology 15, 13021319.

Goffin, S., Aubinet, M., Maier, M., Plain, C., Schnack-Kirchner, H., Longdoz, B., 2014. Characterization of CO_2 and $\delta^{13}CO_2$ production in forest soil layers with the flux-gradient approach, Agricultural and Forest Meteorology 188, 45-57.

Gomez-Casanovas, N., Matamala, R., Cook, D.R., Gonzalez-Meler, M.A., 2012. Net ecosystem exchange modifies the relationship between the autotrophic and heterotrophic components of soil respiration with abiotic factors in prairie grasslands, Global Change Biology, 18, 2532-2545.

Graf, A., Weihermuller, L., Huisman, J.A., Herbst, M., Bauer, J., Vereecken, H., 2008. Measurement depth effects on the apparent temperature sensitivity of soil respiration in field studies, Biogeosciences 5, 1175-1188.

Griffis T.J., Lee, X., Baker, J.M., Sargent, S.D., King, J.Y., 2005. Feasibility of quantifying ecosystem-atmosphere $C^{18}O^{16}O$ exchange using laser spectroscopy and the flux-gradient method, Agricultural and Forest Meteorology 135, 44-60.

Hagen, S.C., Braswell, B.H., Linder, E., Frolking, S., Richardson, A.D., Hollinger, D.Y., 2006. Statistical uncertainty of eddy-flux based estimates of gross ecosystem carbon exchange at Howland Forest Maine. Journal of Geophysical Research 111, D08S03.

Hahn, H., Högberg, P., Buchmann, N., 2006. ^{14}C - a tool for separation of autotrophic and heterotrophic soil respiration, Global Change Biology, 12, 972-982.

Hanson P.J., Edwards, N.T, Garten, C.T. Andrews, J.A., 2000. Separating root and soil microbial contribution to soil respiration: a review of methods and observations, Biogeochemistry 48, 115-146.

Hicks-Pries, C.E., Schurr, E.A.G., Crummer, K.G., 2013. Thawing permafrost increases old soil and autotrophic respiration in tundra: Partitioning ecosystem respiration using $\delta^{13}C$ and $\Delta^{14}C$. Global Change Biology 19(2), 649-61.

Hillel, D., 1982. Introduction to Soil Physics, Academic Press, San Diego.

Hillel, D., 1998. Environmental Soil Physics. Academic Press, San Diego.

Högberg, P., Nordgren, A., Buchmann, N., Taylor, A., Ekblad, A., Högberg, M., Nyberg, G., Ottosson-Löfvenius, M., Read, D., 2001. Large-scale forest girdling shows that current photosynthesis drives soil respiration. Nature 411, 789-792.

Hogberg, P., Hogberg, M.N., Gottlicher, S.G. et al., 2008. High temporal resolution tracing of photosynthate carbon from the tree canopy to forest soil microorganisms. New Phytologist, 177, 220-228.

Holland, E.A., Neff, J.C., Townsend, A.R., Mckeown, B., 2000. Uncertainties in the temperature sensitivity of decomposition in tropical and subtropical ecosystems: Implications for models. Global Biogeochemical Cycles 14, 1137-1151.

Hollinger, D.Y., Aber, J., Dail, B., Davidson, E.A., Goltz, S.M., Hughes, H., Leclerc, M., Lee, J.T., Richardson, A.D., Rodrigues, C., Scott, N.A., Varier, D., Walsh, J., 2004. Spatial and temporal variability in forest-atmosphere CO_2 exchange. Global Change Biology 10, 1689-1706.

Hsu, S.A., Meindl, E.A., and Gilhousen, D.B., 1994. Determining the power-law wind-profile exponent under near-neutral stability conditions at sea. Journal of Applied Meteorology 33, 757-765.

Hutchinson, G. L., Livingston, G. P., 2001. Vents and seals in non-steady-state chambers used for measuring gas exchange between soil and the atmosphere. European Journal of Soil Science 52, 675-682.

IPCC, 2001. Climate Change 2001 - Contribution of Working Groups I, II, and III to the Third Assessment Report of the IPCC, Cambridge University Press, Cambridge.

Irvine, J., Law, B.E., Anthoni, P., Meinzer, F.C., 2002. Water limitations to carbon exchange in old-growth and young Ponderosa pine stands. Tree Physiology, 22, 189-196.

Irvine, J., Law, B.E., Kurpius, M.R., 2005. Coupling of canopy gas exchange with root and rhizosphere respiration in a semi-arid forest. Biogeochemistry, 73, 271-282.

Irvine, J., Law, B.E., Martin, J.G., Vickers, D., 2008. Interannual variation in soil CO_2 efflux and the response of root respiration to climate and canopy gas exchange in mature ponderosa pine, Global Change Biology 14, 2848-2859.

Jarvis, P., Rey, A., Petsikos, C., Wingate, L., Rayment, M., Pereira, J., Banza, J., David, J., Miglietta, F., Borghetti, M., Manca, G., Valentini, R., 2006. Drying and wetting of Mediterranean soils stimulates decomposition and carbon dioxide emission: the "Birch effect". Tree Physiology 27(7), 929-940.

Jassal, R.S., Black, T.A., Cai, T., Morgenstern, K., Li, Z., Gaumont-Guay, D., Nesic, Z., 2007. Components of ecosystem respiration and an estimate of net primary productivity of an intermediate-aged Douglas-fir stand. Agricultural and Forest Meteorology, 144, 44-57.

Kayler, Z.E., Sulzman, E.W., Marshall, J.D., Mix, A.C., Rugh, W.D., Bond, B.J., 2008. A laboratory comparison of two methods used to estimate the isotopic composition of soil $\delta^{13}CO_2$ efflux at steady state. Rapid Communications in Mass Spectrometry 22, 2533-2538.

Kayler, Z., E. Sulzman, W. Rugh, A. Mix, Bond, B., 2010. Characterizing the impact of diffusive and advective soil gas transport on the measurement and interpretation of the isotopic signal of soil respiration. Soil Biology and Biochemistry 42, 435-444.

Keeling, C., 1958.The concentration and isotopic abundance of atmospheric carbon dioxide in rural areas, Geochimica et Cosmochimica Acta 13, 322-334.

Kirchner, J. W., 2006. Getting the right answers for the right reasons: Linking measurements, analyses, and models to advance the science of hydrology, Water Resources Research 42, W03S04.

Kirschbaum, M.U.F, 1995. The temperature dependence of soil organic matter decomposition, and the effect of global warming on soil organic C storage. Soil Biology and Biochemistry 27, 753-760.

Knorr, W., Prentice, I. C., House, J. I., Holland, E.A., 2005. Long-term sensitivity of soil carbon turnover to warming. Nature, 433, 298-301.

Kodoma, N., Barnard, R.L., Salmon, Y., et al., 2008. Temporal dynamics of the carbon isotope composition in a Pinus sylvestris stand: from newly assimilated organic carbon to respired carbon dioxide. Oecologia, 156, 737-750.

Koehler, B., Zehe, E., Corre, M.D., Veldkamp, E., 2010. An inverse analysis reveals limitations of the soil-CO_2 profile method to calculate CO_2 production and efflux for well-structured soils. Biogeosciences 7, 2311-2325.

Ku, H. 1966. Notes on the use of propagation of error formulas. Journal of Research of the National Bureau of Standards Section C: Engineering and Instrumentation 70(c): 263.

Kutsch, W.L., Staack, A., Wotzel,, J., Middelhoff, U., Kappen, L., 2001. Field measurements of root respiration and total soil respiration in an alder forest. New Phytologist 150, 157-168.

Kuzyakov, Y., Sources of CO_2 efflux from soil and review of partitioning methods, Soil Biology and Biochemistry, 38, 425-448, 2006.

Kuzyakov, Y., Gavrichkova, O., 2010. Time lag between photosynthesis and carbon dioxide efflux from soil: a review of mechanisms and controls. Global Change Biology. doi: 10.1111/j.1365-2486.2010.02179.x.

Lee, M.-S., Nakane, K., Nakatsubo, T., Koizumi, H., 2003. Seasonal changes in the contribution of root respiration to total soil respiration in a cool-temperate deciduous forest. Plant and Soil 255, 311-318.

Levin, I., Hesshaimer, V., 2000. Radiocarbon: A unique tracer of global carbon cycle dynamics. Radiocarbon 42, 69-80.

Liu, Q., Edwards, N.T., Post, W.M., Gu, L., Ledford, J., Lenhart, S., 2006. Temperature-independent diel variation in soil respiration observed from a temperate deciduous forest. Global Change Biology, 12, 2136-2145.

Livingston, G. P., Hutchinson, G.L., Spartalian, K., 2005. Diffusion theory improves chamber-based measurements of trace gas emissions. Geophysical Resesarch Letters 32, L24817.

Lloyd, J., Taylor, J.A., 1994. On the temperature dependence of soil respiration. Functional Ecology 8, 315-323.

Lundegardh, H., 1927. Carbon dioxide evolution of soil and crop growth, Soil Science 23, pp. 417-453.

Martin J.G., Bolstad P.V., Norman, J.M., 2004. A carbon dioxide flux generator for testing infrared gas analyzer based soil respiration systems, Soil Science Society of America Journal, 68, 514-518.

Martin, J.G., Phillips, C.L., Schmidt, A., Irvine, J., Law, B.E., 2012. High-frequency analysis of the complex linkage between soil CO_2 fluxes, photosynthesis and environmental variables, Tree Physiology, 32, 49-64.

Maseyk, K., Seibt, U., Ghashghaie, J., Mencuccini, M., Bathellier, C., Almedia, P., Lobo de Vale, R., Pereira, J.S., Yakir, D., Wingate, L., 2009. Biotic and abiotic factors affecting the $\delta^{13}C$ of soil respired CO_2 in a Mediterranean oak woodland. Isotopes in Environmental and Health Studies 45, 343-359.

Massman, W.J., 2006. Advective transport of CO_2 in permeable media induced by atmospheric pressure fluctuations: 1. An analytical model. Journal of Geophysical Research 111, G03004.

McCarthy, K.A., Johnson, R.L., 1995. Measurement of Trichloroethylene Diffusion as a Function of Moisture-Content in Sections of Gravity-Drained Soil Columns. Journal of Environmental Quality 24, 49-55.

McDowell, N.G., Bowling, D.R., Bond, B.J., Irvine, J., Law, B.E., Anthoni, P., Ehleringer, J.R., 2004. Response of the carbon isotopic content of ecosystem, leaf, and soil respiration to meteorological and physiological driving factors in a Pinus ponderosa ecosystem. Global Biogeochemical Cycles 18, GB1013.

Mencuccini, M., Holtta, T., 2010. The significance of phloem transport for the speed with which canopy photosynthesis and belowground respiration are linked. New Phytologist 185, 189-203.

Midwood, A.J., Thornton, B., Millard, P., 2008. Measuring the ^{13}C content of soil-respired CO_2 using a novel open chamber system. Rapid Communications in Mass Spectrometry 22, 2073-2081.

Midwood, A.J., Millard, P., 2011. Challenges in measuring the $\delta^{13}C$ of the soil surface CO_2 efflux. Rapid Communications in Mass Spectrometry 25, 232-242.

Millard, P., Midwood, A.J., Hunt, J.E., Barbour, M., Whitehead, D., 2010. Quantifying the contribution of soil organic matter turnover to forest soil respiration, using natural abundance $\delta^{13}C$. Soil Biology and Biochemistry 18, 935-943.

Moldrup, P., Olesen, T., Schjonning, P., Yamaguchi, T., Rolston, D.E., 2000. Predicting the gas diffusion coefficient in undisturbed soil from soil water characteristics. Soil Science Society of America Journal 64, 94100.

Mora, G., Raich, J. W., 2007. Carbon-isotopic composition of soil respired carbon dioxide in static closed chambers at equilibrium. Rapid Communications in Mass Spectrometry 21, 1866-1870.

Moyano, F.E., Vasilyeva, N., Bouckaert, L., Cook, F., Craine, J., Curiel Yuste, J., Don, A., Epron, D., Formanek, P., Franzluebbers, A., Ilstedt, U., Katterer, T., Orchard, V., Reichstein, M., Rey, A., Ruamps, L., Subke, J-A., Thomsen, I.K., Chenu, C., 2012. The moisture response of soil heterotrophic respiration: interaction with soil properties. Biogeosciences 9, 1173-1182.

Moyes A.B., Schauer, A.J., Siegwolf, R.T., Bowling, D.R., 2010a. An injection method for measuring the carbon isotope content of soil carbon dioxide and soil respiration with a tunable diode laser absorption spectrometer. Rapid Communications in Mass Spectrometry 24, 894-900.

Moyes, A.B., Gaines, S.J., Siegwolf, R.T.W., Bowling, D.R., 2010b. Diffusive fractionation complicates isotopic partitioning of autotrophic and heterotrophic sources of soil respiration. Plant, Cell and Environment 33, 1804-1819.

Nickerson, N., Risk, D., 2009a. Physical controls on the isotopic composition of soil-respired CO_2. Journal of Geophysical Research 114, G01013.

Nickerson, N., Risk, D., 2009b. Keeling plots are non-linear in non-steady state diffusive environments. Geophysical Research Letters 36, L08401.

Nickerson, N., Risk, D., 2009c. A numerical evaluation of chamber methodologies used in measuring the $\delta^{13}C$ of soil respiration. Rapid Communications in Mass Spectrometry 23, 2802-2810.

Nickerson, N., Egan, J., Risk, D., 2013. Iso-FD: A novel method for measuring the isotopic signature of surface flux. Soil Biology and Biochemistry 62, 99-106.

Nickerson, N., Phillips, C., Risk, D., 2014 (in prep.). Using production weighted heat to disentangle the environmental sensitivities of soil respiration. Journal of Geophysical Research - Biogeosciences.

Ochsner, T.E., Horton, R., Ren, T., 2001. A new perspective on soil thermal properties. Soil Science Society of America Journal, 65, 1641-1647.

Ohlsson, K.E.A., Bhupinderpal-Singh, Holm, S., Nordgren, A., Lövdahl, L., Högberg, P., 2005. Uncertainties in static closed chamber measurements of the carbon isotopic ratio of soil-respired CO_2. Soil Biology and Biochemistry 37, 2273-2276.

Ohlsson, K.E.A., 2010. Reduction of bias in static closed chamber measurement of $\delta^{13}C$ in soil CO_2 flux. Rapid Communications in Mass Spectrometry 24, 180-184.

Parent, F., Plain, C., Epron, D., Maier, M., Longdoz, B., 2013. A new method for continuously measuring the $\delta^{13}C$ of soil CO_2 concentrations at different depths by laser spectroscopy. European Journal of Soil Science 64(4), 516-525.

Pataki D.E., Ehleringer J.R., Flanagan L.B., Yakir D., Bowling D.R., Still C., Buchmann N., Kaplan J.O., Berry, J.A., 2003. The application and interpretation of Keeling plots in terrestrial carbon cycle research. Global Biogeochemical Cycles 17(1), 1022, doi:10,1029/2001GB001850.

Pavelka, M., Acosta, M., Marek, M.V., Kutsch, W., Janous, D., 2007. Dependence of the Q_{10} values on the depth on the the soil temperature measuring point. Plant and Soil, 292, 171-179.

Pendall, E., Leavitt, S.W., Brooks, T., Kimball, B.A., Pinter, P.J., Wall, G.W., LaMorte, R.L., Wechsung, G., Wechsung, F., Adamsen, F., Matthias, A.D., Thompson, T.L., 2001. Elevated CO_2 stimulates soil respiration in a FACE what field. Basic and Applied Ecology 2, 193-201.

Phillips C.L., Nickerson, N., Risk, D., Kayler, Z.E., Andersen, C., Mix, A., Bond, B., 2010. Soil moisture effects on the carbon isotope composition of soil respiration. Rapid Communications in Mass Spectrometry 24, 1271-1280.

Phillips, C., Nickerson, N., Risk, D., Bond, B.J., 2011. Interpreting diel hysteresis between soil respiration and temperature. Global Change Biology 17(1), 515-527.

Phillips, C.L., McFarlane, K., Risk, D., Desai, A.R., 2013. Biological and physical influences on soil $^{14}CO_2$ seasonal dynamics in a temperate hardwood forest. Biogeosciences Discussions 10: 10721-58.

Pingintha, N., LeClerc, M. Y., Beasley Jr., J. P., Zhang, G. and Senthong, C., 2010. Assessment of the soil CO_2 gradient method for soil CO_2 efflux measurements: comparison of six models in the calculation of the relative gas diffusion coefficient. Tellus 62B, 47-58.

Pumpanen, J., Ilvesniemi, H., Hari, P., 2003. A process-based model for predicting soil carbon dioxide efflux and concentration. Soil Science Society of America Journal, 67, 402-413.

Pumpanen, J., Kolari,P., Ilvesniemi, H., Minkkinen,K., Vesala,T., Niinisto, S., Lohila, A., Larmola, T., Morero, M., Pihlatie, M., Jandynamicens, I., Curiel Yuste, J., Grunzweig,J.M., Reth, S., Subke,J.A., Savage,K., Kutsch, W., Ostreng, G., Ziegler, W., Anthoni, P., Lindroth, A., Hari, P., 2004. Comparison of difference chamber techniques for measuring soil CO_2 efflux. Agricultural and Forest Meteorology 123, 159-176.

Pypker, T., Hauck, M., Sulzman, E.W., et al., 2008. Towards using $\delta^{13}C$ of ecosystem respiration to monitor canopy physiology in complex terrain. Oecologia 158, 399-410.

Raupach, M.R., Rayner, P.J., Barrett, D.J., DeFries, R.S., Heimann, M., Ojima, D.S., Quegan, S., Schmullius, C.C., 2005. Model-data synthesis in terrestrial carbon observation: methods, data requirements and data uncertainty specifications. Global Change Biology 11, 378-397.

Rayment, M.B., Jarvis, P. G.,1999. Seasonal gas exchange of black spruce using an automatic branch bag system. Canadian Journal of Forest Research 29, 1528-1538.

Rayment M.B., and P.G. Jarvis, An improved open chamber system for measuring soil CO_2 effluxes in the field, Journal of Geophysical Research 102, 28779-28784.

Reichstein, M., Subke, J-A, Angeli, A.C., Tenhunen, J.D., 2005. Does the temperature sensitivity of decomposition of soil organic matter depend upon water content, soil horizon, or incubation time? Global Change Biology 11, 1754-1767.

Reicosky, D.C., Gesch, R.W., Wagner, S.W., Gilbert, R.A., Wente, C.D., Morris, D.R., 2008. Tillage and wind effects on soil CO_2 concentrations in muck soils. Soil Tillage Resesarch 99, 221-231.

Richardson, A.D., Hollinger, D.Y., Burba, G.G., Davis, K.J., Flanagan, L.B., Katul, G.G., Munger, J.W., Ricciuto, D.M., Stoy, P.C., Suyker, A.E., Verma, S.B., Wofsy, S.C., 2006a. A multi-site analysis of random error in tower-based measurements of carbon and energy fluxes. Agricultural and Forest Meteorology 136, 1-18.

Richardson, A.D., Braswell, B.H., Hollinger, D.Y., Burman, P., Davidson, E.A., Evans, R.S., Flanagan, L.B., Munger, J.W., Savage, K., Urbanski, S.P., Wofsy, S.C., 2006b. Comparing simple respiration models for eddy flux and dynamic chamber data. Agricultural and Forest Meteorology 141, 219-234.

Risk, D., Kellman, L., Beltrami, H., 2002a. Carbon dioxide in soil profiles: Production and temperature dependency. Geophysical Research Letters 29(6), 1087.

Risk, D., Kellman, L., Beltrami, H., 2002b. Soil CO_2 production and surface flux at four climate observatories in eastern Canada. Global Biogeochemical Cycles 16(4), 1122.

Risk D., Kellman, L., 2008. Isotopic fractionation in non-equilibrium diffusive environments. Geophysical Research Letters 35, L02403.

Risk, D., Kellman, L., Beltrami, H., Diochon, A., 2008. In situ incubations highlight the environmental constraints on soil organic carbon decomposition. Environmental Research Letters 3, doi: 10.1088/1748-9326/3/4/044004.

Risk, D., Kellman, L., Beltrami, H., 2008. A new method for in-situ soil gas diffusivity measurement and applications in the monitoring of subsurface CO_2. Journal of Geophysical Research 113(G2), G02018.

Risk D., Nickerson, N., Creelman, C., McArthur, G., Owens, J., 2011. Forced Diffusion soil flux: A new technique for continuous monitoring of soil gas efflux. Agricultural and Forest Meteorology 151, 1622-1631.

Risk, D., Nickerson, N., Phillips, C.L., Kellman, L., Moroni, M., 2012. Drought alters respired $\delta^{13}CO_2$ from autotrophic, but not heterotrophic soil respiration. Soil Biology and Biochemistry 50, 26-32.

Riveros-Iregui, D.A., Emanuel, R.E., Muth, D.J. et al., 2007. Diurnal hysteresis between soil CO_2 and soil temperature is controlled by soil water content. Geophysical Research Letters 34, L17404, doi: 10.1029/2007GL030938.

Rochette, P., Flanagan, L.B., Gregorich, E.G., 1999. Separating Soil Respiration into Plant and Soil Components Using Analyses of the Natural Abundance of Carbon-13. Soil Science Society of America Journal 63, 1207-1213.

Ryan, M.G., Law, B.E., 2005. Interpreting, measuring, and modeling soil respiration. Biogeochemistry, 73, 3-27.

Savage, K., Davidson, E.A., Richardson, A.D., 2008. A conceptual and practical approach to data quality and analysis procedures for high frequency soil respiration measurements. Functional Ecology 22, 1000-1007.

Schimel, J.P., Weintraub, M.N., 2003. The implications of exoenzyme activity on microbial carbon and nitrogen limitation in soil: a theoretical model. Soil Biology and Biochemistry, 35, 549-556.

Selker, J.S., Thevenaz, L., Huwald, H., Mallet, A., Luxemburg, W., van de Giesen, N., Stejskal, M., Zeman, J., Westhoff, M., Parlange, M.B., 2006. Distributed fiber-optic temperature sensing for hydrologic systems. Water Resources Research 41(12), W12202.

Senevirathna, D. G. M., Achari, G., Hettiaratchi J. P. A., 2007. A mathematical model to estimate errors associated with closed flux chambers. Environmental Modeling and Assessment 12, 1-11.

Schlesinger, W.H., Andrews, J.A., 2000. Soil respiration and the global carbon cycle. Biogeochemistry 48, 7-20.

Schuur, E.A.G., Trumbore, S.E., 2006. Partitioning sources of soil respiration in boreal black spruce forest using radiocarbon. Global Change Biology 12, 165-176.

Smerdon, J. E., Pollack, H.N., Cermak, V., Enz, J.W., Kresl, M., Safanda, J., Wehmiller, J.F., 2004. Air-ground temperature coupling and subsurface propagation of annual temperature signals. Journal of Geophysical Research 109, D21107.

Smerdon, J.E., Beltrami, H., Creelman, C., Stevens, M.B., 2009. Characterizing land surface processes: A quantitative analysis using air-ground thermal orbits. Journal of Geophysical Research, 114, D15102.

Southon, J. R., 2011. Are the fractionation corrections correct: Are the isotopic shifts for $^{14}C/^{12}C$ ratios in physical processes and chemical reactions really twice those for $^{13}C/^{12}C$?, Radiocarbon, 53, 691-704.

Stoy, P. C., Palmroth, S., Oishi, A.C., Siqueira, M.B.S., Juang, J.Y., Novick, K.A., Ward, E.J., Katul, G.G., Oren, R., 2007. Are ecosystem carbon inputs and outputs coupled at short time scales? A case study from adjacent pine and hardwood forests using impulse-response analysis. Plant, Cell and Environment 30(6), 700-710.

Stuvier, M., Polach, H.A., 1977. Reporting of ^{14}C data. Radiocarbon 19, 355-363.

Subke, J.-A., 2002. Forest floor CO_2 fluxes in temperate forest ecosystems. An investigation of spatial and temporal patterns and abiotic controls. In: Bayreuther Forum Okologie, vol. 96. BITOK, Bayreuth, Germany.

Subke J-A., Inglima I., Peressotti A., Delle Vedove G., Cotrufo M.F., 2004. A new technique to measure soil CO_2 efflux at constant CO_2 concentration. Soil Biology and Biochemistry 36, 1013-1015.

Subke, J.-A., Inglima, I., Cortufo, F., 2006. Trends and methodological impacts in soil CO_2 efflux partitioning: A metaanalytical review. Global Change Biology 12, 921-943.

Subke J.-A., Vallack, H.W., Magnusson, T., Keel, S.G., Metcalfe, D.B., Högberg, P., Ineson, P., 2009. Short term dynamics of biotic and abiotic soil $^{13}CO_2$ effluxes after in situ pulse labeling of a boreal pine forest. New Phytologist 183, 349-357.

Subke, J.A., Bahn, M., 2010. On the "temperature sensitivity" of soil respiration: can we use the immeasurable to predict the unknown? Soil Biology and Biochemistry 42, 1653-1656.

Subke, J.-A., Voke, N.R., Leronni, V., Garnett, M.H., Ineson, P., 2011. Dynamics and pathways of autotrophic and heterotrophic soil CO_2 efflux revealed by forest girdling. Journal of Ecology 99, 186-193.

Suseela, V., Conant, R.T., Wallenstein, M.D., Dukes, J.S., 2012. Effects of soil moisture on the temperature sensitivity of heterotrophic respiration vary seasonally in an old-field climate change experiment. Global Change Biology 18, 336-348.

Takle, E.S., Massman, W.J., Brandle, J.R., Schmidt, R.A., Zhou, X., Litvina, I.V., Garcia, R., Doyle, G., Rice, C.W., 2004. Influence of high-frequency ambient pressure pumping on carbon dioxide efflux from soil. Agricultural and Forest Meteorology 124 (3-4), 193-206.

Tang, J., Baldocchi, D.D., Qi, Y., Xu, L., 2003. Assessing soil CO_2 efflux using continuous measurements of CO_2 profiles in soils with small solid-state sensors. Agricultural and Forest Meteorology 118, 207-220.

Tang, J., Mission, L., Gershenson, A., Cheng, W., Goldstein, A.H., 2005. Continuous measurements of soil respiration with and without roots in a ponderosa pine plantation in the Sierra Nevada Mountains, Agricultural and Forest Meteorology 132, 212-227.

Tang, J., Baldocchi, D.D., Xu, L., 2005. Tree photosynthesis modulates soil respiration on a diurnal time scale. Global Change Biology 11, 1298-1304.

Tedeschi, V., Rey, A., Manca, G., Valentini, R., Jarvis, P.G., Borghetti, M., 2006. Soil respiration in a Mediterranean oak forest at different developmental stages after coppicing. Global Change Biology 12, 110-121.

Trumbore, S. E., Chadwick, O. A., Amundson, R., 1996. Rapid exchange between soil carbon and atmospheric carbon dioxide driven by temperature change, Science 272, 393-396.

Trumbore, S., 2000. Age of soil organic matter and soil respiration: Radiocarbon constraints on belowground C dynamics. Ecological Applications 10, 399-411.

Trumbore, S.E., 2006. Carbon respired by terrestrial ecosystems recent progress and challenges. Global Change Biology 12, 141153.

van t Hoff, J.H., 1898. Lectures on Theoretical and Physical Chemistry. Part 1. Chemical Dynamics. Edward Arnold, London.

Vargas, R., Allen, M.F., 2008a. Diel patterns of soil respiration in a tropical forest after Hurricane Wilma. Journal of Geophysical Research 113, G03021.

Vargas, R., Allen, M.F., 2008. Environmental controls and the influence of vegetation type, fine roots and rhizomorphs on diel and seasonal variation in soil respiration. New Phytologist 179, 460-471.

Venterea, R.T., Baker, J.M., 2008. Effects of Soil Physical Nonuniformity on Chamber-Based Gas Flux Estimates. Soil Science Society of America Journal 72, 1410-1417.

Wang, Y., Amundson, R., Trumbore, S., 1994. A model for soil $^{14}CO_2$ and its implications for using ^{14}C to date pedogenic carbonate. Geochimica et Cosmochimica Acta 58, 393-399.

Wei, W., Weile, C., Shaopeng, W., 2010. Forest soil respiration and its heterotrophic and autotrophic components: global patterns and responses to temperature and precipitation. Soil Biology and Biochemistry 42, 1236-1244.

Welles, J.M., Demetriades-Shah, T.H., McDermitt, D.K., 2001. Considerations for measuring ground CO_2 effluxes with chambers, Chemical Geology, Volume 177(1-2), 3-13.

Winston, G.C., Stephens, B., Sundquist, E.T., Hardy, J.P., Davis, R.E., 1995. Seasonal variability in CO_2 transport through snow in a boreal forest. Biogeochemistry of Seasonally Snow-Covered Catchments. In Biogeochemistry of Seasonally Snow-Covered Catchments. Eds. K.A. Tonnessen, M.W. Williams and M. Tranter. IAHS Publ. 228, 61-70.

Wofsy, S.C., Goulden, M.L., Munger, J.W., Fan, S.M., Bakwin, P.S., Daube, B.C., Bassow, S.L., Bazzaz, F.A., 1993. Net exchange of CO_2 in a mid-latitude forest. Science 260, 1314-1317.

Xu, L., Baldocchi, D.D., Tang, J., 2004. How soil moisture, rain pulses, and growth alter the response of ecosystem respiration to temperature. Global Biogeochemical Cycles 18 (GB4002), doi: 10.1029/2004GB002281.